Characterisation of Defects and Thermoluminescence Yield of Novel Tailor-Made Doped Optical Fibres for Dosimetry

Thesis

By

SITI FAIRUS ABDUL SANI

Submitted for
Degree of Doctor of Philosophy

Centre for Nuclear and Radiation Physics
Department of Physics
Faculty of Engineering and Physical Sciences
University of Surrey
Guildford, Surrey GU2 7XH, UK

May 2015

"Dedicated to My Lovely Husband, Muhammad Hafiz Khalil and My Lovely Son, Ammar Yusuff"

ABSTRACT

This work encompasses characterisation of defects and dosimetric studies of novel tailor made doped SiO_2 fibres. Present studies have been carried out seeking to improve upon the thermoluminescence (TL) yield of commercially produced small diameter telecommunication optical fibres. Using the modified chemical vapour deposition (MCVD) process, the optical fibres have been fabricated to a range of dopant concentrations of nominal value 6- 8- and 10 wt%. In this study, three different types of optical fibres have been utilised, made using the same doped preform. The doped fibres are cylindrical fibres (CF), flat fibres (FF) and photonic crystal fibres (PCF). It should be noted that the process of fibre drawing has been found to produce defect centres, influencing characteristics of optical fibre and TL response. To seek support of this, an X-ray Photoelectron Spectroscopy (XPS) study of a Ge-doped SiO_2 fibres sample has been undertaken to determine the oxidation state of Ge. Results from this have confirmed the efficiency of the surface analysis technique, leading to understanding of the Ge structure. Following on from this, facilities supporting characterization of the fibres are outlined, including an ion beam facility used for Particle Induced X-ray Emission (PIXE)/Rutherford Back Scattering (RBS) analysis to localize and determine the concentration of Ge dopants. Building upon these characterisations, thermoluminescence studies were carried out. For the first of the experiment, undoped flat fibres were used, comparison of response being made with that of conventional TLD-100 and commercial Ge-doped silica fibres. The undoped flat fibres provide competitive TL yield to that of TLD-100, being some 100 times that of the Ge-doped fibres. Pt-coated flat fibres have then been used to increase the photoelectron production and hence local dose deposition, obtaining significant increase in dose sensitivity over that of undoped flat fibres. Using 250 kVp X-ray beams, the TL yield reveals a progressive linear increase in dose for Pt thicknesses from 20 nm up to 80 nm. Finally, to illustrate the potential of novel tailor-made doped SiO_2 optical fibres, the dosimetric characteristics that have been investigated include, dose response, glow curves and energy dependence. Taking TLD-100 as a benchmark, results are presented for Ge-doped, Ge-B-doped and Ge-Br-doped optical fibres. The dose response of doped silica fibres was found to be linear over the range 2 cGy up to 50 Gy, also showing good dosimetric response for low photon energies. Additional investigation of the same doped SiO_2 optical fibres have been conducted for measurement of TL yield from the high linear energy transfer (LET) radiation offered by a liquid ^{223}Ra alpha particle source.

ACKNOWLEDGEMENT

It is a pleasure to thank those who made this project possible. First of all, I am heartily thankful to my supervisor, Professor David Bradley, whose encouragement, guidance and support from the initial until now, enabled me to develop an understanding of the subject. I am indebted to the scientific and technical staff of the Structure Analysis Laboratory and Micro Structural Unit, University of Surrey, Surrey Ion Beam Centre, Royal Surrey County Hospital and UK National Physics Laboratory for their valuable help in all respects during the completion of the project. I offer my regards and blessings to all of those who supported me especially my husband, my family and all my friends for their continuous understanding who become a constant source of moral and emotional support. I would also like to acknowledge the TM R&D/MMU lab, sited at the Multimedia University, for fabricating the fibre preforms. Lastly, I take this opportunity to express my deep gratitude to the University of Malaya for a research grant of University of Malaya - Ministry of Higher Education of Malaysia UM-MOHE High Impact Research Grant UM.C/625/1/HIR/33. The fibres used herein were all fabricated using the University of Malaya Fibre Drawing System, supported by the University of Malaya - Ministry of Higher Education of Malaysia UM-MOHE High Impact Research Grant A000007-50001.

TABLE OF CONTENTS

LIST OF FIGURES

LIST OF TABLES

LIST OF EQUATIONS

LIST OF ABBREVIATIONS

TL	Thermoluminescence
TLD	Thermoluminescence Dosimeter
XPS	X-ray Photoelectron Spectroscopy
PIXE	Particle Induced X-ray Emission
RBS	Rutherford Back Scattering
CF	Cylindrical Fibre
FF	Flat Fibre
PCF	Photonic Crystal Fibre
MMF	Multimode Fibre
COF	Capillary Optical Fibre
MCVD	Modified Chemical Vapour Deposition
NIST	National Institute of Standards and Technology
BJR	British Institute of Radiology
MIT	Massachushetts Institute of Technology
NPL	National Physical Laboratory
LINAC	Linear Accelerator
LET	Linear Energy Transfer
DEF	Dose Enhancement Factor
PDD	Percentage Depth Dose
FSD	Focus-Surface Distance
SSD	Sample Surface Distance

Chapter 1

1 Introduction

Over the past decade and more, optical telecommunication fibres have been widely investigated for application as thermoluminescence dosimeters (TLD), offering relatively high TL yield as a result of extrinsic doping of the fibre core [1,2]. As a result of irradiation, electrons are excited into the point defect traps that have been created by the doping process so that in principle, the concentration and storage capacity of these traps can provide a medium suitable for dosimetric applications. To date, the main dosimetric attributes that have been associated with such small diameter (typically ~100 μm) optical fibres have included the following: the possibility of producing a dosimeter with excellent spatial resolution; a wide dynamic range of dose measurement, from a fraction of a gray to many tens of gray and beyond, providing for applications in radiotherapy and high dose industrial dosimetry; water and corrosion resistance; reusability; and modest cost. Ultimately, this research work is seeking to support fabrication of enhanced TL yield fibres that would extend applications from measurement of the doses that are familiarly used in radiation processing and radiotherapy to diagnostic and environmental radiation doses (milligray down to fractions of a microgray, respectively). As such, one is looking to offer radiation sensitivity approaching or exceeding that of more well established TL dosimeters such as the LiF phosphor-based commercial product TLD-100 [3].

Studies of potential radiation therapy applications of the optical fibre TL dosimetric system have been undertaken by several groups. Various aspects have been studied as for instance, radiation induced attenuation [4], radioluminescence (RL) and optically stimulated luminescence (OSL) [5-7]. Useful TL emission has been observed at the radiation levels familiarly applied in high dose radiation-medicine procedures. The TL response of commercial doped SiO_2 optical fibres has been investigated by a number of researchers, demonstrating promising TL properties with respect to ionising radiation, including for photons [8-12], electrons [9,13], protons [14], alpha particles [15], fast neutrons [16] and synchrotron radiations [17].

Optical fibre is typically made from a preform of silica, comprising two essential components, the doped silica core and an outer silica cladding, such that for telecommunication purposes a difference in refractive index is produced between the core and the cladding. This

refractive index profile is controlled and manipulated through the addition of a dopant. The TL dosimetric system used in this study is tailor-made optical fibres produced by the University of Malaya, and specifically Ge-doped SiO_2 glass. The extrinsically doped silica fibre used herein are composed of silicon (Z=14) and oxygen (Z=8) doped with germanium (Z=32), fabricated via the standard Modified Chemical Vapour Deposition (MCVD) method [18], utilizing $SiCl_4$ and $GeCl_4$ vapour precursor. The cladding layer is exclusively deposited with $SiCl_4$; conversely in the core deposition of this occurs together with $GeCl_4$. Simultaneously the tube is collapsed down to produce what is referred to as a preform, using a high-temperature drawing and fusion process [18] producing an inner core of Ge_2O_3 in amorphous SiO_2.

In brief, for present purposes, the optical properties of silica (specifically the amorphous form) are based on the trapping processes usually reported for crystalline media. It has previously been noted that the TL response of the SiO_2 optical fibre is considerably enhanced by the presence of structural defects in the material, including those produced by extrinsic doping [2]. Such defect centres can also be generated in the glass by either ionization or displacement damage, typically at elevated linear-energy transfer (LET) [19, 20]. Thus said, under certain influencing conditions in the production of the fibres from the preform, it is expected that precursor flow, temperature and drawing speed will all play an important and dominating role in the TL response, influencing the species and population of defects and characteristics of the optical fibre. The Ge atoms (valence 4) directly substitute for the Si atoms (also valence 4) in silica (SiO_2) when Ge is added to the silica glass, therefore affecting the O bonds between Si and Ge atoms; O bonds are lost and form oxygen deficiency centres. The formation of these defects also affect the internal stresses within the glass, it being well understood that the silica fibres become more brittle and therefore less mechanically stable with increasing dopant concentration [21].

In this thesis, many aspects of the generation processes of the defects by irradiation of the Ge-doped optical fibres will be considered, with particular attention to paramagnetic defects Ge(1), Ge(2) and E'Ge, as well as oxygen deficient optically active defects such as the two fold coordinated Ge or Germanium Lone Pair Center (GLPC). Connections between material properties and defects generation will also be investigated. Detailed characterisation of the induced defects will be given, in order to highlight new aspects related to matrix properties and to clarify the spectral features of the defects that are relevant to their recognition. To-date, only limited research has been conducted towards gaining an essential understanding of the magnitude of the TL signal and material characteristics of doped fibres. Such efforts can be traced back to the work of Yusoff et al. [2], in particular concerning TL yield and structural characteristics of sol-gel glass.

In regard to the potential of tailor-made Ge-doped optical fibre for therapeutic dosimetry application, studies have been carried out to investigate the TL response of this candidate dosimeter for various types of radiation beam, covering the energy range from a few eV (from UV sources ~ 1 keV) to several MeV and more (100 MeV). In several dosimetry studies, the main purpose has been to obtain a full performance characterisation of this new candidate TL material for radiation therapy dosimetry applications. In so doing, it has been important to investigate the possible linear dose response between absorbed dose and TL intensity over a wide range of dose, at least over the range of interest for applications covered in this investigation as well as the energy response of the dosimeter.

1.1 Motivation and Goals

The present work utilizes the method of modified chemical vapour deposition (MCVD) for doped silica–glass production, supported by fibre-pulling facilities that can provide for a number of morphologies (cylindrical-, flat- and photonic crystal-fibres for example). The over-arching aim of this PhD project is to improve SiO_2-fibre TLD performance through control of the processes of fabrication. The work demands physical interpretation at the defect level (not only for media whose signal is dependent solely on the presence of intrinsic defects but also for media whose signal is modified by the deliberate inclusion of extrinsic defects). Moreover, this study also aims to establish tailor-made Ge-doped optical fibres as one of the prime thermoluminescent dosimeters of choice in radiation therapy. The specific aims of the current study can be summarised as follows:

1. Study of the oxidation state from the chemical shift information (change in binding energy of a core electron of an element due to a change in the chemical bonding of that element) of the Ge-doped optical fibres, use being made of X-ray photoelectron spectroscopy (XPS). The Auger electrons emitted from the sample surface under the action of X-ray bombardment allows analysis of prominent spectral features and are used to determine the chemical shift of metal surfaces, referred to as the Auger parameter (α') [22].

2. Physical interpretation at the defect level, also ascertaining dopant concentrations and their diffusion in tailor made Ge-doped fibres, ion beam study being undertaken using a combined microbeam proton induced X-ray emission (PIXE)/Rutherford Back Scattering (RBS) analysis [23] arrangement obtained with a 2.5 MeV protons beam.

3. Study of the potential of tailor-made optical fibres of arbitrary dopant concentration as a 1-D dosimetry system, based primarily on TL readout technology, producing dose detection sensitivity (TL yield per unit dose) for various radiation therapy modalities (superficial X-ray beam therapy, linear accelerator beam radiotherapy and the high LET alpha-particles). The associated energies range from keV through to of the order of 10 MeV. Investigation has also been undertaken of the dose enhancement due to photoelectron generation associated with irradiation with kilovoltage potential x-rays for different thicknesses (20-80 nm) of platinum, atomic number (Z) 78, built up as thin layers coated onto the Ge-doped SiO_2 optical fibres.

1.2 Thesis Structure

This thesis is constructed on the basis of three papers published in peer reviewed journals [24-26], all resulting directly from the work conducted during this PhD research. The nature of the investigations embraces the fields of material characterisation and thermoluminescence yield. **Chapter 1,** this chapter provides an introduction to the subject area, outlining the motivation and goals of the work, going on to detail the structure of the thesis.

The layout of the remainder of this thesis is as follows: In **Chapter 2,** the underpinning theoretical basis of the radiations interaction (photons, electrons, protons and alpha-particles) with matter is presented. Also presented is an introductory review of radiation dosimeters (this section providing a more detailed explanation of TL dosimetry, properties of dosimeters and TL measurements). A review is also included of the structure of amorphous silicon dioxide and its main optical defects. This is followed by details of the Ge-doped optical fibre dosimeters and the characterisation methods used in the investigation of doped optical fibres for radiation dosimetry.

Adding to exploration of the physical properties that underpin the thermoluminescence in the tailor-made dosimeters of this investigations, **Chapter 3** is devoted to interpretation and analysis of the results obtained from X-ray photoelectron spectroscopy (XPS). The formation of paramagnetic centres, referred to as the Ge(1) and Ge(2) structures in Ge-doped SiO_2 glass is also discussed in this chapter.

Chapter 4 presents an investigation of the diffusion of the Si and Ge in the core and inner cladding of tailor-made optical fibres, use being extracted of a combined microbeam

proton induced X-ray emission (PIXE)/Rutherford Back Scattering (RBS) analysis arrangement.

Chapter 5 investigates the TL response of the SiO_2 optical fibres, in particular the elevated sensitivity of undoped flat fibres. Further investigation has also been undertaken of dose enhancement close to high atomic number media using coated optical fibre thermoluminescence dosimeters. A particular feature is the experimental technique that has been used in seeking to uniformly coat the selected optical fibres with different thicknesses of platinum. Using tailor made doped optical fibres, studies are performed on thermoluminescent dosimetric studies of a formulation of ^{223}RaCl (the basis of a product called *Xofigo*^{TM}). This is followed by a section on the selection of fibres and characterizing these for dosimetry in terms of, dose response, glow curve and energy dependence for fibres subjected to photon irradiation.

Finally, **Chapter 6** collects together and summarises the experimental results from each chapter, and discusses their significance, providing pointers for future work.

1.3 References

[1] D. A. Bradley, R. P. Hugtenburg, A. Nisbet, A. T. Abdul Rahman, F. Issa, N. Mohd Noor, and A. Alalawi. “Review of doped silica glass optical fibre: their TL properties and potential applications in radiation therapy dosimetry.” *Appl. Radiat. Isot.* vol. 71 Suppl, pp. 2–11, Dec. 2012.

[2] A. L. Yusoff, R. P. Hugtenburg, D. A. Bradley. “Review of development of a silica-based thermoluminescence dosimeter.” *Radiat. Phys. Chem*., vol. 74, no. 6, pp. 459–481, Dec. 2005.

[3] S. W. S. McKeever. Thermoluminescence of Solids Cambridge University Press (1985).

[4] A.L. Huston, B.L. Justus, P.L. Falkenstein, R.W. Miller, H. Ning, R. Altemus, "Remote optical fiber dosimetry." *Nucl. Instruments Methods Phys. Res. Sect. B Beam Interact. with Mater. Atoms*, vol. 184, pp. 55–67, 2001.

[5] M.C. Aznar, C.E. Andersen, L. Botter-Jensen, S.A.J. Back, S. Mattsson, F. KjaerKristoffersen, J. Medin, "Real-time optical-fibre luminescence dosimetry for radiotherapy: physical characteristics and applications in photon beams." *Phys. Med. Biol.*, vol. 49, no. 9, pp. 1655–1669, 2004.

[6] B.L. Justus, S. Rychnovsky, M.A. Miller, K.J. Pawlovich, A.L. Huston, "Optically stimulated luminescence radiation dosimetry using doped silica glass." *Radiat. Prot. Dosimetry*, vol. 74, no. 3, pp. 151–154, 1997.

[7] L.A. Benevides, A.L. Huston, B.L. Justus, P. Falkenstein, L.F. Brateman, D.E. Hintenlang, "Characterization of a fiber-optic-coupled radioluminescent detector for application in the mammography energy range." *Med. Phys.*, vol. 34, no. 6, pp. 2220–2227, 2007.

[8] Y. A. Abdulla, Y. M. Amin, D. A. Bradley, “The thermoluminescence response of Ge-doped optical fibre subjected to photon irradiation,” *Radiat. Phys. Chem.*, vol. 61, pp. 409–410

[9] A.T. Abdul Rahman, A. Nisbet, D.A. Bradley, “Dose-rate and the reciprocity law: TL response of Ge-doped Sio_2 optical fibers at therapeutic radiation doses.” *Nucl. Instruments Methods Phys. Res. Sect. A Accel. Spectrometers, Detect. Assoc. Equip.*, vol. 652, no. 1, pp. 891–895, Oct. 2011.

[10] N. M. Noor, M. Hussein, D. A. Bradley, and A. Nisbet, “The potential of Ge-doped optical fibre TL dosimetry for 3D verification of high energy IMRT photon beams,” *Nucl. Instruments Methods Phys. Res. Sect. A Accel. Spectrometers, Detect. Assoc. Equip.*, vol. 619, no. 1–3, pp. 157–162, Jul. 2010.

[11] N. M. Noor, M. Hussein, D. A. Bradley, and A. Nisbet, “Investigation of the use of Ge-doped optical fibre for in vitro IMRT prostate dosimetry,” *Nucl. Instruments Methods Phys. Res. Sect. A Accel. Spectrometers, Detect. Assoc. Equip.*, vol. 652, no. 1, pp. 819–823, Oct. 2011.

[12] F. Issa, N. A. A. Latip, D. A. Bradley, and A. Nisbet, “Ge-doped optical fibres as thermoluminescence dosimeters for kilovoltage X-ray therapy irradiations,” *Nucl. Instruments Methods Phys. Res. Sect. A Accel. Spectrometers, Detect. Assoc. Equip.*, vol. 652, no. 1, pp. 834–837, Oct. 2011.

[13] S. Hashim, S. Al-Ahbabi, D. A Bradley, M. Webb, C. Jeynes, A. T. Ramli, and H. Wagiran, “The thermoluminescence response of doped SiO2 optical fibres subjected to photon and electron irradiations.,” *Appl. Radiat. Isot.*, vol. 67, no. 3, pp. 423–7, Mar. 2009.

[14] S. Hashim, A. T. Ramli, D. A. Bradley, H. Wagiran, “The thermoluminesce response of Ge-doped optical fibre subjected to proton irradiation” in 5th National Seminar on Medical Physics. Malaysia. Medical Physics Association, Kuala Lumpur, 2006.

[15] A. T. Ramli, D. A. Bradley, S. Hashim, and H. Wagiran, “The thermoluminescence response of doped SiO2 optical fibres subjected to alpha-particle irradiation.,” *Appl. Radiat. Isot.*, vol. 67, no. 3, pp. 428–32, Mar. 2009.

[16] S. Hashim, D. a Bradley, M. I. Saripan, a T. Ramli, and H. Wagiran, “The thermoluminescence response of doped SiO2 optical fibres subjected to fast neutrons.,” *Appl. Radiat. Isot.*, vol. 68, no. 4–5, pp. 700–3, 2010.

[17] A. T. Abdul Rahman, D. A. Bradley, S. J. Doran, B. Thierry, E. Bräuer-Krisch, and A. Bravin, “The thermoluminescence response of Ge-doped silica fibres for synchrotron microbeam radiation therapy dosimetry,” *Nucl. Instruments Methods Phys. Res. Sect. A Accel. Spectrometers, Detect. Assoc. Equip.*, vol. 619, no. 1–3, pp. 167–170, Jul. 2010.

[18] A. C. Pugh, R. P. Stratton, D. B. Lewis. “Investigation of elemental diffusion during the drawing and heat treatment of glass optical fibres.” *J. Mater. Sci*. vol. 29, pp. 1036–1040, 1994.

[19] E. J. Friebele, G. H. Sigel, and D. L. Griscom, “Drawing-induced defect centers in a fused silica core fiber,” *Appl. Phys. Lett.*, vol. 28, no. 9, pp. 516, 1976.

[20] Y. Hibino, H. Hanafusa. “Consolidation atmosphere influence on drawing induced defects in pure silica optical fibres.” *J. Lightwave Technol*., vol. 58, no. 3, pp. 172–178, 1985.

[21] J. Canning, M. Stevenson, S. Bandyopadhyay, and K. Cook, “Extreme silica optical fibre gratings,” *Sensors*, vol. 8, no. 10, pp. 6448–6452, 2008.

[22] J.F. Watts and J. Wolstenholme. "An introduction to surface analysis by XPS and AES." pp. 224. ISBN 0-470-84713-1. Wiley-VCH, May 2003.

[23] L. Pichon, L. Beck, P. Walter, B. Moignard, and T. Guillou, “A new mapping acquisition and processing system for simultaneous PIXE-RBS analysis with external beam,” *Nucl. Instruments Methods Phys. Res. Sect. B Beam Interact. with Mater. Atoms*, vol. 268, no. 11–12, pp. 2028–2033, 2010.

[24] S. F. Abdul Sani, A. I. Alalawi, H. Azhar A.R, G. Amouzad Mahdiraji, N. Tamchek, A. Nisbet, M. J. Maah, and D. A. Bradley, “High sensitivity flat SiO2 fibres for medical dosimetry,” *Radiat. Phys. Chem.*, vol. 104, pp. 134–138, Nov. 2014.

[25] S. F. Abdul Sani, G. W. Grime, V. Palitsin, G. a. Mahdiraji, H. a. Abdul Rashid, M. J. Maah, and D. a. Bradley, “Micro-PIXE analysis of doped SiO_2 fibres intended as TL dosimeters for radiation measurements,” *X-Ray Spectrom.*, vol. 44, no. 2, pp. 33–40, 2015.

[26] S. F. Abdul Sani, G. A. Mahdiraji, A. S. Siti Shafiqah, G. W. Grime, V. Palitsin, S. J. Hinder, N. Tamchek, H. A. Abdul Rashid, M. J. Maah, J. F. Watts, and D. A. Bradley, “XPS and PIXE Analysis of Doped Silica Fibre for Radiation Dosimetry,” vol. 33, no. 11, pp. 2268–2278, 2015.

Chapter 2

2 Literature Review and Underpinning Theory

2.1 Interaction of Radiation with Matter

Radiation therapy is used for the killing of the cancer cells and the halting of further cancer cell proliferation through irradiation of the malignant tissue, use being made of photons (X- or γ-rays) and particles, most commonly electrons, but also protons, carbon ions and neutrons and more recently alpha particles. Radiation interacts with matter (tissue) in a number of ways but it is important to consider the various interaction types that are of significance in radiation measurements. In the following, these interactions will be reviewed.

2.1.1 Interaction of Photons with Matter

In a photon beam (of X- or γ-rays in the present context) energy is lost gradually (10^{-14} s), through the partial or complete transfer of photon energy to electron energy. The intensity *I* (the number of photons) of the original beam is attenuated as it penetrates into the absorber. This is due mainly to the three major interactions that remove photons from the original beam, and which are the predominant mechanism allowing the majority of radiation measurements to be made in medicine (Fig. 2-1): the photoelectric effect, which predominates for the lower energy X- and gamma rays (up to several hundred keV), pair production, which predominates for high energy photons (for tissues, above 5-10 MeV), and Compton scattering, which is the most probable process over the range of energies between the previous two boundaries [1].

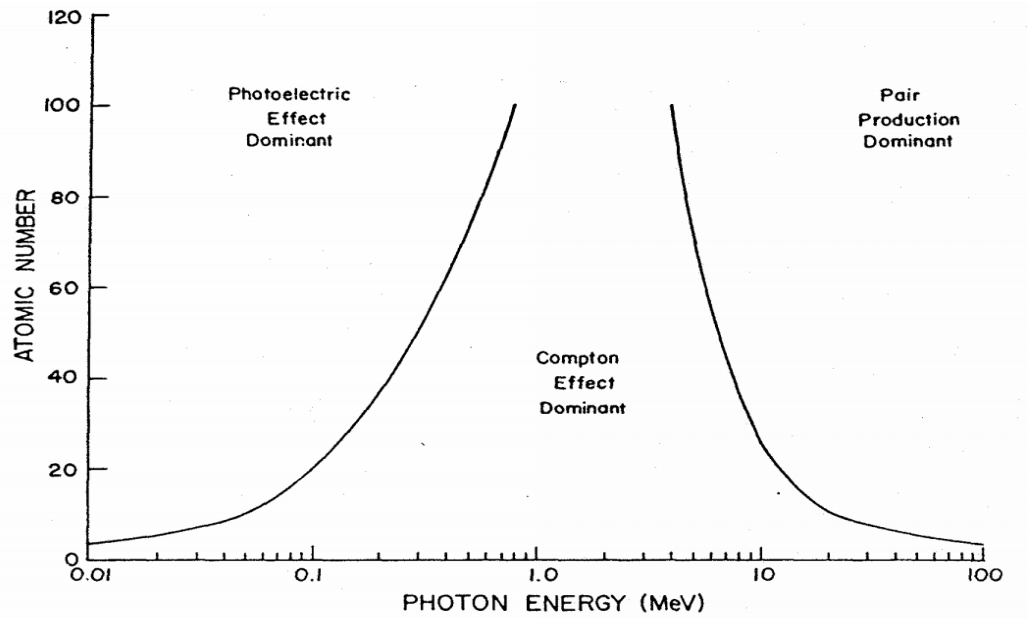

Figure 2-1 The dominant types of photon attenuation processes across the range of energies of interest [1].

When a beam of many photon passes through matter it is attenuated. The value of the linear attenuation coefficient, μ, of photons in an attenuating medium depends on the energy of the photons, the atomic number of the absorber medium and the physical state of the absorber medium (primarily its density). The linear attenuation coefficient is essentially an expression of the total probability per unit path length of a photon interacting with an atom as it penetrates the attenuating medium as shown in equation 2-1.

$$I = I_0 e^{-\mu t} \tag{2-1}$$

where I is the intensity of photons transmitted across some distance x, I_0 is the initial intensity of photons, μ the linear attenuation coefficient, x is the distance traveled and the negative sign shows that the intensity, I decreases as x increases [4].

2.1.1.1 Photoelectron Spectroscopy

In the core of the photoelectric interaction, the incident photons impinge on an atom of the absorbing material and the photon completely disappears; i.e. its energy is completely or partially imparted to an inner shell electron, which is then ejected from its orbit. The ejected electron is called a photoelectron. This energy in general far exceeds the binding energy of the

electron in the host atom. The kinetic energy *(KE)* of the ejected photoelectron is the difference between the incident photon energy E_i *(hν)* and the binding energy of the orbital electron E_0.

$$KE = h\nu - E_0 \qquad \textbf{(2-2)}$$

The photoelectron is typically produced from the K shell, for which the range of binding energies is from a few keV for materials of low atomic number to tens of keV for high Z absorber materials (Fig. 2-1). The process is illustrated in Fig. 2-2 for photons interacting with a K-shell electron.

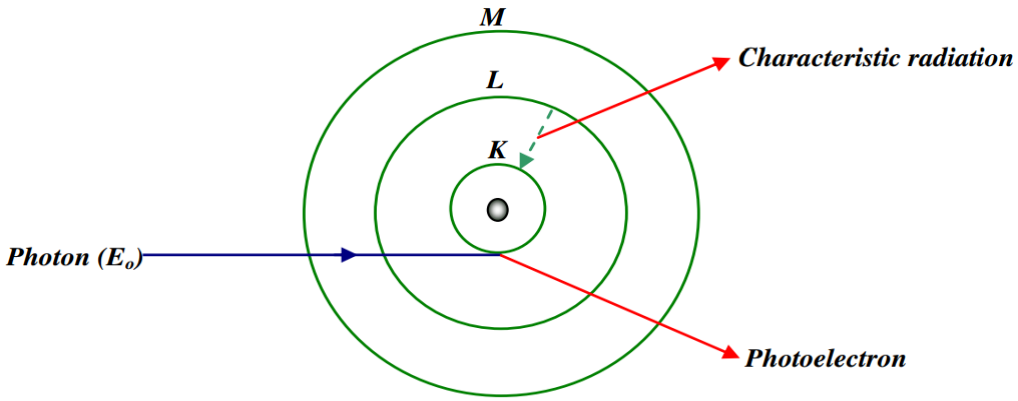

Figure 2-2 Illustration of photoelectric absorption for a K-shell electron and ensuing secondary processes (characteristic X-rays and Auger electron emission).

The vacancy resulting from the electron ejection is filled through the rearrangement of electrons from other shells of the atom (with lower binding energy), leading to the emission of characteristic X-rays and/or Auger electrons. For this to occur, the incident energy should be greater than the binding energy in the atom [1].

The probability of photoelectric absorption depends on the incident photon energy, the electron binding energy and the atomic number of the atom. The probability of the photoelectric interactions is expressed in the following relation [2, 3] where τ is the photoelectric mass attenuation coefficient, Z is the atomic number, E is the incident photon energy and the exponent n is varies between 4 and 5.

$$\tau \propto \frac{Z^n}{E^2} \qquad \textbf{(2-3)}$$

2.1.1.2 Compton Scattering

Compton scattering is an inelastic scattering process, occurring when the incoming photon with energy, $h\nu$, undergoes an interaction with a orbital electron in matter, ejecting the electron, but also incurring partial loss of energy such that the outgoing photon is deflected from the original path of the incident photon [1] (Fig. 2-3). The incident photon loses energy because of the interaction with the electron and part of the energy is transferred to a scattering electron, which then recoils, and the rest of the energy is transferred to the scattered photon. Energy and momentum are conserved in this process therefore, there is dependence on the angle of scattering and not on the nature of the scattering medium.

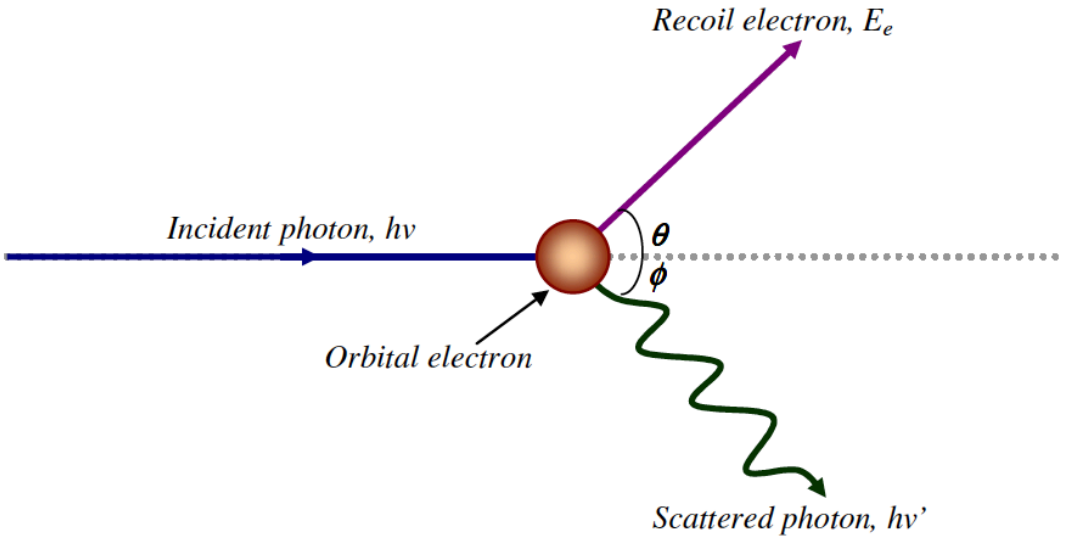

Figure 2-3 A schematic representation of Compton scattering processes.

The energy of the scattered photon, *hv'* and scattering angle, θ are related by:

$$h\nu' = \frac{h\nu}{1 + \frac{h\nu}{m_0 c^2}(1 - \cos\theta)} \qquad \textbf{(2-4)}$$

where m_0c^2 is the electron rest mass energy (0.511 MeV). Compton scattering is almost independent of atomic number, Z compared to photoelectric absorption, however it does depend on the number of electrons available as scattering targets [3].

2.1.1.3 Pair Production

Pair production is observed to occur in nature when the incident photon energy exceeds or is equal to twice the rest-mass energy of an electron (1.022 MeV) where the photon disappears and is replaced by two electronic particles, namely the electron (e-) - positron pair (e+). Fig. 2-4 illustrates the pair production process. Since the rest mass energy of the electron is 0.511 MeV, then 1.022 MeV is the threshold energy for the pair production process to take place. Energy in excess of 1.022 MeV appears as the kinetic energy shared by the electron and the positron.

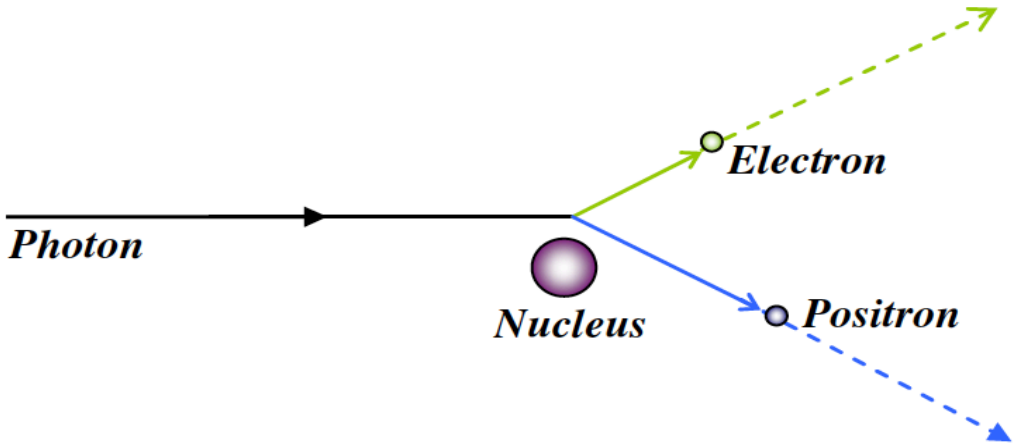

Figure 2-4 A schematic diagram of the pair production process

The positron annihilates with an electron to produce two 0.511 MeV photons, emitted in opposite directions as the secondary products of the interaction, as shown in Fig. 2-5.

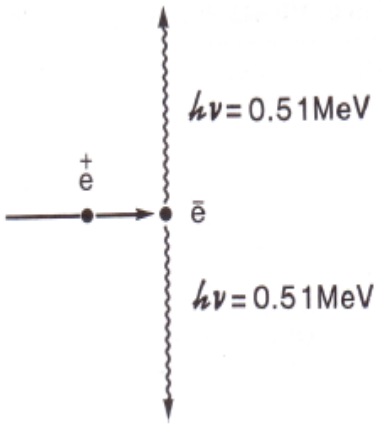

Figure 2-5 Diagramatic illustration the production of annihilation radiation [3].

The probability of the pair production interaction is proportional to the square of atomic number Z, increasing as the square of Z. The pair production mechanism interacts with the electromagnetic field of an atomic nucleus. Also, the probability for it to occur increases as the photon energy increases above the threshold energy [3].

2.1.2 Interaction of Electrons with Matter

As electrons are accelerated into a medium, they interact with the medium through Coulomb interactions with orbital electrons and nuclei of the atoms of the target sample. There are a number of outcomes through these collisions; either the electrons may lose their kinetic energy (through collision and radiative losses) or by changing the trajectory of the electrons (i.e. scattering). For charged particles, the energy loss per particle per unit path travelled (- dE/dx) is described as the stopping power S, typically expressed in units of MeV cm^{-1}, but can also be re-expressed as the mass stopping power S/ρ which may be expressed in MeV cm^2/g, with ρ being the density of the medium. Scattering power is used to define the scattering losses within the medium [4].

Electron bombardment of a sample produces radiation interactions, undergoing interactions with orbital electrons or the nuclei of atoms, experiencing elastic or inelastic collisions. Elastic and inelastic collisions result in a number of outcomes that are used for imaging, quantitative and semi-quantitative information of the target sample and generation of an X-ray source. In the case of an elastic collision, the electron trajectory changes from its original path with no loss of energy (due to large differences between the mass of the electron and nucleus) where the amount of scattering that occurs is dependent on the atomic number of the nucleus. Conversely, inelastic collisions result in loss of energy as it is deflected from its original path, the latter being transferred to an orbital electron or is otherwise released as an X-ray in the form of a bremsstrahlung photon in electron-nucleus interactions [4].

2.1.2.1 Electron-Orbital Interactions

Coulomb interactions between the incident electron and orbital electrons of a medium results in ionizations and excitations of the medium atoms [4]. Ionization transpires if sufficient energy is transferred to an orbital electron to overcome the binding energy to the nucleus, the electron completely escaping from the absorber atom, leaving the atom ionized. If the energy is insufficient to overcome the binding energy then it typically results in excitation of the atom i.e.

promotion of an orbital electron of the medium atom between allowed shells, and subsequent de-excitation to a lower orbital [3, 4].

The liberated electrons generated from the ionisation process are called secondary electrons. These secondary electrons also traverse the medium and interact with the medium atoms, resulting in ionisation or excitation, depositing dose in the medium until stopped [3]. The range penetration of these electrons are typically of the order of 10s to hundreds of microns only, and therefore depositing dose in a highly localised fashion.

2.1.2.2 Electron-Nucleus Interactions

Electrons and nuclei can also interact with the electromagnetic field of the nuclei of the medium. Since the electron mass is small compared to that of nuclei subsequent sudden braking is reduced. The resultant energy loss is produced as X-ray photons referred to as bremsstrahlung. The rate of energy loss as a consequence of bremsstrahlung increases as the energy of electrons and the atomic number of the medium increase. These types of energy loss are characterized through use of the radiative stopping power [3, 4].

2.1.3 Interaction of Heavy Charge Particles with Matter

Heavy charged particles, such as alpha particles, interact with matter predominantly through the Coulomb forces between the positive charge of the alpha particle and the negative charge of the multitude of orbital and free electrons in matter. The most probable process involved in the absorption of alphas, are ionization and excitation of orbital electrons. Ionization occurs whenever the alpha particle is sufficiently close to the electron for the latter to escape from its orbit through coulomb attraction. Each time this occurs, the alpha loses kinetic energy and is thus slowed. The alpha also loses kinetic energy by exciting orbital electrons with interactions that are insufficient to cause ionization. As it becomes slower, the alpha has tendency to cause ionization at an increasing rate. As the alpha nears to the end of its track, its rate of ionization peaks and within a very short distance it stops, collects two electrons and becomes a helium atom. The maximum energy that can be transferred in an interaction process from a heavy particle of mass m with kinetic energy E to a single electron of mass m_e is [4]:

$$\Delta E = 4E\frac{m_e}{m} \qquad \textbf{(2-5)}$$

Because alpha particles are comparatively heavy and have a charge, they react strongly with matter, producing large numbers of ions per unit length of their path. Consequently, they are not very penetrating e.g. 5 MeV alpha particles for instance, will only travel about 3.6 cm in air and will not penetrate an ordinary piece of paper. The average travel distance with respect to air for the other materials is approximately inversely proportional to the respective densities of the material. 5 MeV alpha particles will only travel about 4 μm in mammalian tissue. Alpha particles can interact either with nuclei or orbital electrons in any absorbing medium such as air, water, tissue or metal. Since alphas offer low penetration capability, they are usually not hazardous for external exposure. However, when internally deposited, alpha particles are often more damaging than most other types of particle because comparatively large amounts of energy are deposited within a very small volume of tissue [5].

Measurement of the number of ionisations caused by the radiation per unit distance as it traverses the living cell or tissue is typically expressed in terms of kiloelectron volts deposited per micrometer (keV/μm) and is called the linear energy transfer (LET) of the radiation. The alpha particles cause frequent direct ionization within a narrow diameter around a relatively straight track, thus approximating continuous deceleration. As they slow down, the changing particle cross-section modifies their LET, generally increasing it to a Bragg peak just before achieving thermal equilibrium with the absorber (before the end of the particle range). At equilibrium, the incident particle essentially comes to rest or is absorbed, at which point LET is undefined. The LET of diagnostic x-rays is about 3 keV/μm, whereas the LET of 5 MeV alpha particles is of the order of 100 keV/μm. A plot of the specific energy loss along the track of a charged particle such as that shown in Fig. 2-6 is known as the Bragg curve. The example is shown for an alpha particle of several MeV initial energy. For most of the track, the charge on the alpha particle is two electronic charges, and the specific energy loss per length increases roughly as 1/E. Near the end of the track, the charge is reduced through electron pickup and the curve falls off. Plots are shown for a single alpha particle track.

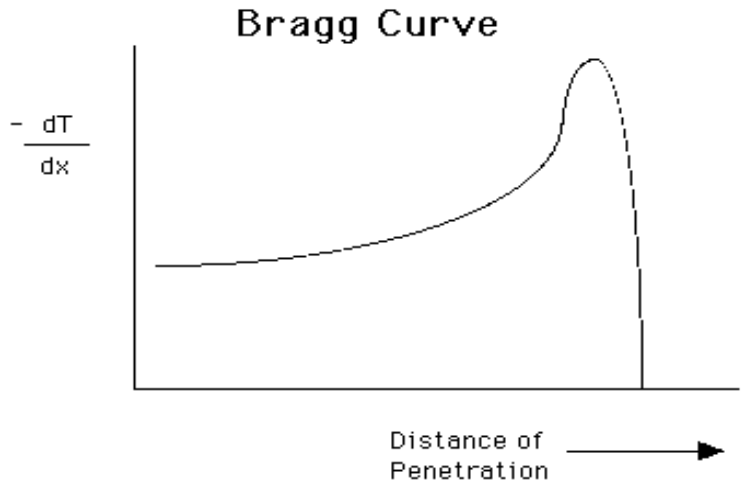

Figure 2-6 Depiction of the energy loss along an alpha track, with dT the loss of energy along an incremental path dx.

2.2 Radiation Dosimeters

The dosimetric quantities such as exposure, kerma (kinetic energy released in the medium), absorbed dose, equivalent dose or dose rate can be measured or evaluated either directly or indirectly with an instrument or device referred to as a radiation dosimeter. With proper calibration, dosimeters must exhibit several desirable characteristics to function effectively for radiation dosimetry including accuracy and precision of dose measurement, linearity of response (dose or dose-rate dependence), a simple or invariant energy response, directional independence and good spatial resolution [4]. Dosimeters are available in a number of types including ionization chambers, films (radiographic and radiochromic), semiconductors (diodes), MOSFET, Gel (e.g. PRESAGE^{TM}) and others. The Ge-doped SiO_2 thermoluminescence dosimeter system is highlighted in this thesis, offering a number of highly desirable characteristics in response to irradiation.

2.2.1 Thermoluminescence (TL) Dosimetry

TL dosimetry (TLD) relies on a system, which comprises a TL medium and a TLD reader, is the measurement of the integrated absorbed radiation dose. Upon irradiation the TL dosimeters store a fraction of the resultant absorbed energy in metastable energy levels, the latter being either intrinsic or introduced as electron traps formed from impurities/dopants. The irradiation energy stimulates electrons to excite and occupy these traps. Conventionally the system is described in terms of a crystalline model formed of a valence and conduction band and

an intermediary forbidden band in which the trapping levels reside. For an amorphous system, as in the case of the doped glass system used herein, it has been found that identical model can be used to interpret the functional TL response of such non-crystalline media. To de-trap a TL system, heat is applied; the de-trapped electrons lose their energy as light, the associated light yield being indicative of the absorbed dose recorded on a photomultiplier tube.

2.2.1.1 Luminescence

The production of light from heat, or incandescence describes the luminescence of a material, typically exhibited in crystalline systems such as for instance gadolinium oxysulphide (GdO_2SO_4), popularly used in film-screen systems. Luminescent materials can absorb energy inside the crystal lattice. This energy is emitted in the form of ultraviolet, visible or infrared light as a result of appropriate stimulation. Two distinct types of luminescence are known, reference being made to the time delay between the stimulation and the releasing of the light, termed fluorescence or phosphorescence. Fluorescence prevails within the period of stimulation of the luminescence material, ejection taking place within a time of between 10^{-10} and 10^{-8} sec; phosphorescence occurs over a time exceeding 10^{-8} sec. If heat is used as the stimulating form of energy, it is referred as thermoluminescence and the material is called a thermoluminescence dosimetric (TLD) material when used for purposes of dosimetry. If light is used as the stimulation form of energy then the phenomenon is known as optically stimulated luminescence (OSL) [3-4, 6].

2.2.1.2 Thermoluminescence Mechanism

As previously mentioned, the TL mechanism in a crystalline material is described in terms of the energy band model. This model represents three electronic energy levels in the crystal lattice, these being the valence band (electrons roam freely), the conduction band (electrons are least tightly bound) and a forbidden gap, which separates the energy between the valence and conduction band. Electrons are normally not present in the forbidden energy band as illustrated in Fig. 2-7 [3]. However, the traps (both the storage traps and recombination centres, explained below) are located in the forbidden energy band; the electron traps engage the states just below the conduction band and the hole traps engage the states just above the valence band [4, 6].

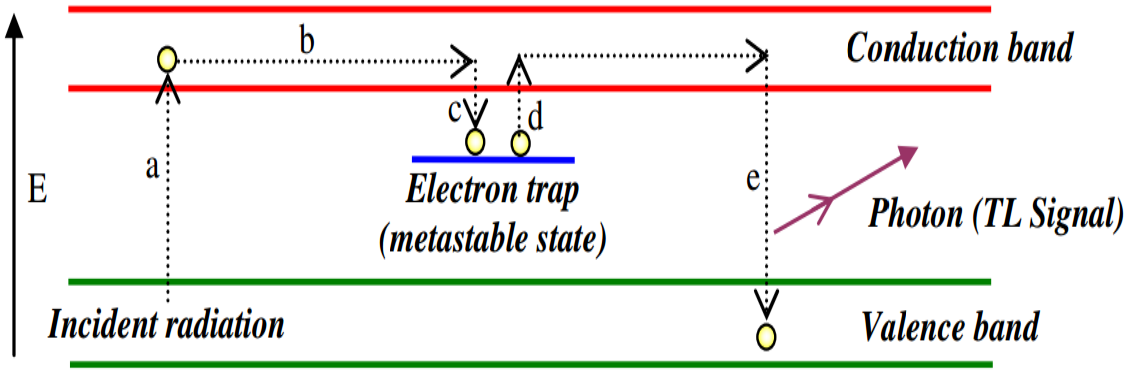

Figure 2-7 Diagram of the energy levels in a crystal lattice and the thermoluminescence process (● - Electron); (a) excited free electron produced by irradiation, (b) electron free to move in crystal, (c) trapping of electron on trap level, (d) release of trapped electron by sample heating and (e) de-excite electron to valence band and photon released as TL signal.

The trapping levels (hole traps and electron traps) are assumed to be empty before irradiation. The exposure of thermoluminescent materials to ionising radiation results in secondary charged particles, most usually electrons that liberate several free low energy electrons and holes [3]. Once stimulated, the electrons are excited from the valence band to the conduction band (if electrons come from the valence band) or leave empty hole traps (in this case of electrons filling hole traps in the forbidden band) [4]. The electrons and holes move freely through their own band until they recombine or fall respectively into the electron trap (E) and hole trap (H). Traps are characterised by the intrinsic defects (vacancies) that exist in the crystal and extrinsic defects (impurities) that are added to the crystal (see section 2.4.1 for details). The traps are represented as below [4] and are illustrated in the diagram of Fig. 2-8:

- Storage traps: release free charge carriers if heated (as in the TL process) or if stimulated by light as in the OSL process [4].
- Recombination centres: charge carriers released from the storage traps recombine with the trapped charge carriers of opposite sign, energy is then emitted due to this recombination in the form of ultraviolet, visible or infrared light, which can be measured using photodiodes or photomultiplier tubes [4].

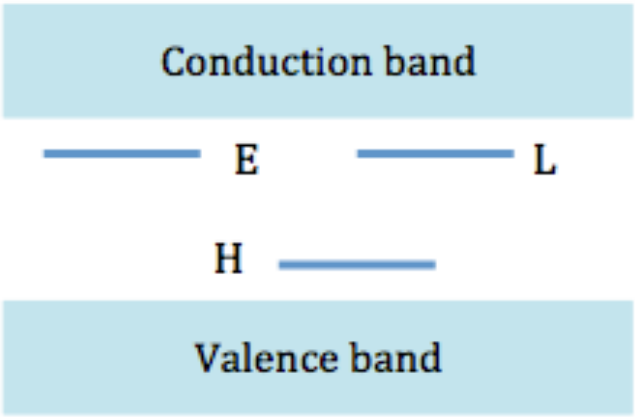

Figure 2-8 Diagram of energy levels in an insulator material where E is the electron trap, H is the hole trap and the trapped electrons recombine with the holes at luminescence centers (L), which is at the stable energy state with emission of light.

As previously mentioned, the fluorescence occurs if the light release due to those transitions is immediate. The emission light of phosphorescence (delayed fluorescence) exists if sufficient energy is provided to eject electrons from the traps, allowing them to fall to the valence band. The phenomenon is referred to thermoluminescence if stimulated by heat (typically at ~300^{0}C and above) to promote the phosphorescence [3]. If the energy traps are superficial then even under ambient light or room temperature conditions release can occur (a process referred to as fading).

Since dosimetry aims to measure integral dose with high precision, the focus is on materials with a high phosphorescence yield. The yield may be improved by adding a controlled amount of artificial impurities into the material, achieved by doping the base medium with other elements called activators, such as LiF: Mg: Ti, the lithium fluoride being doped with magnesium and titanium in this example [7].

2.2.2 Characteristics of Dosimeters

The performance of dosimeters is assessed through the study of characteristics such as linearity, dose response, energy response, reproducibility, stability, effect of the environment on dosimeter performance and others [8].

2.2.2.1 Accuracy and Precision

All measurements in radiation dosimetry are as much subject to error as any other form of measurement system, contributing to the uncertainty of the result and characterized in terms of both accuracy and precision. It is an expectation that there should only be a small standard deviation of the distribution of the measurement results to indicate the high precision of the results in TL dosimetry, as required for instance in their use at radiotherapy levels [4]. The accuracy of any measurements specifies the degree of veracity of how close a measured value is to the actual (true) value for that quantity.

2.2.2.2 Dose Response

In principal, a desirable dosimeter should have a linear response in relationship between the thermoluminescence intensity to the absorbed dose. However, most conventional TL dosimeters exhibit a non-linear growth beyond a certain dose range, being either supralinearity or sublinearity between TL intensity and absorbed dose, as demonstrated in Fig. 2-9. The linearity range and the non-linearity behaviour depend on the type of dosimeter and its physical characteristics [4]. Both supralinearity and the sublinear growth appear to approach saturation, which cause problems of underestimation or overestimation, respectively. The occurrence of non-linear response of a detector does not preclude its use in TLD provided that it is calibrated and corrected for the non-linearity [6].

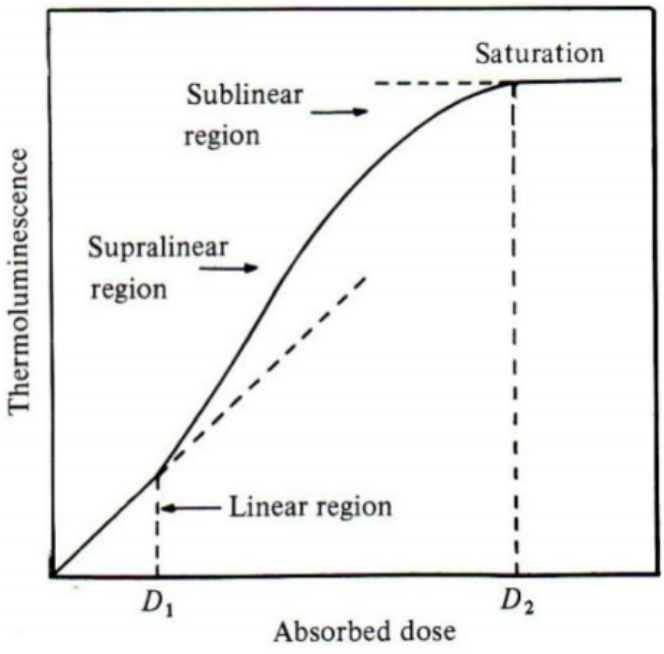

Figure 2-9 Diagram of a typical thermoluminescence growth curve showing linear, supralinear and sublinear regions of a phosphor-based TLD [6].

Supralinearity and saturation can both be affected by previous thermal treatments and exposure to radiation, consequently affecting the reusability of a dosimeter. Due to this, a dosimeter may exhibit a different response upon second and further subsequent use. Therefore, to overcome these sensitization and supralineaity problems, the annealing process is required to re-obtain the original characteristic properties to keep a dosimeter re-useable (its sensitivity remaining the same during multi usage) [6].

2.2.2.3 Energy Dependence

Energy response is defined as a measure of the energy absorbed in the TL material. Since the intensity of thermoluminescence emitted from a material is proportional to the amount of energy initially absorbed by that material, it is important to assess the absorption coefficient of a material with respect to radiation energy. For photon irradiations (X- or γ-rays herein), this evaluation is made via the photon energy response S(E) of the system, derived by calculation of the ratio of the mass energy absorption coefficient for the particular material $(\mu_{en}/\rho)_m$ to the mass energy absorption coefficient of a reference material (air or tissue) $(\mu_{en}/\rho)_{ref}$, where μ_{en} is the linear absorption coefficient and ρ is the density in each case. Thus:

$$S(E)=\frac{\left(\frac{\mu_{en}}{\rho}\right)_m}{\left(\frac{\mu_{en}}{\rho}\right)_{ref}} \qquad \textbf{(2-6)}$$

The mass energy coefficient is dependent upon the energy loss process occurring during energy absorption, including the photoelectric interaction, Compton scattering and pair production. Each process depends upon the energy of the absorbed radiation, the material's isotopic content and its effective atomic number Z [6].

For dosimetry, it is desirable to have a constant energy response over a wide range of energies, thus low Z dosimeter materials are preferable. Additionally, the atomic number Z of a dosimeter is desirable to be close to that of tissue (soft tissue, with effective atomic number, Z_{eff} ~ 7.4), known as a tissue equivalent dosimeter. Fig. 2-10 represents the difference in energy

response for three different Z_{eff} materials; it is notable that the lowest Z_{eff} has the more desirable energy response. CaF_2 (Calcium Fluoride), $CaSO_4$ (Calcium Sulphate), LiF (Lithium Fluoride) have effective atomic numbers of 16.9, 15.6 and 8.14, respectively [6].

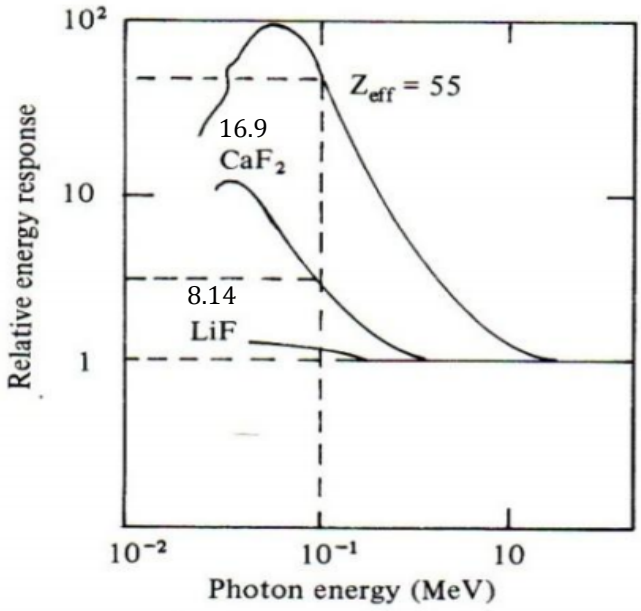

Figure 2-10 Diagram of an energy response of TL materials of various effective atomic number [6].

2.2.2.4 Glow Curve

The glow curve is obtained by measuring the intensity of emitted light against the temperature and the time period during which the temperature is increased. If the heating rate remains constant, the temperature will be proportional to the time during which heating is applied. Fig. 2-11 illustrate the glow curve after irradiation contains five glow peaks up to 250°C temperature. The deconvolved peaks are numbered as a fraction of increasing trap depth. Note that the low temperature peaks have high fading of stored signal and a very short half-life. Peak 1 is not manifested in Fig. 2-11 as it has a very short half-life (10 minute).

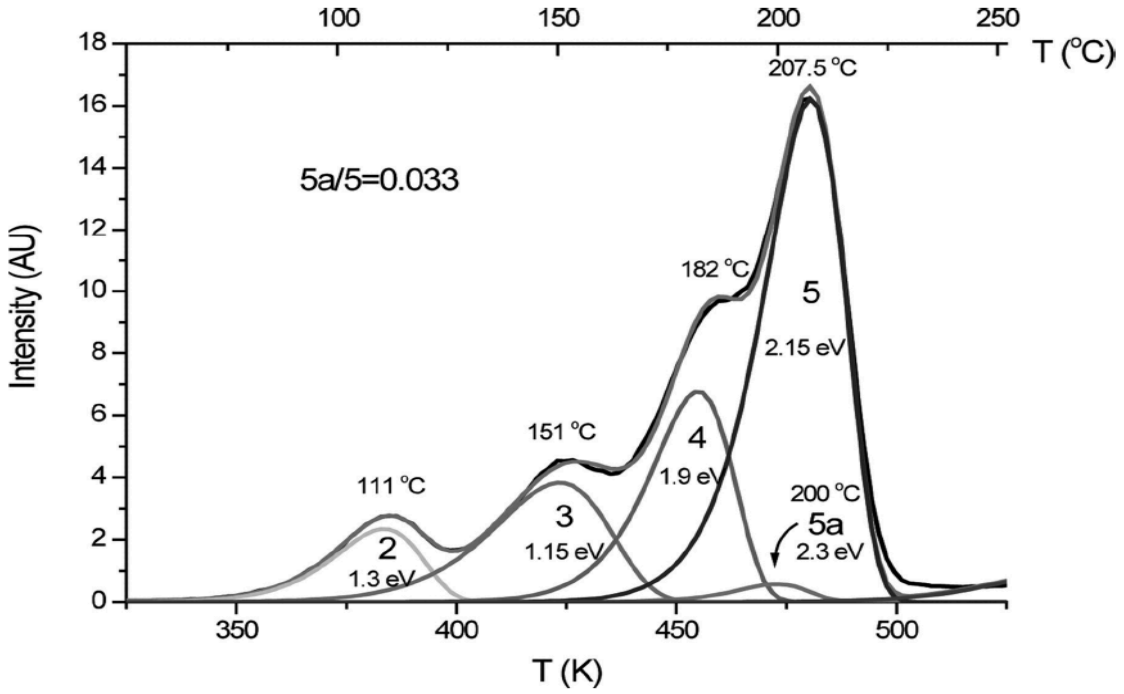

Figure 2-11 Example of glow curve (Glow curve of LiF:Mg,Ti (TLD-100) [9].

The TL medium is initially excited by interaction with radiation, subsequently being exposed to heat to obtain the TL readout. In this, the traps of various energy depths are emptied as the temperature is ramped up, the relative amplitudes of the peaks indicating approximately the relative population of trapped electrons in several trap species, provided the heating-rate (the so-called ramp-rate) is constant throughout the obtaining of the glow curve. In a TL-material the defects or artificial impurities give rise to electron traps at different trapping levels, each trapping level in a TL medium producing a related glow peak maximum that might/might not be determined during readout. Therefore, the shape of glow curve (height and area of glow peak) depends on the type and amount of impurities (the lattice defects), also upon the thermal history and treatment of the dosimeter.

Moreover, there are certain parameters that influence the shape of glow curve, for instance Linear Energy Transfer (LET) of the radiation detected and the amount of radiation deposited, the annealing process, and pre irradiation to high doses. The emission spectrum is the spectral energy distribution of the TL light that is emitted and forms the main peaks. The relative amplitude of the peaks illustrates approximately the relative population of the electrons among the range of traps. The height of the peak, along with the area under the glow curve, can be used as a measure of the absorbed dose in the TL medium. When the peak height is used to measure the absorbed dose, the heating cycle must be sufficiently reproducible to avoid causing peak height fluctuations [10].

2.2.2.5 Fading and Stability

The number of electrons trapped in different trapping levels corresponds to the dose measured by the TL material. The inadvertent loss of TL signal occurs both during irradiation and between irradiation and readout is known as fading, depending in large part upon the depth of traps and the storage temperature. Therefore, it becomes necessary to assess the stability of a dosimeter within the environment in which the dosimeter is operated. The fading can be affected by heat (thermal fading) or light (optical fading). Thermal fading occurs particularly if the trapping depth is rather small so that room temperatures can stimulate release of trapped electrons, during irradiation, between irradiation and during readout [6]. Thermal fading is most apparent within the low temperature peaks of the glow curve [8]. To minimize such effects, it is desirable for the dosimeter to be characterized by a glow-curve with a peak at around 200-250^{o}C, which is sufficiently large to avoid the fading peak but also sufficiently limited to avoid interference from the black-body signal [6]. The amount of fading can be reduced and overcome by pre-irradiation annealing, as previously mentioned. Comparably, a proportion of the traps can be emptied by optical stimulation, referred to as optical fading. In other words, exposure of a dosimeter to sunlight, fluorescent lamps or to other energetic artificial light sources can liberate trapped electrons (emptying of traps) and consequently loss of a part of the TL signal [6].

2.2.2.6 Storage and Handling

The utility of the TLD material in terms of TL sensitivity, stability, precision, re-usability, absorbed dose response and minimum detectable dose may be affected by several factors, relating to physical handling or environmental. The major environmental factors are temperature, humidity, ultraviolet and visible light whereas the physical handling factors are sieving, dispensing and cleaning effects. Therefore, storage and handling of dosimeters are of importance and should be considered during characteristic dosimeter selection.

2.2.3 Thermoluminescence Measurement

2.2.3.1 TLD System

A typical TLD reader consists of the following significant components: 1) a planchet (heater cup) for placing and heating the TLD, using a reproducible heating cycle in order to speed up the yield of phosphorescence; 2) photomultiplier tube (PMT) to detect the TL light emission and convert it into an electrical signal. The magnitude of the electrical signal is

proportional to the relative light intensity; 3) electrometer for recording the PMT signal as a charge or current [11]. Fig. 2-12 illustrates the construction of a typical TLD reader.

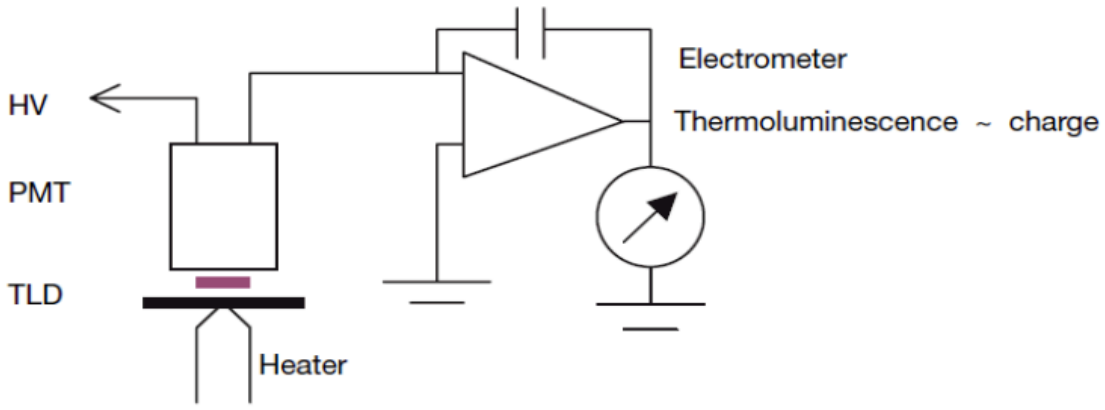

Figure 2-12 Diagram of a TLD reader [4].

A nitrogen atmosphere (N_2) is connected to the TLD reader and made to flow at a steady well-controlled rate during the read out process. The N_2 is used to suppress false light signals due to oxidation during the heating process, the O_2 acting as trapping centres [12].

2.2.3.2 The Light Measurement and Heating Systems

The reader contains a light-tight enclosure for holding the TL dosimeters during analysis. Sometimes a motorised sliding drawer instrument is used to setup the TLDs into their measurement position. With the drawer back in place following loading of the planchet, the heating element is then elevated to contact the planchet holding the detectors. Feedback from thermocouples attached to the heaters is used to control the heating profile and this ensures the reproducibility and accuracy of the heating cycle. Light emitted from the detector is filtered and collected by gain control to the photomultiplier tube (PMT) [13].

2.2.3.3 The Heating Cycle

The primary purpose of the heating cycle is to heat the phosphor until the electrons are released from the traps (readout being confined to a particular range of temperatures selected by the user, this being referred to as the readout phase), it is also used for rapidly fading away any low temperature traps (the so-called pre readout phase or preheat phase) and also to ensure complete removal of all electrons from deep traps prior to reuse (the so-called annealing phase).

The heating cycle used for readout is thus divided into these three phases: preheat, read and anneal as shown in Fig. 2-13 [13].

2.2.3.3.1 Preheat Phase

In this phase the dosimeters are exposed to a temperature that is low relative to those during the reading phase. The intention for this is to stimulate the release of the signal corresponding to the low temperature peaks, which are unstable because of their fading characteristics [13].

2.2.3.3.2 Reading Phase

The light intensity (the TL yield) is recorded in this phase attributed to glow curve. The process starts immediately after the preheat phase and the temperature is raised to a significant level and maintained for a certain time using a programmed temperature ramp rate. The light emitted during this period is integrated and provides the raw data upon which the results are based [13].

2.2.3.3.3 Anneal Phase

The anneal phase is normally intended to remove any residual signal and restores the primary intrinsic background of the detector. This process involves the exposure of the detector to a more elevated temperature than that used in the readout phase, with subsequent cooling using nitrogen gas. As a result, the sensitivity of the detector remains the same for each use [13].

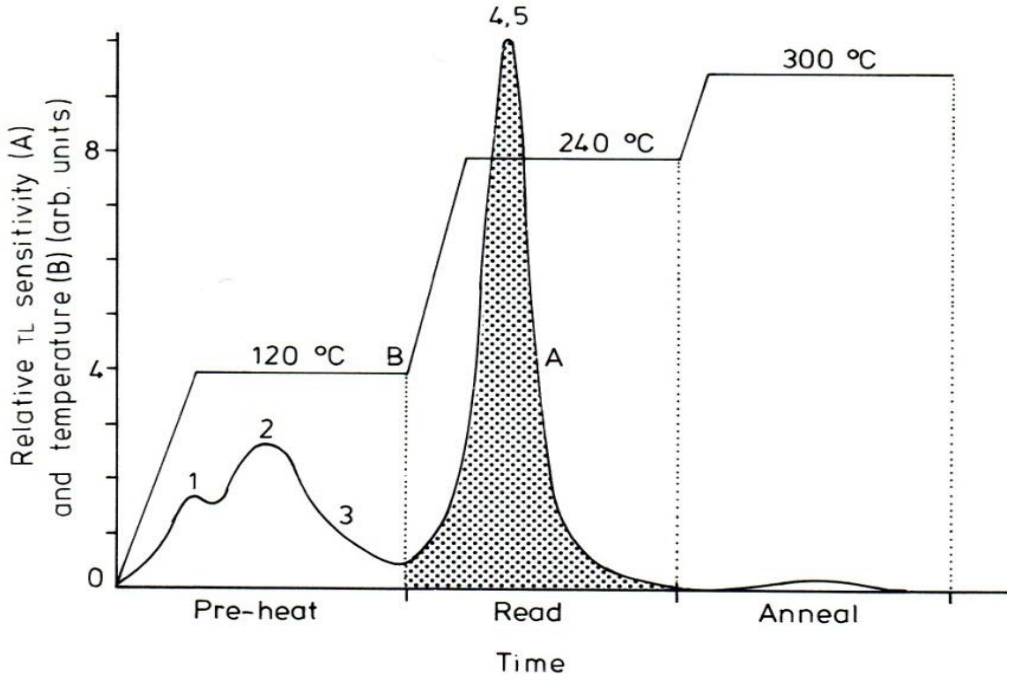

Figure 2-13 Diagram of a heating cycle and glow curve used in the reading of LiF (Mg, Ti): PTFE disc dosimeters. The preheat temperature is used to remove the rapidly fading TL represented by the low-temperature peaks. The area of TL integration is denoted by the shaded portion of the curve [7].

2.3 Amorphous Silicon Dioxide

Amorphous silica is a candidate material for many photonic systems. However, over and above their more typical applications in telecommunications they have begun to find a niche in radiation dosimetry, not least because of their high spatial resolution and relatively good sensitivity in some cases. It has long been known that radiation can modify the optical properties of such photonic material, strongly influenced by defects introduced during the manufacturing processes or produced by photon or particle radiation [14]. Understanding of the intrinsic and extrinsic defects that reside or are introduced into the silica structure and the radiation consequences for SiO_2 optical fibre has major importance in seeking to produce fibres of well-characterised behaviour.

2.3.1 Structure and Types

Silicon dioxide (SiO_2) can exist in different crystalline forms (including quartz, cristobalite, coesite, keatite, stishovite, chalcedon, agate, morganite and others) or

amorphous forms (as opal, hyalite, sintered pearl, lechateierite and natural silica glass). The crystalline forms of SiO_2 have been studied by X-ray and neutron diffraction measurements [15-17], these investigations reveal that the structural order present in crystalline forms is preserved in such glassy media over the short and intermediate length scales (at 0.5 to 2 nm). In particular, the atomic coordination and the first and second neighbour distances of silica are very similar in the amorphous and crystalline forms indicating that the basic building blocks of the two solid states of SiO_2 are similar.

The fundamental structural unit of SiO_2 is the tetrahedron, as is seen in Fig. 2-14. This SiO_2 unit cell is constituted of 4 oxygen atoms, each one located at the vertices of the regular tetrahedron. A single silicon atom is present in the inner center of the tetrahedron. The silicon atom has four hybridized sp3 orbitals; therefore it has four electrons in the outermost energy shell. An oxygen atom has two valence electrons (two electrons in the outermost shell), and then a silicon atom can take four oxygen atoms and form a stable bond [18]. This results in the SiO_2 molecule. The electron remaining from each of the oxygen, linked to the central silicon atom, can be also linked to another silicon atom and thus construct another tetrahedron. The arrangement of the links between tetrahedron units determines the classification of the silicate. If the tetrahedra exist in isolation the material is called nesosilicate, if they are linked in groups of two they are called soroslicate, if all tetrahedra are linked together into rings the material is called cyclosilicate [19].

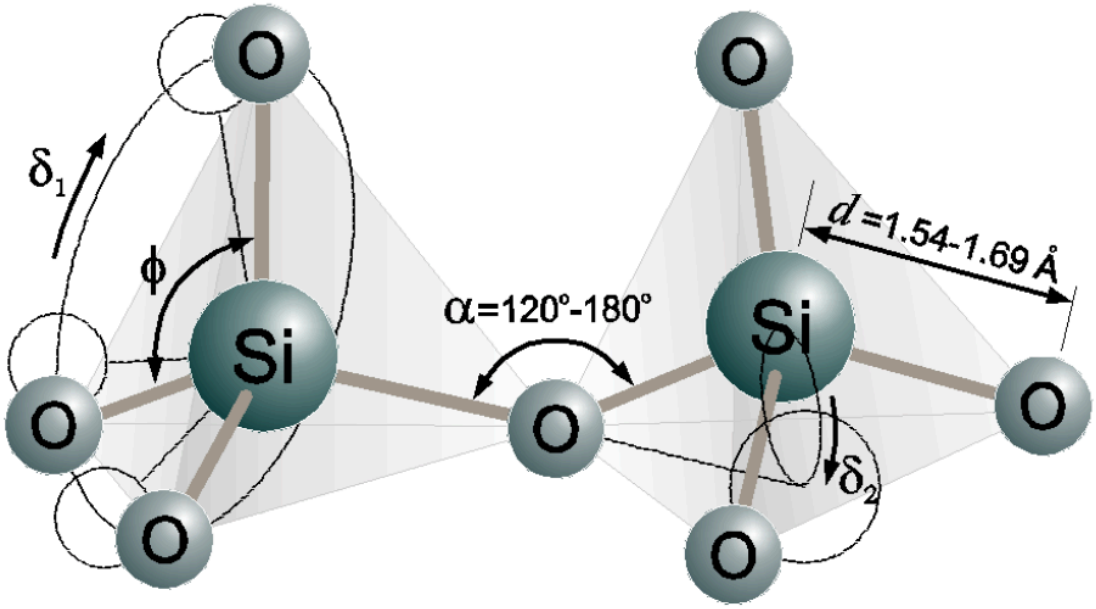

Figure 2-14 The basic structure of the SiO_2. Here d is the Si-O bond length. α is the inter-tetrahedral angle, Φ is the tetrahedral angle, and the δ 's are the bond torsion angle [20].

The Si-O bond length can vary in the range of 0.154 nm to 0.169 nm, while the angle α varies as the silica form changes. For instance, in vitreous silica α varies from 120° to 180° and for quartz it varies from 146° to 155° [20]. The different arrangements of the tetrahedral units produce the different types of silicate structure.

The amorphous silica (a-SiO_2) or vitreous silica can be divided into several types according to its method of fabrication and its OH (hydroxyl group) content. Here the amorphous silica is referred to simply as silica. The silica is divided into four types [21]

- The type I (natural dry) is molten quartz (silica obtained from ground quartz or quartz sand) with low OH content. It is obtained by melting quartz sand or quartz powder, typically by electric fusion. Aluminium is the predominant impurity in natural quartz, and it keeps its presence in the final product making type I silica high in aluminium impurities.
- Type II (natural wet) silica is molten quartz with high content of OH. It is obtained by melting quartz powder. This powder is melted in a H_2/O_2 flame giving rise to a high content of OH molecules in the resulting silica.
- Type III (synthetic wet) is synthetic silica produced by the oxidation and hydrolysis of the $SiCl_4$ in a H_2/O_2 flame. In the process of production this silica is able to absorb great quantities of water from the atmosphere. As a consequence, type III silica has a high content of OH group, even greater than that in type II. Also it has a considerable content of chlorine due to the initial reactants.
- Type IV (synthetic dry) is silica obtained from the oxidation of $SiCl_4$. The difference of this silica type with respect to the type III (synthetic wet) is that a chlorination treatment is applied at high temperatures, reducing the content of OH [22].

2.3.2 Main Optical Defects

Dislocations and intrinsic point defects reside in the silica structure, displacing lattice atoms and with a greater likelihood of existing near to impurities. The defects provide the link to the thermoluminescence that can be observed in undoped silica glass. The presence of mixed ionic and covalent natural bonds in silica cause the appearance of two mechanisms for radiation damage; breaking of covalent bonds and vacancy and interstitials creation. The majority of the defects caused by ionisation radiation occur at impurities. Thus, electrons and holes released by radiation can be trapped, to give rise to optical absorption and luminescence [6].

The defects occurring in amorphous silica are to be contrasted with those in the crystalline material, in which any disruption in the repeated structure can be considered a defect. Since amorphous silica does not possess long-range order, defects in silica are the disruption in the short to mid-range order existing in such media. The defect modes can be divided into two major categories, according to whether one is dealing with intrinsic or extrinsic defects. These will be discussed below.

2.3.2.1 E' Center or Silicon Dangling Bond Centre

The generic E' centre comprises an unpaired electron in a dangling tetrahedral (sp3 hybridized) orbital of the silicon atom which is bonded to three oxygens in the silica network, ≡Si•. The lines represent the three oxygen bonds to the silicon atom and the dot denotes an unpaired electron. This centre is known to be paramagnetic and therefore is detectable using the EPR (electron paramagnetic resonance) signal [23]. The second neighbour environment of the bulk types of E' centres continue to remain a source of discussion. What is apparent is that it is associated with an absorption band at 5.85 eV in quartz and silica glass.

There are four main types of the E' centre defects in vitreous silica, labelled with their corresponding spectroscopic notation as E'α, E'β, E'γ, E'δ. One of the mechanisms that may produce the E'α defect is the rupture of the strained bond (=Si-O-Si=) producing the E'α plus one Non Bridging Oxygen Hole Centre (NBOHC) defect (Fig. 2-15). The absorption of a hydrogen atom by an unrelaxed oxygen vacancy configuration may lead to the formation of an E'β. The rupture of an unrelaxed oxygen vacancy configuration can also lead to the E'γ defect. The electron paramagnetic resonance (EPR) signal of the E`γ (the most abundant type) is related to a strong absortion at 5.8 eV. The dangling Si bond on surfaces has an absorption band at 6.2 eV. If one of the neighbouring O in the silica molecule is substituted by one H an optical band appears at 4.9 eV [24].

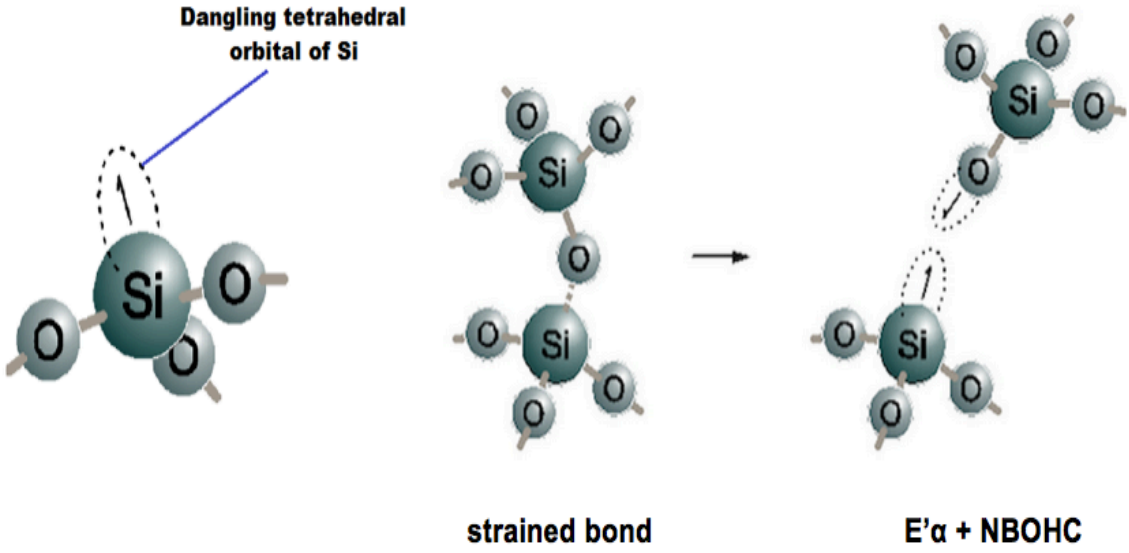

Figure 2-15 The E' center and a creation process of E'α [18].

2.3.2.2 Oxygen Deficient Centres (ODC)

There are two types of ODC. ODC (I) is a simple oxygen vacancy. It is also known as the oxygen deficient vacancy, denoted as ≡Si-Si≡, where the single – represents the two bonded electrons in a chemical reaction (Fig. 2-16 (left)). It is the only optical absorption band that is observed on both silica glass and in alpha quartz (the silica crystal type). The absorption band attributed to ODC (I) is at 7.6 eV. ODC (I) can also be transformed into ≡Si-H through a thermal reaction with hydrogen. This defect is a precursor of the E' centres [25]. The origin of ODC (II) is still a matter of controversy. Two dangling bonds in Si can react forming a Si-Si bond or creating a divalent Si atom =Si•• (ODC (II)) (Fig. 2-16 (right)). These processes occur in the bulk of the silica. Its main difference with respect to the ODC (I) is the unrelaxed state of the oxygen vacancy. The absorption band associated to ODC (II) is about 5 eV. Two photoluminescence bands at 4.4 eV (singlet state to singlet state transition) and 2.7 eV (triplet state to singlet state transition) are related to the excitation of the bands 5 eV and 7.6 eV, evidencing the interaction of the ODC (I) and ODC (II). Both ODC's are diamagnetic defects (nonparamagnetic), which means that they are not detectable by electron paramagnetic resonance (EPR) techniques [26].

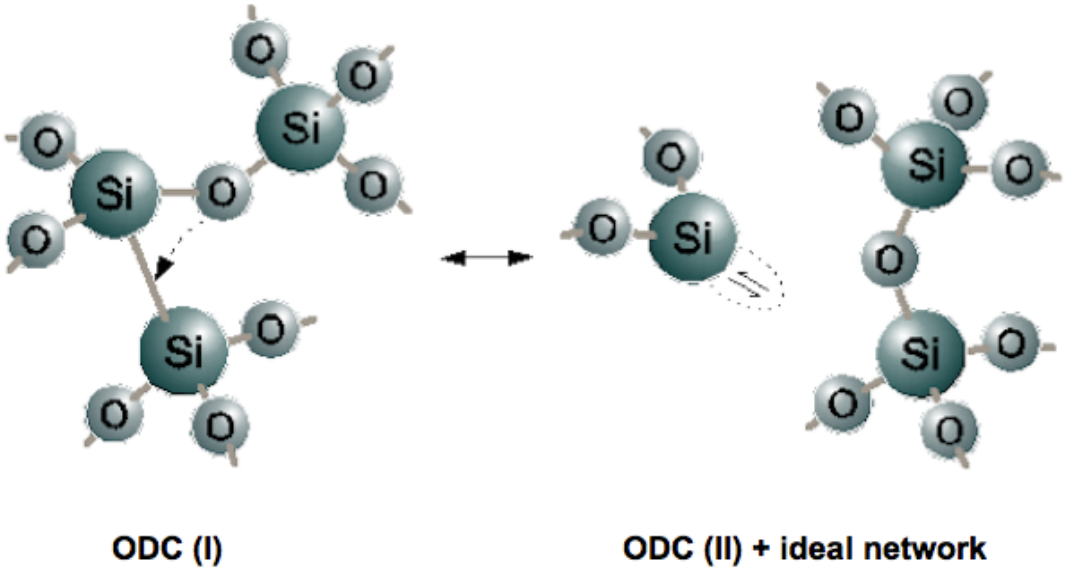

Figure 2-16 ODC (II) from ODC (I) [20].

2.3.2.3 The Non Bridging Oxygen Hole Centre (NBOHC)

The NBOHC is an oxygen dangling bond defect (=Si- O•), a paramagnetic defect absent in alpha quartz, the latter being devoid of amorphous regions. It can be characterized by EPR and optical absorption (OA). It has an absorption band at 4.8 eV with a Full-Width at Half-Maximum (FWHM) of 1.07 eV. It also has a weaker asymmetric absorption band at 1.97 eV, FWHM 0.17 eV. Further, a photoluminescence band at 1.91 eV appears with the excitation of its main absorption bands. This luminescence is centred at the red end of the visible spectra wavelength. There is a third absorption band at 6.8 eV, confirmed by finding an excitation band at 6.4 eV for the 1.9 eV photoluminescence band of NBHOC [24].

As depicted in Fig 2-17, NBHOCs are created when hydrogen atoms are liberated radiolytically (disassociated by atomic radiation) from a hydroxyl radical OH in high OH group silica (wet silica), that is, they are created by the rupture of silanol groups (=Si-O-H). Although the NBOHC can also be created in low OH group silica (dry silica) by the rupture of the strained Si-O bond.

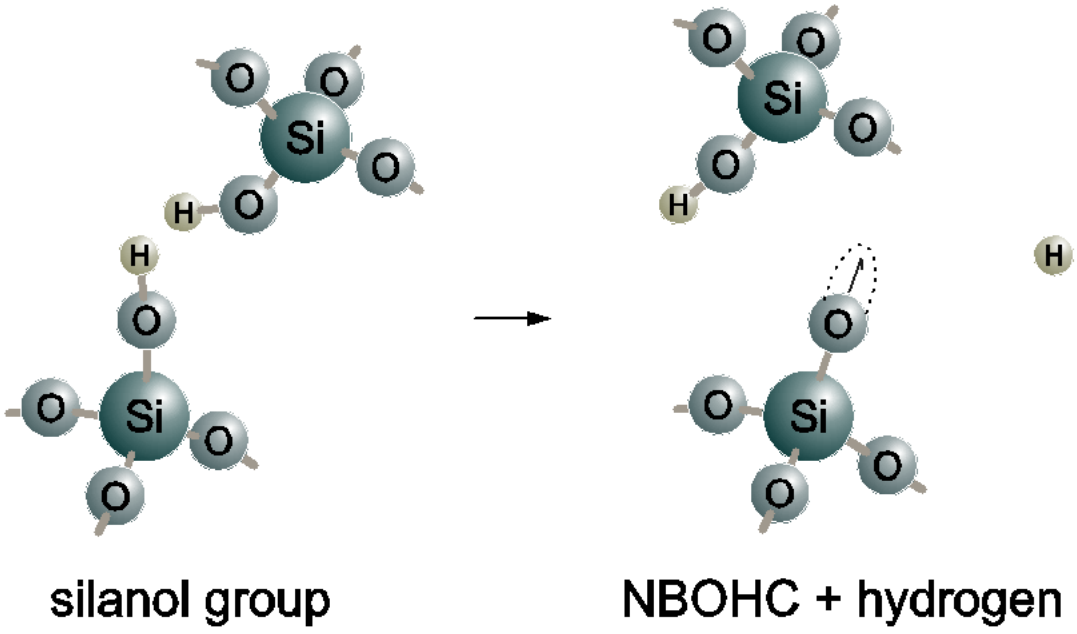

Figure 2-17 One way of creating NBOHC [22]. The NBOHC arises when hydrogen atoms are liberated radiolytically from one member of a pair of OH groups in wet silica (high OH group) [27].

2.3.2.4 The Self-Trapped Exciton (STE)

When an electron is excited in a lattice it will leave a hole in the valence band. This electron will experience a coulombic interaction with the hole, screened by ions and other electrons. This electron-hole pair, termed an exciton, can propagate through the crystal. The STE is defect related to the excitation energy in electron and hole interactions. Self-trapping occurs in an otherwise ideal structure when the excited electron and hole spontaneously create a localized distortion in the lattice, which lowers their total energy and thus localizes and traps them at the distortion [28]. The luminescence band in the range of 2 to 3 eV is considered to belong to the STE. The characteristic blue light in amorphous SiO_2 is attributed to the STE. The decay of a STE associated to an excited Si-O bond can create an oxygen vacancy and peroxy bridge (Fig. 2-18). Also, creating STEs in silica leads directly to the formation of two other important defects, the E' centre and the NBOHC [28], both of which have been discussed above.

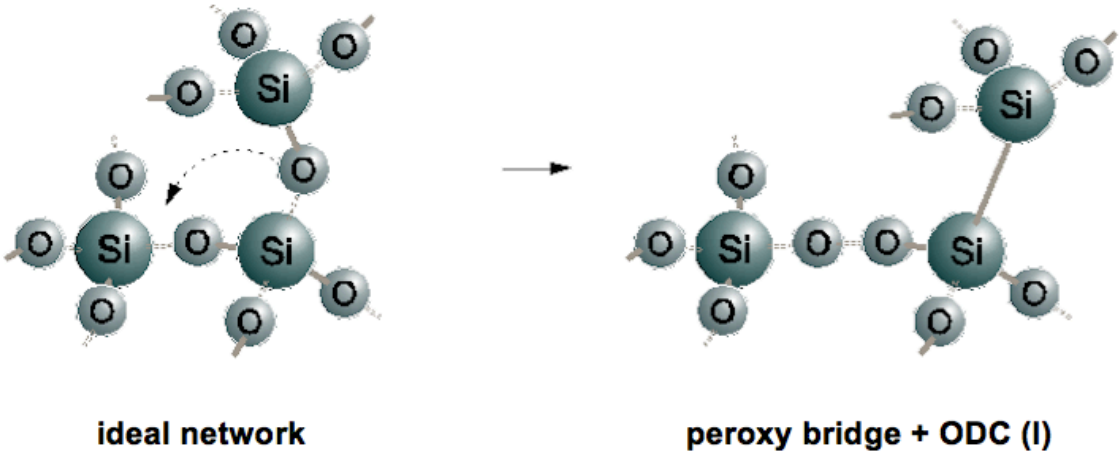

Figure 2-18 Decay of STE due to an excited Si-O bond creating a peroxy bridge and an oxygen vacancy [20].

2.3.2.5 Germanium Impurity

Analysis of luminescence when impurities are added into the SiO_2 substrate involves a model in which the impurity centre becomes either substitutional atoms, interstitial atoms, an impurity-intrinsic complex, or an impurity-impurity complex inside the substrate. Apart from the possibility of introducing a new luminescence band (causing localized energy levels within the forbidden energy gap), impurity atoms might also change the number of electron or hole traps. The presence of the extrinsic defects (impurities) lead to a large increase in the sensitivity of thermoluminescence [6].

Germanium (Ge) is in the same chemical group as silicon, and in nature an amorphous Ge dioxide (a-GeO_2 or germania) having a tetrahedron (a Ge atom at the centre and four oxygen atoms at the vertices) may be arranged within a-SiO_2 in many different configurations, each of which constitutes a specific point defect. It is qualitatively expected that many Ge-related point defects are structurally indistinguishable to Si-related centres since Ge and Si are isoelectronic elements, apart from the substitution of Si with Ge [29]. In [30], in comparing between a Ge-doped silica glass and a pure silica glass, it has been shown that defects related to germanium are predominantly intrinsic. With UV absorption, luminescence is from two to three orders of magnitude more intense in germanosilicate glasses, even before irradiation exposure compared to that of pure silica [31].

Previous research has demonstrated that the photosensitivity of Ge-doped silica,

reflected in the variation observed in the UV optical absorption (OA) spectra, is associated with the Ge-lone pair centre (GLPC) [32-34]. The GLPC is considered to be a marker of the oxygen deficiency in the materials (lack of oxygen atoms in the glass network), denoted in the form of =Ge••, where = represents the two bonds formed with two O atoms and •• is the electron lone pair). This defect is characterised by the presence of an OA band peak at 5.1 eV related to the optical transition $S_0 \longrightarrow S_1$ [31], resulting from the ground state to the first excited singlet state. Furthermore, the GLPC defect is also characterized by two photoluminescence (PL) bands at 4.2 and 3.1 eV, related to the transitions from the excited electronic states of singlet (S_1) and triplet (T_1), respectively, to the ground state (S_0) [29, 35]. The energetic level scheme in Fig. 2-19 consists of a ground singlet S_0 and the excited S_1 and T_1 states, associated with GLPCs. The radiative decay channels from S_1 and T_1 are described by the rates KS and KT respectively, while the ISC process linking S_1 and T_1 is characterized by $KISC_b$. Experimental data in the literature on the defect spatial distribution in fibres exists mainly for elements of intrinsic nature [36, 37].

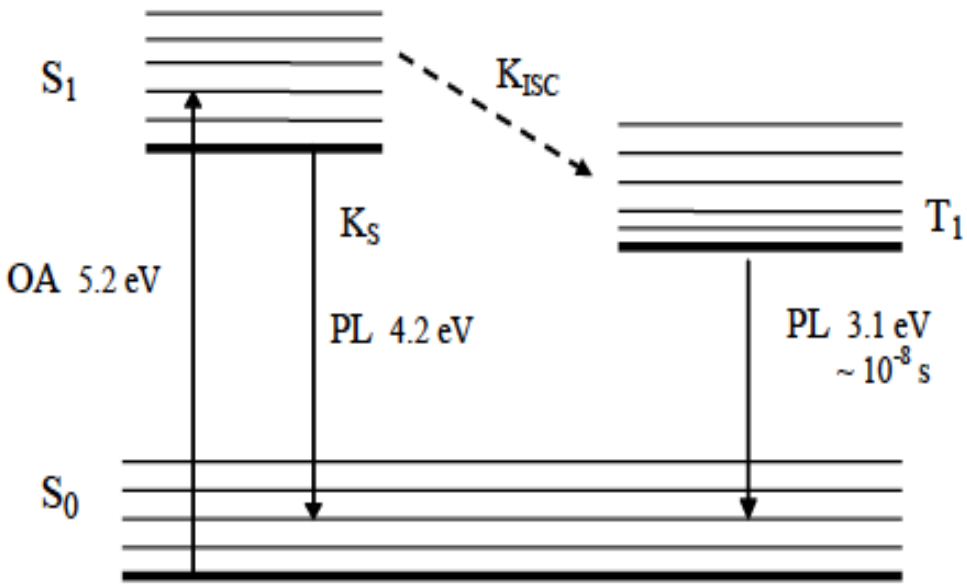

Figure 2-19 Schematic representation of GLPC diamagnetic defect. The solid arrows indicate the radiative transition in absorption and luminescence. The dashed arrows indicate the Inter System Crossing (ISC) non-radiative transition.

The most common Ge-related paramagnetic defects that are detected by electron paramagnetic resonance (EPR) in irradiated Ge-doped a-SiO_2 are the GeE_0 centre and the Germanium Electron Centres (GECs) Ge(1) and Ge(2) (Fig. 2-20).

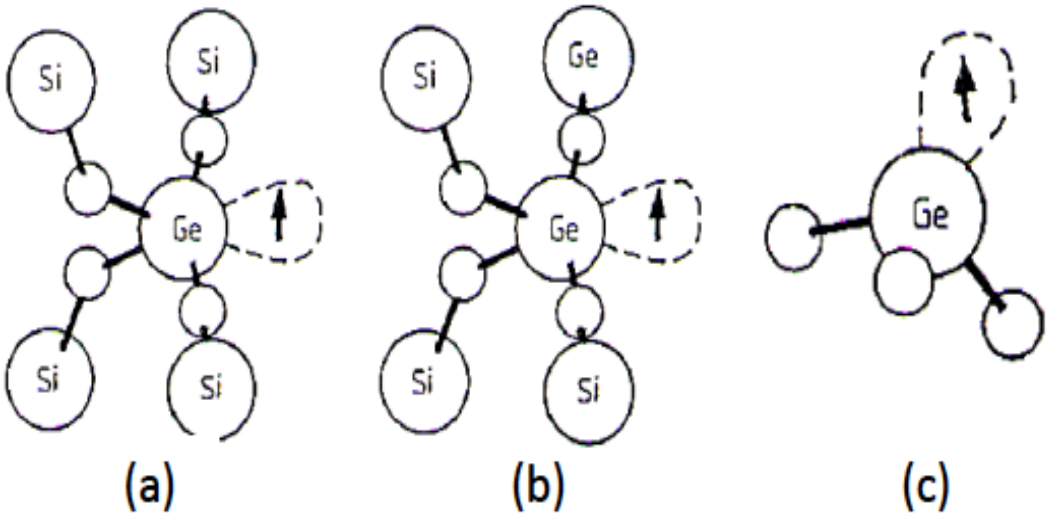

Figure 2-20 Microscopic structures proposed by Neustrev [38] as models for (a): Ge(1), (b): Ge(2) and (c): GeE' defects.

The microscopic structure of GeE_0, which is observed also in pure GeO_2, is structurally identical to the E_0 centre apart from substitution of Si with Ge (≡Ge•) [32, 38, 39] (Fig. 2-20 (c)). This centre was associated with an absorption band at 6.2 eV- 6.4 eV [37, 40]. The Ge(1) consists of an electron trapped at the site of a substitutional 4-fold coordinated Ge precursor ($GeO•_4$) [30, 41] (Fig. 2-20 (a)). An absorption band at 4.4 eV- 4.6 eV has been attributed to this centre [30, 42, 43]. Finally the structure of the defect responsible for the latter EPR signal, the Ge(2) centre, is still being debated. Indeed, its structural model was first ascribed to a trapped electron centre at the site of a GeO_4 unit, such as the Ge(1), on the basis of the similarities of their ^{73}Ge hyperfine coupling constants, differing from Ge(1) for the number of Ge nearest neighbour ions [44]. According to this attribution, an absorption band at 5.8 eV was assigned to the Ge(2) centre [33, 42]. However, subsequent studies, based on the defect annihilation, suggested an alternative model for Ge(2): an ionized twofold coordinated Ge (=Ge••) [29, 44]. Even the circumstance that the paramagnetic centre's electronic structure (g value) of Ge(2) is smaller than 2.0023 does not permit its conclusive assignment to a trapped electron centre because this line of reasoning is only rigorously valid for very simple paramagnetic centres, and generally cannot be extended to point defects in silica [46]. The EPR signals related to GeE_0 and GECs centres are presented in Fig. 2-21.

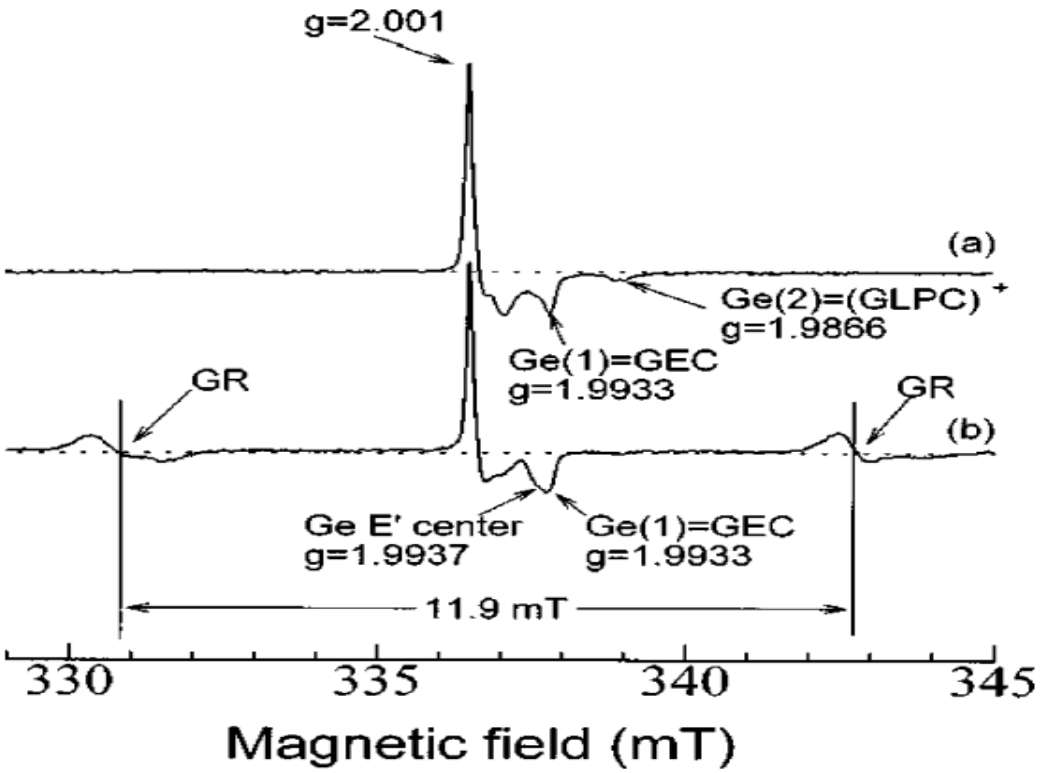

Figure 2-21 EPR signature of the GeE_0, Ge(1) and Ge(2) paramagnetic defects in germanosilicate irradiated silica: (a) irradiated at 77 K; (b) irra- diated at 77 K followed by annealing at 298 K for 5 min [42].

2.4 Ge-doped Silica Optical Fibre Dosimetry

The germanium in the silica matrix, in the form of GeO_2, causes an increase in the refractive index of the glass. This property is often used for the creation of the optical fibre core and Ge was the first and now the most traditional dopant used in fibre telecommunications. The presence of the Ge does not affect the fibre losses, but it can produce the appearance of new energy levels within the silica band gap, leading to a detrimental loss of transmitted signal strength in the fibres.

The major challenge of dosimetry in radiotherapy and in other areas of radiation medicine (a major application interest area for the work herein) is finding a tissue equivalent dosimeter having a well-behaved characterised response across a radiation field associated with a high gradient of radiation dose. Moreover, it is desirable that the dosimeter of choice should be able to measure dose in very small volumes, dose being a point quantity [4].

2.4.1 Development of Ge-doped Silica Optical Fibre Dosimetry in Radiation Therapy Applications

Commercially available Ge-doped SiO_2 telecommunication fibres have been investigated in recent years as a 1-D thermoluminescence (TL) system for high spatial resolution dosimetry within relatively small diameters (~several tens of μm) for therapeutic applications [47-51]. In several dosimetry studies, the main purpose has been to obtain a full performance characterisation of this candidate TL material for radiation therapy dosimetry applications including interface radiation applications [47, 48], brachytherapy dosimetry [49], Intensity-Modulated Radiotherapy (IMRT) verification [50, 51], external beam radiotherapy dosimetry audits by mailed dosimeters [48] and UV radiation dosimetry. To date, the response of these fibres has been tested for UV sources, superficial X-ray beam therapy facilities, a synchrotron microbeam facility, electron linear accelerators, protons, neutrons and alpha particles, covering the energy range from a few eV to several MeV and more. Dosimetric characteristics include, reproducibility, fading, dose response, reciprocity between TL yield and dose rate and energy dependence. The fibres produce a flat response to fixed photon and electron doses to within better than 3% of the mean TL distribution [47, 48, 53, 54]. Irradiated Ge-doped SiO_2 optical fibres show limited signal fading, with an average loss of TL signal of ~0.4% per day. In terms of dose response, Ge-doped SiO_2 optical fibres have been shown to provide linearity to X-ray and electron doses, from a fraction of 1 Gy up to 2 kGy. The dosimeters have also been used in measuring photoelectron generation from iodinated contrast media, the TL yields being some 60% greater in the presence of iodine than in its absence; further work has also been undertaken on thin (a few μm to ~ 100 μm) gold coatings to the fibres [55] showing somewhat greater dose enhancement. The observed presence of useful TL emission at the radiation levels familiar in radiotherapy procedures has provided stimulus in seeking to fully understand the various influencing factors. Primarily this is based on the presence of dopant in the material [56], contributing markedly to the structural defects in the SiO_2 fibres, producing trapping processes for electrons and holes in this amorphous medium.

From the beginning of such studies, it was clear that the application of commercially available Ge-doped telecommunication fibres for medical therapies demonstrated favourable TL characteristics. It was subsequently envisaged that these same favourable characteristics could be harnessed towards development of TLDs that were more sensitive than those available from either commercially available fibres or indeed phosphor-based TL media, based on production of non-commercially available fibres. Recently, as part of a consortium based in Malaysia, three forms of Ge-doped optical fibres, capillary fibre, flat fibre (FF) and photonic crystal fibre (PCF), have been fabricated and tested for sensitivity towards ionizing radiation dose detection in the

energy response several eV to MeV. Abdul Sani et al., [57] has found that the sensitivity of the undoped flat fibre to be markedly greater (by a factor of 100) than that of the commercial Ge-doped cylindrical fibre, being comparable to that of commercially available TLD-100. The findings of that study have paved the way for designing and fabricating high sensitivity optical fibre based dosimeter sensors. By collapsing the doped capillary fibre wall so that the internal surfaces fuse, the arrangement forming a flat fibre, it has been shown that that its TL response increases by approximately 6 times over that of the doped capillary-fibre [58]. The study results are suggestive of defect generation occurring as a result of the collapsing technique in producing the flat fibres, providing a TL response from the optical fibres that can improve upon existing TL system sensitivities. The PCF is fabricated by stacking an array of capillaries inside a glass tube. In this particular instance, the PCF was formed from 168 stacked capillaries, the TL response of the PCF being some 17.5 times that of a single capillary optical fibre. These results suggest that by collapsing capillary fibres until their outer surfaces fuse, strained surface defects are generated, the dose detection sensitivity of the product fibre increasing in a commensurate fashion [58].

2.4.2 Fibres Fabrication

Optical fibre is typically fabricated initially from a carefully prepared preform of doped silica, comprising two essential components, the doped silica core and the outer silica cladding, such that for telecommunication purposes a difference in refractive index is produced between the core and the cladding (Fig 2-22) when the fibre is drawn. This refractive index profile is controlled and manipulated through the addition of dopant to the basic SiO_2 glass. The research of this investigation in this thesis focuses on the Ge-doped cylindrical fibres (CF), flat fibres (FF) and photonic crystal fibres (PCFs). These fibres have been investigated herein in characterising the diffusion of dopant and the presence of other defects as well as the thermoluminescence yield in regard to radiation dosimetry.

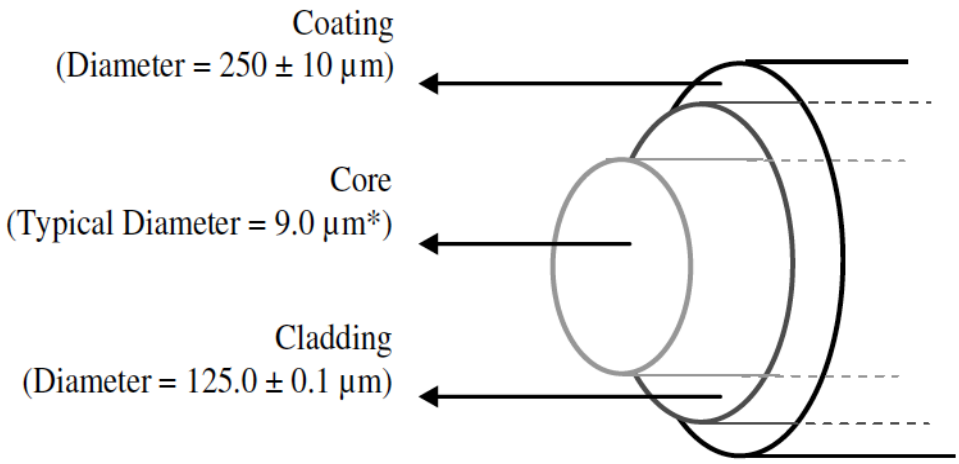

Figure 2-22 Basic structure of typical geometry of commercial silica optical fibre (* from information sheet provided by manufacturer), the core and cladding having differing refractive indices, n, sufficient to provide for the total internal reflection required for communication purposes.

The fibres, produced by a University of Malaya lead collaboration, were doped using the Modified Chemical Vapour Deposition (MCVD) method, with precursor $SiCl_4$, $GeCl_4$ and oxygen (O_2) being made to flow into a rotating high purity silica tube (Suprasil F300). The vapour mixture is subsequently oxidized using a high temperature H_2/O_2 burner/furnace operating in the temperature range 1300-2100°C, and moved forwards and backwards in a number of passes depending on the target dopant concentration value. As the vapour mixture approaches the hot zone, the vapour is turned into a white soot-like powder, to be distributed along the substrate tube by the thermophoretic process, yielding a temperature-dependent particle-size deposition profile. Subsequent to soot deposition, the tube temperature is increased to 1800-2100°C in order to sinter the soot particles, the powder being considered to be fully sintered when the material is judged by eye to be sufficiently transparent [59]. Equation (2-7) and (2-8) represent the chemistry of $SiCl_4$ and $GeCl_4$ oxidation:

$$SiCl_4 + O_2 \leftrightarrow SiO_2 + 2Cl_2 \quad \textbf{(2-7)}$$

$$GeCl_4 + O_2 \leftrightarrow GeO_2 + 2Cl_2 \quad \textbf{(2-8)}$$

It is clear from Equation (2-6) and (2-7), $SiCl_4$ is completely oxidized during the MCVD process [59]. On the other hand, $GeCl_4$ oxidation and incorporation is heavily affected by the unfavorable thermodynamic equilibrium (Equation 2-7). Under the appropriate condition, the addition of Cl_2 (in Equation 2-6) will shift the equilibrium further to the left. Incorporation of

GeO_2 in deposited silica is also affected at higher temperature (especially during the sintering, collapsing and sealing) with evaporation of GeO_2 itself as represented in Equation 2-9 [60].

$$GeO_2 \quad \leftrightarrow \quad GeO + \frac{1}{2}O_2 \qquad \textbf{(2-9)}$$

The optical fibers were pulled using a conventional drawing tower with a furnace hot zone of 3.4 cm. The temperature of the furnace was initially set at 2100 °C for the fiber drop to occur. The final Ge-doped preform with 15.14 mm outer diameter and 2.10 mm core diameter contains 8.49 ± 0.07 wt% and 10.02 ± 0.07 wt% Ge (measured by the Electron Dispersive X-ray (EDX) techique) in the preform core area. Samples of this preform, cut to a length of 1.5 to 2 mm are then prepared, the surface being polished and cleaned in order to avoid interference during optical measurements.

One part of the preform is collapsed during the MCVD process for the purpose of fabricating conventional optical fibre, and the other part is left hollow as shown in Fig. 2-23(a)(b) and 2-23c, respectively. The preform is then pulled into conventional optical fibre (hereafter referred to as cylindrical fibre) with 125 μm diameter using the collapsed part (Fig. 2-23b and Fig. 2-24a). The hollow part of the preform is used to fabricate the capillary optical fibre with 125 μm outer diameter and flat fibre with cross section of 60 μm × 180 μm as shown in Fig. 2-23c, 2-24b and 2-23d, 2-24c respectively at a temperature of 2000 ± 10 °C and drawing speed of 1-2 m/min. The flat fibre (FF) used herein was fabricated using a conventional 5 m high fibre drawing tower (Fig. 2-25), the latter being located at the Flat Fibre Laboratory, Department of Electrical Engineering, University of Malaya. Unlike the more conventional case of a cylindrical fibre (CF) formed from a preform doped silica solid rod, the doped FF preform is a hollow amorphous SiO_2 tube with the internal faces containing the deposited dopant. In this work, to produce the FF, the preform is a commercially available uncollapsed silica tube [61]. The application of a vacuum leads to a quasi-complete collapse of the preform into a flattened shape, with additional TL yield resulting from the stresses produced at the inner contacting faces of the flattened fibre during the cooling process [14]. For obtaining the FF shape, a low vacuum pressure was applied from the top of the preform. The capillaries and FFs were pulled with a drawing speed of 1-1.5 m/min and a temperature of 1990 ± 5 °C. It should be noted that the capillary fibre in this study is fabricated from the boundary between the collapsed and uncollapsed region of the preform, which leads to a smaller hole-to-outer diameter ratio in the capillary compared to the uncollapsed part of the preform.

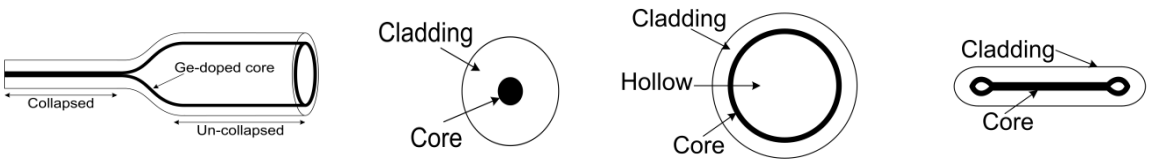

(a) (b) (c) (d)

Figure 2-23 (a) Original Ge-doped preform, (b) Cylindrical fibre, (c) Capillary fibre, and (d) Flat fibre.

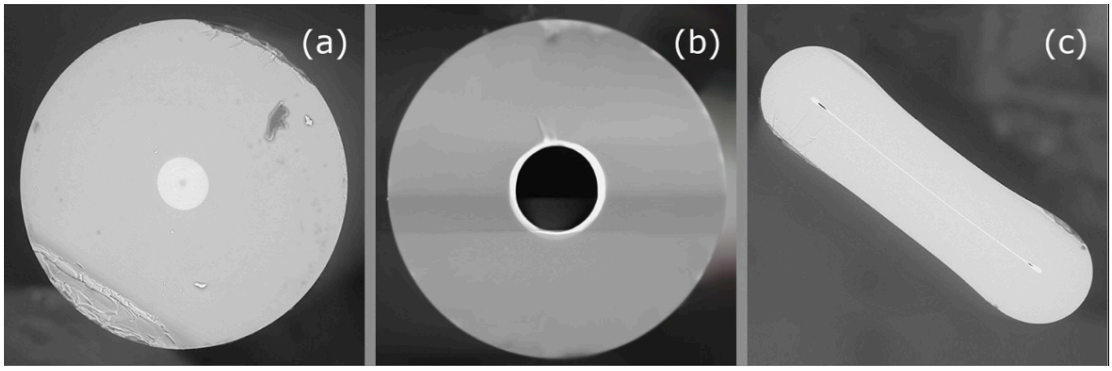

Figure 2-24 From left to right are not-to-scale schematic representations of Scanning Electron Microscope (SEM) images from the cross-section of the common form of; (a) doped single mode telecommunication fibre, 9b) the capillary fibre, and (c) the flattened capillary fibre (flat fibre).

Figure 2-25 Fibre pulling tower located at the University of Malaya, Malaysia. Shown is the heated perform, ready to be pulled by addition of tension (a weight of some few tens of grams).

In this study, the Photonic Crystal Fibres (PCFs) are also fabricated at the University of Malaya using the stack-and-draw method. A Ge-doped silica tube preform made with the aid of the MCVD process fabricated with the same doping concentration and MCVD process parameters as the preform shown in Fig. 2-26 (a) is used here for fabricating the PCF. The Ge-doped tube preform is drawn into capillaries, to obtain a diameter of a few millimeters (1.26 mm diameter is used in this study a for seven-ring PCF). Prior to stacking, the capillaries undergo preparation processes such as cutting to a shorter length of 30 - 40 cm, fusing one end, and cleaning [62]. The capillaries are then stacked into a Suprasil F300 silica tube with outer and inner diameters of 25 and 19 mm, respectively. The central capillary is exchanged with a similar size of solid rod to form a solid-core-PCF. After fixing the capillaries in the tube, the PCF preform is drawn into PCF cane of 1.5-2 mm diameter. A mild vacuum pressure is applied during the PCF cane fabrication to close all interstice holes between capillaries. The PCF cane is then pulled into the standard fibre size of ~125 μm at 1980 °C with solid core diameter of 8.27 μm as shown in Fig. 2-26 (b), hereafter referred to as uncollapsed PCF. A new type of PCF, herein called a collapsed PCF (see Fig. 2-26 (c)), is also fabricated in this study with almost the same core and cladding diameter as the uncollapsed PCF (~125 μm ± 2.0). A PCF cane fabricated from the same PCF preform is used to draw the collapsed PCF at a slightly higher furnace temperature (by 10 °C) by applying a vacuum pressure from the top of the PCF cane to make sure all the capillary holes are fully collapsed.

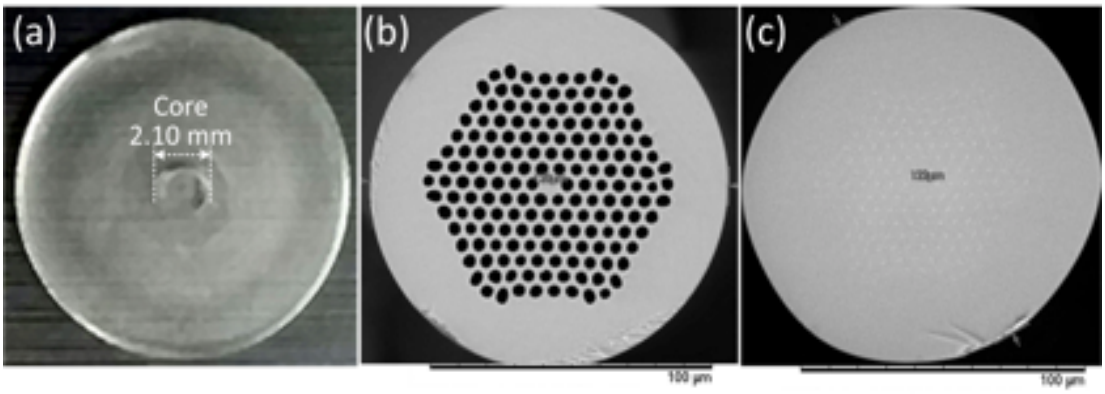

Figure 2-26 (a) Polished surface Ge-doped silica preform. (b) and (c) Scanning Electron Microscope (SEM) images from the cross-section of Ge-doped-cladding uncollapsed PCF and collapsed PCF, respectively.

Both types of optical fibres have been fabricated with similar drawing tension ranges of 20 to 25 g, the one difference being in the case of collapsed PCF that an additional vacuum

pressure was applied. The small tolerance in optical fibre drawing tension is expected to have negligible effect on radiation characteristics of optical fibre. As an example, Girard et al., [63] have shown that fibre drawing tension ranges from 22 to 70 g has no effect or negligible effect on radiation induced attenuation (RIA) over an observed ~500-1600 nm wavelength for a Ge-doped core optical fibre. Alessi et al., [64] have shown the lack of tension variation effect of drawing condition on the fibre radiation response by comparing the RIA of two fluorine-doped optical fibres over ~200-500 nm fabricated with 30 and 140 g tension, with the samples exposed to 400 kGy. In another study, Alessi et al., [65] demonstrated the insignificance of drawing condition variations on structural and radiation sensitivity of an optical fibre fabricated with different tensions from 35 to 80 g, and evaluated these with different measurements (Raman spectroscopy, electron paramagnetic resonance and RIA).

The application of microstructured optical fibres (MOFs) e.g. photonic crystal fibres (PCFs) to TL dosimetry has further improved the sensitivity to radiation dose [66]. Moreover, PCFs have also been used in radiation dose measurements in the form of optically stimulated luminescence (OSL) detection mode, modelling also being undertaken [67, 68]. The enhanced dose detection sensitivity of PCFs could be due to the fusing of the outer wall surface of the stacked capillaries since such high TL response values have also been observed in single capillaries after collapsing the internal bore to form a flat fibre shape; the TL has been observed to be enhanced compared to that before collapse [58]. In addition, a more significant improvement in TL response is observed in flat fibres when extrinsic impurities are added to the collapsing/fusing area, comparison being made with undoped flat fibre. This should be taken into consideration in designing a PCF that may contain hundreds of capillaries stacked in a glass tube; collapsing all capillary holes to form a collapsed-hole-PCF would then be expected to lead to even greater TL response compared to the original PCF. However, it is not clear what silica dependent parameters change during PCF and collapsed-hole-PCF fabrication to the extent that improved luminescence response is indicated.

2.5 Overview of Characterisation Methods in Investigation of Doped Optical Fibres for Radiation Dosimetry

The material characteristics of doped SiO_2 fibre are to be studied herein, the electron traps in the product medium creating a situation attractive for their application in thermoluminescence (TL) radiation dosimetry. To-date, limited research has been conducted towards gaining an essential understanding of the magnitude of TL signal and material

characteristics of doped fibres. Characterisation is being sought to ensure that the mechanism of TL yield in optical fibres is well understood, allowing a favourable well controlled production situation to be established. The intended end point is to specify dosimeters, not only for clinical dosimetry but also for their application in industrial/energy–industry settings. Investigation of the surface oxidation state of the Ge-doped SiO_2 optical preform has been carried out using the X-ray Photoelectron Spectroscopy (XPS) technique. In a further development using the fibre forming technology, Particle Induced X-ray Emission (PIXE)/Rutherford Back Scattering (RBS) measurements have been employed to ascertain dopant concentrations of Ge-doped-cladding photonic crystal fibres (PCFs) with a view to improving TL yield.

2.5.1 X-ray Photoelectron Spectroscopy (XPS)

In the case of XPS, the solid material is bombarded with low energy X-rays (ideally highly monochromatic) (generally in the range 20 - 2000 eV), while simultaneously measuring the kinetic energy of the photoelectrons that are emitted from the sample (Fig. 2-27 and 2-28). In this respect, soft X-rays (Mg-K_α and Al-K_α) are ideally suited to probe the core levels of a solid, which generally show no dispersion due to their highly localised atomic-like character [69]. The ejected electrons from the top 3 to 10 nm of the material are analysed with respect to their kinetic energy and to their direction of propagation in angular resolved photoemission. XPS detects all elements with an atomic number (Z) of 3 (lithium) and above. However, it is difficult to detect hydrogen (Z=1) or helium (Z=2) due to the binding energy of these electrons being very small compared to the excitation energy of the X-ray photon, and hence the absorption efficiency is very small.

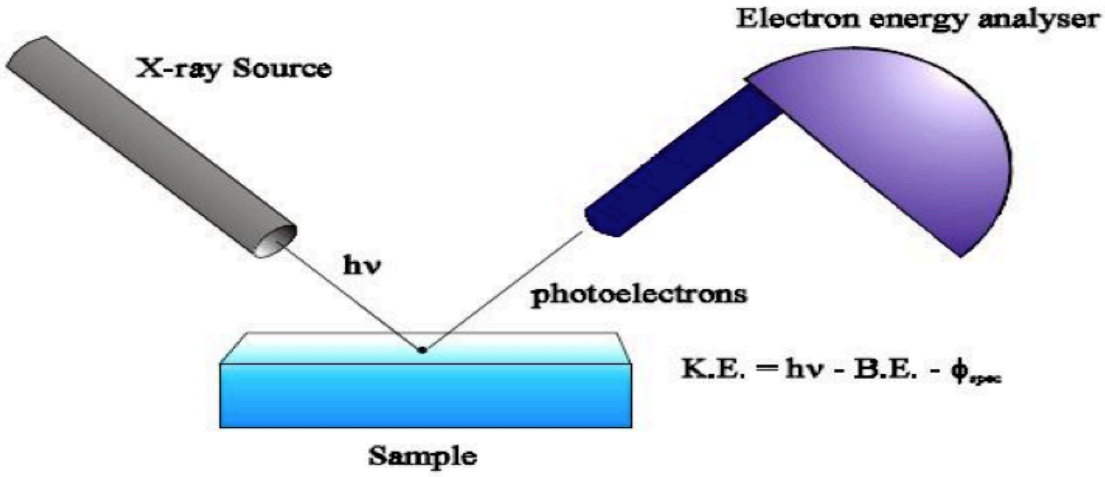

Figure 2-27 Schematic diagram of XPS system, showing photoelectric emission and binding energy equation.

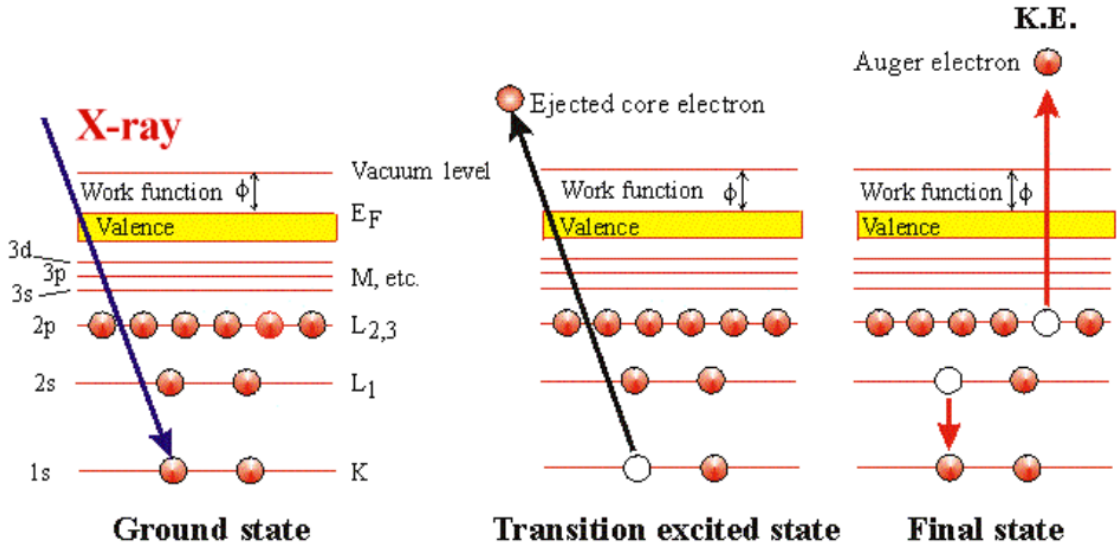

Figure 2-28 The photoelectron and auger emission.

In the photoemission event, the excitation energy must be large enough for the electrons to overcome the work function of the solid, which leaves the n-electron system in a core-ionised state. It obeys the following energy conservation rule:

$$h\nu = E_B + E_{kin} \qquad \textbf{(2-10)}$$

where $h\nu$ is the energy of the X-ray photons being used, E_B is the electron binding energy (BE) relative to the vacuum level prior to ionisation and E_{kin} is the kinetic energy of the photoelectron. In photoelectron spectroscopy, however, reference is generally taken with respect to the Fermi level, so that E_B is replaced by $E_B' + \Phi$ (the BE relative to the Fermi level, plus the sample work function), yielding:

$$h\nu = E_{kin} + E_B' + \phi \qquad \textbf{(2-11)}$$

The photoemission spectroscopy technique is attractive due to its chemical sensitivity and its suitability for solid surface investigation. The photoelectron BEs, in fact already conveys information on the chemical composition of the sample. In addition, the chemical environment in which the core electron is found prior to the photoemission event (the type of bonding, the oxidation state, the possible presence of adsorbates) result in distinctive BE shifts.

The X-ray source consists of a hot filament at high voltage (10 – 15 kV), which emits electrons accelerated to an anode at ground potential. Inelastic electron-atom collisions in the anode produce an inner-shell ionisation, which leads to the emission of either:

a) An X-ray when an electron from a higher level falls into the inner-shell vacancy (core-hole)
b) An Auger electron when the energy released (when the hole is filled by the outer shell electron) is transferred to another electron (the Auger electron)

A common XPS spectrum is represented as a function of the number of electrons detected against the binding energy of the electrons detected (Fig. 2-29). The characteristic peaks correspond to the electron configuration of the electronic shells of the atoms such as 1s, 2s, 2p, 3s etc. The number of detected electrons in each of the characteristic peaks is directly related to the amount of an element within the volume irradiated. The peaks in the spectrum correspond to two distinct processes, namely, electrons ejected due to the photoelectric effect and emission due to the Auger effect. The kinetic energy scale is reported relative to the photon energy of the excitation source and so photoelectric line positions with respect to a binding energy scale become independent of the X-rays used to excite the sample, while the Auger line positions are invariant with respect to the X-ray anode only when plotted against a kinetic energy scale.

The Auger electrons are emitted with kinetic energies that are only dependent on the electronic state of the element responsible for the ejected electron. That is to say, unlike the photoelectric lines, changing the X-ray characteristic energy does not alter the position of the Auger lines in the recorded spectra with respect to a kinetic energy scale. Auger electrons are produced by auto-ionization. The collision processes involved with XPS result in electronic excited states with energies that lie above the ionization threshold. Some of these states are meta-stable with respect to radiative transitions within the neutral atom, but may couple with the continuum states of the ionic form to produce a radiation-less transition where the excess energy is transferred to the emitted electron. For this reason an electron spectrum may include Auger features that, when viewed using a binding energy scale, appear to move as a function of the X-ray source. In reality the Auger peaks always appear at the same kinetic energy and it is the photoelectric lines that move when a different excitation source is used.

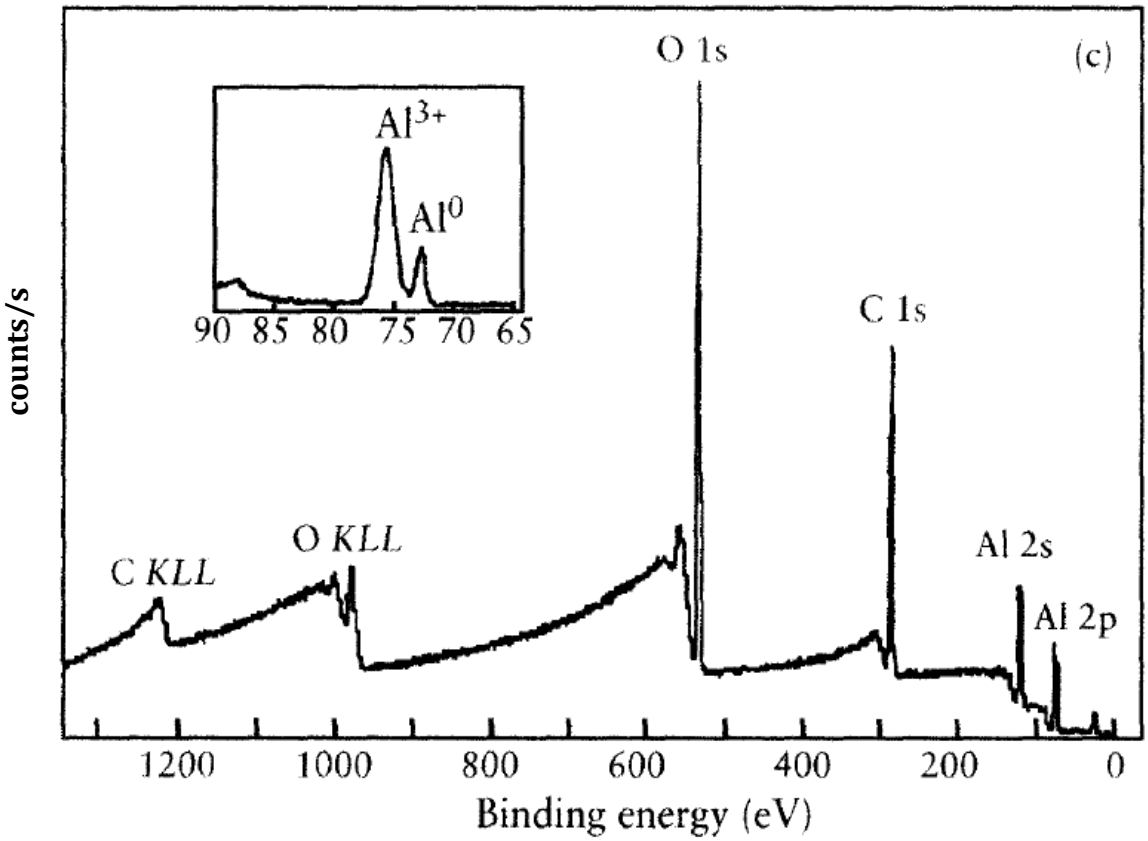

Figure 2-29 The XPS survey spectrum (recorded with monochromatic Al K_α radiation) of oxidized aluminium foil following air exposure; note the large C 1s peak resulting from the deposition of adventitious carbon from the atmosphere; inset is the Al 2p region recorded at higher resolution showing the metallic (Al°) and oxide (A1 3+) components [69].

XPS measures the energy of electrons emitted from a material and able to produce chemical state information (as distinguished from the element that presence within the material) from the first layer of few nm of any surface. This makes XPS a unique and a valuable technique for understanding the chemistry of elements near the surface, either as received, or after physical or chemical treatments. The chemical state can be described as the local bonding environment of a species in question (for the present study, Ge atom is the highlighted element to be worked on). The local bonding environment of a species in question is affected by its formal oxidation state, the identity of its nearest neighbour atom, its bonding hybridization (overlapping) to that nearest neighbor atom, as well as the bonding hybridization between the atom in question (e.g. Ge atom) and the next neighbor atom. Thus said, while the nominal binding energy of the C1*s* electron is 284.6 eV, subtle but reproducible shifts in the actual binding energy, the so-called chemical shift, provide the chemical state information referred to here.

2.5.2 Particle Induced X-ray Emission (PIXE)

Use has been made of particle induced X-ray emission (PIXE) analysis to map the relative presence of Si and Ge. It is known that the pure silica will give rise to a degree of thermoluminescence (TL) following irradiation by ionising radiation; however, the TL signal is considerably enhanced by the presence of certain dopants. The exact amount of dopant added to these fibres is not specified by the manufacturers. The dopants act as defect centres that provide the TL signal. A particular concern is that non-uniformity in the distribution of added dopants and impurity concentration in the core of the commercially available fibres will cause variation in TL yield to an extent that this may limit the application of such fibres. Findings from these PIXE studies may pave the way to conduct more comprehensive investigation of TL from tailor-made doped SiO_2 fibres.

In particular, sample elemental concentrations can be determined using the microbeam PIXE technique. PIXE was introduced in 1970 at the Lund Institute of Technology, following the advent of Lithium drifted Si(Li) detectors in the late 1960's [70]. This detector technology first stimulated the development PIXE and other energy dispersive spectroscopic techniques. The foundation was laid in 1914 by Moseley in his pioneering study of the energy of the characteristic X-ray lines of the different elements of the periodic table [71]. Moseley used a demountable X-ray tube and a flat crystal spectrometer with photographic recording to relate the atomic number of an element with the wavelengths of the element's characteristic X-ray emission. In general, PIXE involves the excitation of atoms in the sample to produce characteristic X-rays caused by bombardment of ions of sufficient energy (usually MeV protons).

The PIXE method is best suited for detection of K-shell transitions in lighter and L-shell transitions in the heavier atoms, the characteristic energies of these transitions being sufficiently separated to discern contributions of different atoms in the spectra. In addition, it is mostly used for elements heavier than Na, the characteristic X-rays of elements with lower Z having insufficient energy to penetrate into the detector sensitive volume.

Bombardment with ions of sufficient energy (usually MeV protons) produced from pure hydrogen by, in our case, a 2.5 MeV Tantedron accelerator (Fig. 2-30), causes inner shell ionization of atoms present in the sample material (predominantly the K and L shells), resulting in an unstable electron atomic configuration. Quantum theory states that orbiting electrons of an atom must occupy discrete energy levels in order to be stable. Outer shell electrons in the atom

then drop down to fill inner shell ion vacancies, and in so doing, emit excess energy in the form of X-rays. The number of X-rays of a certain energy emitted is proportional to the mass of the corresponding element in the sample being analysed. The energies of these X-rays are characteristic of the elements from which they originate and therefore can be used to identify elemental composition (Fig. 2-31). The generation of X-rays in a sample is very strongly influenced by the bombarding proton. The probability of X-ray production depends upon both the total number of incident protons and the proton energy. The total number of incident protons can be expressed as proton current (measured in micro amps). The greater the proton current, the greater the probability for X-ray production.

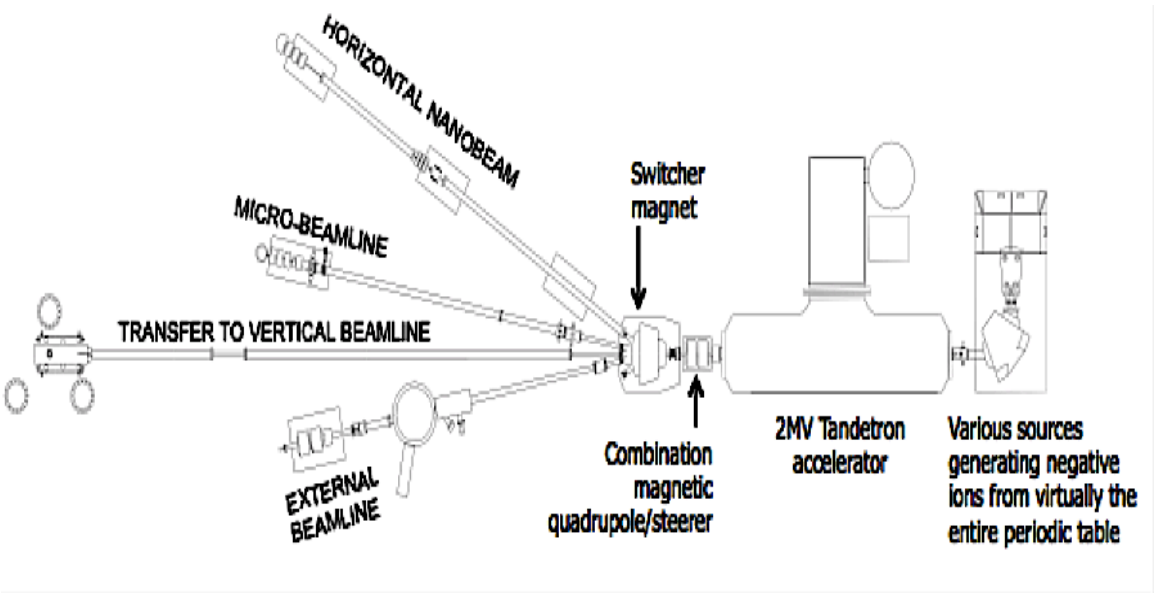

Figure 2-30 Schematic illustration of the experimental beamline employed at the Surrey Ion Beam Centre Tantedron Laboratory, implying electrostatic and magnetic field in the 2 MV implanter to accelerate the ions and for momentum selection, respectively.

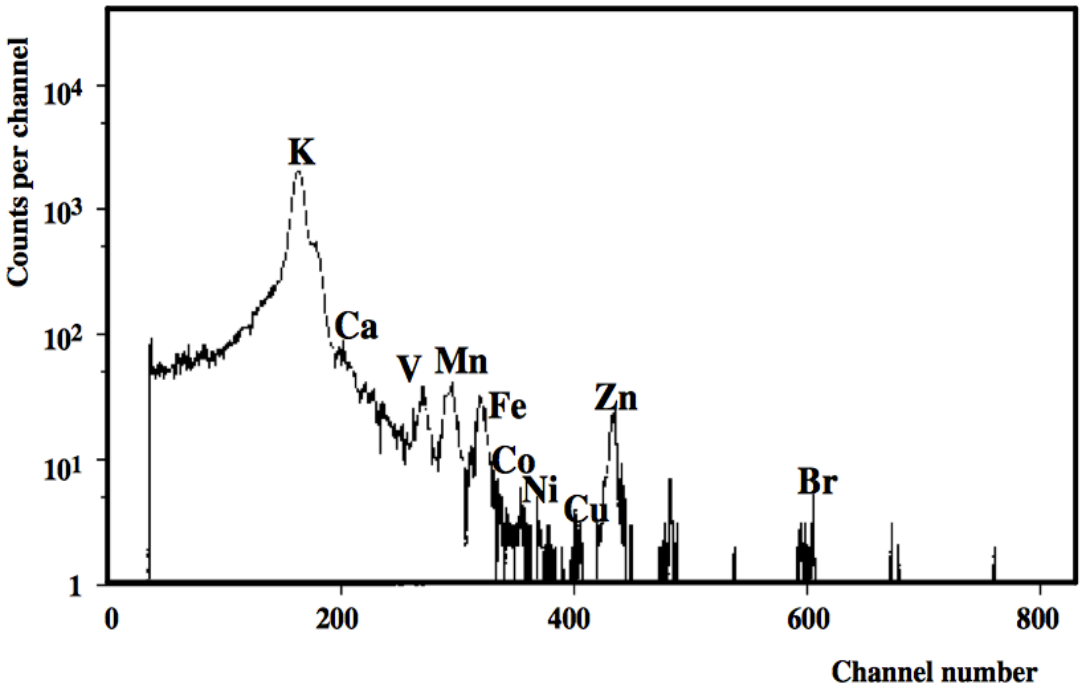

Figure 2-31 A PIXE spectrum of elements found in yeast cell [72], shown as an example of the simultaneous multi-element capability of the PIXE technique, being applicable to a wide range of media as in for instance the cells show herein.

A Lithium drifted Silicon Si(Li) detector is used to record and measure these emitted X-rays and the intensities are then converted to elemental concentrations of almost all elements in the sample to an accuracy of approximately 1 ppm (part-per-million, equivalent to 1 µg of the element of interest in every gram of the sample) (Fig. 2-32). X-ray absorber filters are utilised to attenuate the dominant peaks and allow higher trace element sensitivity (Fig. 2-32). Data reduction is accomplished using an interactive software package, which normalises the detected sample X-ray intensities against those measured from pure standards for each element, as well as analysing and converting raw spectral data into elemental concentrations.

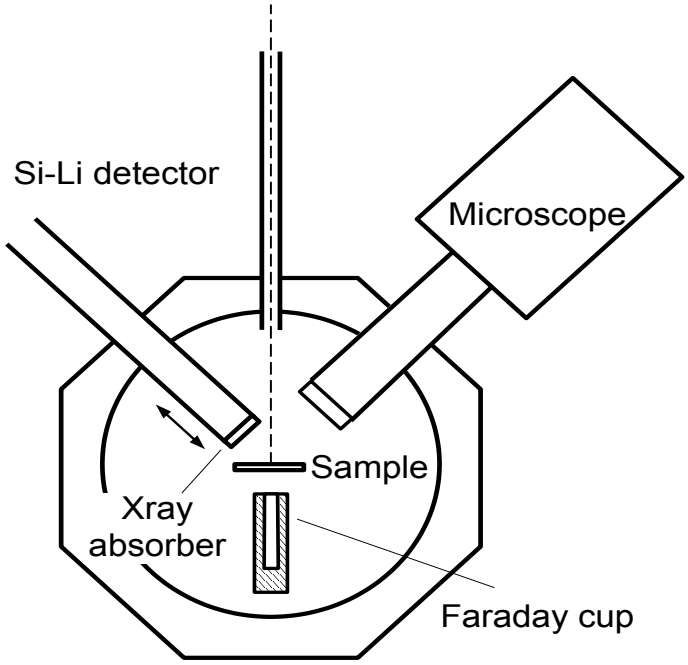

Figure 2-32 A typical PIXE facility contain the following components; Si(Li) detector with facility to fit X-ray absorber, microscope for sample viewing, sample mounted on adjustable stage, faraday cup to measure the incident beam current with thin samples and evacuated sample chamber connected to beamline.

The ability to detect the presence of an element via its characteristic X-ray emission and the generation of background radiation are considered for both proton bombardment and excitation by heavier ions. Background contribution arising from secondary electron bremsstrahlung constitute the limiting factor to sensitivity in the X-ray region below 10 keV, while primary bremsstrahlung and/or Compton scattering of nuclear gamma rays limit sensitivity for the X-ray region above 15 keV. The choice of bombarding ion and energy are examined with regard to optimising the analytical capabilities of PIXE. Protons of 2 to 4 MeV are generally considered to provide optimal sensitivity. In addition, the proton microprobe is a powerful analytical technique combining the multielemental capability and detection sensitivity of PIXE with spatial resolutions approaching 1 μm.

2.6 References

[1] G. F. Knoll. "Radiation detection and measurement." John Wiley & Sons (2000).

[2] J. R. Greening. "Fundamentals of Radiation Dosimetry." Medical Physics Handbook 15, 2nd edition, (1985).

[3] F. M. Khan. "The Physics of Radiation Therapy." Lippincott Williams & Wilkins (2003).

[4] E. B. Podgorsak. "Radiation Oncology Physics: A Handbook for Teachers and Students". Vienna, IAEA (2005).

[5] E. J. Hall, "Radiation biology, A Handbook for Teachers and Students" *Cancer*, vol. 55, no. 9 Suppl, pp. 2051–2057, 1985.

[6] S. W. S. McKeever. "Thermoluminescence of Solids." Cambridge University Press (1985).

[7] R. Chen and S. W. S. McKeever. "Theory of Thermoluminescence and Related Phenomena." London, World Scientific Publishing Co Pte Ltd (1995).

[8] A. F. McKinlay. "Thermoluminescence dosimetry." Bristol, Adam Hilger in collaboration with the Hospital Physicists' Association (1981).

[9] Y. S. Horowitz, E. Fuks, L. Oster, L. Podpalov, Y. Belaish and B. Ben Shachar, "Advanced Multistage Deconvolution Applied to Composite Glow peak 5 in LiF : Mg, Ti (TLD-100)," vol. 126, no. 1, pp. 322–325, 2007.

[10] K. Mahesh, P. S. Weng, C. Kent Furetta. "Thermoluminescence in solids and its applications." Nuclear Technology Publishing (1989).

[11] J. Izewska and G. Rajan. "Radiation Dosimeters. In Podgorsak E.B (ed). Radiation Oncology Physics: A Handbook for Teachers and Students." Vienna: International Atomic Energy Agency (IAEA) (2005).

[12] S. Hashim, S. Al-Ahbabi, D. A Bradley, M. Webb, C. Jeynes, A. T. Ramli, and H. Wagiran, "The thermoluminescence response of doped SiO2 optical fibres subjected to photon and electron irradiations.," *Appl. Radiat. Isot.*, vol. 67, no. 3, pp. 423–7, Mar. 2009.

[13] NE Technology Ltd, "Operators manual for Solaro TLD reader, version 2.00. Reading." NE Technology Ltd., 1996.

[14] K. Lyytikainen, S. Huntington, A. Carter, P. McNamara, S. Fleming, J. Abramczyk, I. Kaplin, and G. Schötz, "Dopant diffusion during optical fibre drawing.," *Opt. Express*, vol. 12, no. 6, pp. 972–7, Mar. 2004.

[15] R. L. Mozzi and B. E. Warren, J. Appl. Crystallogr. 2, 164 (1969)

[16] J. R. G. DaSilva, D. G. Pinatti, C. E. Anderson and M. L. Rudee, Phil. Mag. 31, 713 (1975)

[17] A. C. Wright and R. N. Sinclair, "The Physics of SiO_2, and its Interfaces." Proceedings of the International Topical Conference, ISBN: 978-0-08-023049-8, 1978

[18] N. Wiberg, A. Holleman, E. Wiberg. Inorganic Chemistry (Academic Press, 1st edition, London, 2001)

[19] L. Hobss, X. Yuan. "Defects and disorders in crystilline and amorphous solids." Kluwer Academic Publisher, Dordecht, 2000.

[20] R. Salh, "Defect Related Luminescence in Silicon Dioxide Network : A Review," 1991.

[21] G. Heterington, K. Jack, M. Ramsay. Phys. Chem. Glasses 6, 6 (1965).

[22] M. León Pichel, Doctoral thesis: Efectos de la radiación gamma y neutrónica en las propiedades ópticas del oxido de silicio amorfo, Universidad Autónoma de Madrid, (2011).

[23] R. Magruder III, R Weeks, R.Weller, J. of Non-crystaline Solids 357, 1615 (2011).

[24] L. Skuja, M. Mirano, H. Hosono, and K. Kajihara, Phys. Status Solidi. C2 No 1, 15 (2005).

[25] R. Magruder III, R Weeks, R.Weller, R. Zuhr, J. of Non-crystaline Solids 304, 224 (2002).

[26] K. Moritani, Y. Teraoka, I. Takagi, H. Moriyama. J. of Nuclear Materials 329, 988 (2004).

[27] M. Stapelbroek, D. L. Griscom, E. J. Friebele and G. H. Sigel Jr., "Oxygen-associated trapped-hole centers in high-purity fused silicas." *J. Non-Cryst. Solids,* vol. 32, no. 1-3, pp. 313-326, 1979.

[28] S. Ismail- Beigi, S. Louie. Physical Review Letters 95, 1 (2005).

[29] L. Skuja, "Isoelectronic series of twofold coordinated Si, Ge, and Sn atoms in glassy SiO_2: a luminescence study," *J. Non Cryst. Sol.* vol. 149, pp. 77-95, 1992.

[30] V. B. Neutruev, "Colour centres in germanosilicate glass and optical fibres," *J. Phys. Condens, Matter*. vol. 6, pp. 6901-6936, 1994.

[31] C. M. Carbonaro, V. Fiorentini, and F. Bernardini, "Stability of Ge-related point defects and complexes in Ge-doped SiO_2," *Phys. Rev. B,* vol. 66, pp. 233201, 2002.

[32] J. Nishii, N. Fukumi, H. Yamanaka, K. Kawamura, H. Hosono, and H. Kawazoe, "Photochemical reactions in GeO_2-SiO_2 glasses induced by ultraviolet irradiation: Comparison between Hg lamp and excimer laser," *Phys. Rev. B,* vol. 52, no. 3, pp. 1661-1665, 1995.

[33] H. Hosono, Y. Abe, D. L. Kinser, R. a Weeks, K. Muta, and H. Kawazoe, "Nature and origin of the 5-eV band in SiO_2:GeO_2 glasses," *Phys. Rev. B*, vol. 46, no. 18, pp. 11445–11451, 1992.

[34] M. Cannas and G. Origlio, “Ultraviolet optical properties of silica controlled by hydrogen trapping at Ge-related defects,” *Phys. Rev. B - Condens. Matter Mater. Phys.*, vol. 75, no. 23, pp. 5–8, 2007.

[35] M. Cannas, "Point Defects in Amorphous SiO_2: Optical Activity in the Visible, UV and Vacuum-UV Spectral Regions", Phd thesis, Dipartimento di Scienze Fisiche ed Astronomiche, Università di Palermo, Italy, 1998.

[36] S. Kannan, J. L. M. E. Fineman, and G. H. Sigel-Jr., Appl. Phys. Lett. 63, 3440 (1993).

[37] S. Girard, J.-P. Meunier, Y. Ouerdane, A. Boukenter, B. Vincent, and A. Boudrioua, Appl. Phys. Lett. 84, 4215 (2004).

[38] E. J. Friebele, D. L. Griscom, and G. H. Sigel, “Defect centers in a germanium-doped silica-core optical fiber,” *J. Appl. Phys.*, vol. 45, no. 8, pp. 3424–3428, 1974.

[39] T. E. Tsai, D. L. Griscom, E. J. Friebele, and J. W. Fleming, “Radiation-induced defect centers in high-purity GeO2 glass,” *J. Appl. Phys.*, vol. 62, no. 6, pp. 2264–2268, 1987.

[40] N. Chiodini, F. Meinardi, F. Morazzoni, A. Paleari, and R. Scotti, “Optical transitions of paramagnetic Ge sites created by x-ray irradiation of oxygen-defect-free Ge-doped SiO_2 by the sol-gel method,” vol. 60, no. 4, pp. 2429–2435, 1999.

[41] G. Pacchioni and C. Mazzeo, “Paramagnetic centers in Ge-doped silica: A first-principles study,” *Phys. Rev. B - Condens. Matter Mater. Phys.*, vol. 62, no. 9, pp. 5452–5460, 2000.

[42] J. Nishii, K. Kintaka, H. Hosono, H. Kawazoe, M. Kato, and K. Muta, “Pair generation of Ge electron centers and self-trapped hole centers in GeO2-SiO2 glasses by KrF excimer-laser irradiation,” *Phys. Rev. B*, vol. 60, no. 10, pp. 7166–7169, 1999.

[43] M. Fujimaki, T. Kasahara, S. Shimoto, N. Miyazaki, S. Tokuhiro, K. S. Seol, and Y. Ohki, “Structural changes induced by KrF excimer laser photons in H_2-loaded Ge-doped SiO2 glass,” *Phys. Rev. B*, vol. 60, no. 7, pp. 4682–4687, 1999.

[44] E. Friebele and D. Griscom, “Defects in Glasses,” in Mater Res. Soc. Symp., M. W.F.L. Galeneer, D.L. Griscom, ed., 61, 319, 1986.

[45] M. Fujimaki, T. Watanabe, T. Katoh, T. Kasahara, N. Miyazaki, and Y. Ohki, “Structures and generation mechanisms of paramagnetic centers and absorption bands responsible for Ge-doped SiO_2 optical-fiber gratings,” vol. 57, no. 7, pp. 3920–3926, 1998.

[46] C. P. Slichter, Principles of Magnetic Resonance (Springer-Verlag, Hong Kong, 1991).

[47] A. T. Abdul Rahman, R. P. Hugtenburg, S. F. Abdul Sani, A. I. M. Alalawi, F. Issa, R. Thomas, M. A. Barry, A. Nisbet, and D. A. Bradley, “An investigation of the thermoluminescence of Ge-doped SiO_2 optical fibres for application in interface radiation dosimetry.,” *Appl. Radiat. Isot.*, vol. 70, no. 7, pp. 1436–41, Jul. 2012.

[48] A. T. Abdul Rahman, S. F. Abdul Sani, and D. A. Bradley, “Doped SiO_2

telecommunication fibre as a 1-D detector for radiation therapy dosimetry," vol. 347, pp. 347–353, 2012.

[49] F. Issa, N. A. A. Latip, D. A. Bradley, and A. Nisbet, "Ge-doped optical fibres as thermoluminescence dosimeters for kilovoltage X-ray therapy irradiations," *Nucl. Instruments Methods Phys. Res. Sect. A Accel. Spectrometers, Detect. Assoc. Equip.*, vol. 652, no. 1, pp. 834–837, Oct. 2011.

[50] N. M. Noor, M. Hussein, D. A. Bradley, and A. Nisbet, "The potential of Ge-doped optical fibre TL dosimetry for 3D verification of high energy IMRT photon beams," *Nucl. Instruments Methods Phys. Res. Sect. A Accel. Spectrometers, Detect. Assoc. Equip.*, vol. 619, no. 1–3, pp. 157–162, Jul. 2010.

[51] N. M. Noor, M. Hussein, D. A. Bradley, and A. Nisbet, "Investigation of the use of Ge-doped optical fibre for in vitro IMRT prostate dosimetry," *Nucl. Instruments Methods Phys. Res. Sect. A Accel. Spectrometers, Detect. Assoc. Equip.*, vol. 652, no. 1, pp. 819–823, Oct. 2011.

[52] N.M. Noor, D. A. Bradley, A. Nisbet, "An investigation of the suitability of Ge-doped optical fibres in mailed thermoluminescence dosimetry audits of radiotherapy dose delivery". Radiotherapy Oncol. vol. 99 (1), pp. 196 - 197, 2011.

[53] A. T. Abdul Rahman, D. A. Bradley, S. J. Doran, B. Thierry, E. Bräuer-Krisch, and A. Bravin, "The thermoluminescence response of Ge-doped silica fibres for synchrotron microbeam radiation therapy dosimetry," *Nucl. Instruments Methods Phys. Res. Sect. A Accel. Spectrometers, Detect. Assoc. Equip.*, vol. 619, no. 1–3, pp. 167–170, Jul. 2010.

[54] A.T. Abdul Rahman, A. Nisbet, D.A. Bradley, "Dose-rate and the reciprocity law: Tl response of Ge-doped Sio_2 optical fibers at therapeutic radiation doses." *Nucl. Instruments Methods Phys. Res. Sect. A Accel. Spectrometers, Detect. Assoc. Equip.*, vol. 652, no. 1, pp. 891–895, Oct. 2011.

[55] I. Amani, Alalawia, R.P. Hugtenburg, A.T. Abdul Rahman, M.A. Barry, A. Nisbet, Khalid S. Alzimami, and D.A. Bradley, "Measurement of dose enhancement close to high atomic number media using optical fibre thermoluminescence dosimeters" *Radiat. Phys. and Chem.,* vol. 95, pp. 145–147, 2014.

[56] A. L. Yusoff, R. P. Hugtenburg, and D. A. Bradley, "Review of development of a silica-based thermoluminescence dosimeter," *Radiat. Phys. Chem.*, vol. 74, no. 6, pp. 459–481, Dec. 2005.

[57] S. F. Abdul Sani, A. I. Alalawi, H. Azhar A.R, G. Amouzad Mahdiraji, N. Tamchek, A. Nisbet, M. J. Maah, and D. A. Bradley, "High sensitivity flat SiO2 fibres for medical dosimetry," *Radiat. Phys. Chem.*, vol. 104, pp. 134–138, Nov. 2014.

[58] D. A. Bradley, G. A. Mahdiraji, M. Ghomeishi, E. Dermosesian, F. R. M. Adikan, H. A. Abdul Rashid, and M. J. Maah, "Enhancing the radiation dose detection sensitivity of optical fibres," *Appl. Radiat. Isot.*, vol. 100, pp. 43–49, 2014.

[59] M. L. Zulkifli, S. M. Aljamimi, A. Yusoff, Y. M. Amin, S. Shafiqah, A. P. Technologies, and D. Cyberjaya, "Effect of $GeCl_4$ / $SiCl_4$ Flow Ratio on Germanium Incorporation in MCVD Process Si02 Si02," no. 4, pp. 284–287, 2013.

[60] Tingye Li, Optical Fiber Communications Volume I, Academic Press Inc. 1985

[61] K.D. Dambul, G.A. Mahdiraji, F. A. Amirkhan, D. Chow, G. Gan, W. R. Wong, M. R. Abu Hassan, D.C. Tee, S. Ismail, S.A. Ibrahim, N. Tamchek and F.R. Mahamd Adikan, "Fabrication and development of Flat Fiber". Proc. PGC, pp. 3–5, 2012.

[62] G. A. Mahdiraji, D. M. Chow, S. R. Sandoghchi, F. Amirkhan, E. Dermosesian, Kwok Shien Yeo, Z. Kakaei, M. Ghomeishi, Soo Yong Poh, Shee Yu Gang and F. R. Mahamd Adikan, "Challenges and Solutions in Fabrication of Silica-Based Photonic Crystal Fibers : An Experimental Study," *Fiber and Integrated Optics*, vol. 33, pp. 85–104, Oct. 2014.

[63] S. Girard, C. Marcandella, A. Alessi, A. Boukenter, Y. Ouerdane, N. Richard, P. Paillet, M. Gaillardin, M. Raine, "Transient Radiation Responses of Optical Fibers: Influence of MCVD process Parameters", *IEEE Trans. Nucl. Sci*, Vol. 59, No. 6, pp. 2894-2901, Dec. 2012.

[64] A. Alessi, S. Girard, M. Cannas, S. Agnello, A. Boukenter, and Y. Ouerdane, "Influence of Drawing Conditions on the Properties and Radiation Sensitivities of Pure-Silica-Core Optical Fibers" *Journal of Lightwave Technology*, Vol. 30, No. 11, pp. 1726-1732, Jun. 2012

[65] A. Alessi, S. Girard, C. Marcandella, L. Vaccaro, M. Cannas, A. Boukenter, and Y. Ouerdane, "Influence of the Manufacturing Process on the Radiation Sensitivity of Fluorine-Doped Silica-Based Optical Fibers", *IEEE Trans. Nucl. Sci*, Vol. 59, No. 4, pp. 760-766, Aug. 2012.

[66] M. Ghomeishi, G. A. Mahdiraji, F. R. M. Adikan, and S. Hashim, "The thermoluminescence response of undoped silica PCF for dosimetry application," *2013 Conf. Lasers Electro-Optics Pacific Rim*, pp. 1–2, Jun. 2013.

[67] S. Girard, J. Baggio, and J.-L. Leray, "Radiation-induced effects in a new class of optical waveguides: the air-guiding photonic crystal fibres," *IEEE Trans. Nucl. Sci.*, vol. 52, no. 6, pp. 2683–2688, Dec. 2005.

[68] N. J. Florous, K. Saitoh, T. Murao, and M. Koshiba, "Radiation Dose Enhancement in Photonic Crystal Fiber Bragg Gratings: Towards Photo-Ionization Monitoring of

Irradiation Sources in Harsh Nuclear Power Reactors," *2007 Conf. Lasers Electro-Optics*, vol. 1, pp. 1–2, 2007.

[69] J.F. Watts and J. Wolstenholme. "An introduction to surface analysis by XPS and AES." pp. 224. ISBN 0-470-84713-1. Wiley-VCH, May 2003.

[70] T. B. Johansson, K. R. Akselsson and S. A. E. Johansson, *Nucl. Instr. Meth*., 84, 141 (1970)

[71] S.A. Johansson and J.L. Campbell, (1988). PIXE: A novel technique for elemental analysis.

[72] I. C. Farcasanu, F. Nishiyama and T. Miyakawa, Particle-Induced X-ray Emission (PIXE): A Tool for Multielement Analysis in the Yeast Cells, vol. I-II, pp. 39-43

Chapter 3

3 X-ray Photoelectron Spectroscopy (XPS) Analysis of Doped Optical Fibres

3.1 Introduction

Most of the content of this chapter is published in the journal "Lightwave of Technology": "S.F. Abdul Sani, G. Amouzad Mahdiraji, A.S Siti Shafiqah, G.W. Grime, V. Palitsin, S.J. Hinder, N. Tamchek, H.A Abdul Rashid, M.J. Maah, J. F. Watts and D.A. Bradley, 2015. XPS and PIXE analysis of doped silica fibre for radiation dosimetry" (Appendix A). The right to include the article in any thesis or dissertation has been obtained during assignment of copyright with the publisher.

The study of elemental composition and chemical state of the elements that exist within a surface region of solids is provided by the X-ray photoelectron spectroscopy (XPS) technique, a non-destructive method. XPS was initially used for the spectroscopy of atoms and molecules in the gas phase, excited with monochromatic ultraviolet light (He I: 21.2 eV, He II: 40.8 eV). Subsequently spectroscopic investigations of solids by excitation with soft X-rays (Al-K_α: 1486.6 eV and Mg-K_α: 1253.6 eV) was developed by Kai Siegbahn (Nobel Prize in Physics 1981), who gave the new technique the acronym ESCA (electron spectroscopy for chemical analysis) to emphasise the ability to identify the chemical state of elements [1].

As discussed in section 2.5.1, the bombardment of X-rays on solid material causes photoelectron emission from the outermost atomic layers of the surface, allowing identification of the elemental composition (except for H and He), interpreted via XPS. In this respect, monoenergetic soft X-rays (Mg-K_α and Al-K_α) are ideally suited to probe the core levels of a solid, which generally show no measurable dispersion due to their highly localised atomic-like character. It is important to note that XPS is recognised as a surface sensitive quantitative spectroscopic technique due to the lossless emission of photoelectrons from a thin surface layer. The escape depth varies from 3 to 10 nm on the surface, depending on the kinetic energy (KE) of the photoelectron. The energies and intensities of the photoelectron peaks enable identification and quantification of all surface elements except hydrogen and helium, as previously mentioned. The kinetic energy of the emitted electrons is characteristic of the element from which the

photoelectron originated. The position and intensity of the peaks in an energy spectrum provide the desired chemical state and quantitative information.

Given that XPS can probe core electrons, it has a greater range of potential application beyond identifying the chemical state on surfaces and quantitative analysis. As an example, XPS is capable of detecting the difference in chemical state between samples as well as differentiating between oxidation states of molecules. Moreover, XPS has the ability to analyse insulating materials with relative ease. Since the analysis beam (X-rays) does not consist of charged particles, the insulating material is not required to conduct away any charge build up due to incidence of the analysis beam. The material is only required to conduct away a sufficient amount of charge to compensate for the small number of electrons which have been ejected from the sample. This small positive charge build up is easily compensated for by use of a "flood gun", which directs low energy electrons to the sample surface. Despite the many benefits of XPS, no technique is foolproof, without limitations. The smallest analytical area XPS can measure is ~10 μm. Further, samples for XPS must be compatible with the ultra high vacuum environment. XPS spectra also take a long time to acquire (up to 4 hours); the use of a monochromator can reduce the time per experiment, but increases the resolution of the spectra obtained.

In regard to the medium of interest herein, they are dopants that have been introduced within silica glass fibres, ostensibly to control the refractive index of the glassy host (an amorphous medium) for optical communication purposes. Here it is to be noted that use of commercially available optical communication fibres as thermoluminescence dosimeters (TLD) was the original starting point of the research developed within this thesis. However, presently the doped fibres under study have been tailor made, altering composition and form in an effort to enhance the TL characteristics of the various media. Fortuitously, due to the presence of the dopants, irradiated glass fibres give rise to thermoluminescence (TL) to an extent well beyond that of the silica itself. Useful intensities of TL have been observed at radiation levels familiar in high dose radiation-medicine procedures. In optical fibres, dopants added to the core structure provide for total internal reflection, these defects being distributed under the high temperature and rapid quenching conditions that are required for fibre drawing. It is the defect centres that provide for TL [2]. This chapter describe an investigation elemental and chemical analysis of tailor-made Ge-doped optical fibres, use being made of X-ray photoelectron spectroscopy (XPS).

3.2 Experimental Procedure

Ge-doped optical silica preforms with 15.14 mm outer diameter and 2.10 mm core diameter, containing 8.49 ± 0.07 wt% and 10.08 ± 0.07 wt% Ge (measured by electron dispersive X-ray analysis (EDX)) in the preform core area, were cleaned using an ultrasonic bath, repeated three times in three different solvents; methanol, ethanol and propanol (see Fig. 3-1) of 15 minutes of cycle for each type of alcohol. For XPS measurement, all samples were first annealed at 400 °C for 1 hour, followed by slow cooling to room temperature for 6 hours due to minimize surface contaminant. The sample analysis was performed under ultra-high vacuum (UHV) conditions in a Thermo Fisher Scientific (East Grinstead, UK) theta probe spectrometer (Fig. 3-2). The instrument employs a monochromatic Al K_α X-ray source (hv = 1486.6 eV). The area of analysis was approximately 800 µm diameter. The pass energy was set at 50 eV for core level high-resolution spectra of all elements of interest and at 300 eV for all survey spectra. The preform sample was held in place on the instrument sample stage by a Cu/Be clip. All data were obtained and quantified using the manufacturer's Avantage v4.84 software, which incorporates the appropriate sensitivity factors and corrects for the electron energy analyser transmission function [3]. All spectra were charge referenced against the C1s peak at 285 eV to correct for charging effects during acquisition.

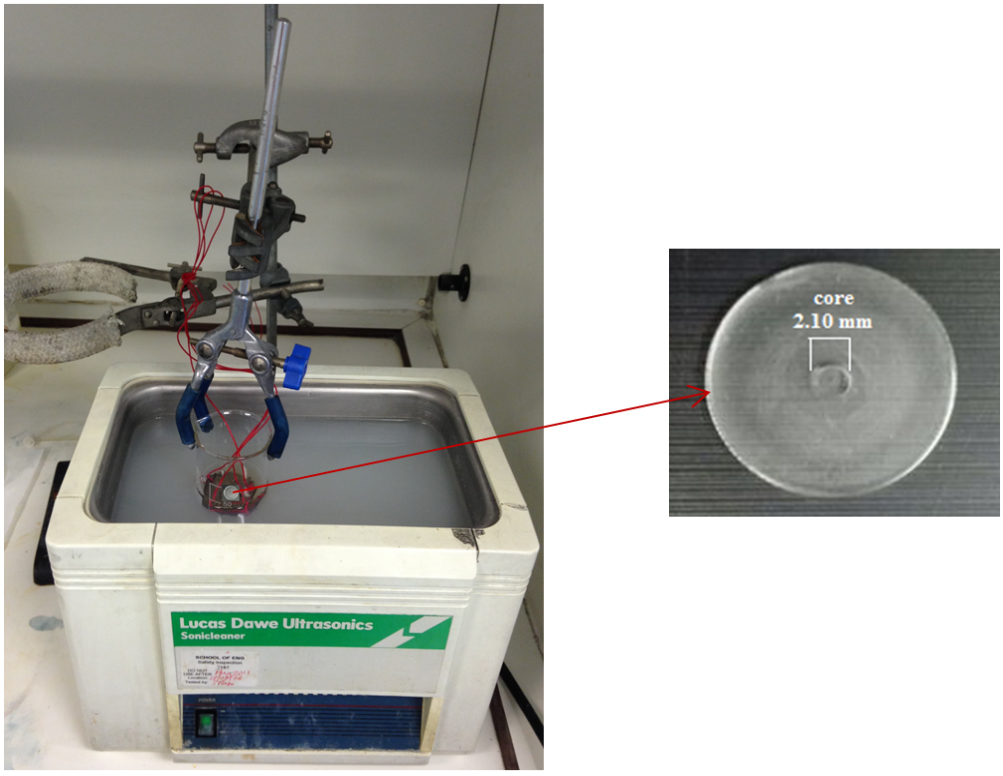

Figure 3-1 The ultrasonic bath and polished surface Ge-doped silica preform.

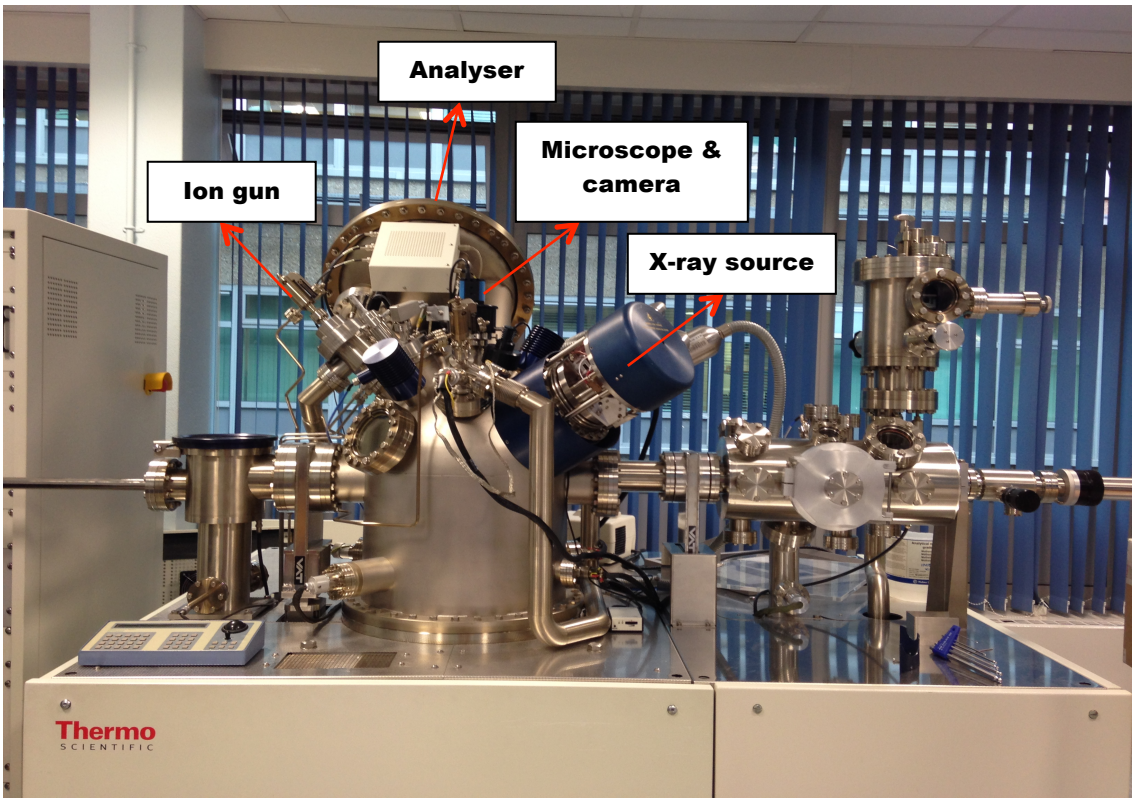

Figure 3-2 XPS Thermo Scientific Theta Probe employed in the Surface Analysis Laboratory of the Faculty of Engineering and Physical Sciences, University of Surrey.

3.3 Results and Discussion

3.3.1 XPS Analysis of Ge-doped Silica Preforms and Ge-doped Capillary Fibres

In XPS the solid material is bombarded with low energy X-rays in order to provoke photoelectron emission from the outermost atomic layers of the surface, thereby allowing identification of the elemental composition (other than H and He). The energy distribution of the emitted photoelectrons is then analyzed by the electron spectrometer and the data presented as a graph of intensity against electron energy. While the kinetic energy of the electron is the experimental quantity measured by the spectrometer, this is nevertheless dependent on the photon energy of the X-rays employed.

Fig. 3-3 shows the survey spectra of the preforms and identifies the presence of elements on the sample surface, the different peaks corresponding to electrons photoejected from the different core levels of the material for nominal 8 wt% and 10 wt% preforms. The high

resolution spectra of the Ge2p3/2 core level peaks are shown in Fig. 3-4. The binding energy and quantitative analyses of the detected elements are presented in Table 3-1. It is observed in Fig. 3-3 that the O1s peak (~528 eV) is the most intense peak in the spectrum, followed by the C1s component peak (~282 eV), attributed to hydrocarbon components. Adventitious carbon contamination detection, resulting from exposure to the atmosphere, is commonly used as a charge reference for XPS spectra to allow calibration of the binding energy scale for XPS measurements with non-conducting specimens; a binding energy of 284.50 eV has been set for this purpose. The presence of Fe2p, N1s, Na1s, Mg1s and Cu2p3 in the preforms under investigation is due in part to contamination during sample handling and fibre pulling.

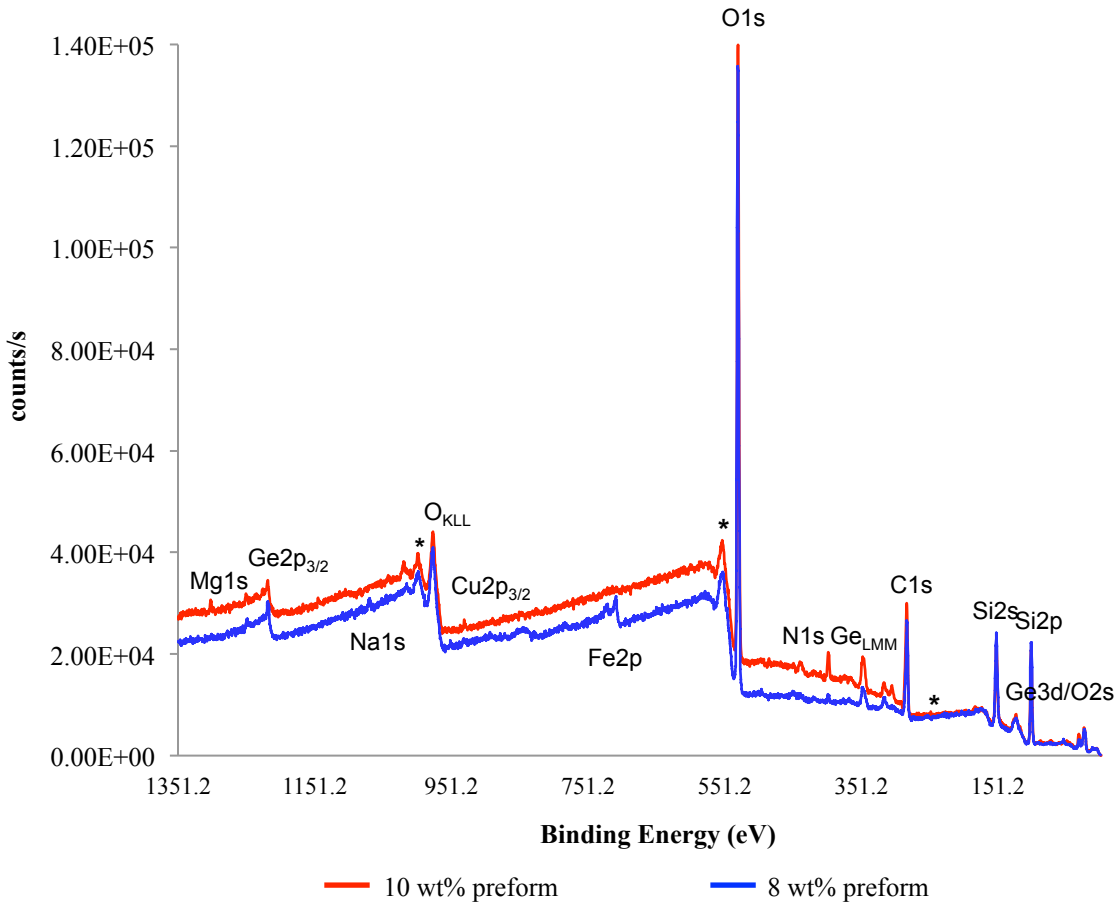

Figure 3-3 A survey spectrum is shown for Ge-doped performs of nominal 8 wt% and 10 wt%, revealing the XPS transitions made accessible using Al K_α radiation (1486.60 eV). The features marked with an asterisk are electron energy loss features due to plasmon excitation. A comparative study is made on two preforms to investigate the reproducibility of the technique, shown to be reliable.

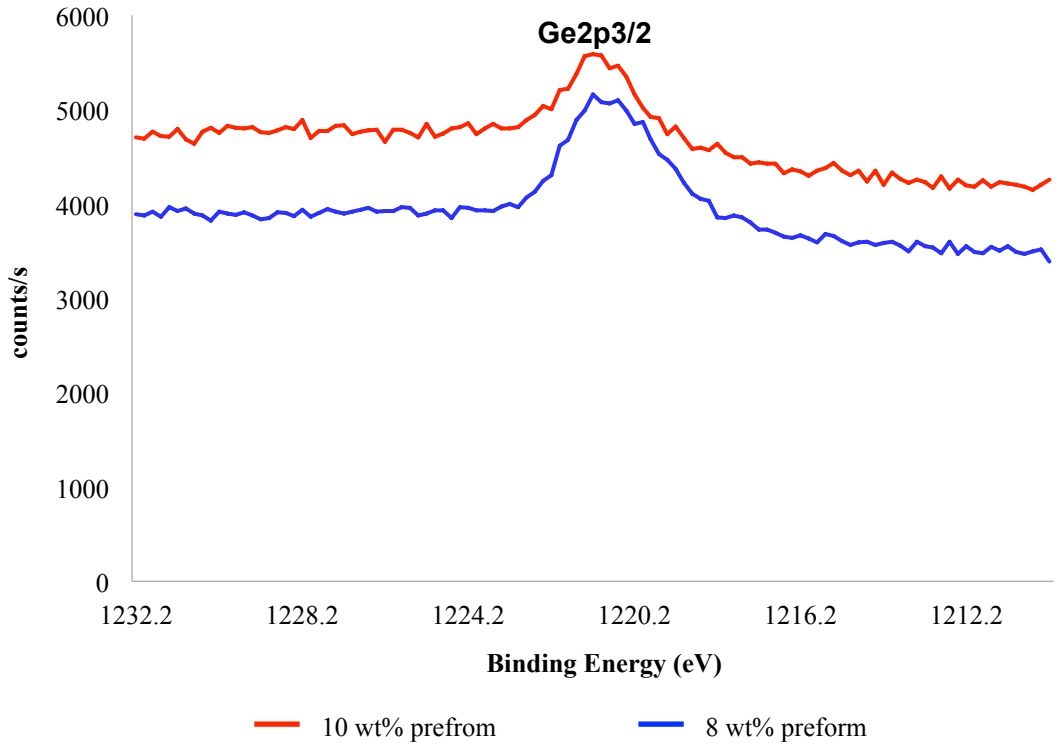

Figure 3-4 High resolution spectra of the Ge2p3/2 of nominal 8 wt% and 10 wt% preforms, revealing the peak binding energy to be located at 1217.39 eV and 1218.08 eV with concentration of 0.82 % and 0.49 % respectively.

Table 3-1 Summary XPS analysis for Ge-doped optical silica preforms of nominal 8 wt% and 10 wt%.

8 wt% preform	***Binding Energy (eV)***	***Atomic Percentage (At%)***	***10 wt% preform***	***Binding Energy (eV)***	***Atomic Percentage (At%)***
Ge2p3/2	1217.39	0.82 ± 5.00	**Ge2p3/2**	1218.08	0.49 ± 5.00
Si2p	99.80	18.70 ± 2.00	**Si2p**	100.20	15.20 ± 2.00
O1s	527.20	60.30 ± 2.00	**O1s**	528.20	55.19 ± 2.00
C1s	282.20	17.35 ± 2.00	**C1s**	282.20	25.31 ± 2.00
Fe2p	705.00	1.37 ± 5.00	**Cu2p3**	930.20	0.12 ± 5.00
N1s	396.89	0.95 ± 5.00	**N1s**	397.20	3.20 ± 5.00
Na1s	1068.81	0.51 ± 0.01	**Mg1s**	1301.40	0.48 ± 5.00

The Ge-doped preform of nominal 10 wt% produces lower Ge concentration being 1.7 times less than that of nominal 8 wt% preform. This is due to the greater presence of hydrocarbon (C1s) in the nominal 10 wt% preform, attenuating the Ge emission as a result of the hydrocarbon rich surface. For further discussion of this, see the section immediately below in which the Ge concentration of annealed and non-annealed capillary fibres are compared, showing the removal of the hydrocarbon contaminant to favourably alter the measured Ge concentration.

The measurement has been repeated using nominal 10 wt% Ge-doped capillary fibres with dopant in the inner ring region (see Fig. 3-5 (a)), being fabricated from the same Ge-doped preforms. The fibres were cut in half to allow scanning on the dopant area (Fig. 3-5 (b)) and cleaned using acetone in an ultrasonic bath.

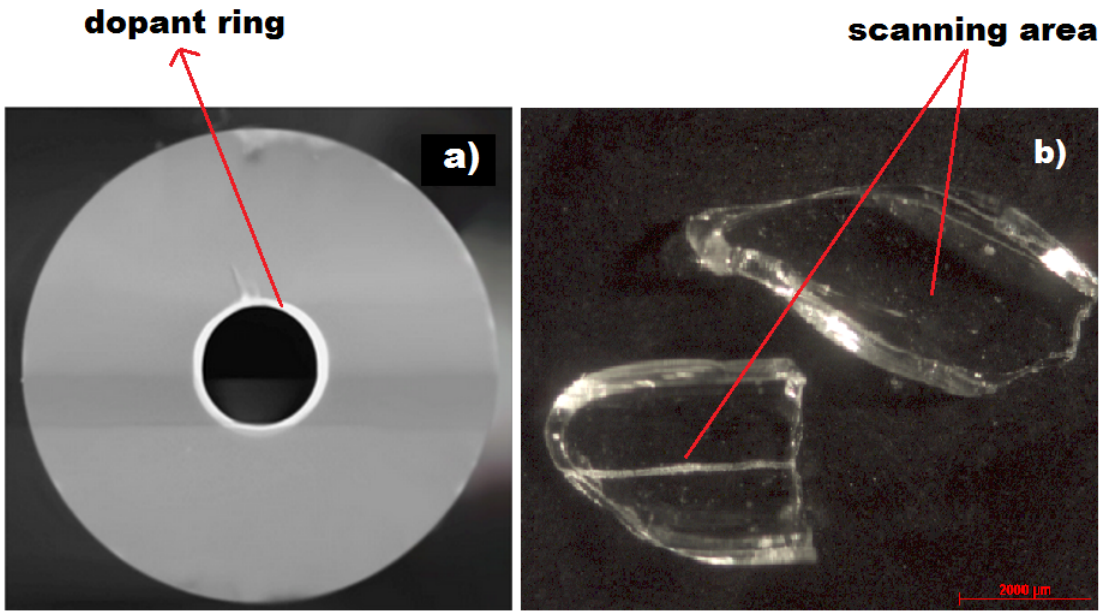

Figure 3-5 (a) The Scanning Electron Microscope (SEM) image from the cross-section of nominal 10 wt% capillary fibre being doped with Ge in the inner ring region, and (b) two pieces of split capillary fibres used for the investigation, allowing access to the doped region.

Fig. 3-6 demonstrates the presence of the Ge dopant, centrally located within the cross-section of the sample surface, for non-annealed and annealed capillary fibres (annealed in the furnace for 400 ^{o}C for a duration of 1 hour). The high resolution Ge2p3/2 core level peak is shown in Fig. 3-7. The summary binding energy and atomic percentages of the detected elements are presented in Table 3-2.

In Fig. 3-6, it is apparent that the concentration of C1s of the annealed capillary fibre is less than that of non-annealed capillary fibre. Many surfaces are known to adsorb hydrocarbon from ambient air, including SiO_2 [4, 5]. Such hydrocarbon adsorption decreases the surface energy of the substrate. Removing the hydrocarbon by thermal annealing (at 400^{o}C) resulted in a concurrent increase of the Ge2p3/2 by factor 4 (Fig. 3-7). This is due to the disproportionate relation of the kinetic energy and the binding energy of Ge2p3/2 electrons. The Ge2p3/2 has a low kinetic energy and will thus have a much smaller attenuation length than the Si2p transition. A layer of carbon will thus reduce the intensity of the Ge2p3/2 signal more significantly than that of the Si2p. The reduction of C1s in the annealed capillary fibre is a consequence of the partial removal of the adventitious hydrocarbon contamination from ambient air exposure as mentioned above. It should also be noted that the cleaning process in acetone in an ultrasonic bath effectively removed many of the contaminant species present in the former measurement on the preforms e.g. Na, Fe etc.

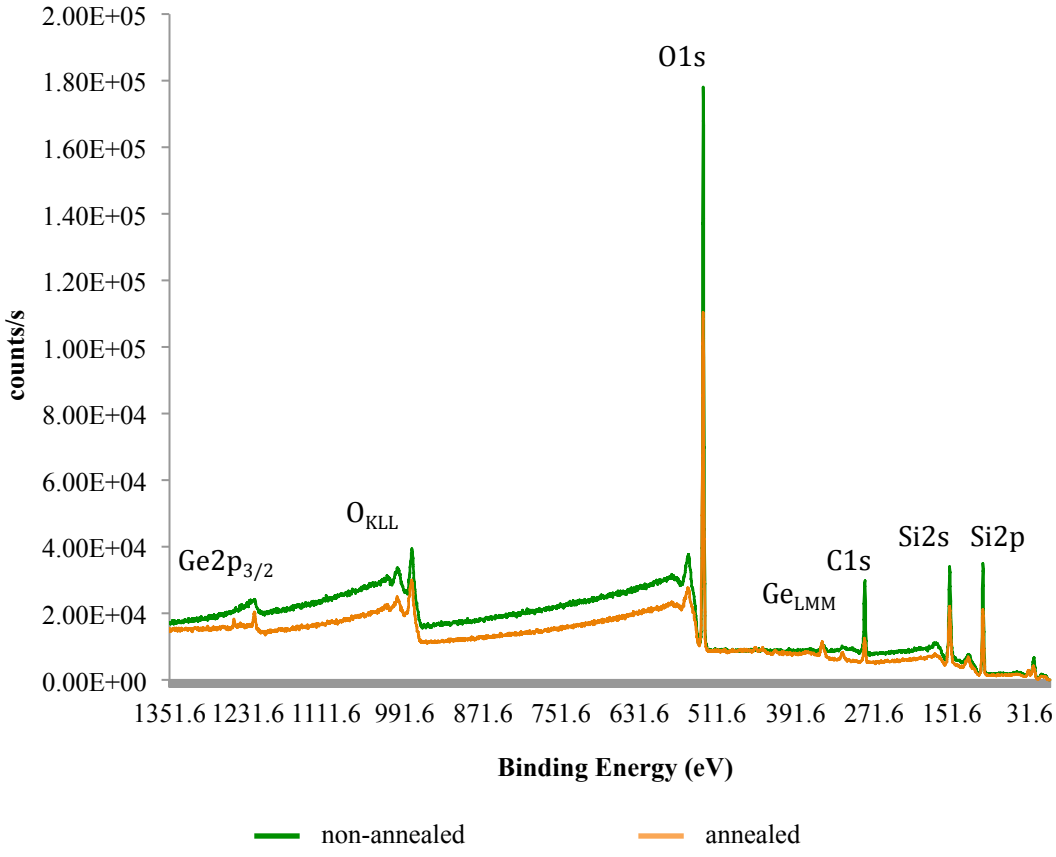

Figure 3-6 A survey spectrum is shown for the example Ge-doped non-annealed and annealed capillary fibres, revealing the XPS transitions made accessible using Al K_{α} radiation (1486.60 eV). The comparative study has been made using samples treated using two different approaches, non-annealed and annealed capillary fibres, examining possible effect upon reproducibility.

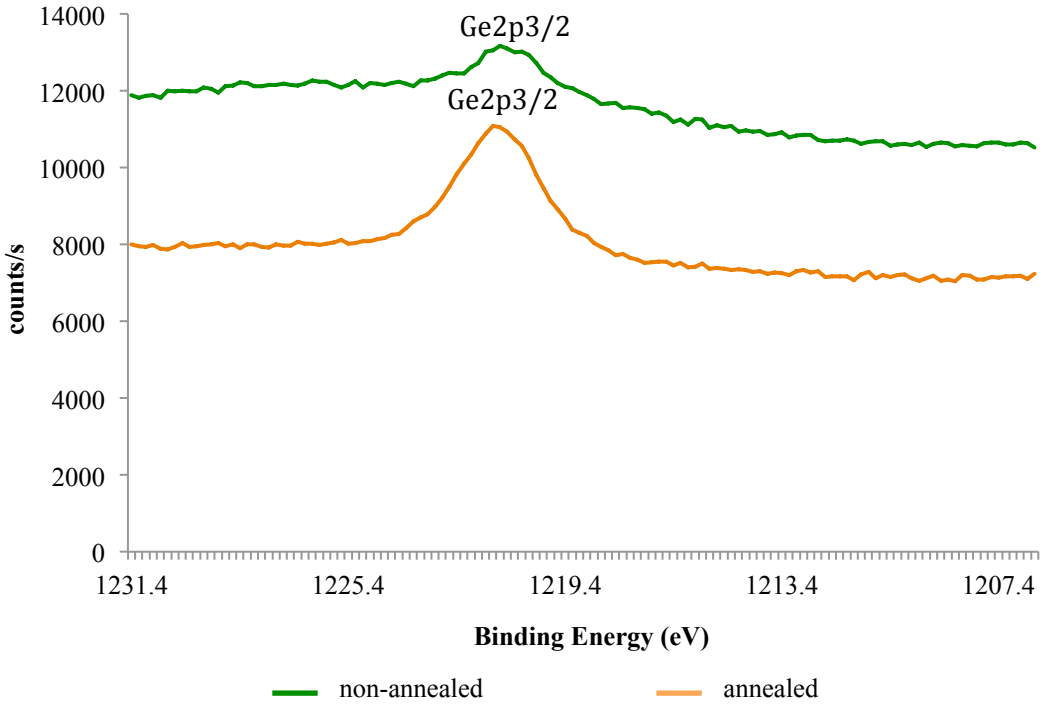

Figure 3-7 A high resolution spectra of the Ge2p3/2 of the non-annealed and annealed capillary fibres, revealing the peak binding energy to be located at 1218.20 eV and 1216.60 eV with atomic percentages of 0.18% and 0.84% respectively.

Table 3-2 Summary XPS analysis for Ge-doped non-annealed and annealed capillary fibres.

Capillary Fibre - non annealed	***Binding Energy (eV)***	***Atomic Percentage (At%)***	***Capillary Fibre - annealed***	***Binding Energy (eV)***	***Atomic Percentage (At%)***
Ge2p3	1218.20	0.18 ± 5.00	**Ge2p3**	1216.60	0.84 ± 5.00
Si2p	99.20	22.62 ± 2.00	**Si2p**	99.60	23.91 ± 2.00
O1s	528.60	62.68 ± 2.00	**O1s**	528.60	65.88 ± 2.00
C1s	282.00	14.52 ± 2.00	**C1s**	281.40	9.38 ± 2.00

Comparisons of calculated electron attenuation lengths (EALs) for XPS with Al K_α X-rays in a range of measurement configurations for two illustrative cases have been reported: Si2p photoelectrons in C (for which elastic-electron scattering effects are relatively strong) at 1385 eV and Ge2p3/2 photoelectrons in C (for which the elastic-electron scattering effects are relatively weak) at 150 eV. The determination of electron attenuation length (AL) is important in

XPS for the determination of layer thicknesses in the nanometer range for a particular electron kinetic energy. The signal intensities of the early overlayer-film depend quasi-exponentially on film thickness, and it is thus natural to refer to the exponential parameters as the attenuation length. For that the following simple relation can be used:

$$I_{\infty}(E) = I_{o}(E)\exp\left[\frac{-d}{\lambda_{\infty}\cos\theta}\right] \qquad \textbf{(3-1)}$$

where $I_{\infty}(E)$ and $I_{o}(E)$ are the respective intensity for a photoelectron peak of energy E for a layer of thickness d of the substrate material and that for the bulk substrate. In equation (3-1), the electrons are detected at an angle θ to the surface normal and λ_{∞} is the AL of the substrate photoelectrons in the overlayer material. With a path length of one λ 65% of all electrons are scattered. Sampling depth is defined as the depth from which 95% of all photoelectrons are scattered by the time they reach the surface (3λ). Most λ's are in the range of 1 – 3.5 nm for AlK_{α} radiation. So the sampling depth (3λ) for XPS under these conditions is 3-10 nm [6].

The EALs (λ_{∞}) is evaluated directly from the software for Quantitative Analysis of Surfaces by Electron Spectroscopy (QUASES), characterizing surface nano-structures by analysis of electron spectra [7]. The ratio of the average EALs for Si2p photoelectrons is found to be 3.68 whereas for the Ge2p3/2 photoelectrons it is 0.86 in the C layer. To compute the effects, some parameters are required for Si2p and Ge2p3/2 and these are the thickness of the substrate material of 1 nm and the angle θ to the surface normal of 52°. The relative intensity of electrons $\left(\frac{I_{\infty}(E)}{I_{o}(E)}\right)$ for Si2p photoelectrons and Ge2p3/2 photoelectrons in the C layer are therefore found to be 0.163 and 0.695 respectively, being consistent with the disproportionate attenuation of the Ge2p3/2 electrons.

At the outset of the project it was initially intended that silica samples would be thermoluminescence (TL) activated using only single element dopants (where Germanium has been used for present investigation). With only a limited number of TL studies on silica material already reported in the literature, it was unclear which dopant concentrations in silica should produce significant thermoluminescence. The yield problem lies in the fact that in many of the studies, the results were not compared to that of any known TLD (this will be discussed in Chapter 5). Another reason concerns the apparent lack of any published account of concentration dependency, to verify if the dopant concentration is at the optimum level for

thermoluminescence. Fig. 3-8 shows the dependence of TL sensitivity in cylindrical fibres (CF) of dimension 241 um Ge-doped to nominal concentrations of 6-, 8- and 10 wt%. Over the range of dopant concentrations, the nominal 6 wt% CF has been observed to be at least 3 times more sensitive than the fibre of greatest dopant concentration, of nominal 10 wt%, while that for the nominal 8 wt% CF lies in between these two dopant concentrations. It might be expected that the TL yield will increase with dopant concentration, the number of electron traps and recombination centres increasing with dopant concentration, however, beyond an optimised concentration (nominal 6 wt%), the TL yield of the samples actually decreases. This occurs because the distance between traps reduces as the number of traps and recombination centres increases, raising the probability for the light emitted from one recombination process to be absorbed by an electron in another trap. This phenomenon is called self-absorption. Alessi et al. [8] have sought to examine differences between the Raman activities of the optical fibres and preforms. It was found that in changing the drawing conditions e.g. tension, no significant differences occurred in the glass structure of the Ge-doped optical fibres and their associated preforms. Thus said, the variations in the drawing parameters were not sufficient to influence the glass structure in a way measurable by the Raman technique.

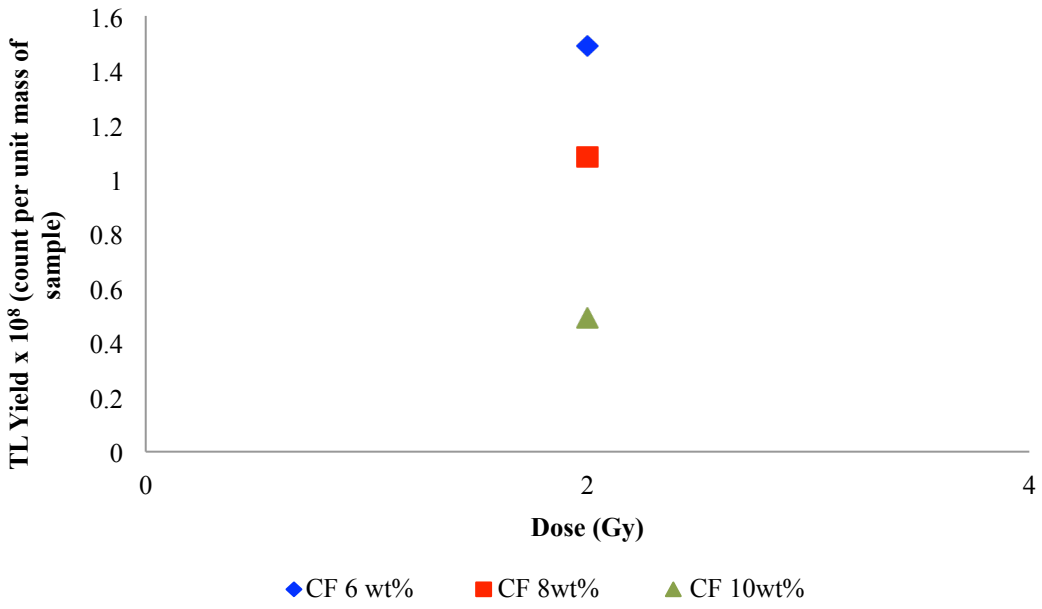

Figure 3-8 The TL response of nominal 6-, 8- and 10 wt% Ge-doped cylindrical fibres of 241 μm diameter, irradiated to a fixed dose of 2 Gy using a Gulmay X-ray machine (Gulmay, UK) operated at a potential of 250 kVp. Prior to irradiation, the fibres were cut to lengths of approximately 5.0 ± 0.1 mm. The irradiations were conducted at the Royal Surrey County Hospital (RSCH). The fibres were then readout 12 hours after irradiation using a TOLEDO TLD reader (Pitman Instruments, Weybridge, UK).

3.3.2 Determination of Oxidation Charge State of Ge-doped Optical Fibres using XPS

Following core-ionization by photoelectron emission, an outer shell electron can fill the created vacancy and the energy released can result in the emission of an Auger electron. The energy of the Auger transition shows dependence on chemical state, more exactly than do the binding energies of the individual electrons involved in the transitions. Therefore, the Auger electrons emitted from surface under the action of X-ray bombardment allows analysis of prominent spectral features and are used to determine the chemical shift (change in binding energy of a core electron of an element due to a change in the chemical bonding of that element) of metal surfaces, referred to as the Auger parameter (α') without interference of surface charging. Originally defined by Wagner [9, 10], the Auger parameter was calculated using (3-2):

$$\alpha' = E_k(C1C2C3) + E_b(C) \qquad \textbf{(3-2)}$$

where $E_k(C1C2C3)$ is the kinetic energy of the Auger transition involving electrons from C1, C2 and C3 core levels and $E_b(C)$ is the binding energy of the core level C. The kinetic energy of the Ge_{LMM} Auger electrons is shown in Fig. 3-9, indicating the kinetic energy value of nominal 8- and 10 wt% preform to be 1137 eV and 1137.40 eV respectively. The observed Ge_{LMM} lineshape and oxidation state shift of nominal 8- and 10 wt% are 2354.39 eV and 2355.48 eV respectively, with respect to pure germanium, indicating that the germanium is predominantly in the form of GeO_2 (+4 oxidation state) within the core [11].

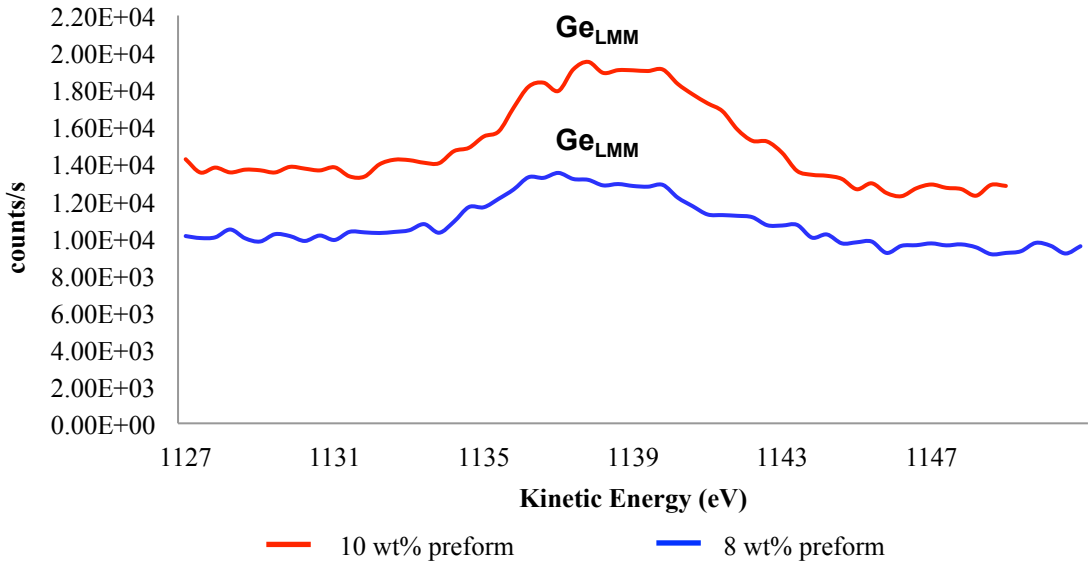

Figure 3-9 High resolution of the kinetic energy for Ge_{LMM} Auger electrons of nominal 8- and 10 wt% preform, showing the kinetic energy to be 1137 eV and 1137.40 eV respectively.

The oxidation state of germanium is of significance because GeO_2 is known to play an important role in the optical fibre performance. The difference in refractive index induced by GeO_2 between the core and cladding structure allows the light signal to propagate as a result of total internal reflection, enabling long distance optical telecommunication. Naturally, oxygen interstitials occupy bond-centered positions of the Ge-Ge bond axis forming a tetrahedral structure similar to silicon. Since the formation energy of GeO_2 is much lower (-106 kJ/mol^{-1}) compared to silicon, the oxygen diffusion rate is higher which leads to increased oxygen-related defects [12]. Mostly, these defects are embedded in an amorphous Si and Ge matrix, being created in the preform during the high temperature fabrication processes.

In recent years, as a result of numerous Ge-doped silica studies, knowledge of oxygen-related defects in Ge has rapidly increased, their signature properties being discussed with emphasis on seeking to understand and utilise these for possible application in optical (e.g. telecoms, sensors), electronic (e.g. semiconductors optoelectric) and dosimetric scenarios.

The oxygen-related defect centre been attributed to a diamagnetic Ge oxygen deficient centre (GODC), and previous research [13, 14] has suggested the most probable microscopic structure is that of a twofold coordinated Ge (=Ge●●), where the (=) represents the bonds with two oxygen atoms, and (●●) denotes a lone electron pair: from this structural model the defect takes the name Ge lone pair centre (GLPC). Previous work [14, 15] has also provided evidence for the presence of GLPC defects induced by ionising radiation where the absorption band peaks

at 5.15 eV, showing two photoluminescence (PL) bands at 4.3 and 3.1 eV. The absorption band has been attributed to an electronic transition from a point defect ground state (S_0) to its first excited singlet state (S_1). The α_E band is attributed to the inverse transition of absorption ($S_1 \rightarrow S_0$) while, in this energy level scheme, the β band is associated with the transition from the first excited triplet state (T_1), supplied by an intersystem-crossing (ISC) process ($S_1 \rightarrow T_1$), to the S_0 state [16, 17]. The other absorption change is the generation of the Ge electron centre (GEC), where an electron is trapped at a fourfold coordinated Ge site. Some defects providing absorption at 5.1 eV strongly contribute to the generation of the paramagnetic centres, referred to as Ge(1) and Ge(2). Fujimaki et al. [14] has explained in detail the generation mechanism of the GEC in Ge-doped SiO_2 glass through absorption and ESR measurements with three different photon sources (exposed to ultraviolet photons from a KrF excimer laser (5.0 eV), a XeCl excimer lamp (4.0 eV), and a KrCl excimer lamp (5.6 eV), proving electrons are released from the GLPCs and the GEC are generated. From this investigation, two paramagnetic centres, named Ge(1) and Ge(2) were induced with the KrF excimer laser. In addition, the 4.0 eV photons from the XeCl excimer lamp induce only a $GeE^{'}$ centre. From these results, Ge(1) and Ge(2) and the positively charged Ge oxygen deficient centre $(GODC)^{+}$, which donated an electron to the GEC.

The GODC formation is accounted for by internal stresses. In the stressed regions, regular bonds are ruptured to produce pairs of oxygen-deficient and oxygen redundant centres. Germanium atoms in SiO_2 directly substitute for the silicon atoms in crystalline quartz, as the Ge^{4+} ion is isoelectronic with Si^{4+}, so only the 4+ valence state is present before irradiation. This indicates that GODC is an electron donor. Studies at 77K [18] have found that the GeO_4 tetrahedra that trap electrons in x-irradiated Ge-doped silica glass, denoted Ge(1) and Ge(2), possess a degree of quartz-like local structure. All of these defects result from trapping of radiation-induced electrons on substitutional Ge^{4+} ions present in the original diamagnetic materials. These features suggest that the main generation mechanism of twofold coordinated Si defects involves the displacing of O from bonding configuration, due to knock–on or radiolysis processes. Such a generation process should depend on the structure of the material (for example on the strength of Si-O bonds).

Fig. 3-10 (a) shows the Ge2p3/2 photoelectron spectrum of the optical preform sample. By fitting the measured spectrum, the binding energy of the Ge was found to be 33.32 eV with a FWHM of about 3.02 eV. Comparing this energy with elemental Ge3d of 29.1 eV [19], the energy is shifted to about 4.22 eV. According to Schmeisser [20], an average chemical shift per oxidation state for Ge3d core level is about 0.85 eV which brings about an oxidation state of greater than 4. From Fig 3-10 (b), the O2s photoelectron is found at 25 eV, about 1 eV more

than the typical value [21]. The quantitative ratios of the photoelectron peak intensity yields a [O/Ge] ratio of about ~3.3 for the present material.

Under high temperature fabrication, the mobility of Ge atoms is increased thus allowing transformation to GeO_x states. Therefore, during prolonged treatments at this temperature, GeO_x precipitates are easily formed. However when heat is suddenly removed, the GeO_x form 'strained GeO_2' to achieve equilibrium states. This leaves vacancies (Frenkel defects), which are responsible for the formation of GEC and GODC centres.

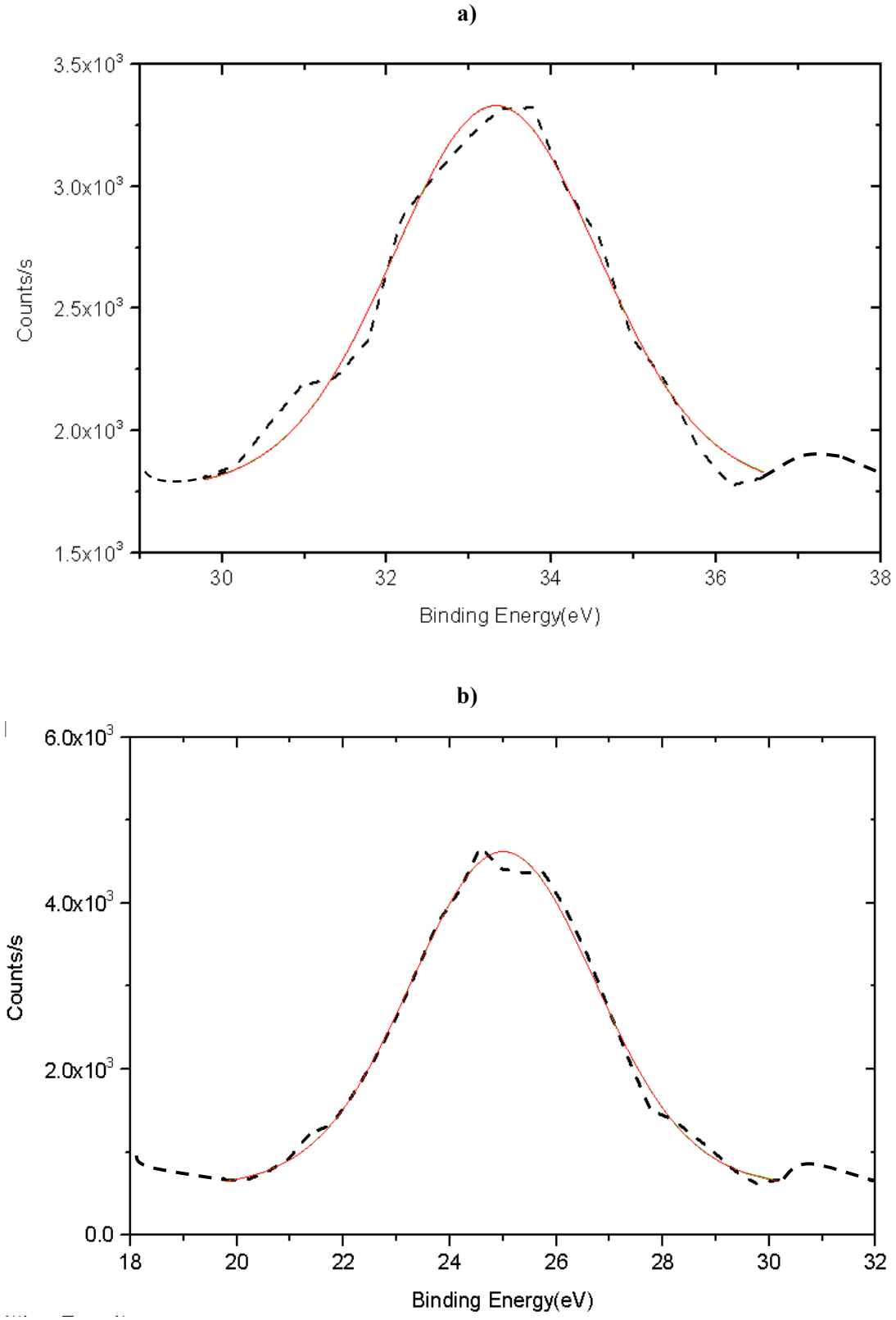

Figure 3-10 (a) The X-ray photoelectron for Ge2p3, (b) O2s. The dotted line is the subtracted counts per second using the Shirley background and the solid line is the fitted curve [22].

3.4 Summary of XPS Analysis of Doped Optical Fibres

Studies using X-ray Photoelectron Spectroscopy (XPS) been used, to investigate the surface chemical charge state of a Ge-doped SiO_2 optical preform. The binding energy of Si2p and Ge2p3/2 of nominal 8 wt% preform were found to be 99.80 eV and 1217.39 eV respectively, the atomic percentages from the XPS analysis being 18.70% and 0.82% respectively. The measurement has been repeated to investigate the reproducibility of the MCVD process using nominal of 10 wt% preform, resulting in binding energies of 100.20 eV and 1218.08 eV for Si2p and Ge2p3/2 respectively, with respective atomic percentages of 15.20% and 0.49%. The observed Ge_{LMM} lineshape and oxidation state shift of nominal 8- and 10 wt% performs of 2354.39 eV and 2355.48 eV respectively with respect to pure germanium, indicate the dopant to be in the predominant form GeO_2 (+4 oxidation state) within the core. Comparison studies have been conducted on non-annealed and annealed capillary fibres, the latter of these indicating the presence of less hydrocarbon components thus elevating the Ge2p3/2 electrons from the surface layer. The capillary fibres used herein were washed in acetone in an ultrasonic bath, advantageously removing surface contamination species resulting from sample handling and fibre pulling.

3.5 References

[1] Kai Siegbahn et al., ESCA: Atomic, Molecular and Solid State Structure studied by means of Electron Spectroscopy, Uppsåla (1967)

[2] A. L. Yusoff, R. P. Hugtenburg, and D. A. Bradley, "Review of development of a silica-based thermoluminescence dosimeter," *Radiat. Phys. Chem.*, vol. 74, no. 6, pp. 459–481, Dec. 2005.

[3] S. J. Hinder, C. Lowe, J. T. Maxted, C. Perruchot, and J. F. Watts, "Intercoat adhesion failure in a multilayer organic coating system: An X-ray photoelectron spectroscopy study," *Prog. Org. Coatings*, vol. 54, no. 1, pp. 20–27, Sep. 2005.

[4] A. Shinozaki, K. Arima, M. Morita, I. Kojima, and Y. Azuma, "FTIR-ATR evaluation of organic contaminant cleaning methods for SiO2 surfaces.," *Anal. Sci.*, vol. 19, no. 11, pp. 1557–1559, 2003.

[5] K. Choi, T. J. Eom, and C. Lee, "Comparison of the removal efficiency for organic contaminants on silicon wafers stored in plastic boxes between UV/O3 and ECR oxygen plasma cleaning methods," *Thin Solid Films*, vol. 435, no. 1–2, pp. 227–231, 2003.

[6] J.F. Watts and J. Wolstenholme. "An introduction to surface analysis by XPS and AES." pp. 224. ISBN 0-470-84713-1. Wiley-VCH, May 2003.

[7] S. Tanuma, C. J. Powell, D. R. Penn: Surf. Interf. Anal.,Vol. 21, 165 (1994)

[8] A. Alessi, S. Girard, C. Marcandella, M. Cannas, a. Boukenter, and Y. Ouerdane, "Raman investigation of the drawing effects on Ge-doped fibers," *J. Non. Cryst. Solids*, vol. 357, no. 1, pp. 24–27, 2011.

[9] C.D. Wagner, Electron Spectroscopy, in: D.A. Shirley (Ed.), Proceedings of an International Conference held at Asilomar, Pacific Grove, California, USA, 7-10 September, 1971, North-Holland, Amsterdam, 1972, p. 861

[10] C.D. Wagner, "Auger lines in X-ray photoelectron spectrometry", Analytical Chemistry, vol. 44, no. 6, pp. 967-973, (1972).

[11] C.D. Wagner, "Chemical shifts of Auger lines, and the Auger parameter." Faraday Discussions of the Chemical Society **60**(0): 291-300, (1975).

[12] V. Markevich, a. Peaker, J. Coutinho, R. Jones, V. Torres, S. Öberg, P. Briddon, L. Murin, L. Dobaczewski, and N. Abrosimov, "Structure and properties of vacancy-oxygen complexes in Si1-xGex alloys," *Phys. Rev. B*, vol. 69, no. 12, pp. 1–11, 2004.

[13] K. Awazu, H. Kawazoe, and M. Yamane, "Simultaneous generation of optical absorption bands at 5.14 and 0.452 eV in 9 SiO2: GeO2 glasses heated under an H2 atmosphere," *J. Appl. Phys.*, vol. 68, no. 6, pp. 2713–2718, 1990.

[14] M. Fujimaki, T. Watanabe, T. Katoh, T. Kasahara, N. Miyazaki, and Y. Ohki, “Structures and generation mechanisms of paramagnetic centers and absorption bands responsible for Ge-doped SiO_2 optical-fiber gratings,” vol. 57, no. 7, pp. 3920–3926, 1998.

[15] A. Alessi, S. Agnello, F. M. Gelardi, S. Grandi, A. Magistris and R. Boscaino, "Twofold coordinated Ge defects induced by gamma-ray irradiation in Ge-doped SiO_2", *Optics Express*, Vol. 16, No. 7, pp. 4895- 4900, March. 2008

[16] M. Leone, S. Agnello, R. Boscaino, M. Cannas, and F. M. Gelardi, “Optical absorption, luminescence, and ESR spectral properties of point defects in silica,” in Silicon-based Materials and Devices: Properties and Devices, H. S. Nalwa, ed., (Academic Press, San Diego, 2001).

[17] L. Skuja, “Isoelectronic series of twofold coordinated Si, Ge, and Sn atoms in glassy SiO_2: a luminescence study,” *J. Non Cryst. Sol.* vol. 149, pp. 77-95, 1992.

[18] T. E. Tsai, D. L. Griscom, and E. J. Friebele, "On the Structure of Ge-Associated Defect Centres in Irradiated High Purity GeO_2 and Ge-doped SiO_2 Glasses", *Diffus. Defect Data*, vol. 53–54, pp. 469-476, 1987

[19] NIST XPS database for the selected elements. http://srdata.nist.gov/xps/EngElmSrchQuery.aspx?EType=AP&CSOpt=Retri_ex_dat&Elm=Ge. Accessed on 13 November 2014.

[20] E. V. Anoikin, A. N. Guryanov, D. D. Gusovskii, V. M. Mashinskii, S. I. Miroshnichenko, V. B. Neustruev, V. A. Tikhomirov, and Yu. B. Zverev, "Photoinduced defects in silica glass doped with germanium and cerium" *Sov. Lightwave Commun.,* vol. 1, pp. 123-131, 1991

[21] D. L. Griscom, “Trapped-electron centers in pure and doped glassy silica: A review and synthesis,” *J. Non. Cryst. Solids*, vol. 357, no. 8–9, pp. 1945–1962, Apr. 2011.

[22] K. Axis, “Peak Fitting in XPS,” *Bioengineering*, pp. 1–29, 2006.

Chapter 4

4 Particle Induced X-ray Emission (PIXE) Analysis of Doped Optical Fibres

4.1 Introduction

Most of the content of this chapter is published in the journal of X-ray Spectrometry: "S. F. Abdul Sani, G. W. Grime, V. Palitsin, G. A. Mahdiraji, H. A. Abdul Rashid, M. J. Maah and D. A. Bradley, 2015. Micro-PIXE analysis of doped SiO_2 fibres intended as TL dosimetrt for radiation measurements 44: 33-40" and in the journal of Lightwave of Technology: "S.F. Abdul Sani, G. Amouzad Mahdiraji, A.S Siti Shafiqah, G.W. Grime, V. Palitsin, S.J. Hinder, N. Tamchek, H.A Abdul Rashid, M.J. Maah, J. F. Watts and D.A. Bradley. 2015. XPS and PIXE analysis of doped silica fibre for radiation dosimetry" (Appendix B). The right to include the article in any thesis or dissertation has been obtained during assignment of copyright with the publisher.

In general, X-ray emission analysis involves both a means of exciting the atoms of a sample, emitting characteristic X-rays caused by bombardment of ions (MeV protons) and a means of detecting and identifying these X-ray emissions so that their intensities can be converted to elemental concentrations in the sample. The potential advantages of the Particle Induced X-ray Emission (PIXE) method, other than its generally non-destructive nature, is the availability of simultaneous multi-elemental analysis of element of atomic number ≥ 11, the short data collection time and the very low background, avoiding primary bremsstrahlung production, with parts per million (ppm) lower detection limits [1]. Given the greater mass of protons relative to electrons, there is less lateral deflection of the beam, a matter which can be used to great benefit in support of the microbeam technique, providing for imaging and elemental mapping at a spatial resolution of about 1 μm. PIXE combines a particular and unique set of advantageous features, but as with any technique, it also has its limitations. The main limitation is in the absolute quantification of PIXE elemental concentrations it suffers from spectral interferences and matrix effects. Added to this is the fact that it does not allow for the direct measurement of ultratrace elements that are present at nanograms per gram levels. The use of simultaneous Rutherford Back Scattering (RBS) analysis can overcome this problem by providing the ratio between the true charge and the measured charge (the so-called 'Q factor').

After obtaining the 'Q factor', the PIXE data can be normalized to provide for accuracy of 5-10% in most cases. Details of the acquisition system have been described by Grime and Dawson [2] and Grime [3].

To-date, only limited research has been conducted towards gaining an essential understanding of the magnitude of the TL signal and material characteristics of doped fibres. The work of Yusoff et al. [4], is an example of one, concerning TL yield and structural characteristics of sol-gel glass. Present interest concerns analysis of Ge-doped SiO_2 fibres intended as high spatial-resolution thermoluminescence (TL) dosimeters for radiation measurements in place of their more typical applications in telecommunications. Dopant diffusion in optical fibres is fundamentally important, determining both the transmission properties of the fibre and in defining the eventual TL yield of the medium. In regard to optical fibres production, germanium is the dopant that has been most frequently reported in diffusion studies. Diffusion of Ge in silica optical fibre has also been observed during splicing, manufacture of fused fibre couplers as well as fibre drawing [5]. PIXE analysis detects characteristic X-rays generated in the sample by MeV ions, usually protons or sometimes alpha particles. Characteristic X-rays produced in PIXE analysis provide information concerning the relative distribution of elements within a sample, as in for instance Ge and Si concentrations, the Ge acting as point defect centres that promote TL.

For doped silica fibres, to establish an underpinning basis for the TL yield, we wish to define the extent of diffusion of the Si and Ge in the core and inner cladding of single-mode optical fibre. In turn, this reflects the underlying influence of fibre-drawing and subsequent heat treatment processes. With the dopant tending to diffuse in and away from the fibre core, it is essential to define the sample matrix composition in order to accurately evaluate the X-ray yield. This is determined in part using simultaneous Rutherford Back Scattering (RBS) analysis. The over-arching aim of the project is to improve SiO_2-fibre TLD performance through control of the processes of fabrication. In support of this, and to ascertain dopant concentrations of tailor-made fibres of cylindrical fibres (CF), flat fibres (FF) and photonic crystal fibres (PCF) that have been fabricated at the University of Malaya, ion beam study has been undertaken using a combined microbeam proton-induced x-ray emission (PIXE)/Rutherford Back Scattering (RBS) analysis arrangement.

4.2 Experimental Procedure

4.2.1 Sample Preparations

The Ge-doped optical fibres have been cut into approximate 2.0 ± 0.1 cm lengths using an optical fibre cleaver (Fujikura, Japan). Preparing for irradiation, the optical fibres, attached to a silicon substrate, were embedded in a 25 mm diameter circular resin casting as shown in Fig 4-1(a). The mould was filled with a liquid synthetic resin made of Durocit Liquid and Durocit Powder (see Fig. 4-1(b)), which then hardened to form what is referred to as a cold mounting resin (Struers, Denmark). Clips were used to hold the samples in the resin to prevent them from floating in the initial resin solution (Fig. 4-2). For the hardened resin, Struers Pedemax-2 (Fig. 4-3) a rotating circular lapping machine was used, to grind the resin blocks in order to present a flat cross section to the beam and to customize the blocks to the desired thickness (~15 mm).

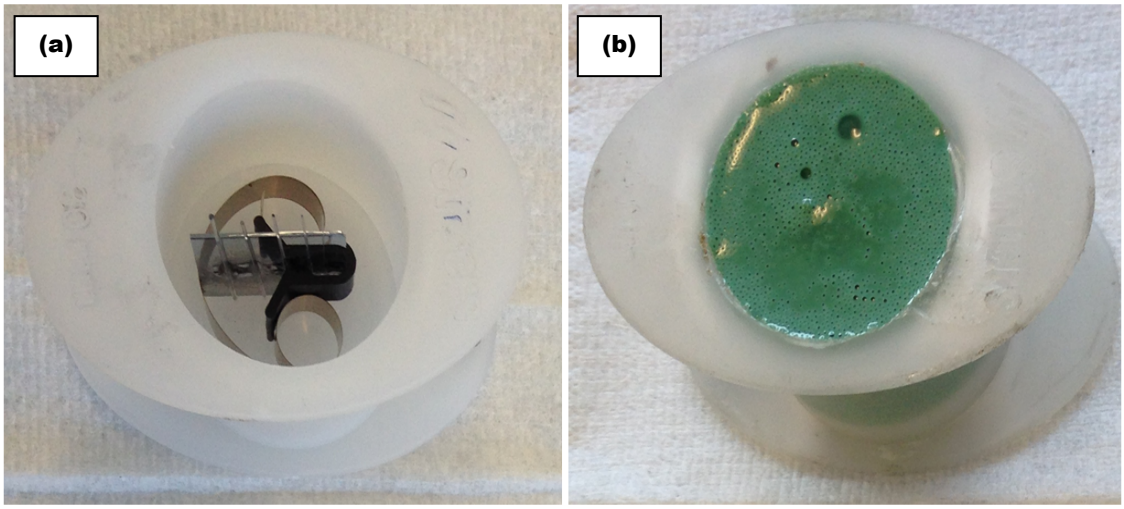

Figure 4-1 a) 2.0 cm length fibres were contained within the silicon substrate, being fixed with retaining clips; b) a mixture of Durocit Liquid and Durocit Powder (Struers, Denmark) was filled into the mould.

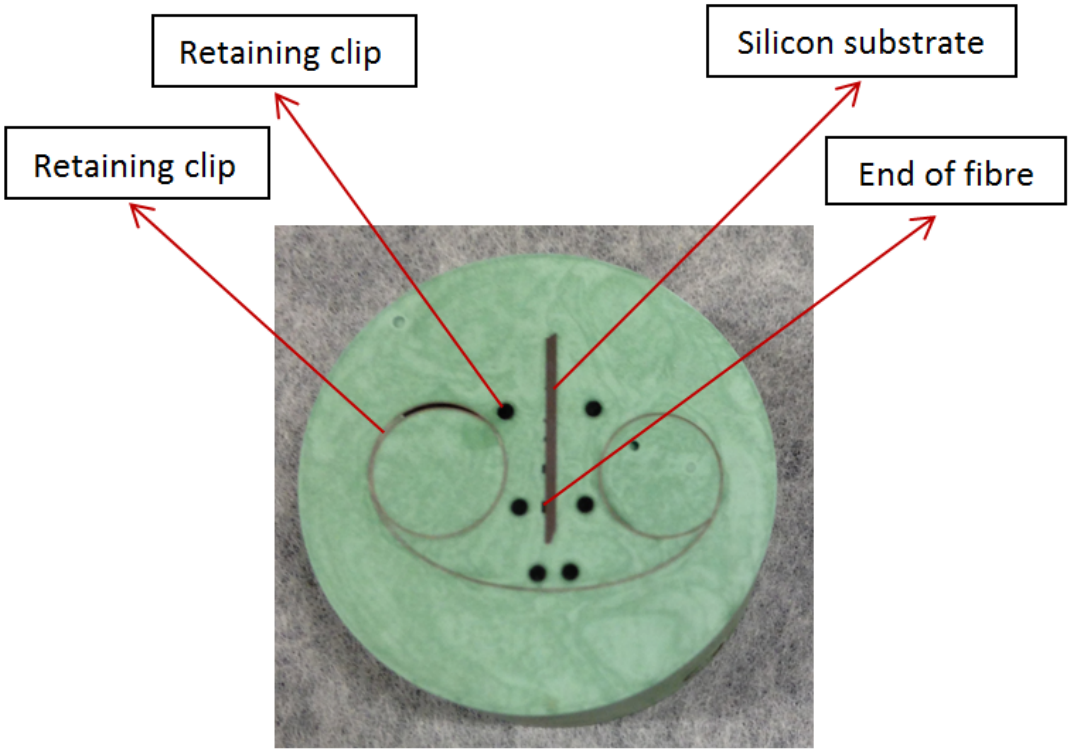

Figure 4-2 Optical fibres were implanted in circular resin blocks for PIXE analysis. The large black dots are the only visible part of retaining clips that are embedded in the resin to prevent the fibres from floating in the initially non-solid resin. The other item seen in the figure is a circular retaining clip, also being introduced to prevent the fibres from floating. Barely visible along the left-hand edge of a centrally-located linear silicon substrate are the ends of the fibres under investigation, appearing as small dots; the silicon substrate was required in order to provide a more rigid structure that would allow the face of the resin blocks to be ground into a flat surface without flexing of the fibres.

Figure 4-3 Pedemax-2 was employed for sample preparations. The rotating circular lapping machine is featured in this photograph; a disc of fine abrasive medium is attached to the lapping surface such that with even pressure a polished flat surface to the sample assembly can be achieved.

In order to minimize sample charging, conductive adhesive tape was fixed to the surface of each resin block, leaving a small window around the samples in the block. Three nominal 4% weight Ge-doped SiO_2 fibres of 125.0 ± 2.0 µm diameter were the first such fibres to be investigated by PIXE analysis; the dimensions of nominal 6% and 8% weight for both Ge-doped cylindrical fibres and flat fibres are detailed in Table 4-1.

Table 4-1. Dimensions of nominal 6- and 8% weight Ge-doped SiO_2 fibres used in PIXE analysis.

Sample Dimension	***Fibre Type***	
	Cylindrical Fibre (CF) (µm)	**Flat Fibre (FF) (µm)**
Sample 1	604 ± 30	200 x 750 ± 20
Sample 2	483 ± 20	165 x 620 ± 20
Sample 3	362 ± 10	100 x 350 ± 20
Sample 4	241 ± 10	85 x 270 ± 5
Sample 5	120 ± 10	60 x 180 ± 5

4.2.2 Microbeam Setup

The University of Surrey supports the Engineering and Physical Sciences Research Council (EPSRC) national ion beam facility. The microbeam facility used herein is based on a 2MV Tandetron™ accelerator, described in detail by Simon et al. [6]. The samples were irradiated on the microbeam line (Fig. 4-4 and 4-5) to 2.5 MeV protons with the beam oriented normal to the sample, comprising a spot size of 2 × 2 μm, and measured using a copper grid (Fig. 4-6) and a proton current in the range 0.3 – 0.8 nA. The resin blocks were mounted inside the target chamber (Fig. 4-7), which was designed to include a moving sample stage and can be used for simultaneous PIXE and RBS analysis. The characteristic X-ray photon emissions were detected using a SGX Si–Li detector (Sensortech Ltd, High Wycombe, UK) of 80 mm^2 active area and 140 eV energy resolution at 5.9 keV, mounted at a scattering angle of 45° to the beam. In order to reduce the intensity of the Si K_α X-rays and to avoid spectrum degradation by high energy recoiling protons, the Si–Li detector was fitted with a two-layer absorber consisting of 130 μm thick beryllium foil and 50 μm thick Kapton foil.

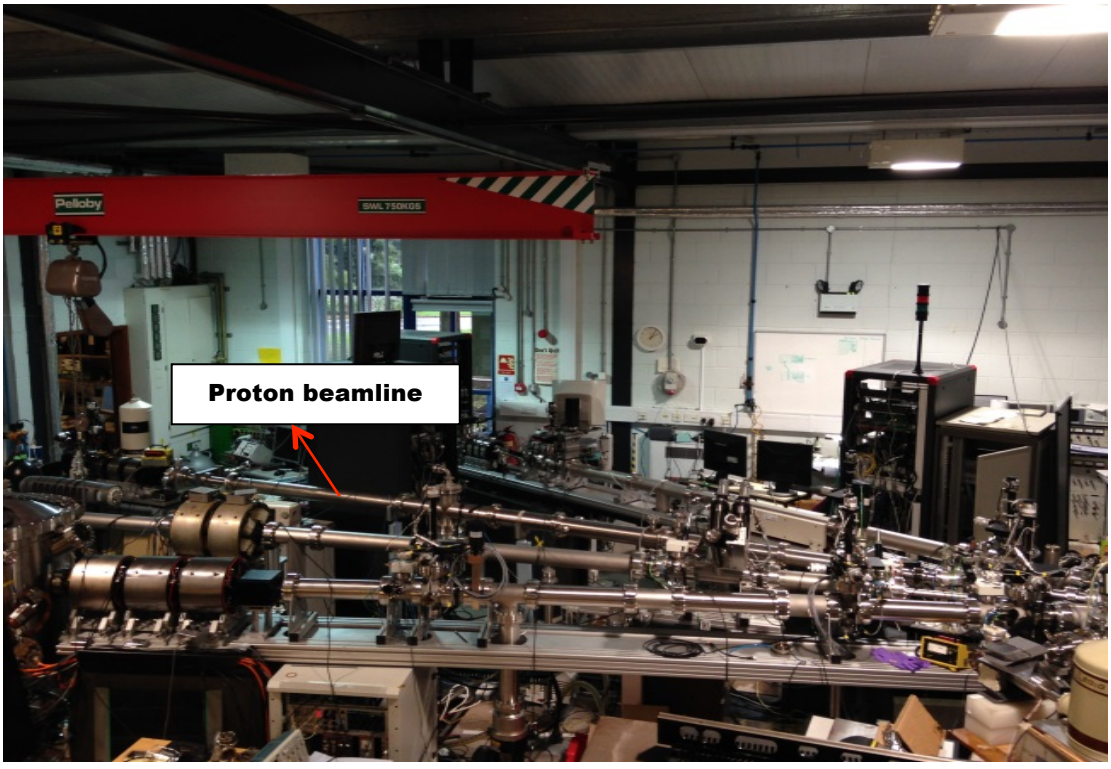

Figure 4-4 The beamlines situated in the Surrey Ion Beam Centre.

Figure 4-5 The High Voltage Engineering Europe 2.0 MV Medium Current Plus Tandetron™ accelerator providing 2.5 MeV protons. The facility is situated in the Surrey Ion Beam Centre.

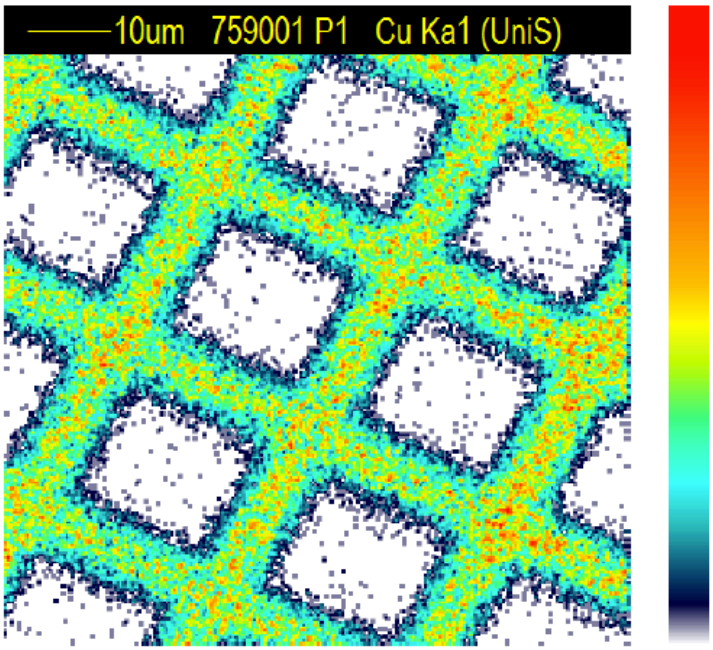

Figure 4-6 A copper grid mounted on a quartz substrate was scanned to demonstrate the beam size. The distance between the 10% and 90% points on the edges of the bars was estimated to be ~2 μm, placing an upper limit on the beam diameter, assumed to be less than this. The 'heat bar' to the right indicates the relative intensity of features in the image.

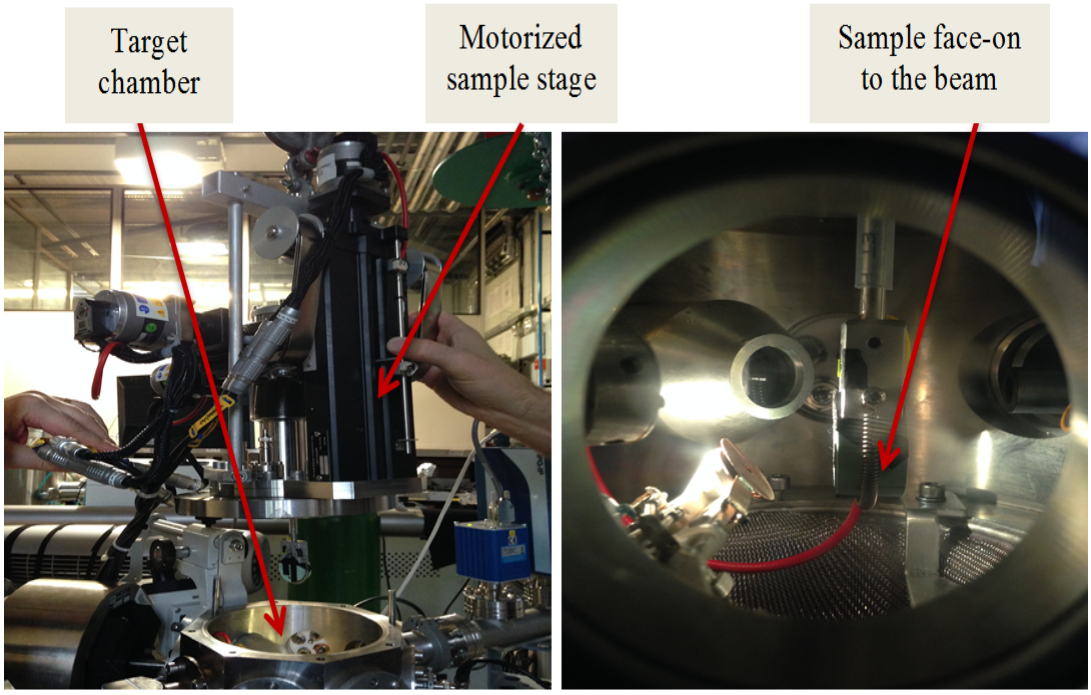

Figure 4-7 In the left-hand panel a fibre sample embedded in resin is lowered into the target chamber, while in the right-hand panel the fibre sample is aligned at the sample position of the microbeam line, ready for proton irradiation. The view is taken through one of the transparent port windows.

Scanning was carried out over the cross-sectional area of the optical fibres implanted in the resin block, producing a pixel-by-pixel map of the sample elemental composition. For each sample, elemental maps were collected for localisation, and then, a line of points was set up in order to obtain the required concentration profiles. This was performed in preference to a continuous line scan along the profile because this allows the local sample matrix composition to be determined at each point, permitting more accurate analysis. Although this is superficially a simple system (only three atoms, Si, O and Ge), PIXE spectrum processing is complicated by the fact that in the high concentration regions of the sample, the yield of the Ge K lines is strongly affected by self-absorption, and so the Ge concentration must be determined independently or an iterative process must be used. Because the O is not visible in the PIXE spectra and it is not possible to iterate assuming atomic stoichiometry, RBS was used to provide an independent measurement of Ge. Pairs of simultaneously collected RBS and PIXE spectra were processed using the 'Q factor' method [3] implemented in the software OMDAQ2007 [7]. In this method, the actual beam charge and the local sample matrix (both of which are required for accurate thick target PIXE analysis) are calculated from the RBS spectrum and transferred automatically to the PIXE processing software within OMDAQ2007. The method requires a determination of the ratio of solid angles of the PIXE and RBS detector and also the parameters used in the model of the variation of the PIXE detector efficiency with X-ray energy. This is

performed during each run as part of the setting-up process using a standard reference material (lead glass BCR 126A [8]) as described in the study of Gomez-Morilla et al [9]. RBS spectra were fitted using the simulation module of OMDAQ2007, which incorporates non-Rutherford cross sections. The PIXE spectra were processed using GUPIX (Guelph University PIXE Group GUPIX and GUPIXWIN Department of Physics University of Guelph Guelph, Ontario, Canada N1G 2W1) [10] accessed via the automated OMDAQ2007 user interface. Fig. 4-8 shows PIXE and RBS spectra for a high Ge concentration region. OMDAQ2007 provides real-time spectrum quality monitoring, and so, each point was analysed until the statistical precision of the Ge K_{α} line area evaluation was better than 5% and the total number of counts in the RBS spectrum was greater than 50000 or for a maximum of 10 min. With the beam currents available, this corresponds to an accumulated charge of up to 300 nC.

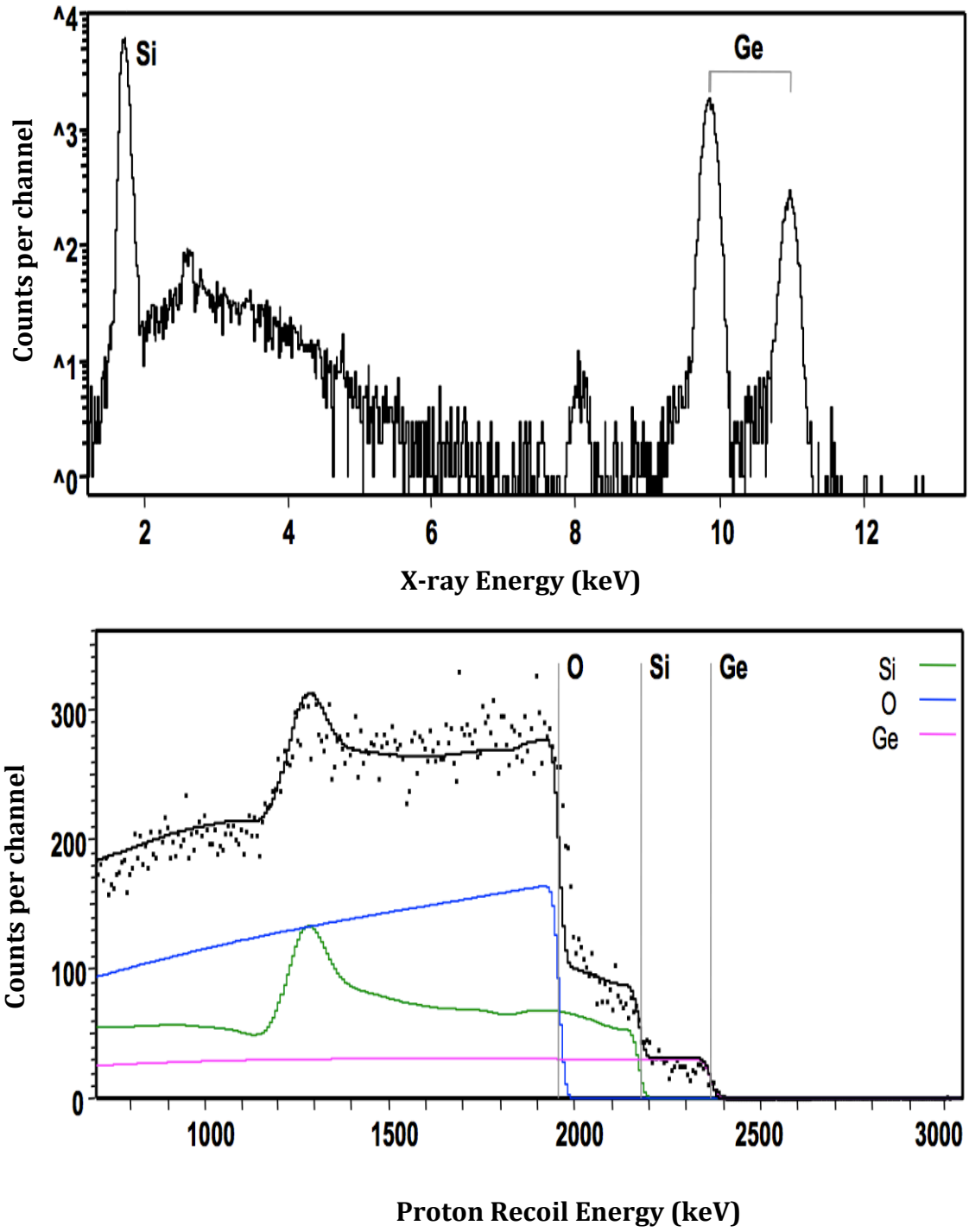

Figure 4-8 PIXE (top) and RBS spectra (below) for a point in a high Ge concentration region of a doped SiO_2 fibre (Si 42%, Ge 9.5%, O 42% w/w). In the RBS spectrum, the surface energies of O, Si and Ge are marked and the solid lines show the fit calculated using OMDAQ2007. (The coloured lines are the partial spectra for each element). The total run time was 2.5 minutes using a beam current of ~150 pA of 2.5 MeV protons corresponding to a beam dose of 22.5 nC.

4.3 Determination of Dopant Concentration for CF and FF

4.3.1 Results and Discussion

Typical PIXE and RBS spectra for a cylindrical fibre of 604 µm diameter, obtained with a 2.5 MeV proton beam, are shown in Figure 4-8. Similar PIXE and RBS spectra were obtained for the other cylindrical fibres and flat fibres investigated herein. Fig. 4-9 represents the elemental maps of Si and Ge for both cylindrical and flat fibres. PIXE and RBS analysis also detected the presence of other elements, including P and Al, due in part to contamination from the fibre pulling facility. However, the concentration of these elements has been found to be relatively small (nowhere greater than ~0.5%) and as such can be considered to have little effect upon the TL yield of these fibres.

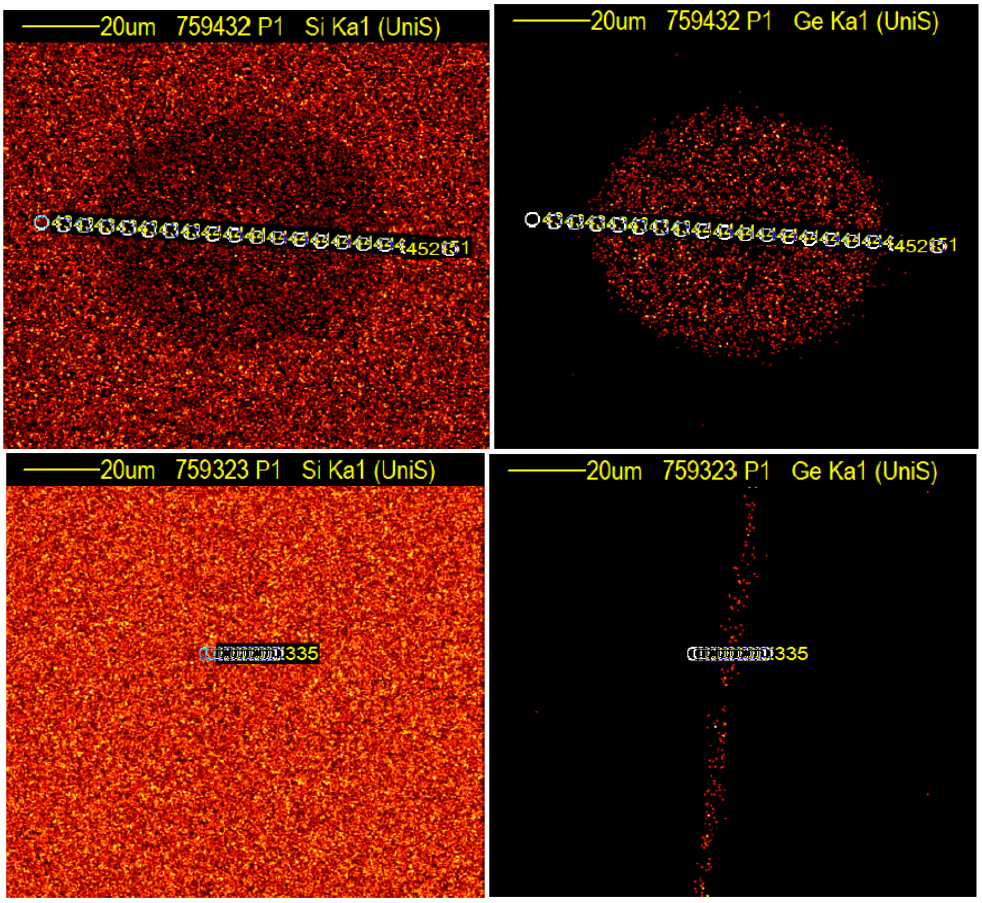

Figure 4-9 Typical elemental maps across the transverse cross section of a SiO_2 cylindrical fibre, 483 µm outer diameter (top) and flat fibre, 165 x 620 µm (bottom), showing the relative presence of the identified elements, from left to right, the images depicted Si (cladding region) and Ge (core region) respectively. Also identified are the lines along which the point data were obtained.

The Ge distribution in the fibres, centrally located as designed, diffuses away from the centre into the fibre cladding, extending out to Ge concentrations measurable to well below 0.1 mol %, strongly dominated by Si in all cases. In the centre of the fibre, a pronounced dip in the Ge concentration is observed (Fig. 4-10 (b)(c)(d)(e) and Fig. 4-11(a)(b)(c)(d)), mirroring that seen in the refractive index profile, again attributed to Ge diffusion, in line with Ge chemistry temperature dependency [5]. Further, in many cases there are one and sometimes two peaks in Si concentration, almost certainly due to $SiCl_4$ vapour deposition and its variations, typically with co-location discrepancies with the Ge dip of the order of 2 to 5 μm, as seen in Fig. 4-10 to 4-11. These illustrate some of the points discussed above.

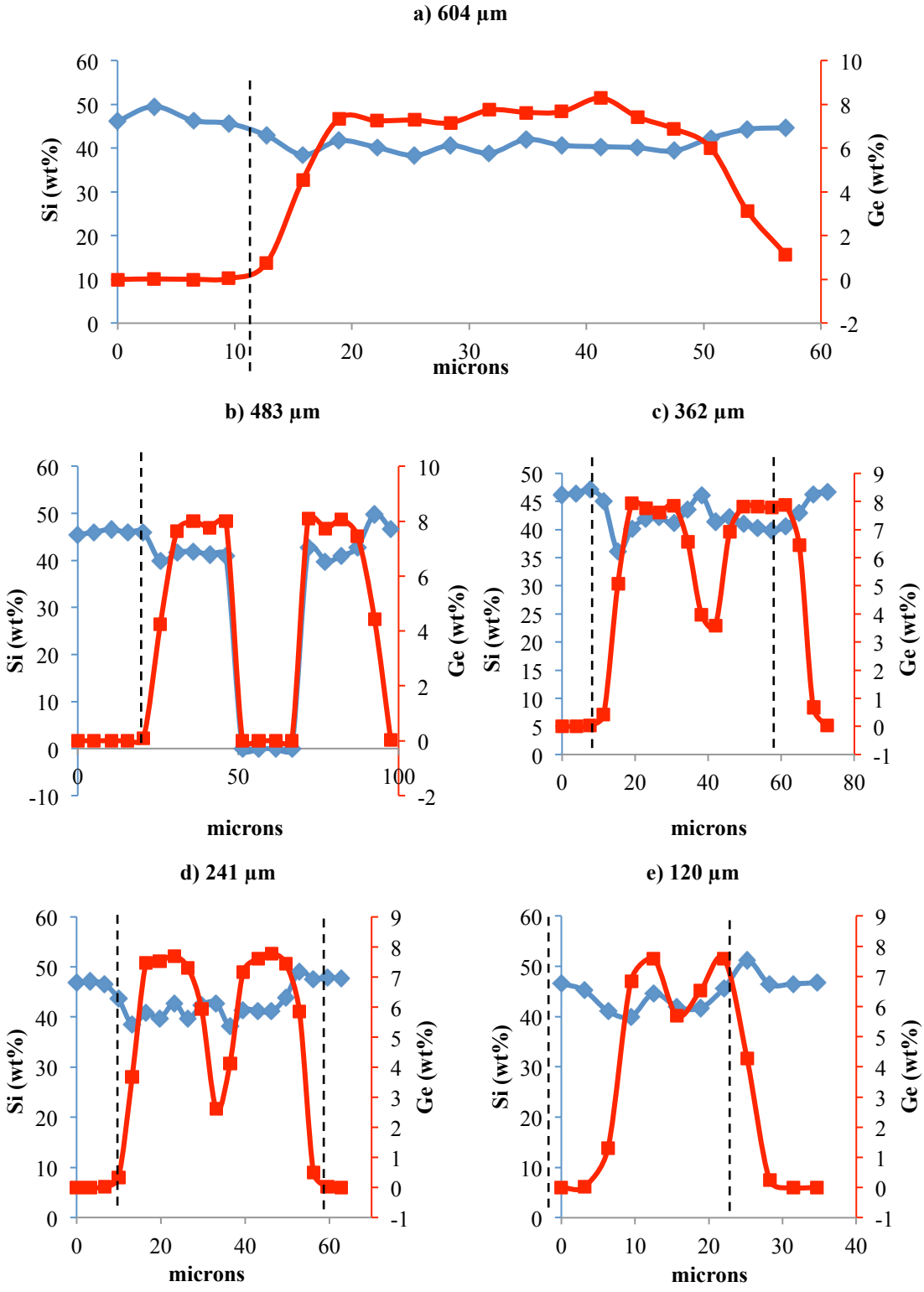

Figure 4-10 The distribution of Si (in blue) and Ge (in red) along a line scan for nominal 6 % weight Ge-doped cylindrical fibres of different dimension: a) 604 µm; b) 483 µm; c) 362 µm; d) 241 µm; e) 120 µm. The data for the largest fibre i.e. that represented in (a) is clearly for one half of the core diameter, the full data showing symmetry between one half and the other, as in (b) – (e). The boundary lines (black dashed) indicate the region between the core and cladding of the Ge-doped cylindrical fibres.

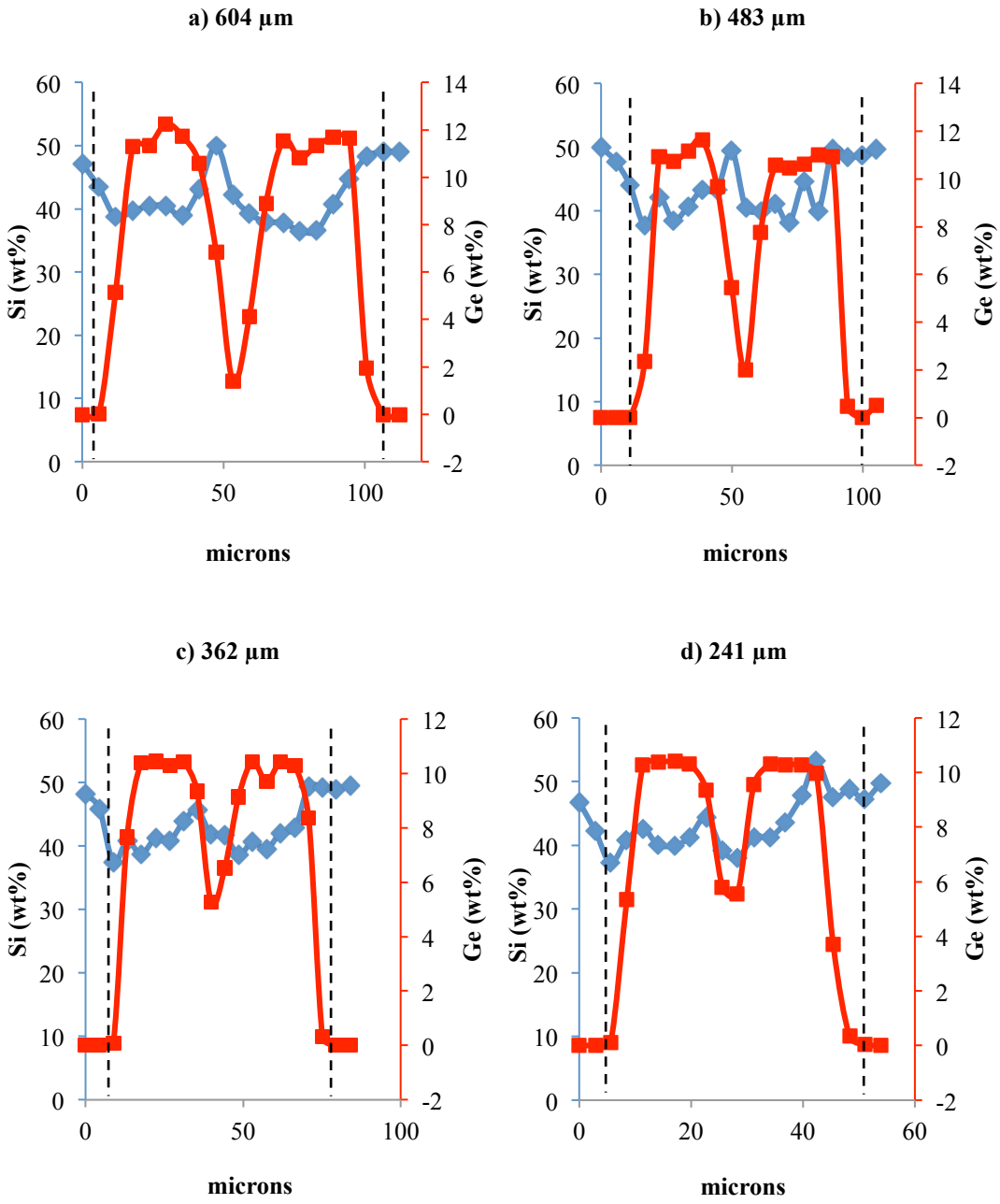

Figure 4-11 The distribution of Si (again in blue) and Ge (in red, as before) along a line scan for nominal 8 % weight Ge-doped cylindrical fibres: a) 604 µm; b) 483 µm; c) 362 µm; d) 241 µm. The boundary lines (black dashed) indicate the region between the core and cladding of the Ge-doped cylindrical fibres.

Also, as previously mentioned, there are challenges in terms of the increasingly brittle nature of the glass with increasing dopant concentration, the predominant effect being illustrated in Fig. 4-12. Here we note that drawing of optical fibres of greater Ge concentration requires elevated drawing temperatures (by some 10-20 °C) compared to similar fibres of lower dopant concentration. This is perhaps best illustrated in efforts towards

fabricating 8% weight Ge FF, incomplete closure of the inner bore to the glass fibre resulting, as shown in Fig. 4-12(a). Using the same drawing conditions for 6% weight Ge doped FF (Fig. 4-12(b)) lead to a fully-closed situation. We have therefore only used 6 % weight Ge flat fibres in investigations herein. The dips may also be due in part to the evaporation of GeO_2, occurring due to the relatively low vapour pressure of GeO_2 compared to that of SiO_2 (Zulkifli et al., 2013).

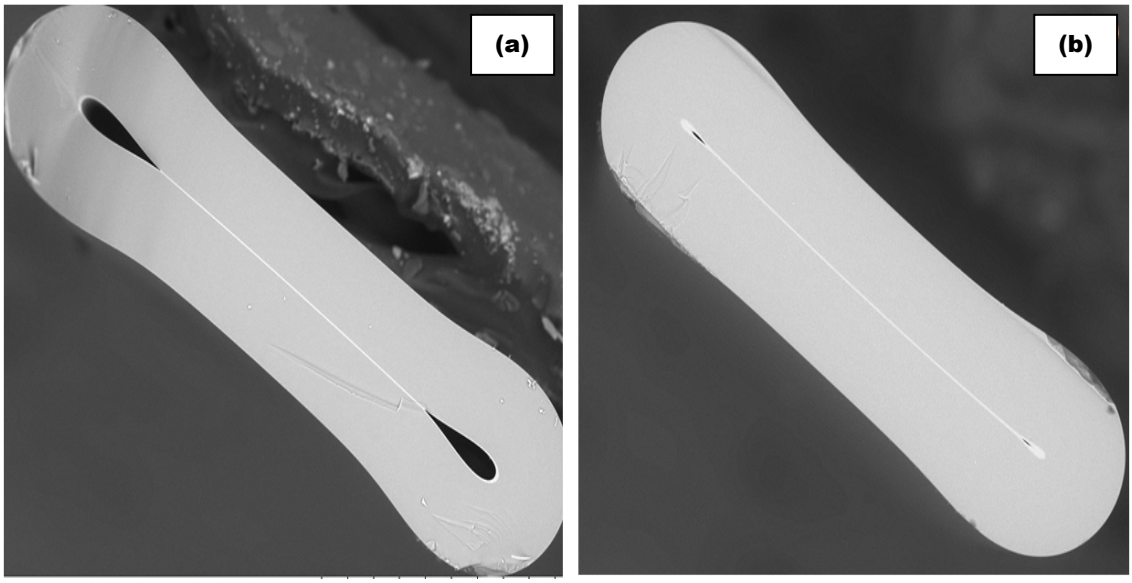

Figure 4-12 FF cross section imagesof two fibres fabricated using identical drawing parameters (a) 8% weight Ge doped FF, with two remaining holes (to be referred as 'eye region') and (b) 6% weight Ge doped FF, the interface being now fully closed.

The results of PIXE/RBS analysis of Ge concentrations in SiO_2 fibres nominally doped to 4-, 6- and 8 % weight are presented in Table 4-2, it being noted by Lyytikainen et al. [5] that dopant distribution in the fibres is affected by temperature during manufacture of fused fibre couplers and by fibre drawing. It is also apparent from Table 4-2 that the shape of fibre strongly influences the variation in Ge concentration in the fibres, specifically in the FF.

Table 4-2 Summary PIXE analysis for fibres of nominal Ge concentrations 4-, 6- and 8 % weight.

Sample No	*Ge dopant concentration (wt%)*	*Sample Dimension*	*Ge dopant concentration (wt%)*		
	4%		**6%**		**8%**
	CF		**FF***	**CF**	**CF**
1	0.87 - 1.25	**Sample 1**	2.43 - 6.55	6.01 - 8.29	10.61 - 12.25
		Sample 2	0.95 - 1.14	7.47 - 8.10	10.48 - 11.62
2	2.45 - 4.56	**Sample 3**	0.15 - 0.17	6.44 - 7.92	10.27 - 10.43
		Sample 4	0.07 - 0.10	7.31 - 7.79	10.38 - 10.42
3	3.10 - 4.26	**Sample 5**	0.07 - 0.12	6.53 - 7.59	-

*Note: As discussed in the text, the FF results are manifestly compromised by the 2 μm spatial resolution. Future further investigation could be useful, use being made of the nm resolution beam line at the Surrey ion beam centre.

With the core region in the flat fibres being highly central and thinly distributed along the width of the fibre, results are clearly expected to show only a very narrow Ge-rich core thickness in the collapsed region. As such, with a scanning resolution of ~2 um, very few scanned points were obtained in the centre of the FF, as seen in Fig. 4-13. Thus, due to the limited spatial resolution, the true peak Ge concentration may not have been obtained. Applying a curve fitting interpolation based on the three points (Fig. 4-13) that are central to the Ge distribution curve would suggest the Ge in the central core to be slightly higher than the evaluated value of 6.55 shown in Table 4-2. The same problem would also be expected to prevail for the Ge core thickness of the other FF samples, becoming increasingly acute with decrease in FF dimensions, the extreme of which would be that of FF Sample 5 in Table 4-2, with a Ge core of less than 500 nm (0.5 μm).

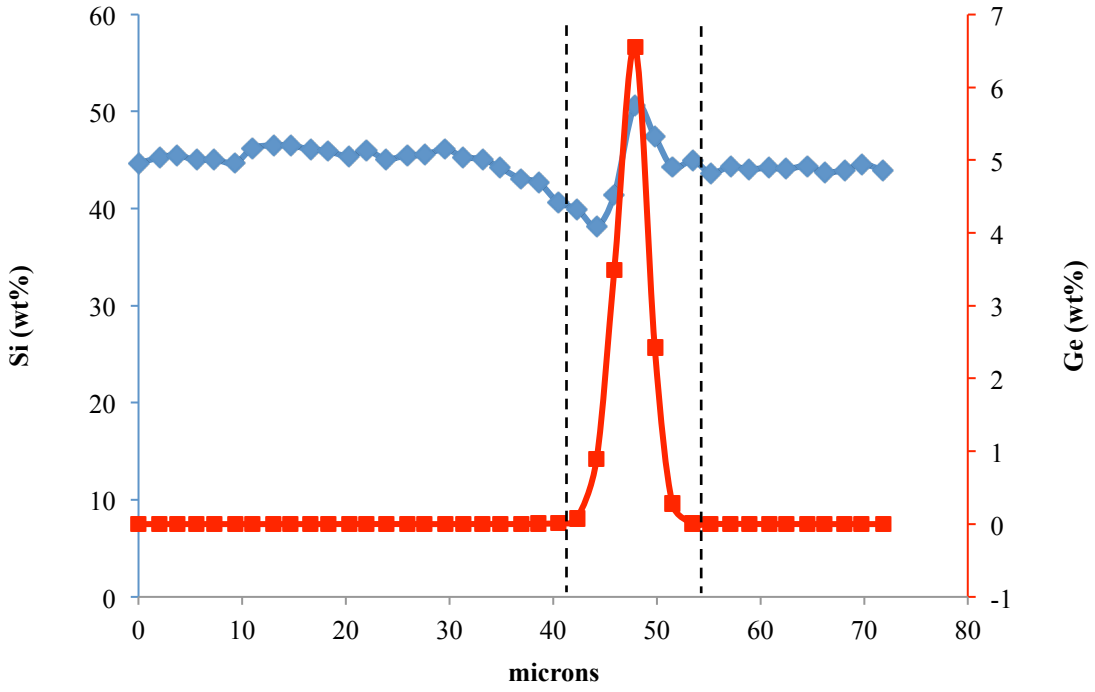

Figure 4-13 Typical plot of distribution of Si (in blue) and Ge (in red) along a line scan for a nominal 6 % weight Ge-doped flat fibre, 200 x 750 µm (FF Sample 1). Similar patterns were obtained for other flat fibre outer diameters. The boundary lines (black dashed) indicate the region between the core and cladding of the Ge-doped flat fibres.

Linearity between dose and TL response has been observed (to be discussed in Chapter 5), the TL response of Ge-doped fibres of the greatest diameter producing superior response to that for smaller dimension fibres. It is clear that non-uniformities in the distribution of added dopants have a direct effect on the TL yield. Variation in TL yield obtained from each batch of Ge-doped SiO_2 fibre is almost certainly explained by point-to-point variation in doping concentration along the length of an optical fibre, as shown in Fig. 4-14. This is reflected in the present PIXE analysis results, as seen in Fig. 4-15 and 4-16 for similar fibres (nominal 4 % weight) with a much greater measured peak Ge concentration of 4.56 % weight in one case compared to the other fibre with a measured peak Ge concentration of 1.25 % weight, respectively.

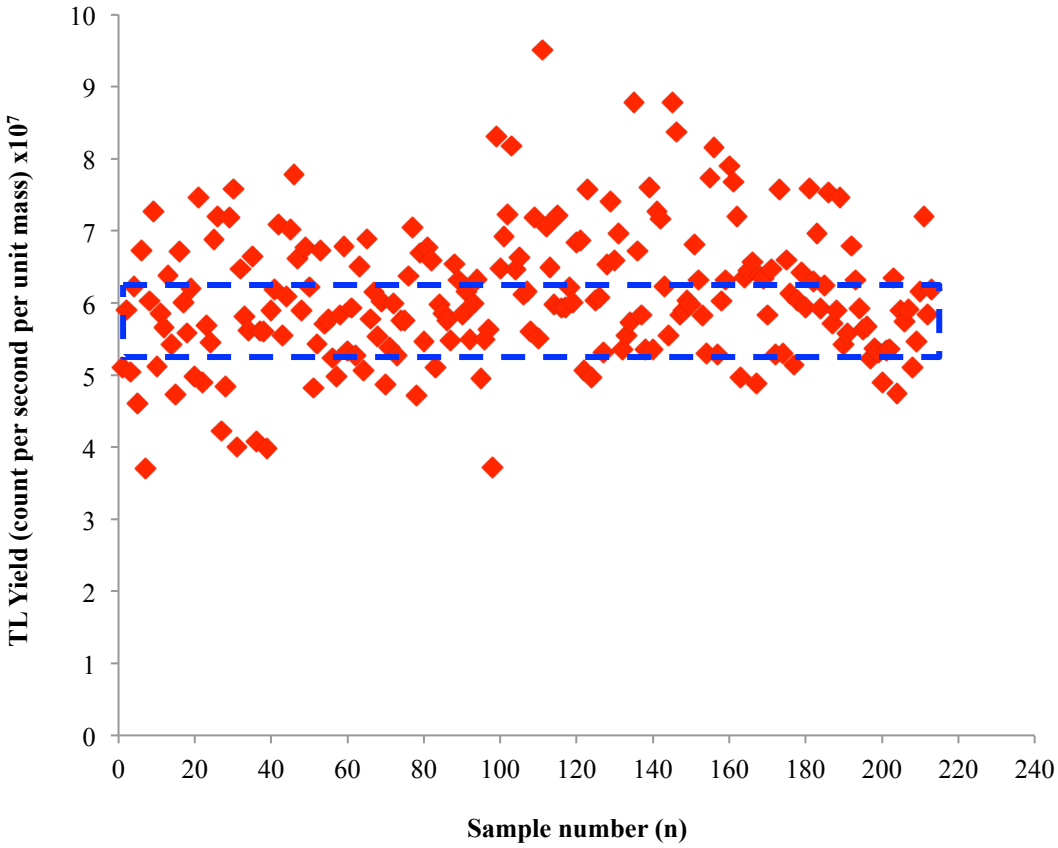

Figure 4-14 Response from 211 6 % weight Ge-doped cylindrical fibres of 604 µm diameter, irradiated at a fixed dose of 3 Gy using a Gulmay X-ray machine (Gulmay, UK) operated at a potential of 250 kVp. Prior to irradiation, the fibres were cut to lengths of approximately 5.0 ± 0.1 mm; variations in response arising from variation in dopant concentration along the length of a fibre are expected to be the largest influencing factor. The irradiations were conducted at the Royal Surrey County Hospital (RSCH). The fibres were then readout 12 hours after irradiation using a TOLEDO TLD reader (Pitman Instruments, Weybridge, UK). The actual number of fibres falling within the selection criteria (± 5 % of the mean TL value is presented within the blue dashed-box.

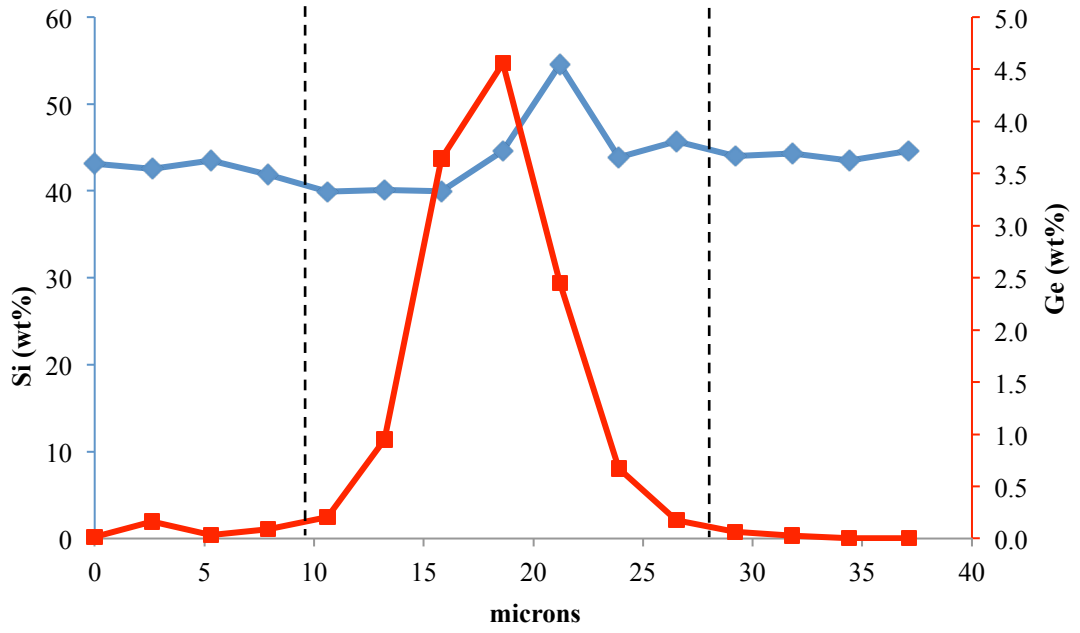

Figure 4-15 Line scan of Si (in blue) and Ge (in red) concentrations for nominal 4 % weight Ge-doped cylindrical fibre of similar dimension (125 µm). The boundary lines (black dashed) indicate the region between the core and cladding of the Ge-doped cylindrical fibres.

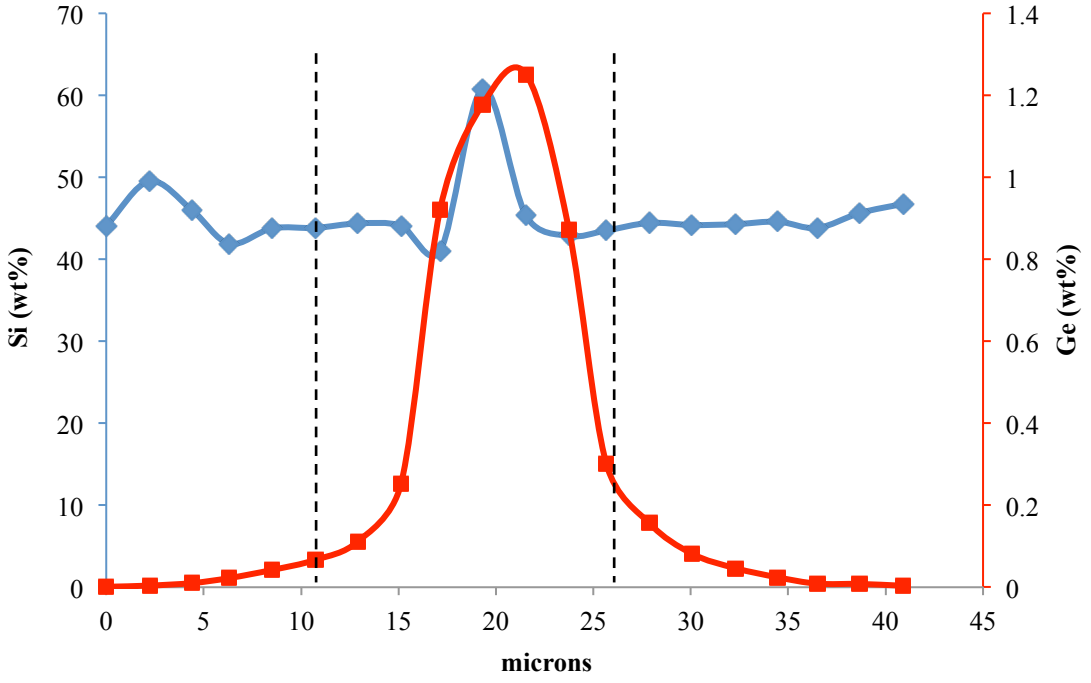

Figure 4-16 Line scan of Si (in blue) and Ge (in red) concentrations for nominal 4 % weight Ge-doped cylindrical fibre of similar dimension (125 µm). The boundary lines (black dashed) indicate the region between the core and cladding of the Ge-doped cylindrical fibres.

Results from these investigations can be compared against that of previous research for doped silica glass. Using the sol-gel route, a notably difficult process to control, Yusoff et. al. [4] have reported the highest TL yield to be obtained from Ge-doped fibres at 0.25 mol%, investigating dopant concentrations from 0.01 mol% up to 33 mol%. Hashim et. al. [11] have found the range of Ge concentration in commercial Ge-doped fibres to be 0.53 - 0.71 mol%. While the application of the MCVD method as used herein, can be used to provide for different dopant concentration fibres which may improve upon the sensitivity of existing TL systems, the TL performance can only be more fully specified by knowledge of the dopant distribution, measured in absolute terms, as herein.

4.3.2 Summary of Determination of Dopant Concentration for CF and FF

The absolute concentration profile of the Ge dopant in tailor-made silica fibre TL dosimeters has been investigated herein; use was made of the PIXE/RBS method. It was found that the nominal 6 wt% and 8 wt% of cylindrical fibres for all dimensions is in the range of 6.01 to 8.10 wt% and 10.27 to 12.25 wt%, respectively. The nominal 4 wt% of similar cylindrical fibres has been observed to have a significant variation in the dopant concentration with a much greater peak Ge concentration of 4.56 wt% in one of the three fibres compared to the other fibre with a measured peak concentration of 1.25 wt%, respectively. This is due to the non-uniformities in the distribution of added dopants along the length of the optical fibre. In addition, the high variation in the dopant concentration of flat fibres (FF) of nominal 6 wt% has been strongly affected by the shape of the fibre. The very thin layer of Ge in the centre of the FF, being less than the spatial resolution of 2 μm, has resulted in few scanned points.

4.4 Determination of Dopant Concentration and Diffusion for PCF uncollapsed and collapsed

The appearance of commercially available microstructured optical fibres (MOFs), such as photonic crystal fibres (PCFs), has further improved the TL sensitivity of fibres for radiation dosimetry [12]. Moreover, PCFs have also been used in radiation measurements in the optically stimulated luminescence (OSL) detection mode, modelling also being undertaken [13, 14]. The dose detection sensitivity of PCFs could be due to the fusing of the outer wall surface of the stacked capillaries since similar elevations of TL response properties

have been observed in single capillaries after the internal bore was collapsed to form a flat fibre shape; the TL has been observed to be enhanced several fold compared to that before collapse (by a factor of 12) [15]. In addition, a more significant improvement in TL response has been observed in flat fibres when extrinsic impurities were added to the collapsing/fusing area, comparison being made with undoped flat fibre. This should be taken into consideration in designing a PCF that could in principle contain hundreds of capillaries stacked in a glass tube; collapsing all capillary holes to form a collapsed-hole-PCF would then be expected to lead to even greater TL response compared to the original PCF.

4.4.1 Results and Discussion

Typical PIXE spectrum for an uncollapsed PCF of 125 μm diameter, obtained with a 2.5 MeV proton beam is shown in Fig. 4-17. A similar PIXE spectrum was also obtained for the collapsed PCF investigated herein. Fig. 4-18 represents the elemental maps of Si and Ge for both uncollapsed and collapsed PCFs. PIXE and RBS analysis also detected the presence of other elements, including P, and Al, due in part to sample handling. However, the concentration of these elements has been found to be relatively small and as such can be considered to have little effect upon the TL yield of these fibres.

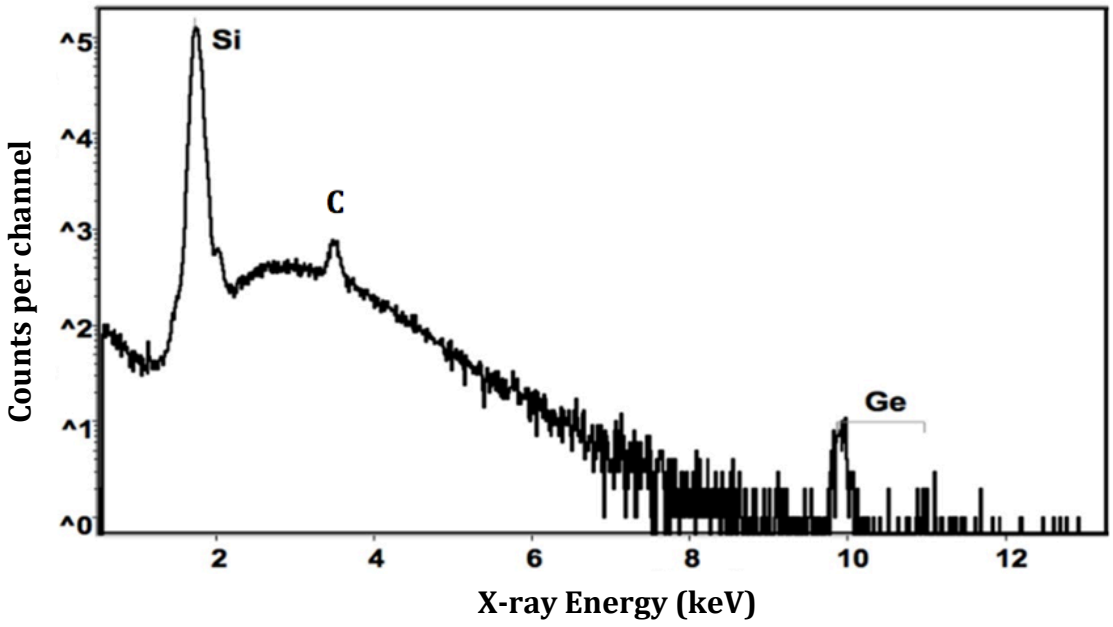

Figure 4-17 PIXE spectrum for a point in a Ge concentration region of Ge-doped SiO_2 PCF uncollapsed fibre. The total run time was 2.5 minutes using beam current of ~150 pA of 2.5 MeV protons corresponding to a beam dose of 22.5 nC.

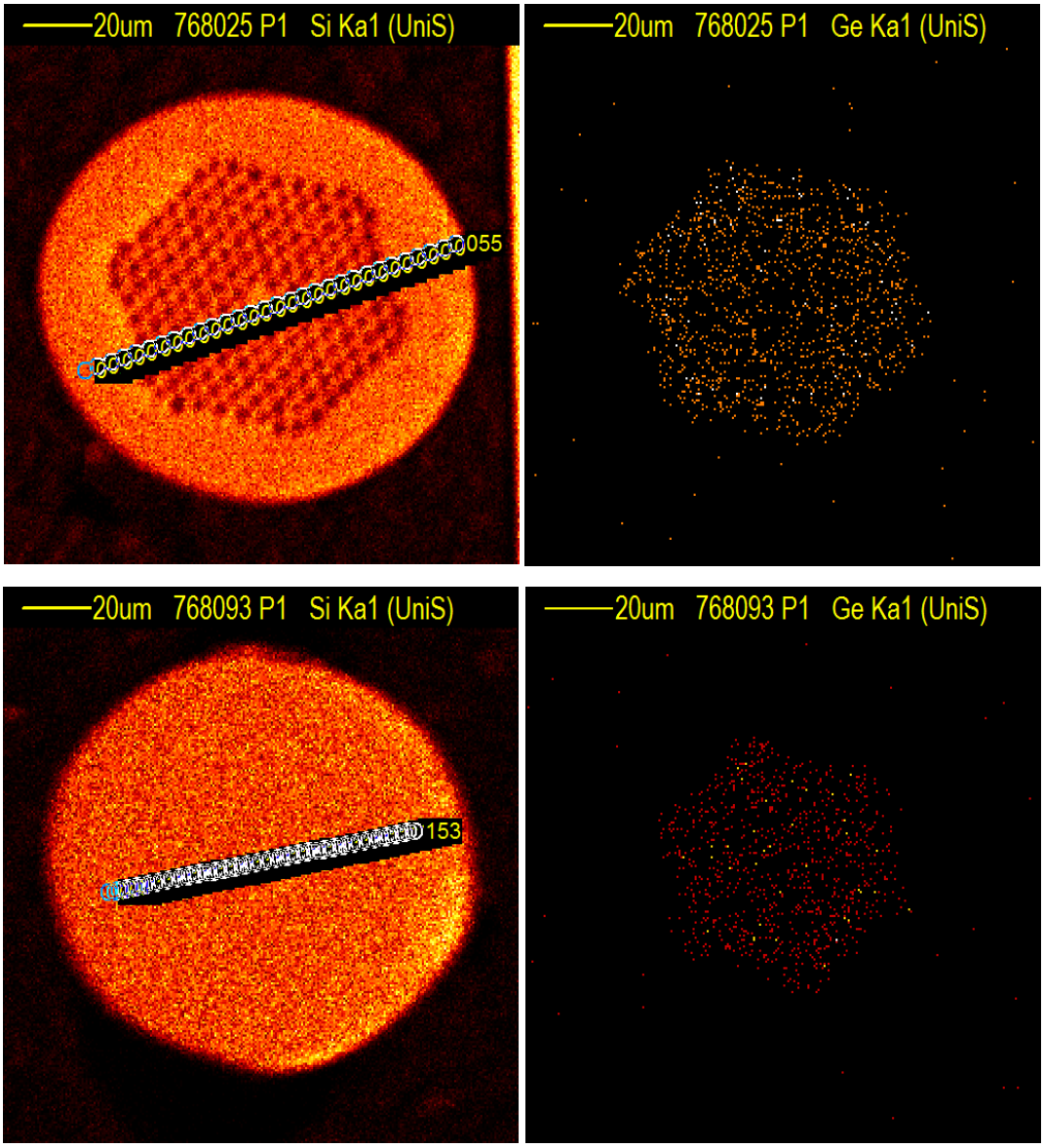

Figure 4-18 Elemental maps across the transverse cross section of an uncollapsed PCF (top) and collapsed PCF (bottom), showing the relative presence of the identified elements, Si, and Ge respectively. Also identified are the locations of the point scans

A complementary analysis for the concentration of the elements Si and Ge has been obtained by line scanning across the uncollapsed and collapsed PCFs, as presented in Fig. 4-19 and 4-20, respectively. The lower Ge concentration measured from the fibre cross-section area in uncollapsed PCF, in the range of 0.0238 - 0.1826 compared to collapsed PCF, 0.0376 - 0.2183 is in agreement with results of the line scan in Fig. 4-19 and 4-20. This is mainly due to the relatively large beam size, 2 x 2 μm^2, in each PIXE measurement, the elemental concentration in uncollapsed PCF being the result of mixture between Ge, Si, and/or air hole regions, and in collapsed PCF the mixture of Ge and Si regions. However, there is a very great difference between the Ge concentration measured in the preform compared to that

observed in uncollapsed and collapsed PCFs. Apart from the small percentage of diffusion of elements during fibre drawing process, it should be noted that the measurement in the preform was made directly from a large core area of around 2.10 mm doped with Ge.

However, in the case of PCFs, elemental analysis was performed in the PCF cross-section area, including Ge-doped cladding and 8.27 μm pure silica central core. The Ge-doped cladding is made of capillary tubes with a thin layer of Ge core existing in the inner layer of the capillaries, the area of Ge layer being approximately 52 times smaller than the area of the pure silica capillary cladding (refer to the core and cladding area of the preform shown in Fig. 2-25 (a) (from Chapter 2), assuming these to have the same core to cladding area ratio compared to the Ge-doped preform tube used for PCF fabrication). The output of the elemental analysis is thus the average of Ge and Si from the collapsed PCF cross section area, which is expected to have a Ge concentration up to 52 times lower than that of the preform core. This is in agreement with the maximum Ge concentration observed from collapsed PCF cross section compared to the preform, which is about 38.9 times (8.49 wt% in preform measured by EDX divided by 0.2183 wt% in collapsed PCF measured by PIXE). The difference between the expected Ge concentration in collapsed PCF (with Ge concentration greater than 52 time lower) and the measured concentrations (38.9 times lower) is mainly due to the use of two different elemental measurement methods, i.e., EDX and PIXE.

Here it is to be noted that the issue of spatial resolution in electron beam induced X-ray analysis (EDX) is complex, the reasoning behind the assertion of superior spatial resolution of the PIXE-based method is as follows: while the beam diameter in electron probe machines is routinely significantly smaller than that achieved in the proton microprobe, the spatial resolution is primarily determined by the shape of the excitation volume beneath the surface of the sample. For electrons, this is a 'teardrop' created by multiple scattering of the primary electrons from electrons in the sample. The effective dimensions of this are determined by the primary beam energy, the material of the sample and the mass absorption coefficient of the X-ray being observed. For electrons with energy sufficient to excite the germanium K lines, the depth and diameter of the excitation volume may be in the micrometre range. For MeV protons, the excitation volume is a cylinder with a diameter equal to the diameter of the beam at the surface (1 μm) and a length dependent on beam energy and the material of the sample. For present samples, the penetration depth before the beam starts to broaden significantly is around 80 μm, and since X-rays from this depth will be attenuated by the overlying material, the resolution is effectively equal to the beam diameter, offering superior spatial resolution.

However, it is to be emphasised that the primary reason for the choice of PIXE is the much lower detection limit (10^{-8} - 10^{-10} g in standard practice) [16]. X-rays from the germanium in the lesser doped samples were not visible using the electron probe technique.

Recently, the Ge concentration of conventional optical fibre fabricated from the same preform presented in Fig. 2-25 (a) (from Chapter 2) using PIXE has been measured, showing a Ge concentration of around 10-12 wt% in the fibre core area [17]. Considering the highest Ge concentration of 12 wt%, this confirms that the Ge concentration in collapsed PCF cross section is about 55 times lower than the Ge concentration in the conventional fibre, due to the averaged concentration between Ge and Si.

In uncollapsed PCF, in addition to Si and Ge, the air holes are also present. Each air hole has a diameter of around 4.3 μm and a wall thickness between two adjacent holes of about 2.0 μm. Averaging the elements Si, Ge, and air holes in the cross section area of uncollapsed PCF would result in a very much lower Ge concentration for this fibre. It should be noted that in the uncollapsed PCF, if the fibre samples under the measurement were not aligned exactly perpendicular to the applied PIXE beam then there would be a greater probability that part of the beam area focused on the inner wall surface of the capillaries (where the Ge layer exists) instead of the hollow area. The results in Fig. 4-19 and the range of Ge concentrations suggest that the uncollapsed PCF were not very far from exact perpendicularity with the applied beam, otherwise a much lower Ge concentration would have been observed from the surface of this fibre.

The variations of Ge concentration in the line scan presented in Fig. 4-19 are the result of an inexact knowledge of the focusing point of the PIXE beam over the uncollapsed PCF cross-section area. With a 2 x 2 μm^2 PIXE beam size, the possibility of having the beam located in an area involving Si, Ge, and/or air is very high. Thus, as the line scan in Fig. 4-19 shows, the Ge concentration to the two sides of the PCF central core is not symmetric, being mainly dependent on the position of the applied PIXE beam on the surface of the PCF, a situation similarly applicable for Si concentration variation.

The lower Ge concentration in the central core of the PCFs is due to the pure silica rod used in these PCFs. However, the small Ge concentration at the central core of PCFs shown in Fig. 4-19 and 4-20 suggest that besides a small diffusion of Ge that might be induced from the cladding part into the core, the line scan did not pass through the exact central core or diameter of the PCFs. Instead, it is passed through a hypotenuse close to the core, resulting in an average Ge concentration overlapped value between the pure silica

central core and the Ge doped capillaries in the cladding. This is clearly observed from Fig. 4-18 (top), the line scan failing to pass exactly through the central core of the PCF.

The lower Ge concentration at the outer diameter of the PCFs (for example before 15 μm and after 95 μm in Fig. 4-20) is due to the use of pure silica tube that is used to stack the capillaries inside this jacket.

An appreciable presence of carbon is visible (Fig. 4-17), which affects the quantitation. It is possible that this is the embedding medium, which has entered the lumen of the fibres. Given that the PIXE analysis assumes a 'flat homogenous slab' approximation, the presence of variable amounts of carbon in the vicinity of each point could also lead to scatter in the results (Fig. 4-20).

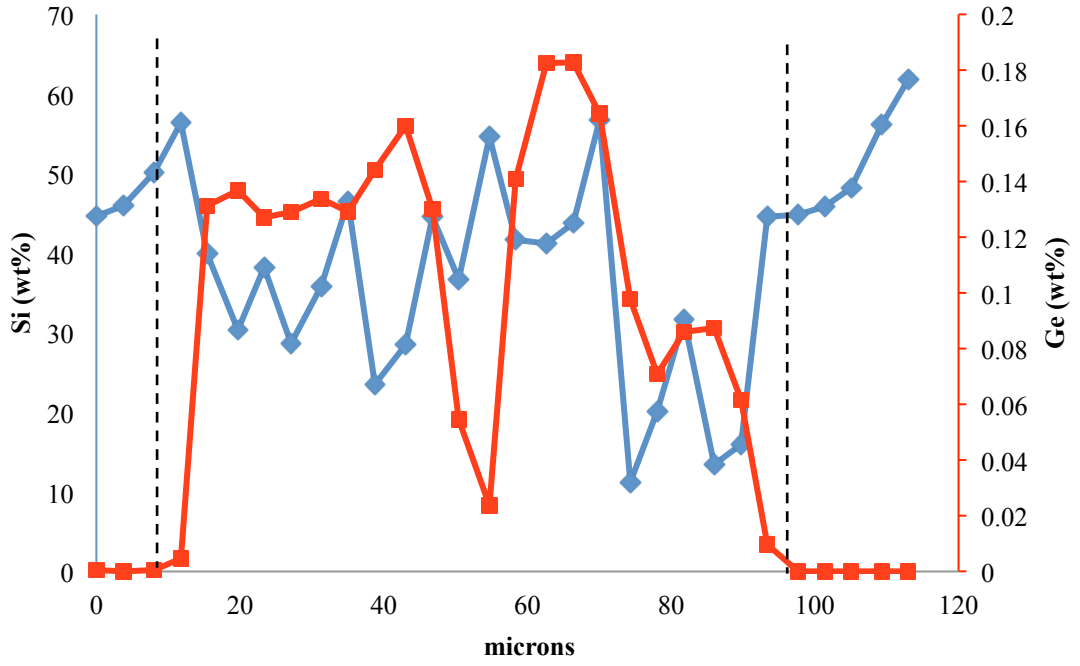

Figure 4-19 The distribution of Si (in blue) and Ge (in red) along a line scan for a Ge-doped uncollapsed PCF. The boundary lines (black dashed) indicate the region between the core and cladding.

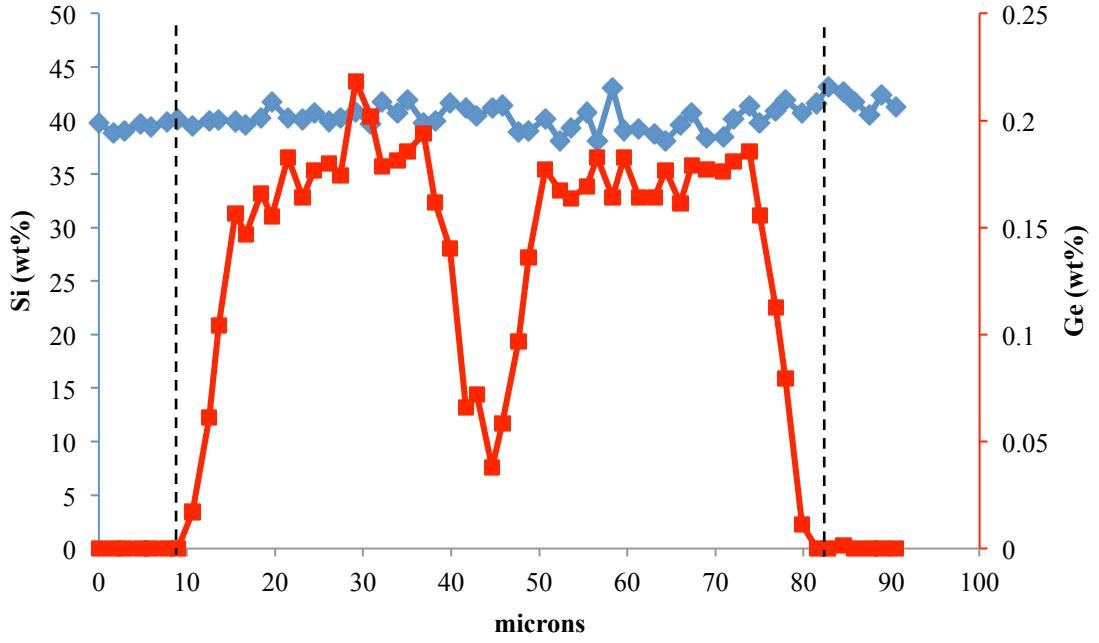

Figure 4-20 The distribution of Si (in blue) and Ge (in red) along a line scan for a Ge-doped collapsed PCF. The boundary lines (black dashed) indicate the region between the core and cladding.

4.4.2 Summary of Determination of Dopant Concentration and Diffusion for PCF uncollapsed and collapsed

The dopant concentrations of Ge-doped photonic crystal fibres (PCFs) using the Particle Induced X-ray Emission (PIXE)/Rutherford Back Scattering (RBS) measurements have been investigated. Using the optimum 2.5 MeV proton energy, the results presented in this chapter have demonstrated the characteristics of uncollapsed and collapsed PCFs. The Ge concentration in uncollapsed PCF is found to be lower than that in the case of the collapsed PCF, in the range of 0.0238 - 0.1826 and 0.0376 - 0.2183, respectively. This can be explained with regard to average of the mixture between Ge and Si in collapsed PCF whereas the Ge concentration in uncollapsed PCF is the result of mixture between Ge, Si and/or hole regions. Moreover, the small Ge concentration at the central core of the uncollapsed and collapsed PCFs is suggested to be due to the small diffusion of Ge that might be induced from the pure silica core. Additionally, the line scan with spatial resolution of 2 μm, which is thought to have been made across the hypotenuse close to the core results in an average Ge concentration value, which overlaps between the pure silica core and the Ge doped capillaries in the cladding hence producing a slightly distorted value.

4.5 References

[1] S. A. E. Johansson, J. L. Campbell, K. G. Malmqvist, Particle-induced X-Ray Emission Spectrometry (PIXE), John Wiley & Sons, New York, 1995.

[2] G. W. Grime and M. Dawson, "Recent developments in data acquisition and processing on the Oxford scanning proton microprobe," *Nucl. Instruments Methods Phys. Res. Sect. B Beam Interact. with Mater. Atoms*, vol. 104, no. 1–4, pp. 107–113, Sep. 1995.

[3] G. W. Grime, "The ' Q factor' method: quantitative microPIXE analysis using RBS normalisation," *Nucl. Instruments Methods Phys. Res. Sect. B Beam Interact. with Mater. Atoms*, vol. 109–110, pp. 170–174, Apr. 1996.

[4] A. L. Yusoff, R. P. Hugtenburg, and D. A. Bradley, "Review of development of a silica-based thermoluminescence dosimeter," *Radiat. Phys. Chem.*, vol. 74, no. 6, pp. 459–481, Dec. 2005.

[5] K. Lyytikainen, S. Huntington, A. Carter, P. McNamara, S. Fleming, J. Abramczyk, I. Kaplin, and G. Schötz, "Dopant diffusion during optical fibre drawing.," *Opt. Express*, vol. 12, no. 6, pp. 972–7, Mar. 2004

[6] A. Simon, C. Jeynes, R. P. Webb, R. Finnis, Z. Tabatabaian, P. J. Sellin, M. B. H. Breese, D. F. Fellows, R. van den Broek, and R. M. Gwilliam, "The new Surrey ion beam analysis facility," *Nucl. Instruments Methods Phys. Res. Sect. B Beam Interact. with Mater. Atoms*, vol. 219–220, pp. 405–409, Jun. 2004.

[7] Oxford Microbeams Ltd. Available fromhttp://www.microbeams.co.uk/download.html (accessed 19 November 2014)

[8] European Commission, Joint Research Centre, Institute for Reference Materials and Measurements (IRMM), Geel, Belgium.

[9] I. Gomez-Morilla, A. Simon, R. Simon, C. T. Williams, Á. Z. Kiss, and G. W. Grime, "An evaluation of the accuracy and precision of X-ray microanalysis techniques using BCR-126A glass reference material," *Nucl. Instruments Methods Phys. Res. Sect. B Beam Interact. with Mater. Atoms*, vol. 249, no. 1–2 SPEC. ISS., pp. 897–902, 2006.

[10] J. L. Campbell, N. I. Boyd, N. Grassi, P. Bonnick, and J. A. Maxwell, "The Guelph PIXE software package IV," *Nucl. Instruments Methods Phys. Res. Sect. B Beam Interact. with Mater. Atoms*, vol. 268, no. 20, pp. 3356–3363, 2010.

[11] S. Hashim, S. Al-Ahbabi, D. A Bradley, M. Webb, C. Jeynes, A. T. Ramli, and H. Wagiran, "The thermoluminescence response of doped SiO2 optical fibres subjected to photon and electron irradiations.," *Appl. Radiat. Isot.*, vol. 67, no. 3, pp. 423–7, Mar. 2009.

[12] M. Ghomeishi, G. A. Mahdiraji, F. R. M. Adikan, and S. Hashim, "The thermoluminescence response of undoped silica PCF for dosimetry application," *2013 Conf. Lasers Electro-Optics Pacific Rim*, pp. 1–2, Jun. 2013.

[13] S. Girard, J. Baggio, and J.-L. Leray, "Radiation-induced effects in a new class of optical waveguides: the air-guiding photonic crystal fibres," *IEEE Trans. Nucl. Sci.*, vol. 52, no. 6, pp. 2683–2688, Dec. 2005.

[14] N. J. Florous, K. Saitoh, T. Murao, and M. Koshiba, "Radiation Dose Enhancement in Photonic Crystal Fiber Bragg Gratings: Towards Photo-Ionization Monitoring of Irradiation Sources in Harsh Nuclear Power Reactors," *2007 Conf. Lasers Electro-Optics*, vol. 1, pp. 1–2, 2007.

[15] D. A. Bradley, G. A. Mahdiraji, M. Ghomeishi, E. Dermosesian, F. R. M. Adikan, H. A. Abdul Rashid, and M. J. Maah, "Enhancing the radiation dose detection sensitivity of optical fibres," *Appl. Radiat. Isot.*, vol. 100, pp. 43–49, 2014.

[16] G. Gauglitz and T. Vo-Dinh, (Eds.). Handbook of Spectroscopy. *John Wiley & Sons*, 2006.

[17] S. F. Abdul Sani, G. W. Grime, V. Palitsin, G. a. Mahdiraji, H. a. Abdul Rashid, M. J. Maah, and D. a. Bradley, "Micro-PIXE analysis of doped SiO_2 fibres intended as TL dosimeters for radiation measurements," *X-Ray Spectrom.*, vol. 44, no. 2, pp. 33–40, 2015.

Chapter 5

5 Thermoluminescence Response of Doped SiO_2 Fibre Dosimeter

5.1 Introduction

The commercially available thermoluminescence (TL) dosimeter is a solid-state system, taking advantage of the electron band structure of solids to allow detection of energetic radiations (including uv, x, gamma, protons, neutrons and alpha particles. Electrons in the valence band may absorb sufficient energy to lift the electrons into the conduction band. In an active dosimeter (e.g. such as a pn junction device) this will create electrons and hole pairs in the crystal lattice, to be collected at electrodes. Conversely in the case of the passive TL system such as LiF (Mg, Ti), the trapped electrons will fall back to the valence band through the action of heating subsequently emitting photons. This can be measured using a photomultiplier tube built into the light-tight readout system.

A TL material intended for dosimetric purposes is generally doped with impurity atoms to create metastable traps in between the valence band and conduction band (within the forbidden band). The luminescence measured is proportional to the amount of energy absorbed via irradiation, allowing use of TL materials for dosimetry.

One particular interest herein are ion beams that are used in radiotherapy to deliver a more precise dose to the target volume while minimizing dose to the surrounding healthy tissue. For optimum dose monitoring in ion-beam therapy, it is essential to be able to measure the delivered dose with a sensitivity, spatial resolution and dynamic range that are sufficient to meet the demands of the various therapy situations. Optical fibres have been demonstrated by other researchers to show promising thermoluminescence properties with respect to photon, electron, proton, alpha particles and neutrons irradiation [1 - 8]. In particular, and also given the flexibility and small size of optical fibres, these fibres have the potential to fulfill the above requirements.

More recently, tailor made optical fibres have been investigated to improve the sensitivity of optical fibres beyond TLD-100 limits in high radiation dose studies [9]. In

further work, new types of Ge-doped fibres (flat- and photonic crystal fibres (PCF)) have been fabricated from a single fibre pulling production run [10, 11], demonstrating potential dosimetric performances that will be discussed more in section 5.3.

In this chapter, study focuses on characterisation of diverse type of Ge-doped SiO_2 fibres of nominal 8 wt% dopant concentration as a potential TL system for radiotherapy dosimetry. The performance of pure (undoped) flat fibres (FF) is compared with the conventional TLD-100 and commercially available Ge-doped optical fibres. It is demonstrated that the photoelectron enhancement can be produced through use of a high atomic number (Z) coating of platinum to create, at the surface of the fibre, an interface to the undoped flat fibres. In addition, the Ge-doped cylindrical fibres (CF), flat fibres (FF) and photonic crystal fibres (PCF), fabricated with the same germanium dopant concentration of nominal 8 wt% were irradiated over a wide range of doses using X-ray radiation energy and compared against high linear energy transfer (LET) of alpha particles, of ^{223}Ra.

5.2 Situations towards Enhanced Thermoluminescence Yield: Part 1

5.2.1 Introduction

In this section, the investigation of the TL response of the undoped flat fibres is compared to that of conventional TLD-100 and commercial Ge-doped telecommunication optical fibres. Additional and separate to this investigation, the undoped flat fibres have also been coated with platinum to enhance the photoelectron emissions, leading to improvement in the sensitivity of that undoped fibres.

5.2.1.1 High Sensitivity of Undoped Flat SiO_2 Fibre

Most of the content of this section is published in the journal of Radiation Physics and Chemistry: "Siti.F. Abdul Sani, Amani I. Alalawi, Hairul Azhar A.R, Ghafour Amouzad Mahdiraji, Nizam Tamchek, A. Nisbet, M.J. Maah, D.A. Bradley. 2014. High sensitivity flat SiO_2 fibres for medical dosimetry" (Appendix C). The right to include the article in any thesis or dissertation has been obtained during assignment of copyright with the publisher.

The sensitivity of a TLD system can be described in terms of TL yield per unit dose per unit mass of the particular medium, dictated by the concentrations and types of activators and defects within the medium, inherent or otherwise. If the medium has a high concentration of luminescent centres, then high energy conversion efficiency might be expected. In practice, variation in sensitivity is observed, even for dosimeters from the same batch [12, 13], a situation resolved by pre-screening and consequent selection. This chapter describes a

preliminary study of the response of undoped flat fibres and commercial Ge-doped SiO_2 fibres irradiated to X-rays generated using megavolt potentials. The sensitivity of these two types of fibre are compared against the standard photon TL material, TLD-100, the study being considered a precursor to future investigation of flat fibres as dosimeters for doses delivered in diagnostic applications.

5.2.1.2 Thermoluminescence Response of Undoped Platinum Coated SiO_2 Flat Fibres and Kilovolt Photon Irradiations

A previous study investigated the use of optical fibre TLD in radiation synovectomy, which is the removal of the inflamed synovium membrane from a joint caused by rheumatoid arthritis [14]. The dose measured in application of this procedure has been referred to by this group as interface radiation dosimetry. In that study, iodine (Z = 53) based contrast medium was used to enhance the treatment dose for the procedure. It was found that the contrast medium gave ~60% increase in TL yields compared against measurements without the contrast medium [14]. This study inspired a subsequent study, where the fibres were coated with gold (Z = 79), which is a high atomic number metal that can increase the probability of radiation interaction, resulting in higher TL yield [15]. Although the result did show a linear increase of TL yield as suggested, an unexpected variation from this for thick coatings was later observed. This was later shown to be due to incomplete removal of the gold coating, reducing the light intensity transmitted to the photomultiplier tube. The study [7] suggests exploration of the dose enhancement factor (DEF) for other metallic element coatings, being one of the aims of this study, this time of platinum (Z=79).

In regard to applications, platinum has been used in the field of therapeutic medicine and examples include implants and platinum based chemotherapy drugs [16, 17]. A study suggests that platinum implants can inadvertently enhance the radiation dose delivered in the use of diagnostic X-rays [18]. Also, platinum based chemotherapy drugs are well developed [16]. Concomitant chemoradiotherapy is where chemotherapy and radiation are simultaneously administered to improve loco-regional and systemic tumour control [19]. Therefore there is a possibility for the need for small field radiation dosimeters such as those based on the present fibres, which together with platinum based towards designing for an improved therapeutic outcome. Therefore it seems to be logical to explore platinum as a candidate coating material to the fibre dosimeters. In this section, studies were extended to validate photoelectric enhancement through platinum-coated undoped SiO_2 flat fibres irradiated using X-rays generated at kilovolt potentials.

5.2.2 Experimental Procedures

5.2.2.1 Sample Preparations

5.2.2.1.1 High Sensitivity of Undoped Flat SiO_2 Fibre

Present research has focused on the TL response of commercially produced single-mode doped silica telecommunication optical fibres, undoped silica flat fibres (FF) and TLD-100 chips. For the first of these, use has been made of Ge-doped silica (INOCORP, Canada) comprising a 9.0 μm doped core in a cladding of diameter (124.7 ± 1.0) μm and an outer polymer coat leading to an outer fibre diameter of (250 ± 10) μm. Prior to use, a mechanical fibre stripper (Miller, USA) (Fig. 5-1 (a)) was used for removing the plastic coating from the optical fibre, allowing investigation of the TL yield of the fibre. Following removal of the outer polymer coat, the fibres were then cleaned with a cotton cloth containing methyl alcohol to remove any remnant polymer. The Ge-doped fibres have been cut into approximate 0.5 cm lengths using an optical fibre diamond wedge scribe (Gilmore, USA) (Fig. 5-1 (b)). The undoped flat fibres used herein have been fabricated using a 5 m fibre drawing tower located in the Department of Electrical Engineering, University of Malaya [20]. The flat fibres have been fabricated using a high grade amorphous SiO_2 tube (Suprasil F300), outer and inner dimensions 25 mm and 19 mm, respectively. As the SiO_2 tube preform is pulled into capillary form (Fig. 5-2(left)) of around 1–2 mm diameter, vacuum pressure is applied to collapse the capillary into the flat form (Fig. 5-2(middle) and Fig. 5-3) as explained in detail in section 2.4.2. The flat fibres have been cut using a diamond wedge scribe (Gilmore, USA) (Fig. 5-1 (b)) and the dimensions of the flat fibres, obtained by digital calipers (DURATOOL), are detailed in Table 5-1. For comparison of response, use has also been made of TLD-100 (LiF:Mg,Ti), comprising 99.99% ^{7}Li, the form of the dosimeter being a disc of diameter 8.81 mm and 0.35 mm thickness.

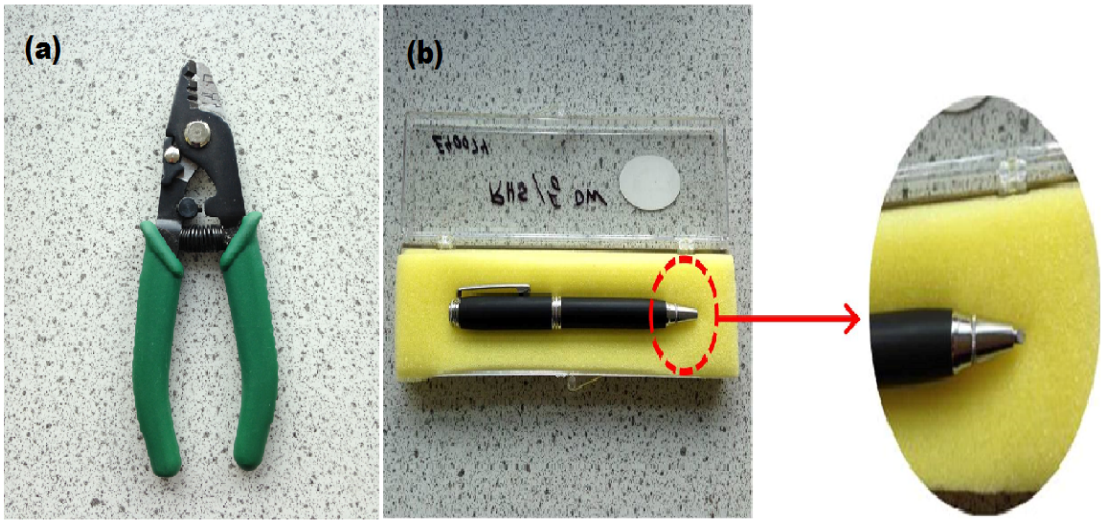

Figure 5-1 Equipment used for sample preparation of the TL dosimetric system studied; (a) fibre stripper (Miller, USA) to cut the round fibre, and (b) diamond wedge scribe (Gilmore, USA) to cut the flat fibre

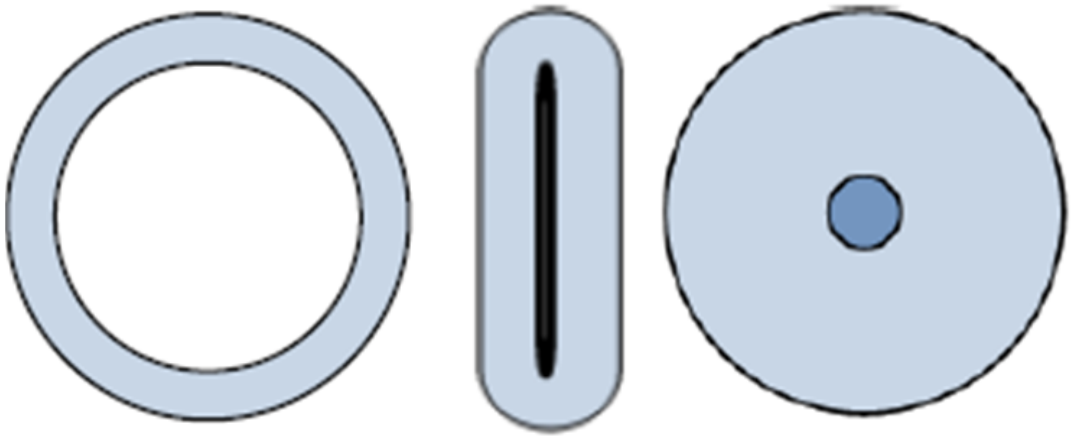

Figure 5-2 From left to right are not-to-scale schematic representations of capillary fibre and flattened fibre created from an initial hollow doped fibre.

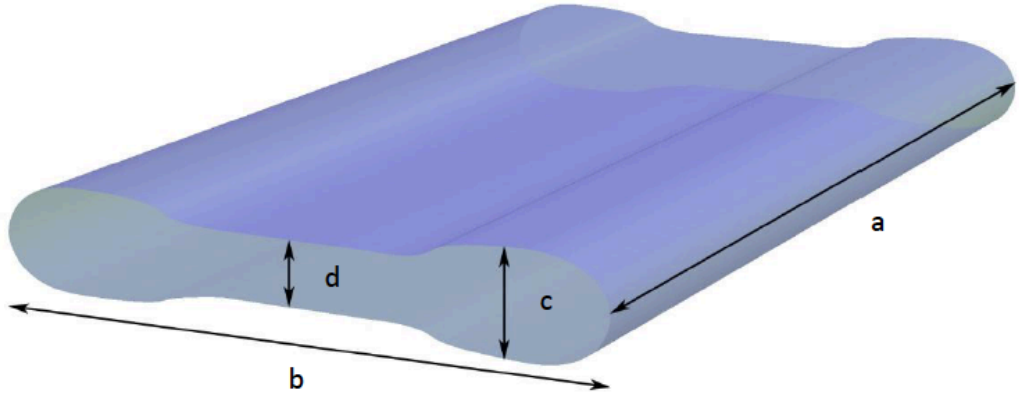

Figure 5-3 A 3D representation of a flat fibre, a: length, b: width, c: thickness, d: mid-thickness.

Table 5-1 Mean dimensions of eleven undoped silica flat fibres (see Fig. 5-3)

Dimension	***(mm)***
Thickness	1.13 ± 0.01
Mid-thickness	1.00 ± 0.01
Width	3.72 ± 0.01
Length	10.00 ± 0.01
Weight (g)	**0.085 ± 0.001**

5.2.2.1.2 The Thermoluminescence Response of Undoped Platinum Coated SiO_2 Flat Fibres and Kilovoltage Photon Irradiations

Sputtering is the gaseous glow discharge of the target material, in this case platinum in cathode tube arrangement. Inert gas such as argon is included in the cathode tube, a current is then passed through the target material and as voltage increased some ionisation is produced by collision with the gas atoms, and this process is called the 'Townsend' discharge. The process is shown in Fig. 5-4.

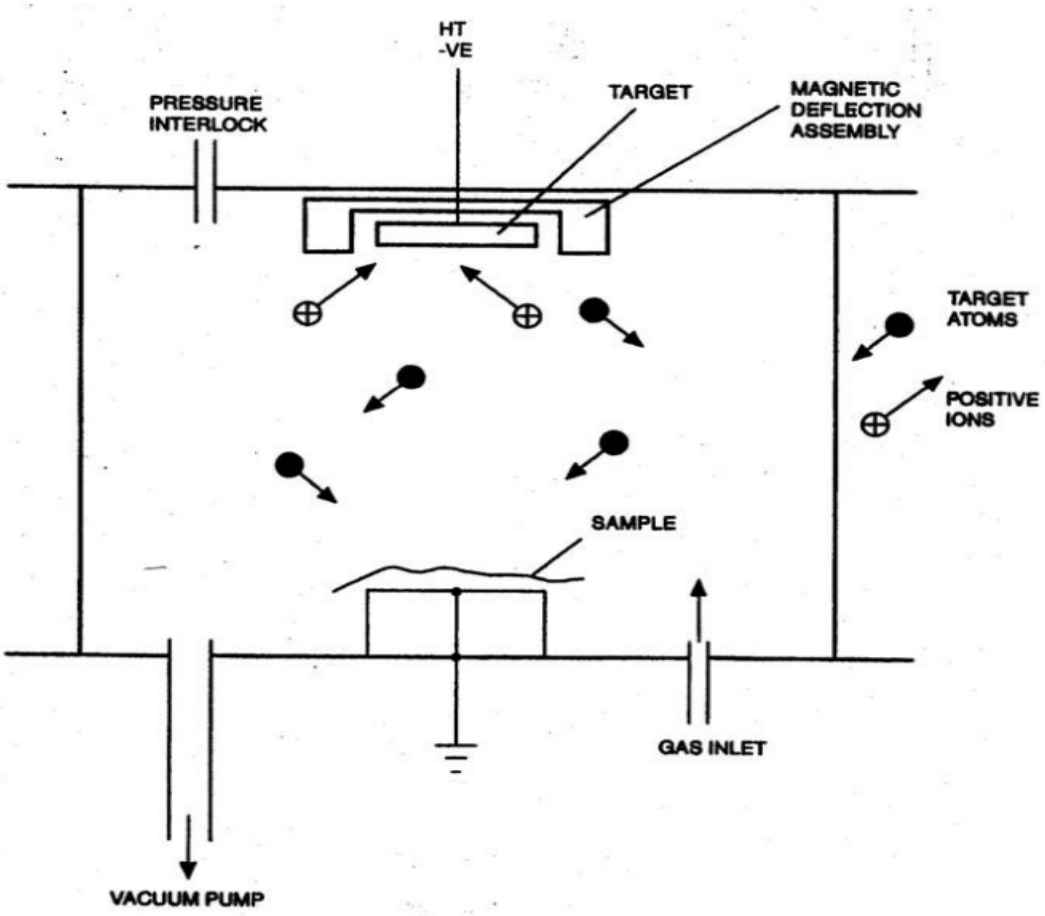

Figure 5-4 Diagram of a 'cool' sputtering head [21].

The undoped flat fibres were coated with platinum (Pt) using a sputter coating unit (Emitech K575X) (Fig. 5-5 (a)) provided by Surrey Materials Institute. The fibres were coated with 20, 40, 60, 80 and 100 nm of Pt. Pairs of fibres were coated with each thickness of coating and an additional uncoated fibre was kept as a comparitor. The sputter current was set to 70 mA and 20 nm terminate value was selected. Once the cycle stopped, a pair of fibres was taken out of the sputterer and the rest would be coated with another 20 nm of Pt. The procedure was repeated until all five pairs of fibres were coated with the required thickness of Pt. A pressure sensitive adhesive medium (Blu-Tack) was used to secure the fibres on the specimen stage (glass slide) as shown in Fig. 5-5 (b). The photographic results of the coated flat fibres are illustrated in Fig. 5-6.

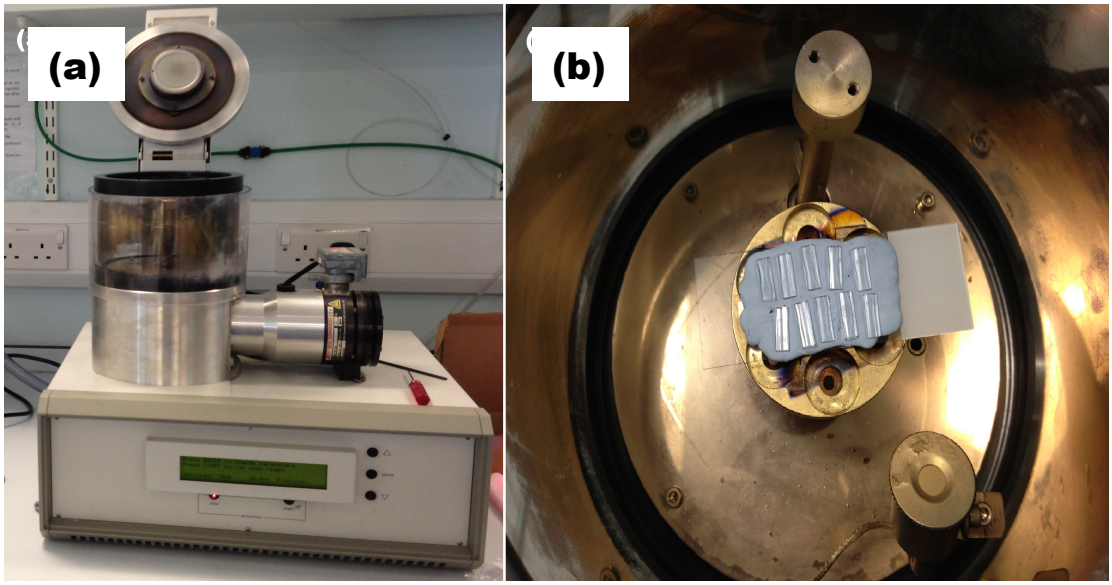

Figure 5-5 (a) sputter coating unit (Emitech K575X) provided by Surrey Materials Institute, and (b) fibres attached to blu-tack inside the sputter coating unit.

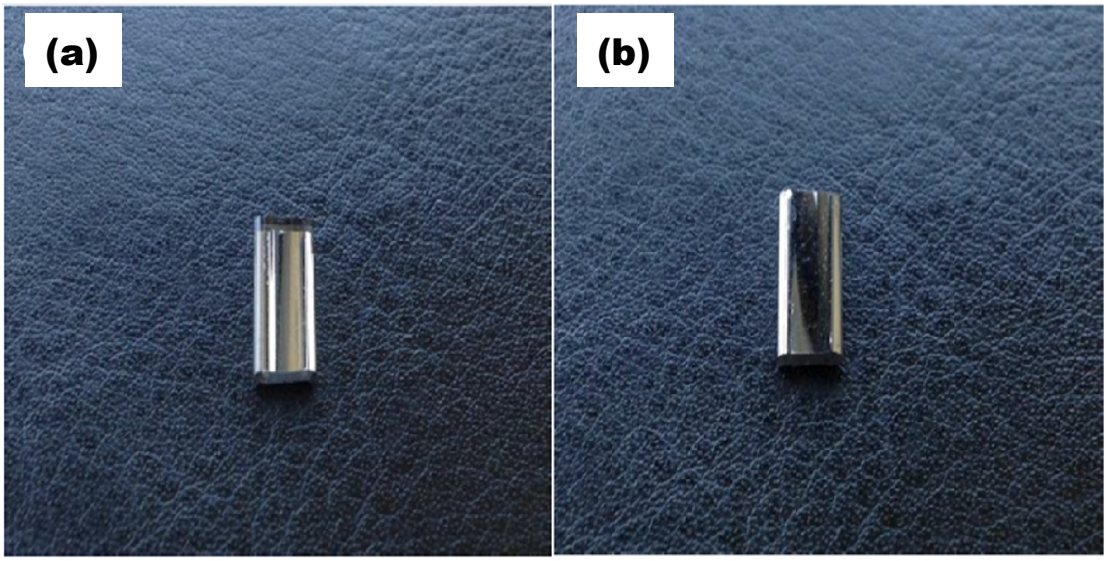

Figure 5-6 (a) Flat fibre with coated side at the bottom, and (b) Flat fibre with coated side on the top.

5.2.2.2 Sample Handling

The properties of the TLD material may be affected by both physical and environmental factors. The physical factors include, transporting and cleaning of the samples. Environmental factors include temperature, humidity, UV and visible light. To minimise these problem, it is therefore important to correctly handle and store the samples. The fibres were handled herein using a vacuum tweezer (Dymax 30, Charles Austen Pump LTD, England) to avoid surface scratches (Fig. 5-7 (a)). The mass of each of the Ge-doped optical

fibres, flat fibres and TLD-100 chips were determined using an electronic balance (PAG, Switzerland) (Fig. 5-7 (b)), allowing TL yield to be normalized to unit mass of the irradiated dosimeter. The mean mass was found to be (1.75 ± 0.01) x 10^{-4} g, (0.085 ± 0.01) g and (0.052 ± 0.01) g respectively. For routine storage and handling, each of the fibres were retained inside gelatine capsules as to allow statistical analysis of reproducibility (Fig. 5-7 (c)). Subsequently they were held within a black case in order to minimize the light effects before and after irradiation, until readout.

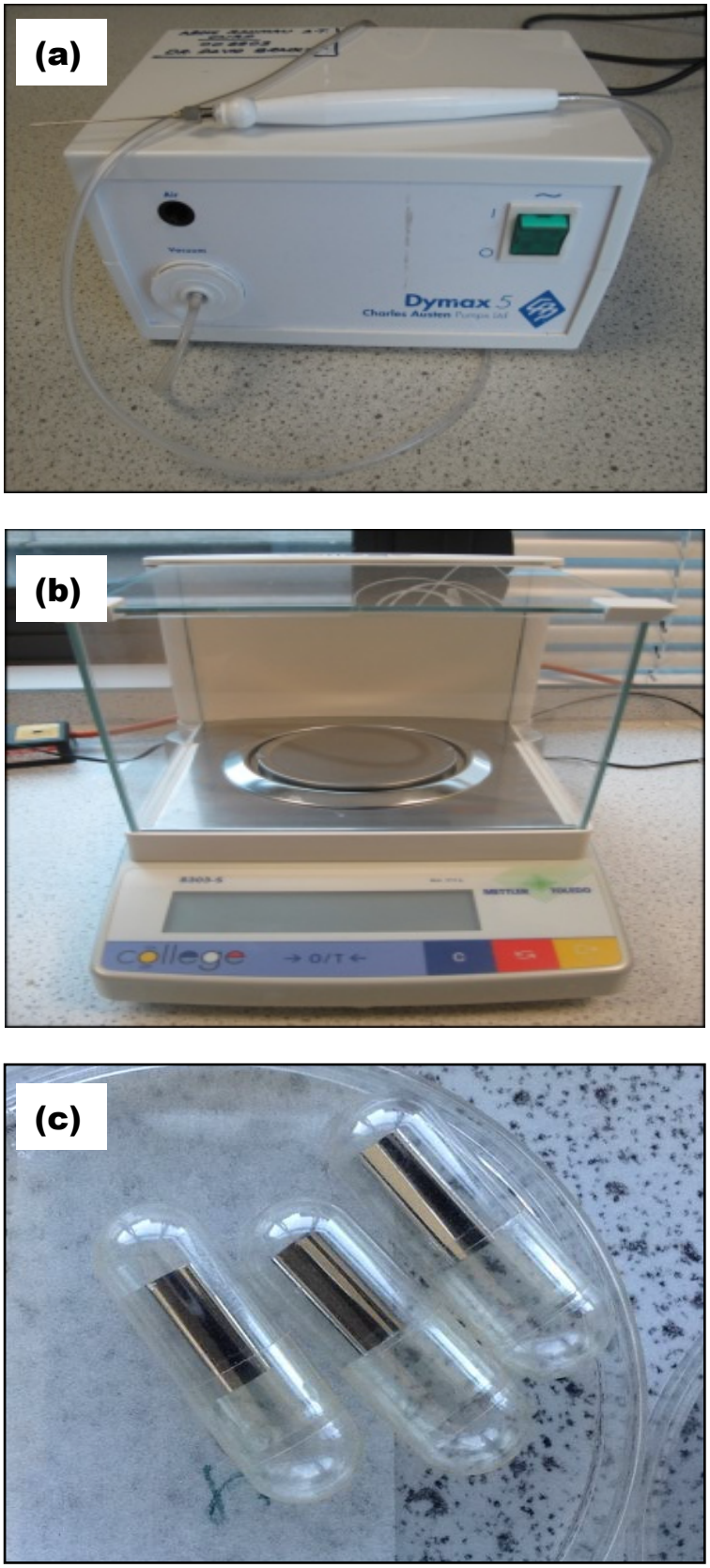

Figure 5-7 Equipment used for sample preparation of TL dosimetric system studied; (a) vacuum tweezer, (b) balance, (c) gelatine capsules.

5.2.2.3 Sample Annealing

Prior to irradiation, the samples (all unscreened) were first annealed in a furnace (Carbolite, UK). This was carried out to provide for a stable situation, for both background and TL signals, the annealing allowing elimination of any previous irradiation history, standardizing the thermal history as well as sensitivity, also erasing the unstable low-temperature glow peaks. For annealing, the samples were retained in an alumina ceramic boat and covered with aluminium foil and a preset annealing and preparation sequence was performed. The sequence consists of an hour of heating at 420 ^{o}C, a steady decrease in temperature (60 ^{o}C per hour) to 80 ^{o}C allow slow cooling and finally the samples were rested for 16 hours at 80 ^{o}C to minimise thermal stress before irradiation.

5.2.2.4 Sample Irradiation

The undoped flat fibres have been irradiated for investigation of high sensitivity of undoped flat SiO_2 fibres; comparison has been made with the Ge-doped telecommunication optical fibres and commercially available TLD-100 (5.2.2.4.1). Following to this, the thermoluminescence response of undoped platinum coated SiO_2 flat fibres and kilovoltage photon irradiations is discussed in 5.2.2.4.2.

5.2.2.4.1 High Sensitivity of Undoped Flat SiO_2 Fibre

The samples were irradiated at the Royal Surrey County Hospital (RSCH), use being made of a Clinac^{TM} 2100C linear accelerator (LINAC) (Fig. 5-8 (a)). The TL media was exposed to 6 MV x-ray beams, to give a dose of 3 Gy. The source to sample surface distance (SSD) was set at 100 cm, with a field size of 20 x 20 cm^2 selected. In all cases, the fibres were placed at the centre of the field. The irradiation was repeated using an X-ray machine (Gulmay, UK) (Fig. 5-8 (b)) generated at an accelerating potential of 140 kVp, giving dose of 0.1 Gy for comparison in energy response, the arrangement of TLD materials being placed at the centre of the phantom as shown in Fig. 5-9.

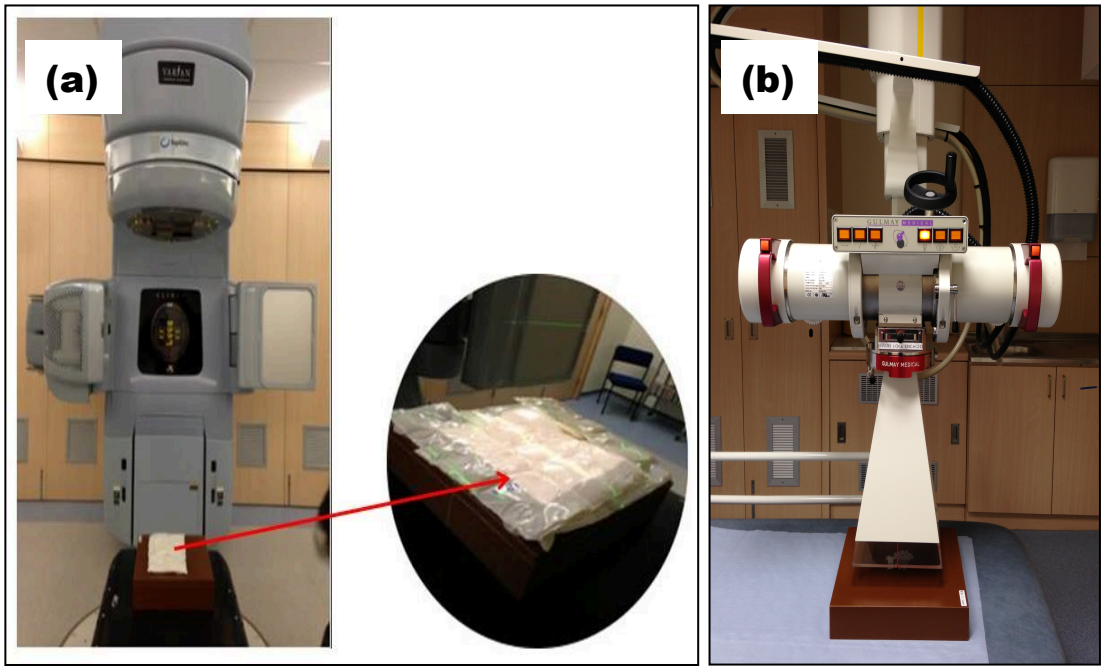

Figure 5-8 a) The irradiation set up of 6 MV potential energy using Clinac^{TM} 2100C linear accelerator (LINAC). Bolus was placed on top of the TLD materials to provide a flat surface for normal beam incidence and (b) the X-ray machine (Gulmay, UK) operating at 140 kVp using closed-ended applicator.

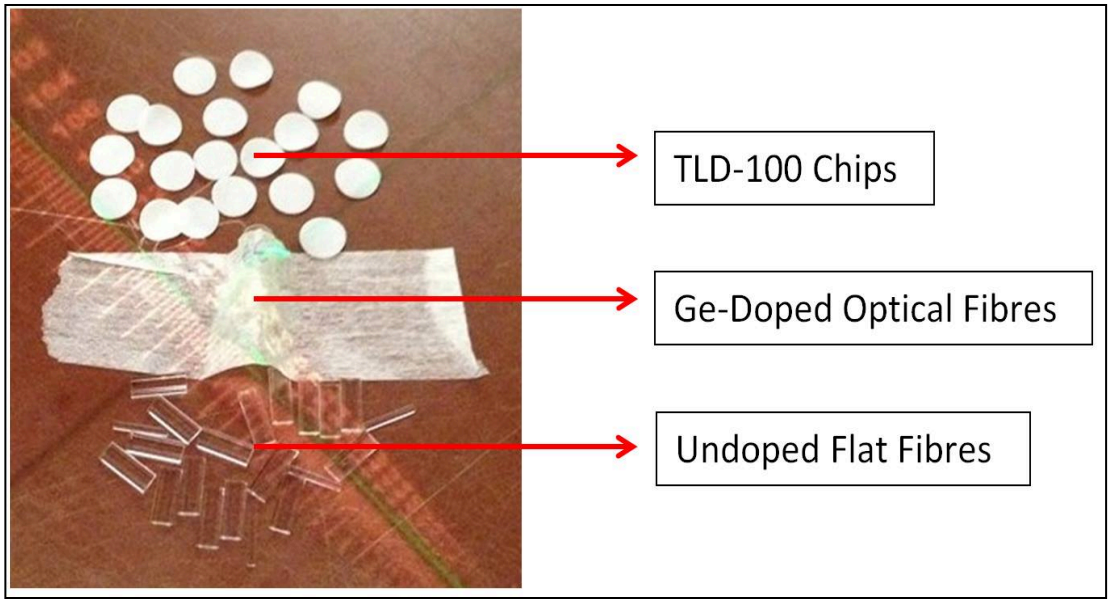

Figure 5-9 Arrangement of TLD materials being placed at the centre of the phantom.

5.2.2.4.2 The Thermoluminescence Response of Undoped Platinum Coated SiO_2 Flat Fibres and Kilovoltage Photon Irradiations

The fibres were placed on top of a 30 x 30 cm^2 water equivalent phantom (solid water^{TM}) with thickness of 6 cm to simulate scattering of human tissue. The fibres were placed in the centre of the phantom (i.e. 3 cm depth) with the coated side faced up towards the X-ray tube and aligned with the applicator of the X-ray unit with 3 cm stand off from the phantom to the applicator. The X-ray unit used was a superficial X-ray therapy unit (Gulmay, UK) provided by St Luke's Cancer Centre, Royal Surrey County Hospital. 3 Gy of X-rays was delivered under tube potential of 250 kVp and tube current of 12 mA.

5.2.2.5 Sample Readout

The samples were read 12 hours after irradiation, this would allow uniform control of thermal fading. Once the samples rested for 12 hours, they were read using a TOLEDO thermoluminescence dosimetry reader (Pitman Instruments, Weybridge, UK). The readout was carried out in a nitrogen gas rich atmosphere to suppress oxidation and triboluminescence effects. Oxidation may occur on the surface of the dosimeter causing absorption of yielded light and result in inaccurate readings [22]. Since triboluminescence is caused by mechanical disturbance, for instance, friction and grinding [22], the samples may trap such energy during transport and handling of the fibres. A scintillating ^{14}C doped radioactive source was installed to calibrate the output of the reader, hence ensuring consistency of readings. The sequence used for this reader was; preheat at 120 ^oC for 28 s, readout at 300 ^oC for 25s with ramp rate of 38 ^oC/second and anneal at 300 ^oC for 10 s to provide initial erasing of any residual signals. The arrangement provided for an optimal glow curve.

5.2.3 Results and Discussion

5.2.3.1 High Sensitivity of Undoped Flat SiO_2 Fibre

Using the 6 MV photon beam at a dose of 3 Gy, eleven flat fibre samples (unscreened), TLD-100 chips and Ge-doped fibres were irradiated to obtain their TL yield and TL yield per unit mass as shown in Fig. 5-10 and Fig. 5-11 respectively. Interest focuses on the previously unexplored sensitivity of the flat fibres. As can be seen from Fig. 5-10, for the particular photon spectrum a much greater TL response to 6 MV photons is obtained from the flat fibres compared to the Ge-doped fibres, of the order of 100 times that produced by the Ge-doped fibres, similar to that from TLD-100. This is due in part to the differential mass of the two dosimeter types, the Ge-doped fibre mass being approximately 100 times less than

that of the flat fibre, and also due to the undoped nature of the flat fibres. In a previous study, the sensitivity of the Ge-doped of 50 µm core was found to be 39 times greater than that of a Ge-doped 8 µm core fibre irradiated at kilovoltage potential [14]. This was mainly due to the larger core size (50 µm), containing proportionately more Ge dopant than that of the 8 µm core fibre.

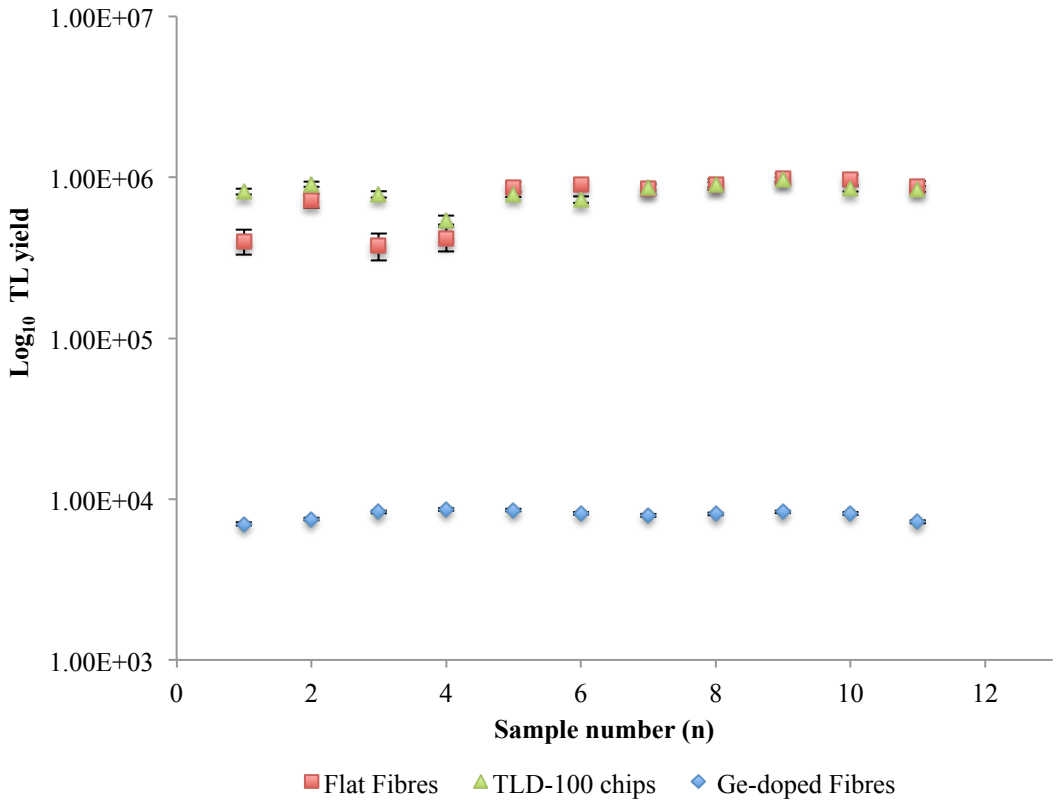

Figure 5-10 Logarithmic plot of the TL yield distribution for flat fibres, TLD-100 chips and Ge-doped fibres subjected to 6 MV photon irradiation at a dose of 3 Gy. (Note: the error bars for the Ge-doped fibres are smaller than the data points)

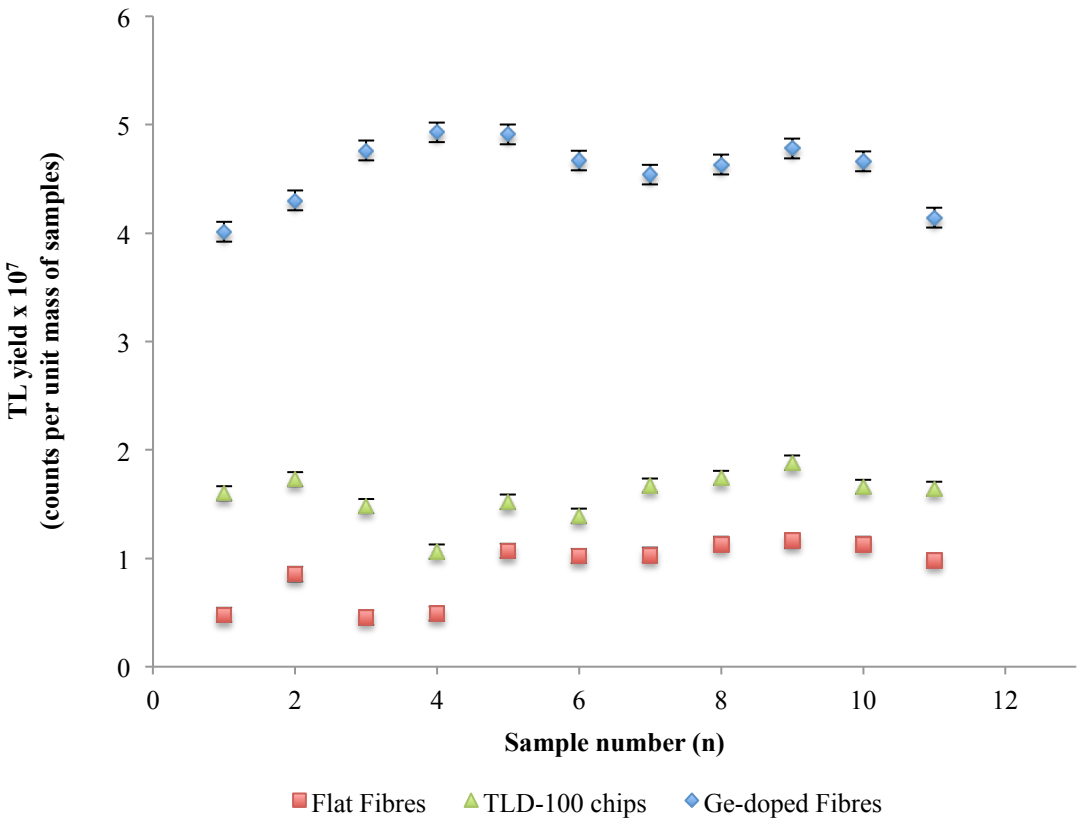

Figure 5-11 TL yield per unit mass for flat fibres, TLD-100 chips and Ge-doped fibres subjected to 6 MV photon irradiation at a dose of 3 Gy.

It is first to be acknowledged that the response of the undoped FFs is closely linked with the SiO_2 vacancy defects and the dangling bonds previously addressed. In addition to TL from the foregoing, the fibres, whether doped or undoped, are further affected by drawing-induced defect centres, all of the fibres produced by the University of Malaya collaboration having been made with Suprasil F500 (Heraeus Quarzglas GmbH, Germany), providing a reduced OH content (typically 0.02 ppm) fused silica with a great many defects when compared against crystal or Quartz glass. As such, it is apparent that defect centres in fibres made from the Suprasil preform can be manipulated, to an extent presently unknown, by controlling the pulling parameters, reflected by changes in the TL response for fibres of the same size and type. By controlling the pulling parameters (temperature, pulling speed, and pressure), there is potential to make the fibre of higher or lower TL response [23].

Alawiah et. al., (2013) [23] observed that the number of electrons released from traps (area under the glow curve) is maximum at 203°C for flat fibres subjected to 21 MeV electron irradiation for a dose of 2.0 Gy while the number of electrons released from the trap is maximum at 243°C for TLD-100. It can be concluded that the number of electrons released

from the trap is proportional to the TL yield. Currently, TLD-100 chips provide superior precision and accuracy but the flat fibres are easier to handle and lower in cost. In studies herein, it is intended to significantly increase the sensitivity of the flat fibre through the addition of suitable dopants such as Ge and through the application of high atomic number coatings to enhance photoelectron production.

Fig. 5-12 demonstrates results for the undoped fibres, irradiated to a dose of 3 Gy using 6 MV photons and to a dose of 0.1 Gy using 140 kVp photons, the data all being normalised to a dose of 3 Gy to allow a direct comparison. Most immediately apparent is that the TL yields from the current batch of FFs, irradiated at 140 kVp, offer a sensitivity which while less than that of the TLD-100 chips, are nevertheless somewhat comparable and hence capable of measuring doses at diagnostic levels. Further apparent is that for 6 MV irradiations the response of the TLD-100 chips is close to an order of magnitude greater than that of the 50 µm Ge core dopant diameter, which in turn is > an order of magnitude that of the 9 µm Ge core dopant diameter.

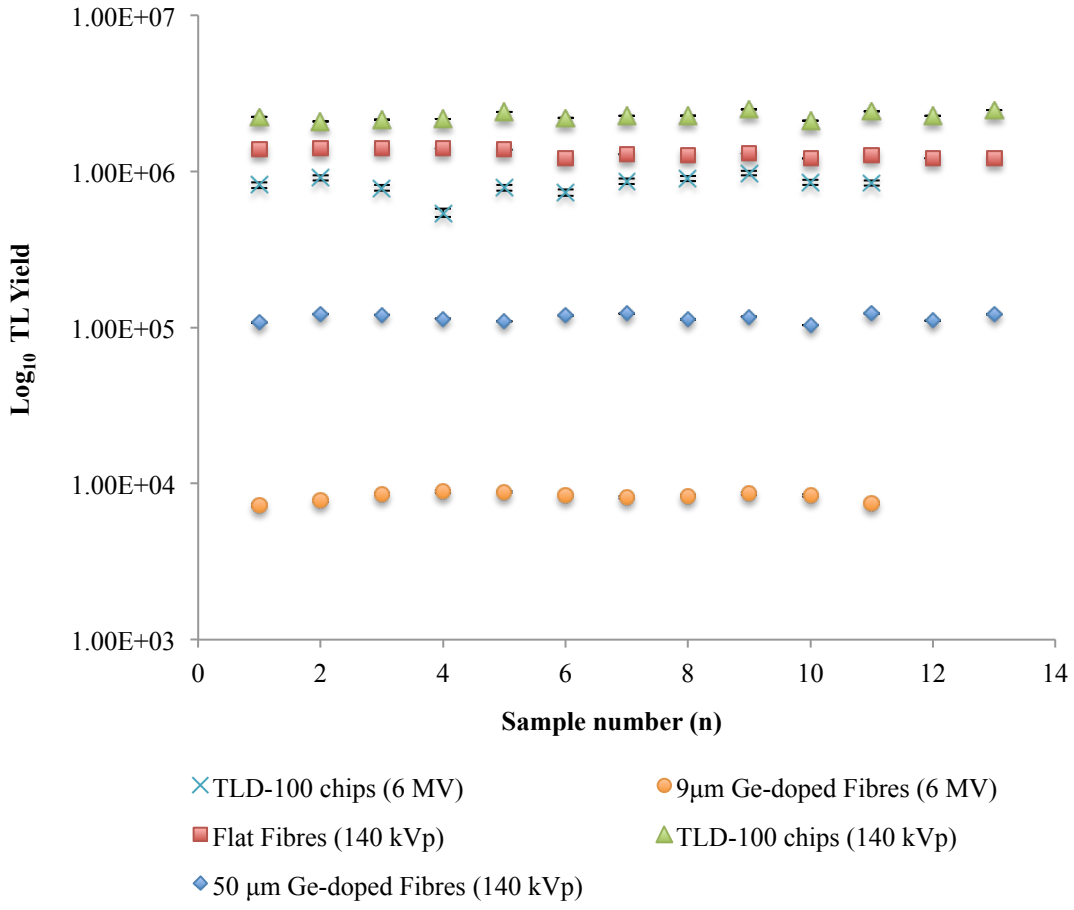

Figure 5-12 A comparison of TL yield from undoped flat fibres, doped cylindrical fibres and TLD-100 chips, normalised to a dose of 3 Gy.

5.2.3.2 The Thermoluminescence Response of Undoped Platinum Coated SiO_2 Flat Fibres and Kilovoltage Photon Irradiations

5.2.3.2.1 Dose Enhancement with Different Thickness of Pt Coating

The fibres were readout 12 hours after irradiation. However, the first set of results was unusable due to sensitivity setting that was erroneously set too high for the flat fibres. The reader was originally set to optimize readout for fibres with very small form factor compared to the fibres used in this project. Hence, the increased size and enhanced dose effect caused the readout to exceed the limit that the reader was tuned to display. This problem was resolved by readjusting the sensitivity of the reader. The fibres were then annealed and irradiated again with the same parameters. The results of the second experiment are shown in Figure 5-13 as those with the blue diamond symbol.

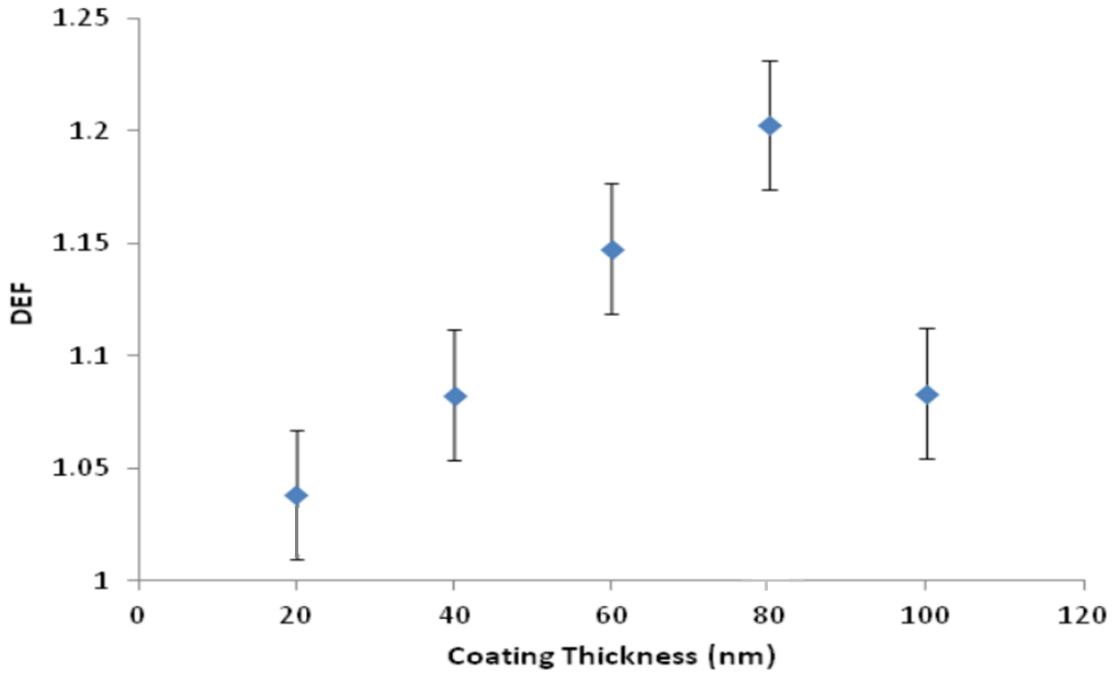

Figure 5-13 Second and third experimental results, showing as dose enhancement factor for different thickness of platinum coating.

The dose enhancement factor (DEF) is described as the ratio of dose deposited in the Pt-coated fibre to the dose deposited in the uncoated fibre. The result shows a linear increase in the dose enhancement factor (DEF) for thickness ranging from 20 nm to 80 nm. At 80 nm the DEF attains its highest value of 1.20 ± 0.03, which is 0.0150 ± 0.0003 nm^{-1}. The result obtained is comparable to a previous study by Alalawi et al. (2013) [15] that used gold as coating material, which shows a maximum DEF of 0.0160 ± 0.0001 nm^{-1}. The difference

between the experimental result was calculated to be 6 %. The difference between Au and Pt photoelectric effect probability was calculated to be 5 %. This shows that the result is also comparable with the theory. However, there is a sudden drop in DEF at 100 nm and this trend of result is very similar to the one obtained by Alalawi et al. (2013) [15], where it was found to be caused by the incomplete removal of the gold coating. This explanation does not apply in the present study, since the platinum was purposely coated on one side only to avoid the removal problem. However, in the more substantial flat fibre, differential heating effect may explain such behaviour where the DEF falls off for the higher values of coating thickness. When annealing, the metal experiences a steady rise of temperature, up to 420 ^{o}C followed by a steady drop down to 80 ^{o}C and eventually to room temperature. Although the melting point of platinum is 1768.3 ^{o}C, however it is uncertain how these fluctuations of temperature would affect the metal coating. In addition, the surface layer of platinum may perhaps not completely bond to the silica surface, which may cause easier removal of Pt on thicker coated fibres. The method of sputter coating may also contribute to this problem. In this study layers of 20 nm platinum were sputter coated each time to add up to the desired thickness. For example, 60 nm coating would be applied as 3 separate coatings. This may affect the bonding of the metal, which may enable differential heating causing degradation of TL yield. However, these are only conjectures that may explain the TL yield degradation at thicker metal coating.

5.2.4 Summary of the High Sensitivity of Undoped Flat SiO_2 Fibre and The Thermoluminescence Response of Undoped Platinum Coated SiO_2 Flat Fibres and Kilovoltage Photon Irradiations

5.2.4.1 High Sensitivity of Undoped Flat SiO_2 Fibre

In the present study, the dosimetry of undoped flat fibre has been shown to possess a number of desirable characteristics, demonstrated using photons of 6 MV irradiations. The sensitivity of the flat fibre is found to be markedly higher (by a factor of 100) than that of Ge-doped fibre, being comparable to that of TLD-100. Given their ease of handling and low cost, these various features make the flat fibres a promising TL material for use as a dosimetric system in a number of clinical applications. Extending beyond present study, it is now the intention of this group to proceed with the development of flat fibres. These will be characterised with respect to well-controlled conditions, concentrations of particular dopants and high atomic number coatings, which will provide for the highest TL yield for both therapeutic and diagnostic applications.

5.2.4.2 The Thermoluminescence Response of Undoped Platinum Coated SiO_2 Flat Fibres and Kilovoltage Photon Irradiations

The investigation of the effect of different thickness of platinum coating on the thermoluminescence response of tailor-made undoped SiO_2 flat fibres has been highlighted above. The result shows a maximum dose enhancement factor of 0.0150 ± 0.0003 nm^{-1}, which is comparable to gold-coated fibres. However, there is a drop in DEF at 100 nm thickness of coating. This has been attributed to the differential heating effect from annealing and sample handling which leads to damage of the coating. Damage to the coating was visually observed, and the result of the damage was reflected in the dose response experiment. This opens up possibility of small field dosimetry in conjunction with concurrent chemo-radiotherapy which uses platinum based chemotherapy agents and dose enhancement of optical fibres TLD with platinum coating as discussed previously in section 5.2.3.2.

5.3 Situations towards Enhanced Thermoluminescence Yield: Part 2

5.3.1 Introduction

In this section, the TL response of six types of doped optical fibres, Ge-B-PCF (collapsed), Ge-Br-PCF (collapsed), Ge-PCF (collapsed), Ge-PCF (uncollapsed), Ge-CF and Ge-FF, each type being subjected to X-rays and alpha particles irradiations have been investigated.

5.3.1.1 Measurement of Dose from X-ray Irradiation using Doped Silica Fibre

The TL response of commercially available Ge-doped fibres to photon irradiations has been the subject of investigations for in excess of a decade [24 - 26]. It should be noted that to date the TL response of Ge-doped fibres to low energy X-ray irradiations has not been studied in detail; discussion will initially cover some of the previous studies of Ge-doped fibres as dosimeter in radiotherapy.

Abdul Rahman et al. (2010) [27] evaluated the TL-response of Ge-doped optical fibres for synchrotron microbeam radiation therapy (the beam having 107 keV mean x-ray energy and an energy spectrum in the range 50-350 keV). This particular radiation therapy facility employs a very high dose gradient, with dose changing by hundreds of Gy within ~ 10 μm. The TL-yield was found to increase linearly from 1 Gy to 2 kGy, being adequate for the intended synchrotron microbeam radiotherapy dosimetry requirements, saturating beyond this due to the filling of all defects centres (dopant ions). Within the linear range, the TL yield was found to be 2.5 times greater than that obtained in a previous study by Hashim et al. (2009)

[5] for the same kind of Ge-doped optical fibres, irradiated with 6 MV photons, this being due to dose-rate non-reciprocity. The TL-yield reproducibility was found to be better than 4% (1SD).

Issa et al. (2011) [4] investigated the Ge-doped fibre response to kilovoltage X-ray therapy irradiations generated at 90 and 300 kVp. The parameters under study included dose response, reproducibility and fading. Relative dose measurements were performed, obtaining central axis percentage depth dose (PDD) values, use being made of doped fibres irradiated in water and solid water phantoms. TL yields were compared with published data and ionization chamber measurements. At 90 kVp and 300 kVp, Ge-doped optical fibres were shown to provide good reproducibility to within ± 2 % and linear dose response over a useful range of therapeutic doses (0.1 to 45 Gy) [4]. TL fading was found to be minimal, at < 1.5% over a seven days period. The RMI-457 solid water phantom correction factor at 2 cm depth was found to be 1.155 ± 0.152 and 0.955 ± 0.221 at 90 kVp and 300 kVp respectively. Percentage Depth Dose (PDD) evaluations made with Ge-doped optical fibres irradiated at 90 kVp in a water phantom, agreed to within 3.1% with measurements made in a RMI 4571 solid water phantom and to within 2.3% with British Journal of Radiology (BJR) tabulated data. PDD measured values for 300 kVp, beams obtained using Ge-doped optical fibres in water, were in good agreement with BJR tabulated data and ionization chamber measurements to within 1.1% and 1.5 % respectively [4]. This study indicates that for all PDD measurements, doses measured in the solid water phantom agreed with those measured in water, within measurement uncertainties. The small size and sensitivity of the optical fibre dosimeters offer considerable potential in providing PDDs for small field size applicators, overcoming the alignment problems mentioned in the addendum to the Institute for Physics and Engineering in Medicine (IPEMB) code [28].

This dissertation builds on previous experience, as above, and investigates the use of Ge-doped optical fibres in the dosimetry of kilovoltage therapeutic X-ray beams. In this section the response of various types of Ge-doped optical fibres to low energy X-ray photons using a superficial kVp X-ray set are studied. Sensor characteristics including dose response, reproducibility, glow curves and energy response are determined. The identified characteristics are important features and through use of an X-ray set, the exploratory investigation could be carried out relatively quickly. It has been established that the TL performance of an irradiated fibre is not only influenced by radiation parameters such as energy, dose-rate and total dose but also the type of fibre. The results that accompany the above section are discussed in section 5.3.1.2.

5.3.1.2 Measurement of Dose from ^{223}Ra Irradiation using Doped Silica Fibre

Alpha particles do not penetrate sufficiently deeply (losing energy at an elevated rate compared to lower linear energy transfer (LET) radiations) to allow for teletherapy unless accelerated to high energies of few 100 MeV [29]. Conversely, the implementation of isotopic alpha sources in targeted alpha therapy has been proven to be useful in cancer treatment as reported by Allen et al. [30]. The ionizing power of alpha particles is concentrated near the ends of their paths, producing what is referred to as the Bragg peak. Hence they can deliver destructive energy to a tumour while causing relatively little damage to nearby healthy tissue. The energy can be delivered with considerable precision by controlling uptake and dosage, the resulting alpha particle radiotherapy being uniquely suited for treating highly localised tumours near sensitive normal tissue. Validation of dose using sensitive systems of dosimetry offering good spatial resolution would appear necessary in support of such charged particle therapy.

Ramli et al. (2009) [7] have investigated the Ge-doped SiO_2 optical fibre response to alpha-particles emitted from an ^{241}Am source (1.77 MBq) of energy 5.486 MeV and compared the TL characterisation with that of TLD-100 rods. In this work, at the irradiation distance of 1 cm, the air kerma dose rate has been estimated to be 0.57 Gy/h. The TL yield of the dose response of TLD-100 was reported to be approximately 10 times that of Ge-doped fibres and approximately 30 times that of Al-doped fibres, each of 5 mm length. However, unlimited by the hygroscopic nature of TLD phosphors, for heavy charged particle beams, present results indicate there to be potential for use of SiO_2 optical fibres, offering the possibility of improved positional sensitivity (fibre diameters are sub-millimetre, typically ~125 μm compared with the ~ millimetre dimensions of the phosphor dosimeters).

Using tailor-made doped silica fibres, thermoluminescent dosimetric studies of a formulation of $^{223}RaCl_2$ (the basis of a product called Xofigo^{TM} (Algeta, Norwegian)) has been carried out. Due to the intrinsic high LET, the short path length (< 100 μm) of the α-particles emitted by the nuclide (and decay progeny) and the high uptake in metabolically active bone metastases the radiopharmaceutical technique is being used for treatment of bone metastatases caused by late-stage castration resistant bone cancer [31]. In this study, the TL yield of various forms of doped SiO_2 optical fibres has been investigated for in vitro dosimetry of α-particles originating from the ^{223}Ra decay series. The six-stage-decay of ^{223}Ra to ^{207}Pb occurs via short-lived daughters, and is accompanied by a number of alpha, beta and gamma emissions with different energies and emission probabilities. The fraction of energy emitted from ^{223}Ra and its daughters as alpha particles is 95.3 % (energy range of 5.0 - 7.5

MeV). The fraction emitted as beta-particles is 3.6 % (average energies are 0.445 MeV and 0.492 MeV), and the fraction emitted as gamma-radiation is 1.1 % (energy range of 0.01 - 1.27 MeV) [32]. The half-life ^{223}Ra was evaluated using a power moderated weighted mean of selected experimental values, with a new value of the recommended half-life for ^{223}Ra of 11.4354 days [33]. Moreover, SiO_2 optical fibres offer many advantages over conventional dosimetry systems including the calcified tissue equivalence of the dosimetric material, the value of Z_{eff} being close to that of bone (being for the fibres, in the range 11.6 - 13.8) [34]. The outcome of the current research is expected to be useful in developing and characterizing tailor-made doped optical fibres as new potential candidate TL dosimeter materials for skeletal radiation dosimetry. The results that accompany the above section are discussed in section 5.3.2.2.

5.3.2 Experimental Procedures

This section is divided into two separate investigations utilising six types of doped silica fibres of nominal 8 wt% for measurement of dose from X-ray irradiation (5.3.2.1) and measurement of dose from ^{223}Ra irradiation using doped silica fibres (5.3.2.2).

5.3.2.1 Measurement of Dose from X-ray Irradiation using Doped Silica Fibres

The types of Ge-doped SiO_2 silica fibres of nominal 8 wt% dopant concentration used herein are presented in Table 5-2. The performance of the Ge-doped optical fibres is compared against the Ge-B-doped and Ge-Br-doped SiO_2 optical fibres, fabricated with the same germanium dopant concentration. Prior to irradiation, the optical fibres were cut into length of approximately 0.5 cm using the optical fibre cleaver (Fujikura, Japan). The mass of each individual fibre was determined using an electronic balance (PAG, Switzerland), allowing TL yield to be normalized to unit mass of the irradiated fibre (see Table 5-2). The optical fibres were first annealed in a furnace (Carbolite, UK) before receiving any irradiations and subsequent TL measurements in order to eliminate any irradiation memory from the dosimetric material.

Table 5-2 Summary of the type, the dimension and the mass of SiO_2 optical fibres used herein.

Fibres Type	*Dimension (μm)*	*Mass x 10^{-4} (g)*
Ge-Cylindrical Fibre (CF)	120 ± 10	1.6 ± 0.01
Ge-Flat Fibre (FF)	(100 x 350) ± 5	7.0 ± 0.01
Ge-PCF (uncollapsed)	125 ± 10	1.6 ± 0.01
Ge-PCF (collapsed)	125 ± 10	1.6 ± 0.01
Ge-B-PCF (collapsed)	140 ± 10	1.6 ± 0.01
Ge-Br-PCF (collapsed)	140 ± 10	1.6 ± 0.01

The doped SiO_2 fibres were irradiated using an X-ray tube facility (Comet, Switzerland) located at the Department of Physics, University of Surrey, over a wide range of doses from 2 cGy up to 50 Gy using 60 kV nominal energy. The optical fibres were attached on sticky paper and subsequently located on a MDF board positioned 30 cm away from the uncollimated X-ray beam as shown in Fig. 5-14 and Fig. 5-15. Two focal spot sizes of the X-ray beam are available, 1.0 mm and 5.5 mm. The small focal spot is generally used at relatively low power (kV and mA) settings. The large focal spot is used when the machine must be operated at power levels that exceed the rated capacity of the small focal spot. The power being supplied is the range 640 W to 3000 W, with a supply voltage of 225 kV. The X-ray tube utilised an 0.8 mm beryllium filter. The filament voltage and tube current is controlled by using the Comet MXR225/22 X-ray tube software. The X-ray tube should be prepared in a warm-up cycle prior to work, this takes approximately 35 minutes.

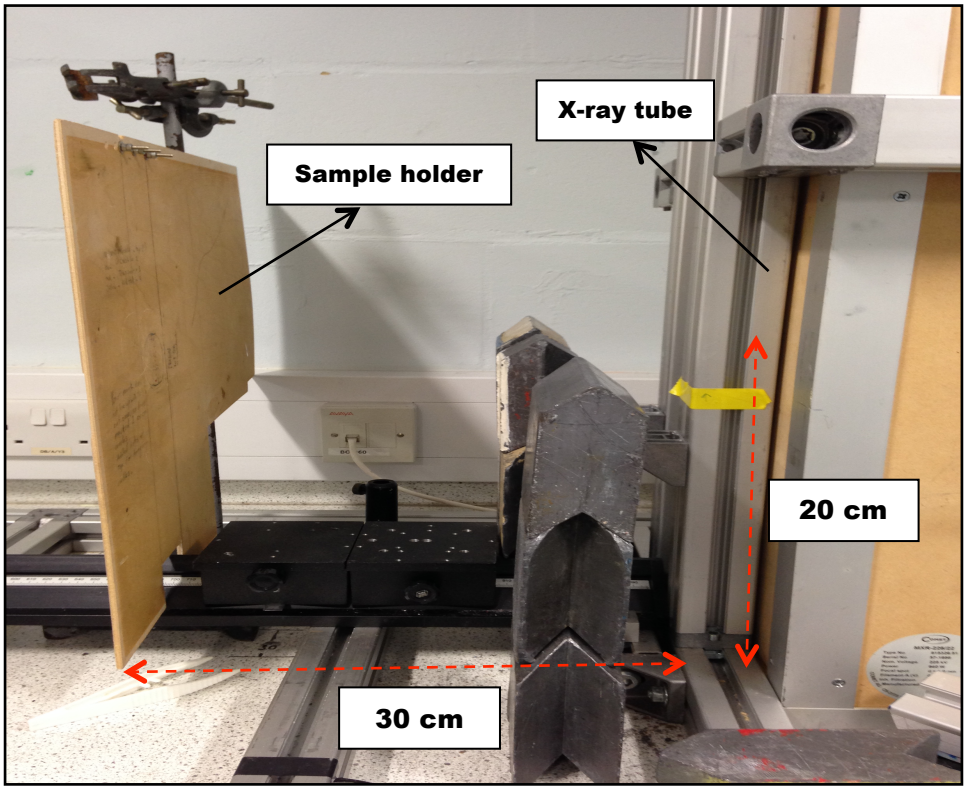

Figure 5-14 Experimental setup using X-ray tube (COMET, Switzerland) located at the University of Surrey. The sample holder (MDF board) is positioned 30 cm from the X-ray beam, being the beam height of 20 cm.

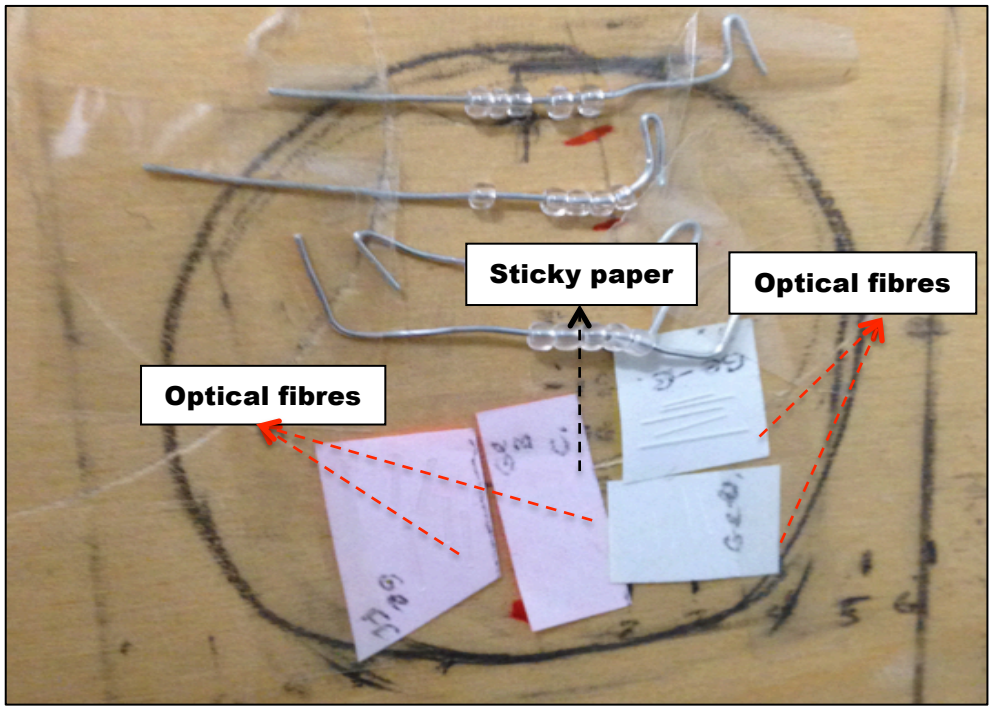

Figure 5-15 Arrangement of the sticky papers containing optical fibres attached at the sturdy board.

Preceding results were attained by exposing the doped optical fibres to an orthovoltage X-ray generator (Gulmay, UK) with photons generated at an accelerating potential of 80 kVp, 140 kVp and 250 kVp (Fig, 5-16 (a) and (b)) as well as being irradiated using a Varian Linac 2100 linear accelerator of nominal photon energy at 6 MV (Fig. 5-16 (c)) to a dose of 2 Gy. For the first of these, the sticky papers containing dosimeters were placed on the surface of a 30 x 30 x 6 cm Solid Water slab and standard output setups were obtained for each nominal beam energy as detailed in Table 5-3. A 10 x 10 cm^2 field size for clinical photon beams of 6 MV was used with a standard Focus-Surface Distance (FSD) of 100 cm. The sticky paper containing the dosimeters was placed in a water-equivalent phantom (Solid Water®) at a depth of 1.5 cm, being restricted to this value due to the limited thicknesses of available phantom slabs. This process was carried out in Royal Surrey County Hospital (RSCH), Surrey.

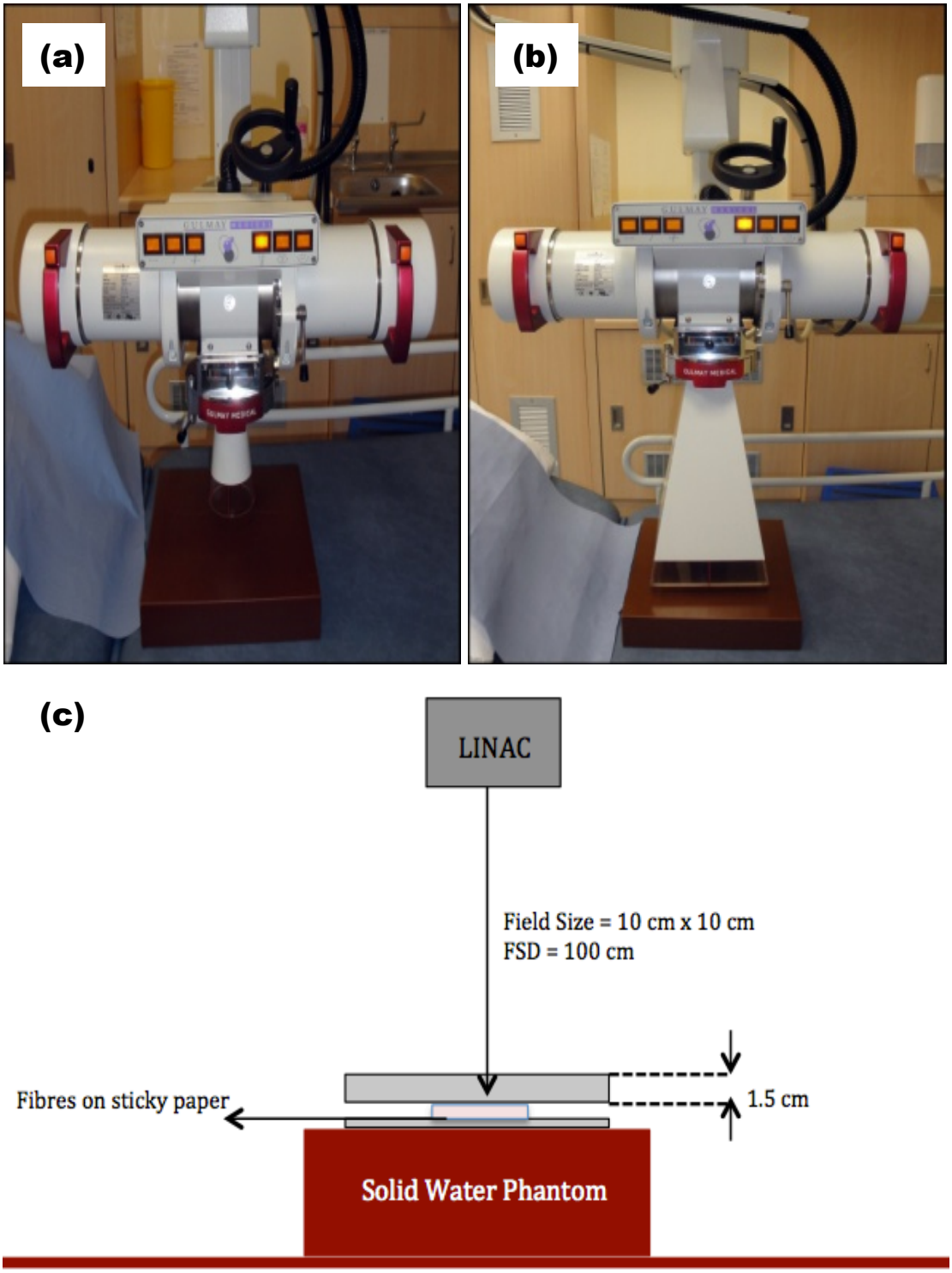

Figure 5-16 (a) and (b) The X-ray machine with different applicators for different values of X-ray energy with respect to 80 kV and 140 kV together with 250 kV, (c) The experimental setup using Varian LINAC linear accelerator.

Table 5-3 X-ray beam parameters

Tube Potential (kVp)	*Added Filtration*	*HVL*	*FSD*	*Field size applicator*	
				Applicator dimension	*Applicator specification*
80	2 mm Al	2.4 mm Al	30 cm	-	circular-open-ended applicator
140	1.4 mm Al + 0.1 mm Cu	6.6 mm Al	50 cm	20 x 20 cm	Close-ended applicator
250	1.5 mm + 0.25 mm Cu + 0.5 mm Sn	2.7 mm Cu	50 cm	20 x 20 cm	Close-ended applicator

HVL: Half Value Layer. FSD: Focus Skin Distance.

The dosimeters were placed in an epoxy resin solid water phantom at 1.5 cm depth for the photon irradiations, using a standard Source Surface Distance (SSD) of 100 cm (Fig. 5-16). Each doped optical fibre was irradiated to a fixed dose of 2 Gy. A Harshaw 4500 planchet TLD reader was employed to readout the dosimeters. The heating cycle consisted of preheat, readout, anneal and cool segments. The time-temperature profile in this study was set at a preheat temperature of 140 ºC within 10 s, with the readout segment set at the temperature 300ºC at a rate of 35 ^{o}C/s. The planchet, of ~ 0.8 cm diameter, could accommodate optical fibres cut to a length of ~ 0.5 cm. The weight of each optical fibre was measured by taking the average of the number of fibres in each capsule. The weight of each fibre varied in the range 0.16 - 0.17 mg. The TL measurements were corrected to provide counts per second per unit mass of fibre. The net measurements were obtained by subtracting the background values.

5.3.2.2 Measurement of Dose from ^{223}Ra Irradiation using Doped Silica Fibre

The present work provides a comparison of the performance of the Ge-doped SiO_2 optical fibres e.g. Ge-PCF (collapsed), Ge-PCF (uncollapsed), Ge-CF and Ge-FF with the Ge-B-doped PCF (collapsed) and Ge-Br-doped PCF (collpased) optical fibres. These tailor made silica fibres, all doped with nominal 8 wt% Ge, were cut into approximate 10 cm lengths. Similarly, as in previous measurement on X-ray irradiation, the mass of these optical fibres

were determined using an electronic balance (PAG, Switzerland), allowing TL yield to be normalized to unit mass of the irradiated dosimeter. The mean masses of these optical fibres were presented in Table 5-2 as shown in section 5.3.2.1. The fibres were first annealed in a furnace (Carbolite, UK) before making any irradiations and subsequent TL measurements to eliminate any irradiation memory from the dosimetric material.

The University of Surrey is not currently licensed to handle liquid alpha nuclei sources, with insufficiently arrangements in place to handle the radiation and security risks. The material used herein, namely *Xofigo*^{TM} could be administered only by persons authorised to handle radiopharmaceuticals in designated clinical settings. Therefore, the irradiation was performed at the UK National Physical Laboratory (NPL). Algeta ASA (Norway) supplied a radiochemically pure solution of nominally 50 MBq $^{223}RaCl_2$ in 10 ml sodium citrate buffer solution to the NPL. To prevent thermodynamic instability of the solution, which had been previously observed with similar solutions at NPL, the solution was diluted to nominally 3 MBq g^{-1} of $RaCl_2$ in 1 M HCL before use [33]. As ^{223}Ra emits ^{219}Rn, the ampoule was held in a lead pot and placed in a fume cupboard in order to reduce the contamination from out-gassing. A hypodermic needle was carefully pushed through the rubber bung in the top of each vial, ensuring that the needle did not go into the solution (Fig. 5-19). Each optical fibre was placed through each hypodermic needle and into the solution so that ~1 cm of the fibre was submerged in the solution. The fibres were inserted at the same time and removed individually over the course of a half-life (11.43 days) of ^{223}Ra. After 12 hours of irradiation, the samples were read out using a Toledo TLD reader. The sequence used for this reader was; preheat at 160 ^{o}C for 10 s, readout at 300 ^{o}C for 25 s with ramp rate of 25 ^{o}C/second and anneal at 300 ^{o}C for 10s to eliminate residual signals.

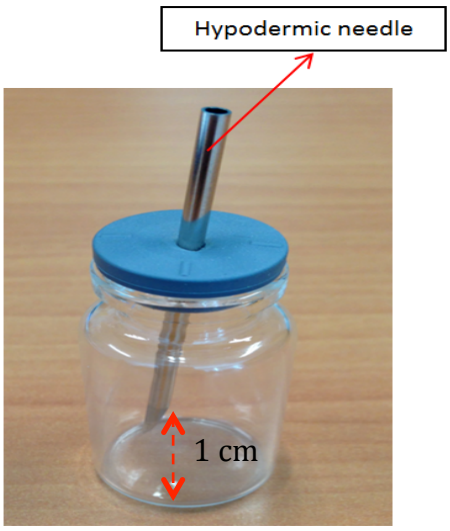

Figure 5-17 The optical fibres were placed through the hypodermic needle inserted in the ampoule so that ~1 cm of the fibres length was submerged into the solution.

5.3.3 Results and Discussion

Section 5.3.3.1 discusses the results and discussion on measurement of dose from X-ray irradiation using doped silica fibres. Following to this, in section 5.3.3.2, the measurement of dose from ^{223}Ra irradiation using doped silica fibres have been discussed.

5.3.3.1 Measurement of Dose from X-ray Irradiation using Doped Silica Fibres

The measurement of dose from X-ray irradiation using doped silica fibres is divided into four discussions, including beam profile (5.3.3.1.1), dose response (5.3.3.1.2), glow curve (5.3.3.1.3) and energy response (5.3.3.1.4).

5.3.3.1.1 Beam Profile

Using an ion chamber (QADOS, Guildford), the beam profile of the X-ray tube (Comet, Switzerland) used herein was measured within the 'flattened area' at a distance of 30 cm from the X-ray beam source. The profile measurements were normalised to the dose at the central axis for a 5 x 5 cm^2 field size defined at the surface (Fig. 5-18) irradiated with 160 kV X-rays and 100 mA current, giving a dose reading of approximately 2 Gy. A time of 20 s was set for each individual measurement. It is very convenient to measure the beam profile with an ionisation chamber because their use is fast and also gives some information about the temporal stability of the beam. The resulting scan clearly shows whether the peak dose distribution is correctly centred and symmetrical. For the purpose of the present results, on

average, the beam flatness was found to be 3.6 ± 0.3 % across the whole field of 5 x 5 cm^2 field size. Flatness is the ratio of maximum to minimum dose anywhere in the beam. In X-ray beams the minimum is usually close to the central axis of the beam, usually because of a beam flattening filter referred to as 'bow-tie' filter. The present result is compared with the International Electrotechnical Commission (IEC) specification [35], allowing an asymmetry of 3 %, being of sufficient measurement accuracy for a quick check. However, it should be easier to achieve better beam symmetry with a modern accelerator. The profiles obtained in this way should not be taken into account as absolute measurements of flatness and should be compared to a similar measurement made at the time of commissioning. It is important to check that the profile has not changed significantly since the beam data were measured.

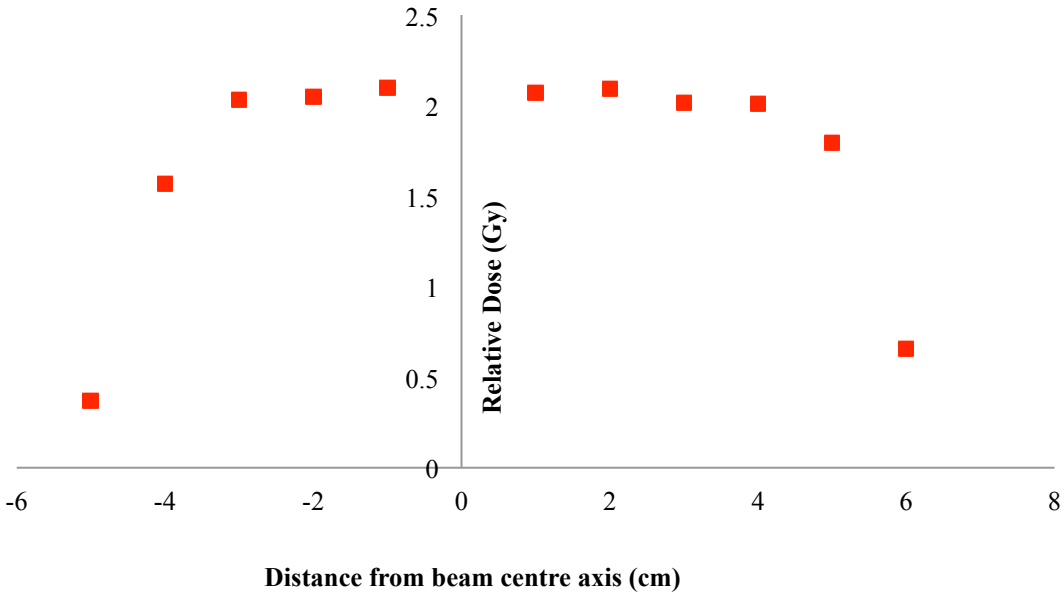

Figure 5-18 Beam profiles at 160 kV in a 5 x 5 cm^2 field, measured with an ionisation chamber.

5.3.3.1.2 Dose Response

To investigate dose response over a wide range (2 cGy to 50 Gy) loaded fibres on sticky paper (each containing 3 individual fibres) were irradiated by kilovoltage X-ray beams of 60 kVp. Fig. 5-19 represents the dose response of the Ge-doped SiO_2 optical fibres for PCF (collapsed), PCF (uncollapsed), CF, FF, together with Ge-B-doped of PCF (collapsed) and Ge-Br-doped of PCF (collapsed), in comparison with TLD-100 TL yields for the accelerating potential. Least square fits to the data have been obtained while the error bars represent the standard deviation from the mean. The obtained values of correlation coefficient (R^2) of the optical fibres confirm linearity, presented in Table 5-4.

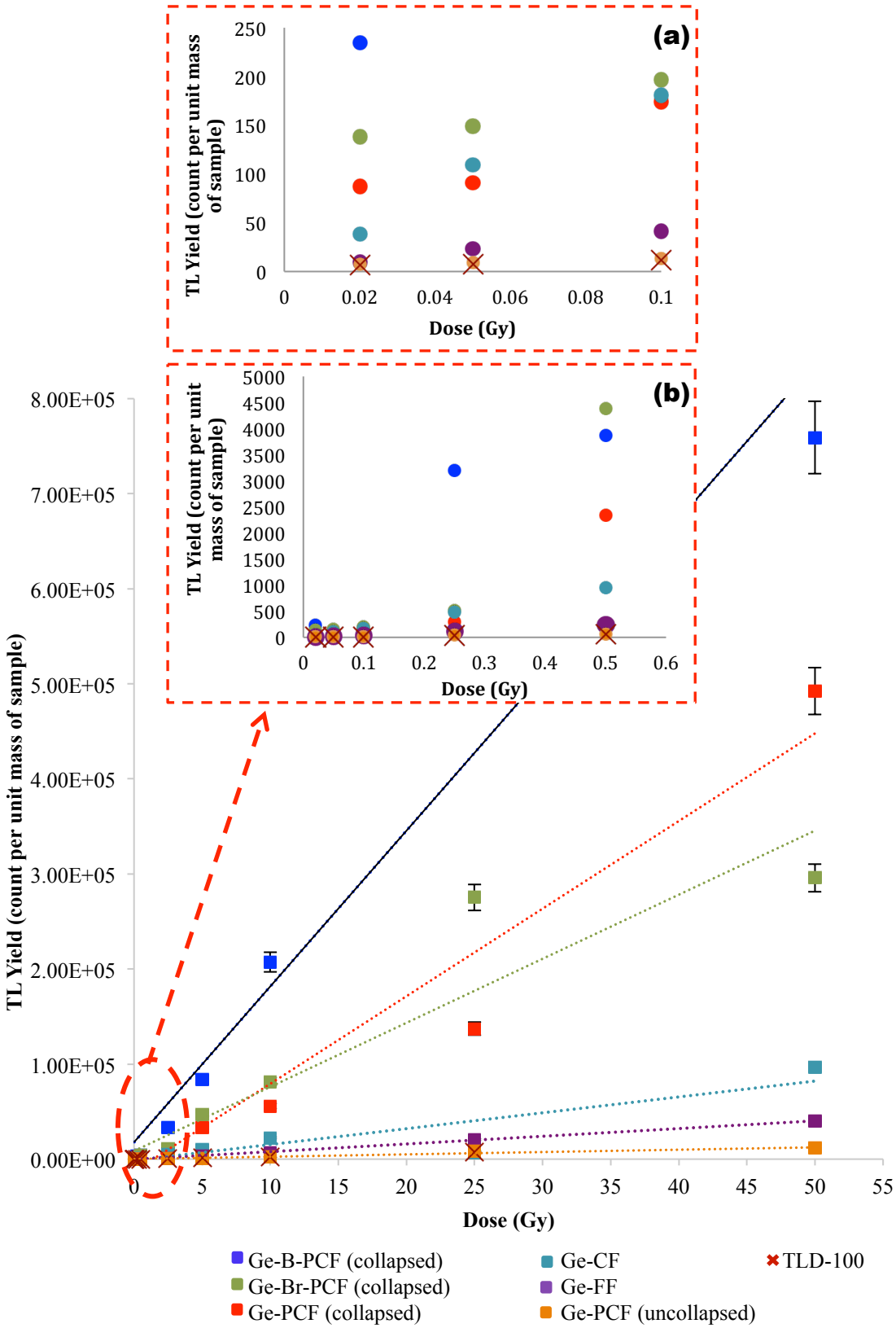

Figure 5-19 The dose response for Ge-B-PCF (collapsed), Ge-PCF (collapsed), Ge-Br-PCF (collapsed), Ge-CF, Ge-FF and Ge-PCF (uncollapsed) in comparison with TLD-100 together with standard error of the mean. The dotted lines are least square fits to the data. (Note: the error bars are smaller than the data points). The inset provides an enlarged view, (a) showing the TL yield variation for the 0 to 5 Gy doses and (b) showing the TL yield variation for the 0.02 to 0.1 Gy doses.

Table 5-4 Summary of the TL output as a function of dose and correlation coefficient of the doped SiO_2 optical fibres used herein.

Fibres Type	*TL output as a function of dose (count per mass per unit dose)*	*Correlation Coefficient (R^2)*
Ge-B-PCF (collapsed)	y = 16383x + 17785	0.9482
Ge-Br-PCF (collapsed)	y = 6740.4x + 8547.3	0.8945
Ge-PCF (collapsed)	y = 9215.1x - 12951	0.9544
Ge-Flat Fibre (FF)	y = 1669.9x - 1363.6	0.8212
Ge-Cylindrical Fibre (CF)	y = 811.02x - 284.05	0.9991
Ge-PCF (uncollapsed)	y = 245.73x + 82.439	0.9689
TLD-100	y = 273.79x - 146.39	0.98439

It is desirable in radiotherapy dosimetry for the measurement system to produce a linear response to absorbed dose. In terms of linearity, from Table 5-4, most of the samples show a highly linear response (linear fitting curve $R^2 > 94.8\%$) over the investigated dose range, 2 cGy to 50 Gy except two of the samples that are Ge-Br-PCF (collapsed) and Ge-FF, producing linear fitting curve $R^2 > 80\%$. Taking TLD-100 as the benchmark, Ge-B-PCF (collapsed), Ge-Br-PCF (collapsed), Ge-PCF (collapsed) and Ge-CF, exhibit significantly greater response, on average, respectively, of some 60, 33, 21 and 11 times to that TLD-100. These results confirm that doped PCFs (collapsed) significantly outperform TLD-100. Meanwhile, Ge-FF and Ge-PCF (uncollapsed) produce relatively small differences of factor 3 and 1 times to that TLD 100 respectively.

Comparison can be made with previous measurement on the potential of the same type of PCF (collapsed) and PCF (uncollapsed) compared against CF. In irradiation made using 6 MeV electrons over a dose range 0.2 mGy up to 10 Gy, Amouzad Mahdiraji et al. [36] demonstrated improved TL response in the PCF (collapsed) of some 16 times greater than that conventional silica glass optical fibres. However, the PCF (uncollapsed) shows a TL response some 4 times lower than that of the CF. This is in line with expectation, given the greater detection efficiency of fibres at the lower photon energy used herein (60 kVp). The comparison underlines the impact of collapsing down the holes with surface fusion of the optical fibre occurring, generating additional defects and thereby, greater TL response. In use

of Ge-B and Ge-Br dopants, the defect centers in the internal wall surface of the fibres are much greater than in the Ge-doped fibre case. It is therefore to be expected that there will be amplified induced defect centers/strained bond rupture in the Ge-B-PCF and Ge-Br-PCF, with an associated increase in TL response. Regardless of the type of defect, a matter not within the scope of this study; the results suggest generation of additional defects in the PCFs, causing additional increase in TL response. However, it is apparent that the Ge-Br-PCF experience greater sensitivity compared to pure Ge-PCF (collapsed) from 2 cGy to 25 Gy and become abruptly saturated at a dose in the range 25 to 50 Gy. This indicated that whenever TL yield become saturated, a linear dose dependence can no longer be expected. As mentioned previously in Chapter 2 (section 2.2.2.2) the occurrence of non-linear response of a detector does not preclude its use in TLD provided that it is calibrated and corrected for the non-linearity [22].

To the best of my knowledge there exist no previous reports showing CFs to outperform TLD-100, certainly not to the present extent. Recently, Benabdesselam et al. [37] reported TL glow curve analysis of a multimode fibre (MMF) with 62.5 μm diameter with 2-layer Ge-doped fibre compared with TLD-500 and -600. The MMF is shown to be relatively more sensitive compared to TLD-500 and -600. Zahaimi et al. [38] demonstrated that the TL yield in a CF with 8 - 9 μm diameter can be improved upon by up to 6 times using a larger core MMF with 50 μm diameter with the same cladding size. In the present work, CFs with 120 μm diameter have been shown to be more sensitive than that TLD-100 irradiated with photon energy (60 kVp).

Analysis of the present results suggests that Ge-PCF (uncollapsed) is significantly less sensitive compared to the other types of fibres. With the sensitivity of these ionising radiation dosimeters depending on structural defects in the materials, the greater TL generated by the PCF (collapsed) for instance, occurs on a result of greater defects introduced in the development of the PCF (collapsed) compared to the PCF (uncollapsed). This is due to fusing of the hole surfaces in the PCF (uncollapsed) during the fibre drawing process. Furthermore, it has been shown herein that the TL response of the Ge-FF is greater than that Ge-PCF (uncollapsed). In the Ge-PCF (uncollapsed), 168 capillaries were fused together from their outer circumferences, inducing lower defects, as a result, a relatively low TL response. However, a more detailed analysis is required to understand the type of the defects induced in the collapsing region of the doped PCFs and FFs.

The TL yield of the Ge-FF is observed herein to have lower sensitivity compared to that Ge-CF, albeit being collapsed into flat form, inducing more defects. This is considered to

be due to the progressive increase in inner surfaces contact length. From the PIXE analysis of FF (as discussed in Chapter 4), the fibres become progressively thinner as the cross-section dimensions of the fibres increase. In association with this is the observed increase in inner surfaces contact length of the FF. The greater TL yield per unit mass is obtained for the smaller dimension fibres as used herein, an observation supported by analyses of the effect of light transportation through the silica component of the fibre medium of various dimensions with the associated multiple scattering, based on a simple Beer-Lambert (monochromatic, single scattering) approximation (personal communication, Siti Nurasiah Mat Nawi, 2015) [39].

In addition, since the optical fibre samples were cut manually to a mean of 5 mm with a tolerance of 0.5 mm, the non-uniformity in length results in greater variation in TL response compared to TLD-100. Due to the very low mass of individual fibres, in present practice the mean mass has been used to normalise each fibre sample, instead of seeking to obtain individual fibre corrections. This variation in TL yield of optical fibre can otherwise be reduced by cutting the fibre samples with an automated fibre cleaver.

5.3.3.1.3 Glow Curve

Fig. 5-20 and 5-21 represent the glow curves of Ge-B-PCF (collapsed), Ge-PCF (collapsed), Ge-B-PCF (collapsed), Ge-CF, Ge-FF and Ge-PCF (uncollapsed) from X-rays irradiation at 60 kV, delivering doses of 2 cGy, 5 Gy and 50 Gy. To provide intercomparison between all these samples, the curves have been normalised to dosimeter mass, the channel-temperature profile covering temperatures from 150 ^{o}C to 300 ^{o}C. In all such cases, it is apparent that as expected the glow curve generated by 50 Gy dose has proportionally greater TL intensity peak compared to the 5 Gy dose and followed by the 2 cGy dose (Fig. 5-20). It is not possible to observe any trend with the 2 cGy values as there are generally in the 10^{7} range, but are shown more clearly on Fig. 5-21. This can be explained the more shallow traps being preferentially emptied as the material is first heated, light yield subsequently falling off as these traps are depleted. As heating continues, the electrons in deeper traps are released, resulting in additional peaks, in this case producing a peak value corresponding to a temperature of 300°C. The area under the curve representing the radiation energy deposited. The glow curve area is given in terms of TL yield per unit mass of fibre per unit dose for a particular source of radiation (i.e. TL yield.mg^{-1}.Gy^{-1}).

The glow curve produced by Ge-B-PCF (collapsed) at 2 cGy is at slightly lower temperature (around 236 ^{o}C), whereas for 50 Gy and 5 Gy is around 245 ^{o}C as can be seen in

Fig. 5-21. The fibre properties differences between PCF (collapsed), PCF (uncollapsed), FF and CF, indicates that even small changes in the fibre properties in terms of defect centers can manifest in change in the TL emission, resulting in change in the glow curve shape and peak temperature. The changes suggest the formation of new defect centres in the PCF (collapsed) and FF not available in the PCF (uncollapsed) and CF.

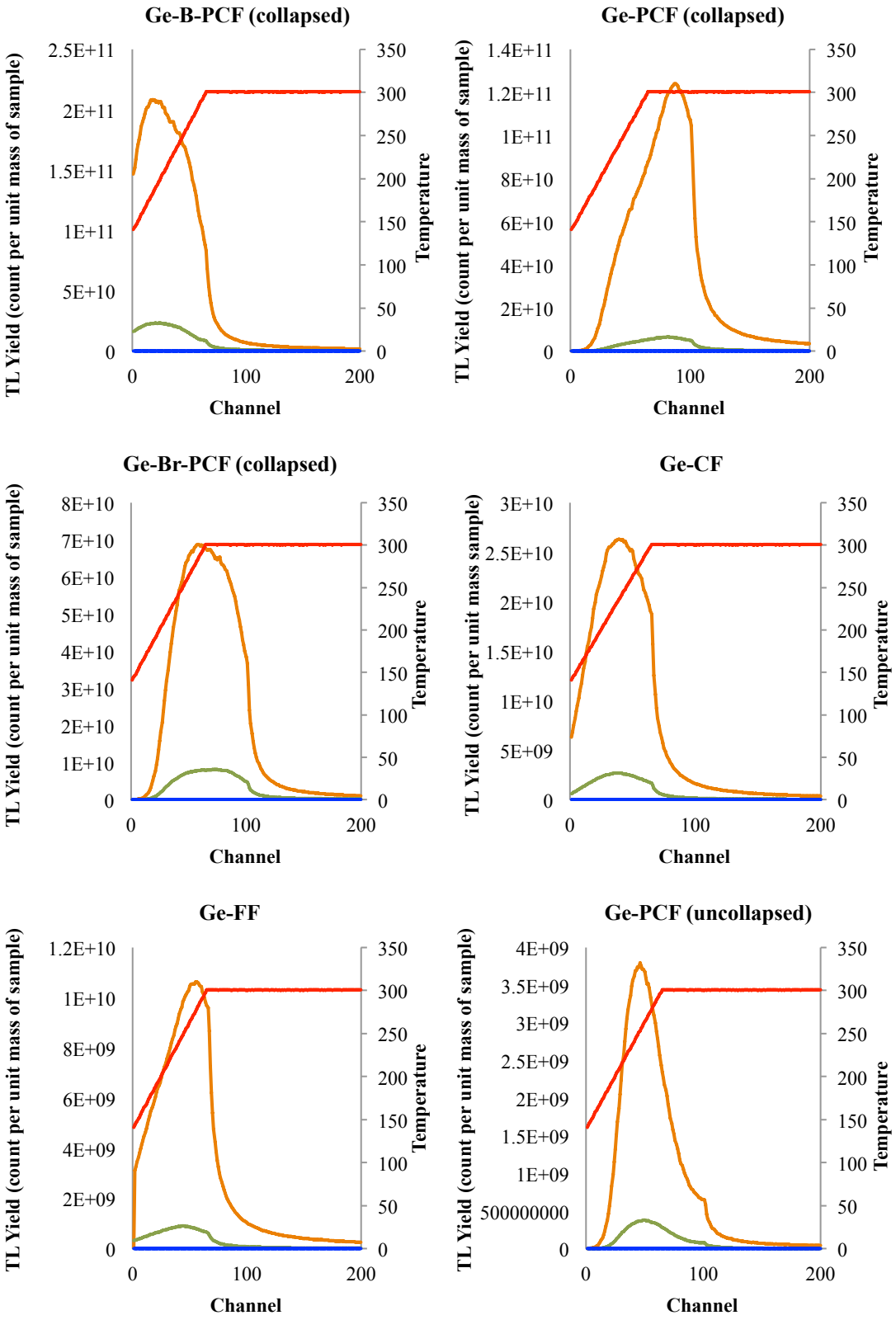

Figure 5-20 Glow curves for Ge-B-PCF (collapsed), Ge-PCF (collapsed), Ge-Br-PCF (collapsed), Ge-CF, Ge-FF and Ge-PCF (uncollapsed), respectively, obtained with 60 kV X-rays irradiation, all normalised with sample mass. Note that the orange line indicates 50 Gy dose, the green line indicates 5 Gy dose, the blue line indicates 2 cGy dose and red line represents the heating rate used.

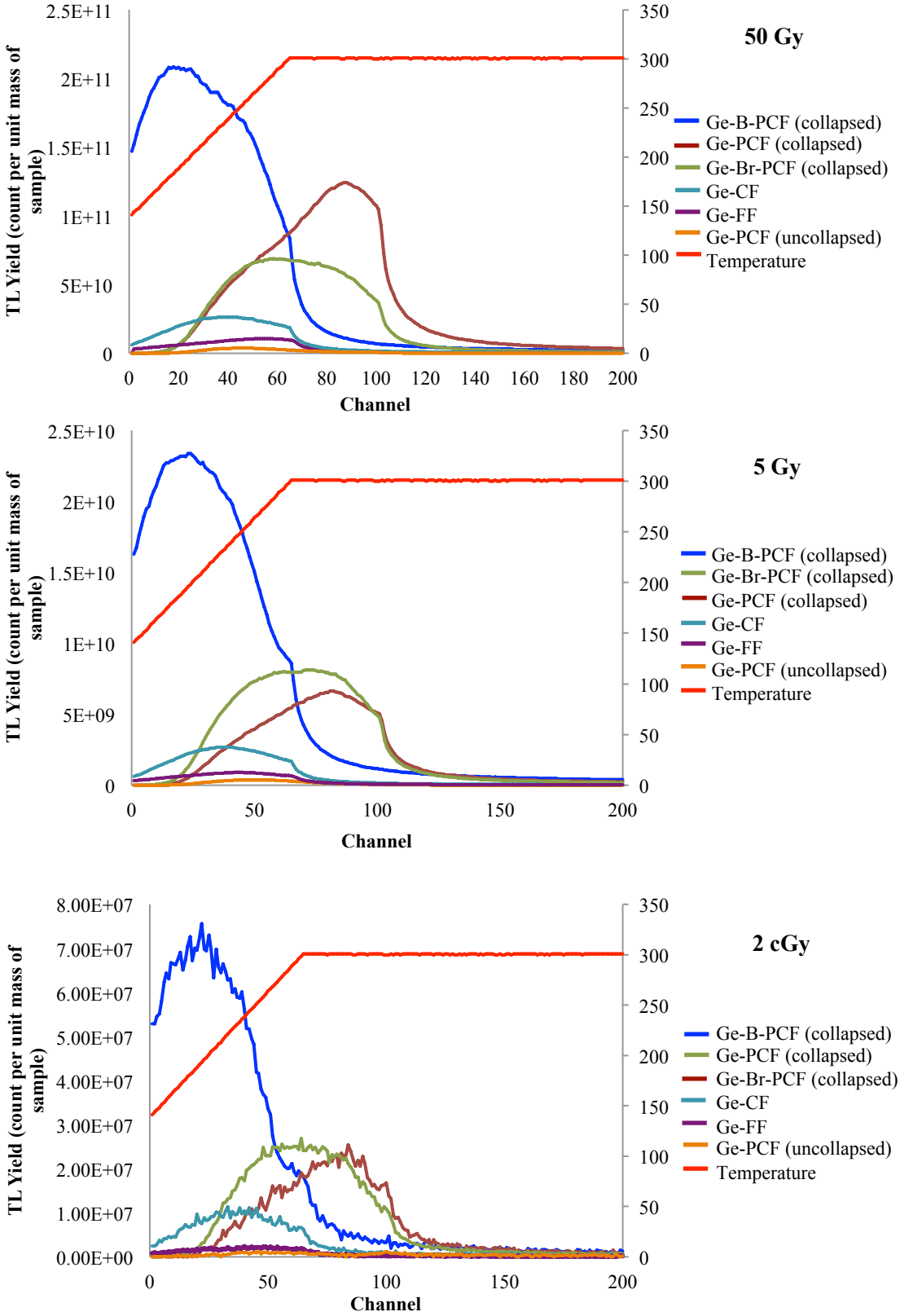

Figure 5-21 Combination glow curves of Ge-B-PCF (collapsed), Ge-PCF (collapsed), Ge-Br-PCF (collapsed), Ge-CF, Ge-FF and Ge-PCF (uncollapsed), irradiated by X-rays at 60 kV for 50 Gy, 5 Gy and 2 cGy doses, respectively.

5.3.3.1.4 Energy Response

It is important in use of the fibres that any energy dependence be characterized. It is apparent that at higher photon energy (i.e. that associated with a potential of 6 MV) (Fig. 5-22), the TL yields response decreases due to the lower mass energy absorption coefficient at higher photon energy. As expected, any type of fibres have a higher response at lower energies than at higher photon energies. The mean energy response of the Ge-B-PCF (collapsed), Ge-PCF (collapsed), Ge-PCF (uncollapsed), Ge-CF and Ge-FF for the X-rays generated at 80, 140 and 250 kV compared to that 6 MV photons is presented in Table 5-5.

Table 5-5 Summary of the average ratio of energy response for doped optical fibres generated at 80, 140 and 250 kV normalized to that of 6 MV photons.

Fibres Type	***Average Ratio of Energy Response***		
	80 kV : 6 MV	***140 kV : 6 MV***	***250 kV : 6 MV***
Ge-B-PCF (collapsed)	5.2	3.2	1.5
Ge-PCF (collapsed)	6.8	4.9	1.5
Ge-Cylindrical Fibre (CF)	8.2	7.0	2.1
Ge-Flat Fibre (FF)	3.5	3.1	1.4
Ge-PCF (uncollapsed)	3.3	2.4	1.0

The greater energy dependence of doped optical fibres in this lower energy range can be explained by the non-soft tissue equivalence of glass, in accordance with the associated energy absorption coefficients, dominated by the photoelectric effect at lower photon energies [40].

Results from these studies (refer Table 5-5) can be compared with previous work specifically for the Ge-PCF (collapsed), Ge-PCF (uncollapsed) and Ge-CF at 80 kV potential energy, respectively, some 5.4, 1.6 and 8.9 times greater compared to the average of the TL response generated by 6 MeV electrons and 6 MV photons [11].

The significant energy dependency of the doped optical fibres in the kV range point to a potential for energy discrimination of the incident photons if these SiO_2 optical fibres are used in conjunction with another TLD type such as TLD 100.

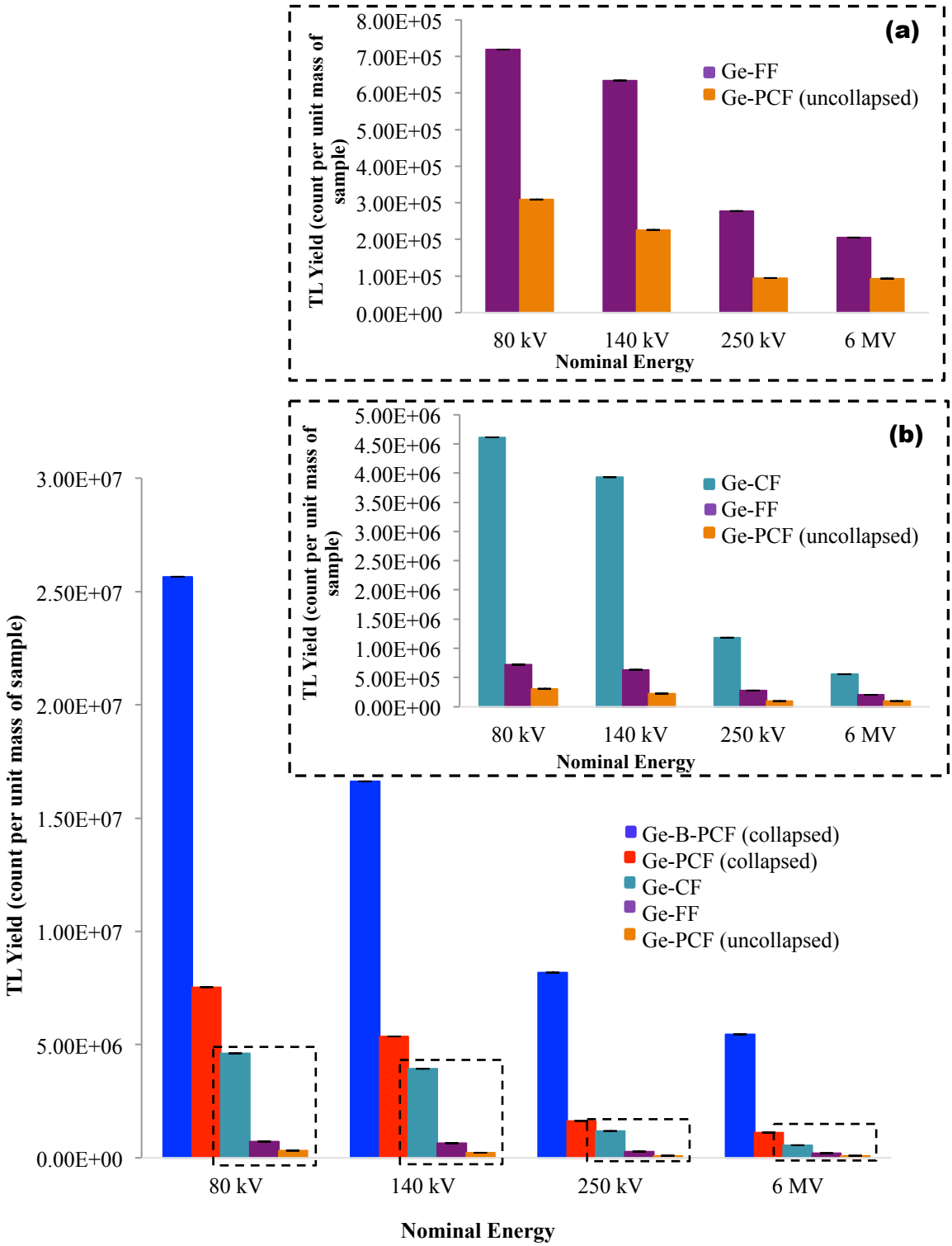

Figure 5-22 Energy response of Ge-B-PCF (collapsed), Ge-PCF (collapsed), Ge-CF, Ge-FF and Ge-PCF (uncollapsed), irradiated to a dose of 2 Gy with kV X-rays of 80 kV, 140 kV, 250 kV and MV photons of 6 MV together with the standard error of the mean. (Note: the error bars are smaller than the data points). The inset provides an enlarged view, (a) showing the TL yield variation for the kV X-rays and MV photons of Ge-CF, Ge-FF, and Ge-PCF (uncollapsed) and (b) showing the TL yield variation for the kV X-rays and MV photons of Ge-FF and Ge-PCF (uncollapsed).

5.3.3.2 Measurement of Dose from ^{223}Ra Irradiation using Doped Silica Fibre

In this investigation, use has been made of $^{223}RaCl_2$ solution to allow *in-vivo* irradiation of doped SiO_2 optical fibres. The initial activity of the ^{223}Ra used herein was 139.6 kBq/g. Since the half-life ($T_{1/2}$) of the ^{223}Ra alpha particles is 11.43 days (273.6 hours), the decay constant, λ can be found using the following equation (5-1), being $\lambda = 2.53 \times 10^{-3}$ units of per hour.

$$\lambda = \frac{\ln 2}{T_{1/2}} \tag{5-1}$$

According to the Massachushetts Institute of Technology (MIT) Open Courseware (2004) [41], the absorbed dose rate has the form:

$$\dot{D} = AE \frac{MeV}{g.s} x\left(1.6x10^{-13}\right)\frac{J}{MeV} x\left(10^{3}\right)\frac{g}{kg} \tag{5-2}$$

$$\dot{D} = 1.6x10^{-10}\left(AE\right)Gy.s^{-1}$$

where A is the activity concentration in Bq.g^{-1} of the radionuclide in the tissue and E is the average alpha particle energy, in MeV per disintegration (5.5 MeV). The rate of energy absorption per gram tissue is AE (MeV.g^{-1}.s^{-1}). The summary of the calculated absorbed dose and activity of the doped optical fibres are presented in Table 5-6.

Table 5-6 Summary of the calculated absorbed dose and activity of the doped optical fibres

Fibres Type	***Total Irradiation Time (hours)***	***Activity (kBq.g^{-1})***	***Absorbed Dose Rate (J/kg.s)***	***Absorbed Dose (kJ/kg)***
Ge-B-PCF (collapsed)	24	2.61	130.57	3.13
Ge-PCF (collapsed)	25	1.30	64.89	1.62
Ge-Br-PCF (collapsed)	22	0.65	32.34	0.71
Ge-CF	24	0.26	13.15	0.32
Ge-PCF (uncollapsed)	24	0.26	12.81	0.31
Ge-FF	31	0.17	8.68	0.27

The TL response stored in the Ge-B-PCF (collapsed), Ge-Br-PCF (collapsed), Ge-PCF (collapsed), Ge-PCF (uncollapsed), Ge-CF, Ge-FF SiO_2 optical fibres subjected to ^{223}Ra is shown in Fig. 5-23 for an absorbed dose range from 250 Gy to 3500 Gy. The absorbed dose is calculated using equation 5-2. Considering the Ge-CF as the benchmark, the Ge-B-PCF (collapsed), Ge-PCF (collapsed) and Ge-Br-PCF (collapsed) show a TL response some 18 times, 8 times and 4 times greater than that of the Ge-CF respectively. The performance of the Ge-PCF (uncollapsed) is very similar to that Ge-CF. Similarly, as explained in the previous section on X-ray measurement, the comparison of the performances of the PCF (collapsed) related to the fact that the other optical fibres generate additional defects by collapsing down the holes with surface fusion and therefore produces greater TL response. However, that the TL response of the Ge-PCF (uncollapsed) is relatively small compared with that of Ge-CF and less sensitive compared to the PCF (collapsed) is due to the uncollapsed structure where the induced defects are rather low. This can be explained by comparing the TL response of an undoped and doped capillary optical fibre (COF) before and after collapsing the fibre [36]. It was reported that the TL response of an undoped COF can be marginally improved upon in collapsing the inner wall surface of the COF into the form of flat fibre (FF). A more significant TL improvement is observed in a FF compared with a Ge-doped COF, where the Ge-dopant exists in the inner wall surface of the COF (in the collapsing region). However, in the present work, the Ge-FF is observed to have the lowest TL yield in ^{223}Ra irradiation even being exposed for the longest time of 31 hours compared to that other doped optical fibres. This is partly due to the dopant region of the FF significantly diluted when compressed to flat form as reported in PIXE analysis (discussed in Chapter 4), a thin layer of Ge dopant in inner surfaces along the length of the FF is found particularly in the smallest size fibre of dimension (100 x 350) μm, which is used herein, this manifestly challenges the ability of alpha particles to travel to points within the doped layer, as illustrated in Fig. 5-24. The arrangement is viewed using a centrally located fixed position TLD Reader photomultiplier tube, TL light along the central bisector to the longer of the two cross-section dimensions of the fibre being received normal to the upper surface of the fibre (Fig. 5-25).

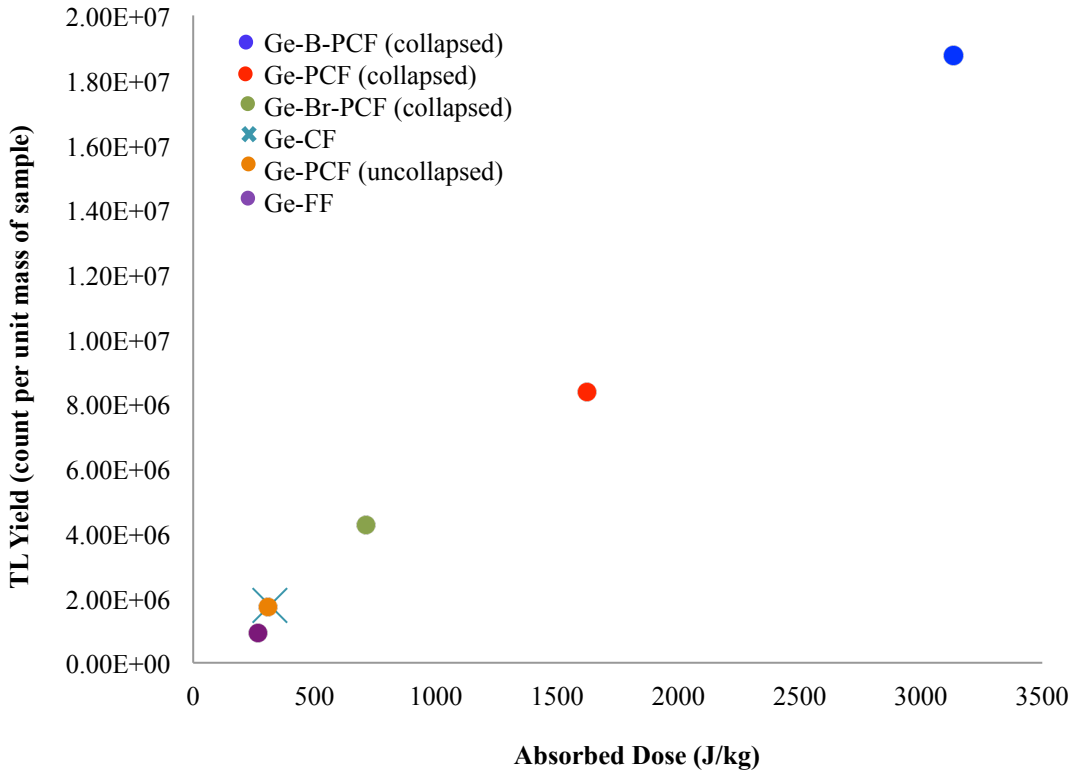

Figure 5-23 TL yield for a range of absorbed dose from 250 Gy to 3500 Gy for Ge-B-PCF (collapsed), Ge-PCF (collapsed), Ge-B-PCF (collapsed), Ge-CF, Ge-FF and Ge-PCF (uncollapsed), irradiated to ^{223}Ra alpha particles of some 20 to 30 hours of irradiation time.

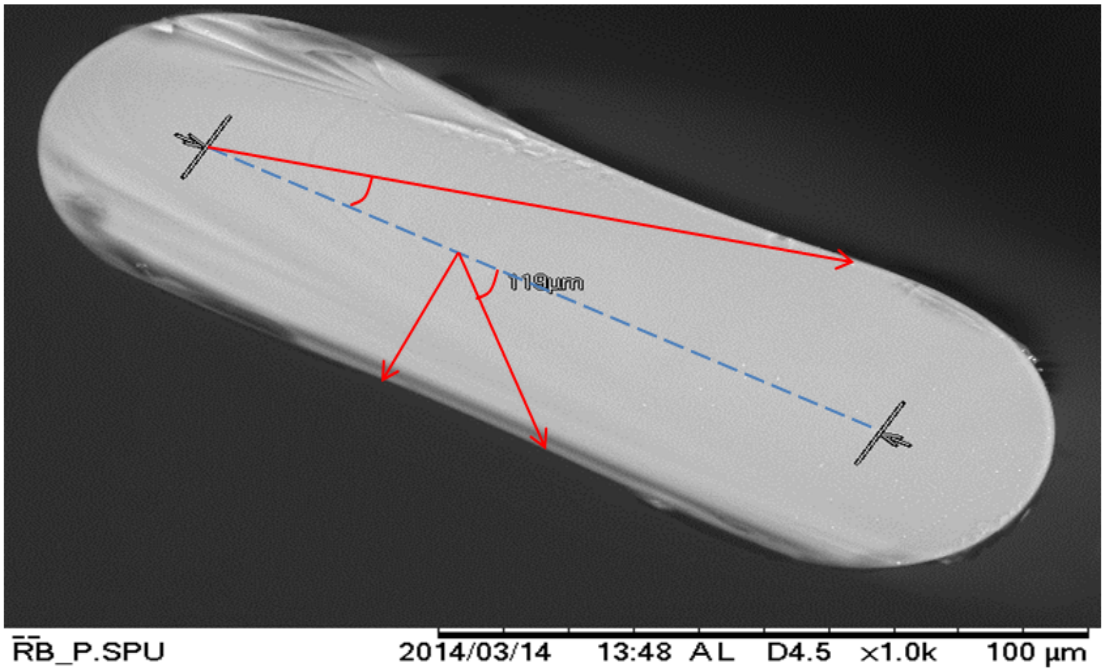

Figure 5-24 Typical cross-sectional image of a cut flat Ge-doped optical fibre. At the centre of the fibre, indicated by the blue dotted line representing the location of the core containing the Ge dopant. The red lines indicate the path of the particles transversing through the medium.

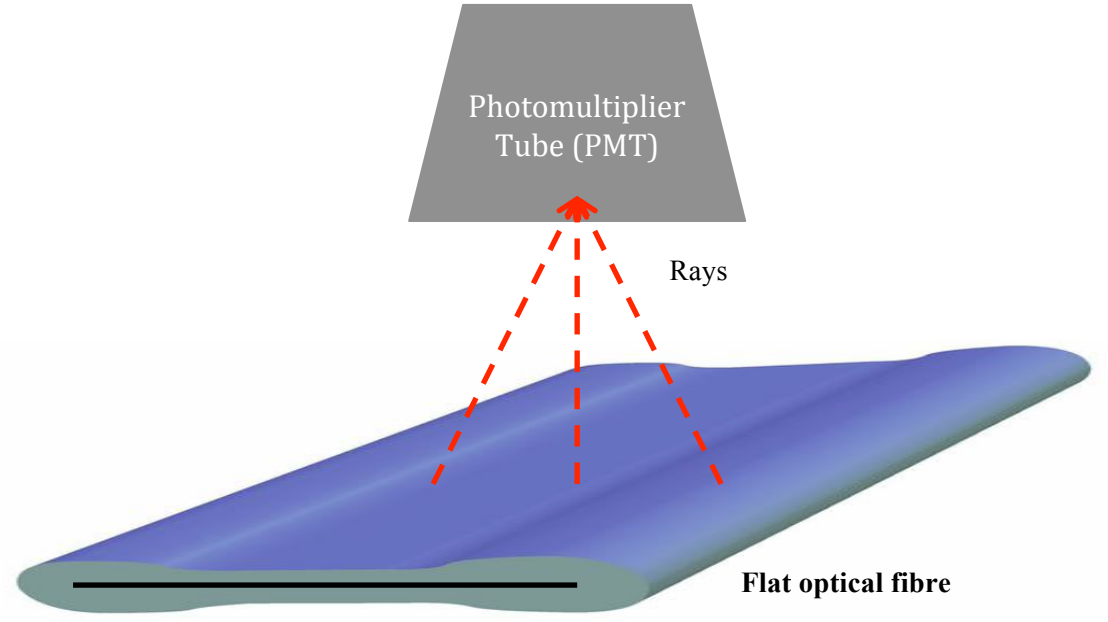

Figure 5-25 Schematic diagram of the position of flat optical fibre viewed using a centrally located fixed position TLD Reader photomultiplier tube (PMT).

One of the major advantage to be considered in using SiO_2 optical fibres sensors for radiation detection subjected to alpha particles is the small diameter of optical fibres of around ~125 µm. The dopant is centrally located with a radius of around ~ 60 µm and since the linear energy transfer (LET) of alpha particles is ~ 80 keV/µm, thereby, the energy absorbed through the optical fibres is approximately 4800 keV (~ 5 MeV). This means the average alpha particle energy is completely transferred to the material, the Bragg peak occurring at the depth of the dopant location.

The alpha particle-emitting isotope ^{223}Ra, mimics the uptake of calcium in bone and forms complexes with the bone mineral hydroxyapatite in areas of increased bone turnover, such as bone metastases. Jafari et al. has reported on the calculated mass attenuation coefficients for a few keV to 100 keV for glass beads, being closely matched to that of NIST B-100 Bone Equivalent Plastic (Jafari et al., 2014). The effective atomic number, Z_{eff} of glass beads was calculated to be 10.6 [42] whereas the Z_{eff} optical fibre was found to be in the range 11.6 - 13.8 [34] close to that bone.

Fig. 5-26 shows the combination of results from two different types of measurement obtained from the six types of doped SiO_2 fibres previously described. One used X-rays generated at 60 kVp to deliver a dose of 50 Gy and the other used ^{223}Ra alpha particles to deliver a range of doses, from the therapeutic level to doses above this, dependent on the

sensitivity of the particular fibres. Present analysis has made comparison of the LET ratio for matched fibres, irradiated by the two different sources.

According to the NIST database tabulating the stopping power of photoelectrons produced by X-rays for electrons in water [44], at 60 keV and 10 keV are 0.580 and 2.256 keV/μm respectively. The energy (dE) and track length (dS) of the electrons can be calculated using Monte Carlo simulation, utilising DOSRZnrc and FLURZnrc [45]. With the assumption of a simple cylindrical fibre and utilizing a Monte Carlo approach as described, a subsidiary calculation can then be made to yield the stopping power of electrons in water, obtaining a weighted LET including both tracks and stoppers (electrons transporting through and stopping in the fibres) of 2.0 keV/μm with an uncertainty of about 10%.

The ratio of the LET of ^{223}Ra alpha particles (~ 80 keV/μm) to that for electrons from a 60 kVp spectrum (~ 2 keV/μm) is therefore found to be around ~40. The normalisation of the TL response of the ^{223}Ra alpha-particles irradiation of the Ge-B-PCF (collapsed), Ge-PCF (collapsed), Ge-Br-PCF (collapsed), Ge-CF, Ge-FF and Ge-PCF (uncollapsed) are found to be 25, 17, 14, 18, 22 and 150 times greater than that X-ray irradiation at a dose of 50 Gy, respectively. It is clear that exposure to the ^{223}Ra alpha particles of the PCF (uncollapsed) produced a more significant change in relative response than that for the other types of fibres. As discussed previously, the sensitivity of the PCF (uncollapsed) subjected to X-rays has the least TL response compared to that of the other fibres, consequently affecting the ratio of response between that obtained for ^{223}Ra alpha particles and X-rays. The unique geometrical situation for the PCF (uncollapsed) has yet to be explored and more detailed analysis is required.

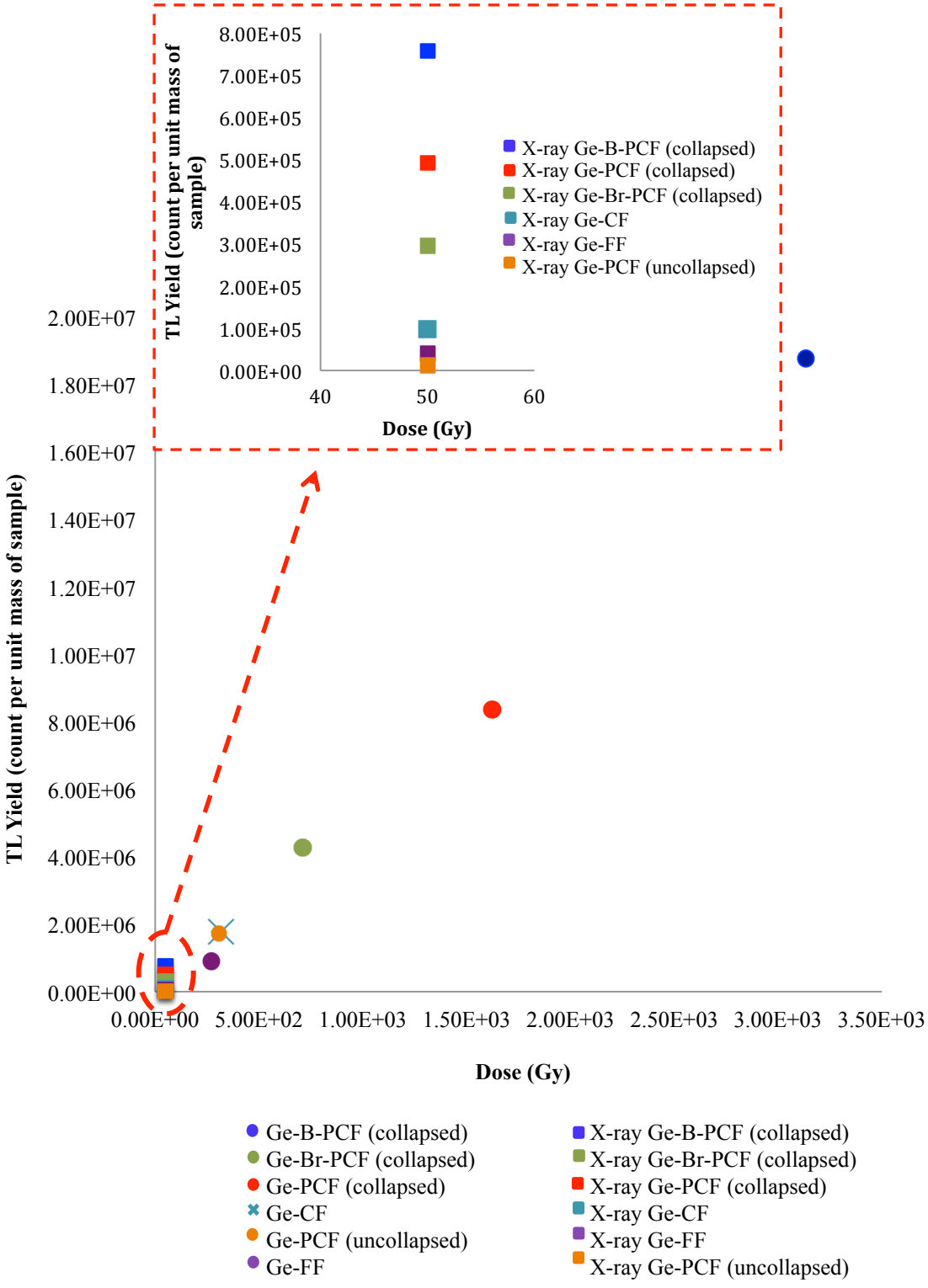

Figure 5-26 Combined analysis for ^{223}Ra irradiation and X-rays irradiation for Ge-B-PCF (collapsed), Ge-Br-PCF (collapsed), Ge-PCF (collapsed), Ge-PCF (uncollapsed), Ge-CF and Ge-FF. The inset provides an enlarged view, showing the TL yield variation for the 60 kV X-rays at a dose of 50 Gy.

5.3.4 Summary of Measurement of Dose from X-ray and ^{223}Ra Irradiation using Doped Silica Fibre

The present studies in this investigation have been aimed at characterising the doped silica optical fibre system as a 1-D dosimeter for applications in radiation therapy. In this section (5.3.3.1), studies have been carried out to establish the extent of dose linearity and energy response of the Ge-B-PCF (collapsed), Ge-Br-PCF (collapsed), Ge-PCF (collapsed), Ge-PCF (uncollapsed), Ge-CF, Ge-FF in comparison to that of TLD-100 at various photon energies. The dosimeter showed good linearity of response up to a dose of 50 Gy (the largest dose applied) for photon beams. Over the range of doses delivered (2 cGy - 50 Gy), for the nominal X-ray energy of 60 kV investigated, linearity of TL yield normalised to unit mass of the fibres has been obtained, the correlation coefficient (R^2) being observed to be greater than 0.9482 for Ge-B-PCF (collapsed), Ge-PCF (collapsed), Ge-PCF (uncollapsed), and Ge-CF. However, the Ge-Br-PCF (collapsed) is observed to produce a linear response only over the more limited dose range 2 cGy to 25 Gy, with saturation of TL yield beyond that (up to 50 Gy) with a correlation coefficient of 0.8945. It should also be noted that Ge-FF produces a correlation coefficient of 0.8212. Ge-doped FF and Ge-doped PCF (uncollapsed) produced the least TL yield of all of the fibre types, a result that is again expected to be linked to the rather unusual geometry of these compared to the other fibre types, a matter which again could be explored in greater detail in simulation studies. In comparison to the response to 60 kVp X-rays for TLD-100, the performance of all of the tailor-made doped fibres of this work is significantly enhanced. With consideration to energy response, a marked reduction in TL yield is observed with increase in nominal photon energy over the range 80 kVp, 140 kVp, 250 kVp and 6 MV, due to the lower mass energy absorption coefficient at the more elevated photon energies.

Studies were also made using the six different types of fibres, recording the absorbed dose from ^{223}Ra alpha particles (as discussed in section 5.3.3.2) referred to above. The calculated absorbed dose of ^{223}Ra alpha particles for Ge-B-PCF (collapsed), Ge-PCF (collapsed), Ge-Br-PCF (collapsed), Ge-CF, Ge-PCF (uncollapsed) and Ge-FF were found to be 3.13, 1.62, 0.71, 0.32, 0.31 and 0.27 kJ/kg, respectively, for irradiation durations in the range 22 to 31 hours. In all of the above cases, the TL response of Ge-B-PCF (collapsed), Ge-Br-PCF (collapsed) and Ge-PCF (collapsed) irradiated to 60 kVp X-rays and 5.5 MeV ^{223}Ra have enhanced the sensitivity compared to that for Ge-CF, Ge-FF and Ge-PCF (uncollapsed). A particular issue yet to be dealt with is the sensitivity of the Ge-FF and Ge-PCF (uncollapsed), which is thought to be related to the unusual geometries presented, producing

non-uniform irradiation. Thus said, the response of all six types of fibre are at least an order of magnitude greater than that for X-rays and for TLD-100. The present results therefore indicate enormous potential for use of SiO_2 doped fibres dosimetry for evaluations of dose in support of the novel use of alpha particle radiotherapy, not least also overcoming the hygroscopic issue of TLD-100.

5.4 References

[1] Y. A. Abdulla, Y. M. Amin, D. A. Bradley, "The thermoluminescence response of Ge-doped optical fibre subjected to photon irradiation," *Radiat. Phys. Chem.*, vol. 61, pp. 409–410

[2] N. M. Noor, M. Hussein, D. A. Bradley, and A. Nisbet, "The potential of Ge-doped optical fibre TL dosimetry for 3D verification of high energy IMRT photon beams," *Nucl. Instruments Methods Phys. Res. Sect. A Accel. Spectrometers, Detect. Assoc. Equip.*, vol. 619, no. 1–3, pp. 157–162, Jul. 2010.

[3] N. M. Noor, M. Hussein, D. A. Bradley, and A. Nisbet, "Investigation of the use of Ge-doped optical fibre for in vitro IMRT prostate dosimetry," *Nucl. Instruments Methods Phys. Res. Sect. A Accel. Spectrometers, Detect. Assoc. Equip.*, vol. 652, no. 1, pp. 819–823, Oct. 2011

[4] F. Issa, N. A. A. Latip, D. A. Bradley, and A. Nisbet, "Ge-doped optical fibres as thermoluminescence dosimeters for kilovoltage X-ray therapy irradiations," *Nucl. Instruments Methods Phys. Res. Sect. A Accel. Spectrometers, Detect. Assoc. Equip.*, vol. 652, no. 1, pp. 834–837, Oct. 2011

[5] S. Hashim, S. Al-Ahbabi, D. A Bradley, M. Webb, C. Jeynes, A. T. Ramli, and H. Wagiran, "The thermoluminescence response of doped SiO2 optical fibres subjected to photon and electron irradiations.," *Appl. Radiat. Isot.*, vol. 67, no. 3, pp. 423–7, Mar. 2009

[6] A.T. Abdul Rahman, A. Nisbet, D.A. Bradley, "Dose-rate and the reciprocity law: Tl response of Ge-doped Sio_2 optical fibers at therapeutic radiation doses." *Nucl. Instruments Methods Phys. Res. Sect. A Accel. Spectrometers, Detect. Assoc. Equip.*, vol. 652, no. 1, pp. 891–895, Oct. 2011.

[7] A. T. Ramli, D. A. Bradley, S. Hashim, and H. Wagiran, "The thermoluminescence response of doped SiO2 optical fibres subjected to alpha-particle irradiation.," *Appl. Radiat. Isot.*, vol. 67, no. 3, pp. 428–32, Mar. 2009.

[8] S. Hashim, D. a Bradley, M. I. Saripan, a T. Ramli, and H. Wagiran, "The thermoluminescence response of doped SiO2 optical fibres subjected to fast neutrons.," *Appl. Radiat. Isot.*, vol. 68, no. 4–5, pp. 700–3, 2010.

[9] G. A. Mahdiraji, M. Ghomeishi, E. Dermosesian, S. Hashim, N. M. Ung, F. R. M. Adikan, and D. A. Bradley, "Optical fiber based dosimeter sensor: Beyond TLD-100 limits," Sensors Actuators A Phys., vol. 222, pp. 48–57, 2015.

[10] D. A. Bradley, G. A. Mahdiraji, M. Ghomeishi, E. Dermosesian, F. R. M. Adikan, H. A. Abdul Rashid, and M. J. Maah, "Enhancing the radiation dose detection sensitivity of optical fibres," *Appl. Radiat. Isot.*, vol. 100, pp. 43–49, 2014.

[11] G. Amouzad Mahdiraji, E. Dermosesian, M. Safari, F. R. Mahamd Adikan, and D. Bradley, "Collapsed-hole Ge-doped Photonic Crystal Fiber as a Diagnostic Radiation Dosimeter," J. Light. Technol., vol. 8724, no. c, pp. 1–1, 2015.

[12] R. Chen and S. W. S. McKeever. "Theory of Thermoluminescence and Related Phenomena." London, World Scientific Publishing Co Pte Ltd, 1995.

[13] A. L. Yusoff, R. P. Hugtenburg, D. A. Bradley. "Review of development of a silica-based thermoluminescence dosimeter." *Radiat. Phys. Chem*., vol. 74, no. 6, pp. 459–481, Dec. 2005.

[14] A. T. Abdul Rahman, S. F. Abdul Sani, and D. A. Bradley, "Doped SiO_2 telecommunication fibre as a 1-D detector for radiation therapy dosimetry," vol. 347, pp. 347–353, 2012.

[15] A. I. Alalawi, R. P. Hugtenburg, A. T. Abdul Rahman, M. A. Barry, A. Nisbet, K. S. Alzimami, and D. A. Bradley, "Measurement of dose enhancement close to high atomic number media using optical fibre thermoluminescence dosimeters," *Radiat. Phys. Chem.*, vol. 95, pp. 145–147, Feb. 2014.

[16] A. Abundes-Velasco, C. Zabal-Cerdeira, J.A. García-Montes, M.O. De los Ríos-Ibarra, J.E. Gallegos and G.Q. Peña, "Treatment of Seven Patients with Coarctation of the Aorta Treated Using a Mexican-made Platinum/Iridium Stent", Archives of Medical Research, vol. 38, no. 8, pp. 853-857, 2007.

[17] S.A. Bhide, S. Gulliford, U. Schick, A. Miah, S. Zaidi, K. Newbold, C.M. Nutting and K.J. Harrington, "Dose–response analysis of acute oral mucositis and pharyngeal dysphagia in patients receiving induction chemotherapy followed by concomitant chemo-IMRT for head and neck cancer", Radiotherapy and Oncology, vol. 103, no. 1, pp. 88-91, 2012.

[18] J.Y. Cheung, and F.H. Tang, "The calculation of dose enhancement close to platinum implants for skull radiography", Health physics, vol. 93, no. 4, pp. 267-272, 2007.

[19] C. Guida, P. Maione, A. Rossi, M. Bareschino, C. Schettino, D. Barzaghi, M. Elmo and C. Gridelli, "Combined chemo-radiotherapy for locally advanced non-small cell lung cancer: Current status and future development", Critical reviews in oncology/hematology, vol. 68, no. 3, pp. 222-232, 2008.

[20] K.D. Dambul, G.A. Mahdiraji, F. A. Amirkhan, D. Chow, G. Gan, W. R. Wong, M. R. Abu Hassan, D.C. Tee, S. Ismail, S.A. Ibrahim, N. Tamchek and F.R. Mahamd Adikan, "Fabrication and development of Flat Fiber". Proc. PGC, pp. 3–5, 2012.

[21] Quorum Technologies 2002, Sputter Coating: Technical Brief, Quorum Technologies Ltd.

[22] S.W.S McKeever, "Thermoluminescence of Solids." Cambridge University Press, 1985.

[23] A. Alawiah, A. M. Intan, S. Bauk, H. A. Abdul-rashid, Z. Yusoff, and M. R. Mokhtar, "Thermoluminescence characteristics of flat optical fiber in radiation dosimetry under different electron irradiation conditions," vol. 8775, pp. 1–12, 2013.

[24] E. J. Friebele, C. G. Askins, M. E. Gingerich, and K. J. Long, "Optical fiber waveguides in radiation environments, II," *Nucl. Instruments Methods Phys. Res. Sect. B Beam Interact. with Mater. Atoms*, vol. 1, no. 2–3, pp. 355–369, 1984.

[25] E.J. Friebele, M.E. Gingerich, K.J. Long, "Radiation damage of optical fibre waveguides at long wavelengths". *Appl. Opt.* vol. 21, issue 3, pp. 547–553, 1982.

[26] E.J. Friebele, P.C. Schattz, M.E. Gingerich, "Compositional effects on radiation response of Ge-doped silica core optical fibre waveguides." *Appl. Opt.* vol. 19, issue 17, pp. 2910–2916, 1980.

[27] A. T. Abdul Rahman, D. A. Bradley, S. J. Doran, B. Thierry, E. Bräuer-Krisch, and A. Bravin, "The thermoluminescence response of Ge-doped silica fibres for synchrotron microbeam radiation therapy dosimetry," *Nucl. Instruments Methods Phys. Res. Sect. A Accel. Spectrometers, Detect. Assoc. Equip.*, vol. 619, no. 1–3, pp. 167–170, Jul. 2010.

[28] R. J. Aukett, J. E. Burns, a G. Greener, R. M. Harrison, C. Moretti, a E. Nahum, and K. E. Rosser, "Addendum to the IPEMB code of practice for the determination of absorbed dose for x-rays below 300 kV generating potential (0.035 mm Al-4 mm Cu HVL).," *Phys. Med. Biol.*, vol. 50, no. 12, pp. 2739–2748, 2005.

[29] S. Jayaraman, L.H. Lanzl, "Clinical Radiotherapy Physics." Springer, Berlin, 2004.

[30] B. J. Allen, C. Raja, S. Rizvi, Y. Li, W. Tsui, D. Zhang, E. Song, C. F. Qu, J. Kearsley, P. Graham, and J. Thompson, "Targeted alpha therapy for cancer.," *Phys. Med. Biol.*, vol. 49, no. 16, pp. 3703–3712, 2004.

[31] D. Heymann, "Bone Cancer: Primary Bone Cancers and Bone Metastases." Elsevier, 2014. ISBN: 978-0-12-416721-6

[32] Summary of Product Characteristics, European Medicines Agency. Accessed on web site: http://www.ema.europa.eu 13 April 2015.

[33] S. M. Collins, a. K. Pearce, K. M. Ferreira, a. J. Fenwick, P. H. Regan, and J. D. Keightley, "Direct measurement of the half-life of 223Ra," *Appl. Radiat. Isot.*, vol. 99, pp. 46–53, 2015.

[34] S. Hashim, M. I. Saripan, A. T. A. Rahman, N. H. Yaakob, D. A. Bradley, and K. Alzimami, "Effective Atomic Number of Ge-Doped and Al-Doped Optical Fibers for Radiation Dosimetry Purposes," *IEEE Trans. Nucl. Sci.*, vol. 60, no. 2, pp. 555–559, Apr. 2013.

[35] J. Olofsson, T. Nyholm, A. Ahnesjö, and M. Karlsson, "Optimization of photon beam flatness for radiation therapy.," *Phys. Med. Biol.*, vol. 52, no. 6, pp. 1735–1746, 2007.

[36] G. A. Mahdiraji, F. R. M. Adikan, and D. a. Bradley, "Collapsed optical fiber: A novel method for improving thermoluminescence response of optical fiber," *J. Lumin.*, vol. 161, pp. 442–447, 2015.

[37] M. Benabdesselam, F. Mady, and S. Girard, "Assessment of Ge-doped optical fibre as a TL-mode detector," *J. Non. Cryst. Solids*, vol. 360, no. 1, pp. 9–12, 2013.

[38] N. A. Zahaimi, M. H. R. Ooi Abdullah, H. Zin, A. L. Abdul Rahman, S. Hashim, M. I. Saripan, M. C. Paul, D. a. Bradley, and A. T. Abdul Rahman, "Dopant concentration and thermoluminescence (TL) properties of tailor-made Ge-doped SiO2 fibres," *Radiat. Phys. Chem.*, vol. 104, pp. 297–301, Nov. 2014.

[39] Personal communication with Siti Nurasiah Mat Nawi, 2015, "The thermoluminescence response of Ge-doped flat optical fibre dosimeters to gamma radiation".

[40] D. A. Bradley, S. F. Abdul Sani, A. I. Alalawi, S. M. Jafari, N. M. Noor, a. R. Hairul Azhar, G. A. Mahdiraji, N. Tamchek, S. Ghosh, M. C. Paul, K. S. Alzimami, a. Nisbet, and M. J. Maah, "Development of tailor-made silica fibres for TL dosimetry," *Radiat. Phys. Chem.*, vol. 104, pp. 3–9, 2014.

[41] Massachusetts Institute of Technology (MIT) Open Courseware (2004), Principles of Radiation Interactions: Dose Calculations of Absorbed Dose from a Charged Particle Beam, http://ocw.mit.edu/courses/nuclear-engineering/22-55j-principles-of-radiation-interactions-fall-2004/lecture-notes/dos_calculations.pdf. Accessed in 13 October 2014.

[42] S. M. Jafari, T. J. Jordan, M. Hussein, D. a. Bradley, C. H. Clark, a. Nisbet, and N. M. Spyrou, "Energy response of glass bead TLDs irradiated with radiation therapy beams," *Radiat. Phys. Chem.*, vol. 104, pp. 208–211, 2014.

[43] NIST database of Stopping Power and range tables for electrons http://physics.nist.gov/PhysRefData/Star/Text/ESTAR.html. Accessed on 23 April 2015.

[44] D.W. Rogers DW, I. Kawrakow, J.P. Seuntjens, B.R.B Walters, E. Mainegra-Hing. NRC User Codes for EGSnrc. NRCC Report PIRS-702 (revB). Ottawa, ON: National Research Council of Canada; 2010. Available from: http://www.irs.inms.nrc.ca/EGSnrc/pirs702.pdf

Chapter 6

6 Conclusion and Suggestions for Future Work

6.1 Conclusion

Modern radiation therapy treatment techniques place an increasingly greater demand on the performance of the associated radiation dosimetry systems, and markedly so in the light of recent advances in dose delivery. The essential aim of radiation therapy is to obtain the greatest possible local and regional tumour control i.e. through complete all mortality, with the least complications, leading to considerable need for precision and accuracy of dosimetry. Modern approaches that seek to deliver dose in conformation with the size and shape of the tumour (conformal radiotherapy) have become possible through use of for example intensity modulated radiotherapy, delivered at relatively high dose compared to more conventional techniques, with fine beams generating high dose gradients in these relatively small field sizes. Thus there is need for a large dynamic range to allow measurements across the high dose gradients and fine spatial resolution to accommodate the small field sizes. In addition, the motivations for dosimeters include the possibility of creating devices of size sufficiently small to negate the need for tissue equivalence, linked to the Bragg-Gray cavity theory. Another motivation for having a fibre dosimeter concerns the possibility of inserting such devices into a catheter for brachytherapy applications. At the outset of this project, it was thus envisaged that having access to tailor-made fibres, present studies might provide the basis for characterisation of defects and thermoluminescence (TL) yield of such novel tailor-made doped fibres for dosimetry.

In pursuing such an aim, it was clearly recognised that the basic issue concerns development in fabrication of enhanced TL response silica material. The entire project was therefore geared toward this objective. In support of the aim, studies were carried out to verify the extent to which there was success in the doped-silica processing method using the MCVD technique, with further studies focusing on determining the dopant concentrations, structure of the Ge-doped silica-glass samples, and in addition the thermoluminescent characterization measurements themselves. Here, a summary of the studies that have been carried out together with the results that have been obtained is provided. A number of

experimental limitations that have been encountered will also be discussed and finally suggestions for future work will also be presented.

Following on from the introductory material provided in Chapters 1 and 2, in **Chapter 3**, the surface oxidation state and elemental studies of the Ge-doped optical preforms and capillary fibres were investigated using the X-ray Photoelectron Spectroscopy (XPS) method. All solid materials interact with their surrounding through their surfaces. The physical and chemical composition of these surfaces determines the nature of the interactions. Surfaces crucially influence a number of important properties of the solid, for instance, catalytic activity. Despite the undoubted importance of surfaces, only a very small proportion of the atoms of most solids are found at the surface, at approximately 1 in 10^{17} or 100 part per billion (ppb). If one wishes to detect impurities at the SiO_2-GeO_2 surface at a concentration of 1% then the need is to detect materials at a concentration of 1 ppb within the medium. It should be noted that the exact proportion of atoms at the surface is dependent upon the shape and surface roughness of the material and its composition. In electron spectroscopy, the facility consists of the sample under investigation, a source of primary radiation, and an electron energy analyser, all contained within a vacuum chamber preferably operating in the ultra-high vacuum (UHV) regime, measuring the energy of electrons emitted from a material.

Using the ultra-high vacuum (UHV) conditions it was obtained that the surface oxidation state of the Ge-doped preforms and capillary fibres (fabricated from the same preform) is predominantly in the form of GeO_2 (i.e. the +4 oxidation state) within the core. The oxidation state of germanium is of significance because GeO_2 is known to play an important role in the optical fibre performance. The oxygen diffusion rate is high in GeO_2 compared to that in silicon due to its low formation energy, resulting in an increased concentration of oxygen-related defects. These defects are mostly located in an amorphous Si and Ge matrix, being generated in the preform during the high temperature fabrication processes. Previous researchers have investigated the generation mechanisms of the Ge related paramagnetic defects, namely Ge(1) and Ge(2) centres in a fibre and in its original preform, giving greater radiation sensitivity of the fibre when compared to the preform. This is as a result of induced germanium lone pair centres (GLPC) in the fibre, generated by the drawing process, indicating that the GLPC are the donor of electrons trapped by the tetra-coordinated Ge atoms. Moreover, it has been suggested that the generation probability for Ge(1) and Ge(2) centres in the fibre and preform are similar. A further study has been performed, comparing between annealed and non-annealed samples of split capillary fibres, resulting in depletion of the hydrocarbon (C1s) in the annealed sample, thus consequently with intensification of the Ge2p3 peak by a factor of some 4 times. This occurs because such

hydrocarbon adsorption decreases the surface energy of the substrate and subsequently decreases the sampling depth.

Two major issues were confronted during the sample preparation stage and samples measurement. These were that the samples need to be cut smoothly (to obtain a flat surface) and cleaned meticulously due to the surface sensitive factors as mentioned earlier where the detection limit is confined to a depth of a few ~ nm. Two approaches in samples cleaning using an ultrasonic bath have been carried out using three types of alcohol (i.e. methanol, propanol and ethanol) as well as acetone. The latter effectively removed the contamination resulting from sample handling and fibre pulling. The problem of making samples measurement arose in using Ge-doped fibres of 2 to 10 μm of Ge-doped core diameter (the doped region being located at the centre of the fibres, defining where the scanning area should be focused upon). High spatial resolution was needed to be utilised, resulting in low intensity of detection. This issue was substantially solved through the use of preform offering 2 mm of Ge-doped core diameter and split capillary fibres (examining the doped region in the whole inner surface). To this end, present studies have established procedures and methodology for analysing the surface chemical charge state of Ge-doped SiO_2 fibres.

In **Chapter 4**, use was made of the Particle X-ray Induced Emission (PIXE) technique in determining the elemental concentration of Ge-dopant in the samples. The multi-elemental detection capability is a prominent feature of PIXE, as is the excellent spatial resolution and signal to background ratio that are on offer. PIXE analysis identified the elements in the target from the energies of the characteristic peaks in the X-ray emission spectrum and the quantity of a particular element in the target is determined from the intensities of emission lines in the characteristic X-ray emission spectrum. This powerful technique can easily analyse various elements at the same time with atomic number as low as 12, all in the ppm range.

It is natural to compare proton microbeams with the electron microprobe, since these two instruments compete to a certain degree. The former can achieve a spatial resolution of approximately 1 μm in actual trace element analysis whereas the resolution for the latter is better than 0.1 μm. However, the excellent resolution of the electron microprobes is limited to sample interrogation of a surface, down to a thickness of about 0.1 μm. Elemental analysis for thicker samples is considerably worse due to scattering of the electrons, broadening the beam into a 'teardrop' volume, the penetration depth now being limited to 5 - 10 μm, with an effective spatial resolution of the order of 10 μm. The proton beam, on the other hand,

maintains the same resolution of 1 - 2 μm for tens of micrometers of penetration. Hence, for samples with thickness greater than a few micrometres a proton microbeam has a superior lateral resolution to that of an electron microbeam.

The dopant concentration of tailor-made SiO_2 fibre TLDs of improved performance through use of Particle Induced X-ray Emission (PIXE)/Rutherford Back Scattering (RBS) measurements has been investigated. This was important, with optimisation of fibre design relying heavily on the fabrication technique used and on accurate characterisation of the dopant profile. GeO_2, commonly used for doping the core region to alter the refractive index, produces significant TL yield in addition to enhancing light transmission along the length of the fibre. The fibre production process is typically seen to result in wide variation in dopant concentration and distribution, critical parameters in controlling the behaviour of the dosimeter. However, it does need to be commented with regard to the flat fibre (FF) samples, that the large variation observed in doping concentration was due to the very thin Ge-rich core, being less than the dimension of the scanning beam. The proton energy used (2.5 MeV) is the optimum for PIXE analysis in this system. The 'noise' in the silicon profile in the uncollapsed PCF is due to the fact that the analysis points were not selected to fall on either the core (Ge), the air hole or the wall (Si) and so there is a consequent large variation. The output of the elemental analysis from the collapsed PCF cross-section area is the average of Ge and Si, diffusing away from the centre into the fibre cladding. These results are expected to help in understanding the influence of the doped silica structure, also involving characterisation of the fundamental parameters that control thermoluminescence yield of the media under investigation.

In regard to the FF results, investigated with a scanning resolution of ~2 μm, the dopant concentration could be a result of tilt of the fibres when being set in the resin block, perhaps to the extent of just a few microns (hardly capable of being detected). In such circumstance the beam area may be focused for instance on the inner wall surface of the capillaries instead of the hollow area (specifically for PCF-uncollapsed samples) and on the cladding. Towards this end, present studies have established procedures and methodology for investigating the dopant concentration of Ge-doped SiO_2 fibres. With improving alignment in mind, it is possible that future further investigation could look to make highly benefitial use of the nm resolution beam line at the Surrey ion beam centre.

The overall aim of the project has been to enhance the performance of silica based TL material, the intention being to investigate the feasibility of using this dosimeter for applications in radiation dosimetry, going beyond the capabilities of conventional TLD-100.

Application could then perhaps move to evaluation of diagnostic doses in radiation medicine and beyond that to measurement of environmental radiation doses (milligray down to fractions of a microgray, respectively).

Chapter 5 concerned two means for increasing the TL yield of fibres: (i) defects generation through fuses surfaces relaxation, and; (ii) photoelectron generation through the use of high atomic number coatings. For the first category of investigations, initial TL studies involved examination of the TL sensitivity of undoped flat fibre (FF), a form previously unexplored, comparison being made with that of TLD-100 and commercial Ge-doped fibres exposed to 6 MV photons. As soon became apparent, undoped FF was found to produce greater sensitivity (by a factor of ~100) than that of Ge-doped fibre, being comparable in sensitivity to that of TLD-100. Also as previously addressed, the fibres, whether doped or undoped, have also been found to be affected by drawing-induced defect centres. The work was then extended to an investigation of the photoelectron enhancement through use of high atomic number coatings of platinum (Z = 79) on the undoped FF, leading to a dose enhancement factor of 0.0150 ± 0.0003 nm^{-1}, a factor comparable to that from gold-coated fibres (Z = 78). This work has opened up the possibility of small field dosimetry in conjunction with concurrent chemo-radiotherapy using platinum based chemotherapy agents (eg cisplatin and carboplatin) and dose enhancement of fibres TLD with platinum coating. Degradation of the platinum coating was observed following several cycles of irradiation and annealing, causing irregularity in TL response (a non-linear effect). As such, the accuracy of the results could be improved by keeping the fibres between foam separators, avoiding damage to the coatings brought about by abrasion against the walls of the gelatine capsules. Measures should be taken to avoid the coated side of a flat fibre making contact with any other abrasive surfaces. Future studies of coated SiO_2 fibres should also investigate the effect of annealing against the coating material. This could be done by microscope studies of the fibre surfaces augmented by X-ray fluorescence spectrometry, the latter evaluating the composition of the coated fibre before and after annealing. The actual thickness of the coating could also be confirmed by use of a scanning electron microscope at each stage of experimentation, such that the degree of damage can be observed.

Dosimetric parameters for doped fibres, particularly of nominal 8 wt% dopant concentration were investigated, the fibres including Ge-B-PCF (collapsed), Ge-Br-PCF (collapsed), Ge-PCF (collapsed), Ge-PCF (uncollapsed), Ge-CF and Ge-FF. Comparison was made with conventional TLD-100, including dose response and glow curves investigated for X-rays generated at 60 kVp over a dose range from 2 cGy to 50 Gy. The energy response of the fibres was also performed, for X-rays generated at peak accelerating potentials of 80 kVp,

140 kVp, 250 kVp and 6 MV photons for a given dose of 2 Gy. The results clearly show the samples to be suitable for use as TL dosimeters, with good linearity of response and a simple glow curve i.e., a simple trap distribution. For the 60 kVp photon irradiations a linear dose response for all of the types of fibre under study was observed, from 2 cGy up to 50 Gy, noting that Ge-B-PCF (collapsed) provided greater sensitivity than that of TLD-100 as well as the other fibres, due to the elevated presence of intrinsic defects and extrinsic impurity/dopants, some presenting as deeper traps as revealed in the glow curves. Moreover, the result shows that the TL response of uncollapsed Ge-PCF can be significantly improved upon by collapsing all holes in a PCF to form collapsed-hole-PCF (PCF-collapsed). Therefore, the results strongly suggest the collapsing technique to be a promising method for designing and fabricating high sensitivity fibre based irradiation dosimeter sensors. As expected, at higher photon energies the TL response of the doped fibres decrease, due to the lower mass energy absorption coefficient.

In further extension of the study, the same doped SiO_2 fibres have been utilized to measure absorbed dose from high linear energy transfer (LET) ^{223}Ra alpha particle source produced in liquid form used for treatment of bone sarcomas. Previous and present studies have shown that the doped fibres used herein provide for spatial resolution far superior to many other forms of dosimeter and is of importance in measuring absorbed dose to sensitive tissue structures (particularly for bone tissue where the effective atomic number is not greatly different to that of the silica fibre). In summary, the TL response of all six types of fibre irradiated to ^{223}Ra alpha particles are at least an order of magnitude greater than that for X-rays and for TLD-100. However, a particular issue yet to be dealt with is that the sensitivity of the Ge-FF and Ge-PCF (uncollapsed) is thought to be related to the unusual geometries presented, producing non-uniform irradiation.

Current evaluations offer support in understanding the basis of the relative dose measurements that have thus far been made. However, the range of fibre types that have been studied to date undoubtedly limits our ability to make broader generalisations. Given that suitable Ge-doped TL material has been obtained, it is also now appropriate to study the mechanism of luminescence involved in phosphor and aluminium-doped optical fibres. Extended investigations may show whether the results hold true for other types of dopant such as these and other potential variables beyond the ones explored here, including fibre drawing speed and fibre tension during the drawing process. Towards this end, present studies have nevertheless established procedures and methodology for investigating the TL characteristics of doped SiO_2 fibres. A particular interest of these studies is that the production of the different types of fibres have resulted in the generation of different types of

defect, creating variation in TL response. Findings from present studies, summarised above, are thus expected to pave the way for more comprehensive investigations of TL from tailor-made doped SiO_2 fibres.

6.2 Other Suggestions for Future Work

Current dose evaluations concern levels of irradiation that are familiar within the realms of radiotherapy. Given the knowledge accrued from the production of fibres providing for increased TL yield, it is clear that there is an ability to improve the lower limits of detection to the levels of dose observed in radiodiagnosis and nuclear medicine, of the order of a fraction of a mGy through to some 10s of mGy. It is also apparent that the spatial resolution demands of these diagnostic medicine techniques are not nearly so stringent as those of radiotherapy. Thus improvement in the lower limits of detection can also be achieved by using dosimeters of greater mass or otherwise making use of groups of fibres irradiated at the same time, subsequently readout at the same time.

The above needs can be further augmented by expansion of the underpinning studies that have been undertaken to date, including spectral analysis including Raman microspectrometry as well as other analytical forms such as atomic force microscopy, examining surface morphology. In terms of spectrometry, it is well known for instance that when MeV ions beam impacts on matter, visible light is often observed, termed ionoluminescence (IL). As with any other luminescent techniques, IL is suitable for studying radiation-matter interaction processes and can be considered a very useful method not only for characterising the material, but can also be applied during material modification with ion beams in order to follow the creation of intrinsic defects in crystalline short range intermediate ordered material. The beam-solid interaction populates states in the band-gap introduced by activator impurity ions or structural defects. Future studies are needed in regard to understanding the intrinsic and extrinsic luminescence phenomena present at the parts per million (ppm) level across the range of wavelengths emitted by doped fibres. Of note is that the ionoluminescence method can be run together with the other ion beam techniques.

Results of X-rays radiation and alpha particles of ^{223}Ra radiation obtained in Chapter 5 confirm that Ge-doped fibre dosimeters are of considerable utility in studying the so-called bystander effects seen in radiobiological investigations. Bystander effects tend to exaggerate the effect of low doses by eliciting damage in nonirradiated cells as reported elsewhere, in

particular that cells lethally irradiated with alpha particles could induce mutagenesis in neighboring cells.

Since optical fibre dosimeters are applicable *in vivo,* due to their glassy nature and relatively small size of some few microns, they are also expected to play a significant role in dose measurement from high through to low doses. In addition, out-of-field dose measurements made outside of the Planned Target Volume (PTV) have been made by others using Ge-doped optical fibres distributed along the length of a RANDO phantom at specific (x,y) coordinates, irradiated at 6 MV and above, for doses from 2300 down to 40 mGy, indicating there to be a thermal neutron component at the higher energies. As a result of the finite but relatively small Ge neutron absorption cross-section for photon energies above the photo-neutron production threshold (~ 10 MV), it is clear that the optical fibres do over-respond as result this photo-neutron component. Further investigation concerning the magnitude of this effect should be taken into account. Moreover, these high resolution dosimeters can be expected to be applied in the near future in obtaining dose measurement in exposure of high collimated beams as for instance for occupational health and heavy metal exposure using X-Ray Fluorescence (XRF) techniques, specifically in study of the effects of lead (Pb), cadmium (Cd) and mercury (Hg).

In final regard to TL studies, it is apparent that in place of silica fibres there is the possibility of the use of high temperature polymers, with melting points up to and beyond 400 ^{o}C, allowing easier fabrication of shapes, being more malleable and less brittle, and also being easier to handle. The added benefit is that the effective atomic number would then approach that of soft tissues.

Finally, it is intended to extend present research work to that of optically stimulated luminescence (OSL), paving the way for a remote, real time measurement system for measuring absorbed radiation dose. Such capability, combined with optical fibre communication technology would have tremendous technological applications, for instance, to a wide variety of scintillator media for clinical dosimetry, medical imaging applications in nuclear medicine (PET, CT), radiotherapy and environmental monitoring systems. The small size, high dynamic range (from fractions of a mGy to several Gy), flexibility and optical transmission characteristics of the fibres make this a promising technology in placing the sensors in areas that are either difficult to access or hazardous in terms of the radiation dose levels or both.

List of Publications and Presentations

1. Submission to journal of Radiation Physics and Chemistry; **Siti. F. Abdul Sani**, Amani I. Alalawi, Hairul Azhar A.R, Ghafour Amouzad Mahdiraji, Nizam Tamchek, A. Nisbet, M.J. Maah and D.A.Bradley. High Sensitivity Flat SiO_2 Fibres for Medical Dosimetry. Radiation Physics and Chemistry, November 2014

2. Submission to journal of X-ray Spectrometry; **Siti. F. Abdul Sani**, Amani I. Alalawi, Hairul Azhar A.R, Ghafour Amouzad Mahdiraji, Nizam Tamchek, A. Nisbet, M.J. Maah and D.A.Bradley. Micro-PIXE analysis of doped SiO2 fibres intended as TL dosimeters for radiation measurements. X-ray Spectrometry, December 2014

3. Submission to journal of Lightwave Technology; **S.F. Abdul Sani**, S.J. Hinder, G.W. Grime, V. Palitsin, G. Amouzad Mahdiraji, H.A Abdul Rashid, S.S Ahmad Shaharuddin, N. Tamchek, M.J. Maah, J. F. Watts and D.A. Bradley. XPS and PIXE Analysis of Doped Silica Fibre for Radiation Dosimetry. Lightwave Technology, February 2015.

4. **Siti. F. Abdul Sani**, Amani I. Alalawi, Hairul Azhar A.R, Ghafour Amouzad Mahdiraji, Nizam Tamchek, A. Nisbet, M.J. Maah and D.A.Bradley, "High Sensitivity Flat SiO_2 Fibres for Medical Dosimetry". Radiation Physics and Chemistry, November 2014. DOI:10.1016/j.radphyschem.2014.03.043.

5. **S.F. Abdul Sani**, G.W. Grime, V. Palitsin, G. Amouzad Mahdiraji, H.A Abdul Rashid, M.J. Maah and D.A. Bradley, "Micro-PIXE analysis of doped SiO_2 fibres intended as TL dosimeters for radiation measurements". X-ray Spectrometry, November 2014. DOI: 10.1002/xrs.2575.

6. **S.F. Abdul Sani**, S.J. Hinder, G.W. Grime, V. Palitsin, G. Amouzad Mahdiraji, H.A Abdul Rashid, S.S Ahmad Shaharuddin, N. Tamchek, M.J. Maah, J. F. Watts and D.A. Bradley, "XPS and PIXE Analysis of Doped Silica Fibre for Radiation Dosimetry". IEEE/OSA Journal of Lightwave Technology, February 2015. DOI 10.1109/JLT.2015.2406394

7. Abstract submission and presented at 1st International Conference on Dosimetry and its Applications (ICDA-1), Prague, Czech Republic, 23 – 28 June 2013. **Siti. F.**

Abdul Sani, Amani I. Alalawi, Hairul Azhar A.R, Ghafour Amouzad Mahdiraji, Nizam Tamchek, A. Nisbet, M.J. Maah and D.A.Bradley. *High Sensitivity Flat SiO_2 Fibres for Medical Dosimetry.*

8. Abstract submission and presented at European Conference on X-ray Spectrometry (EXRS2014) Bologna, 15 - 20 June 2014. **S.F. Abdul Sani**, G.W. Grime, V. Palitsin, G. Amouzad Mahdiraji, H.A Abdul Rashid, M.J. Maah and D.A. Bradley. *Micro-PIXE analysis of doped SiO_2 fibres intended as TL dosimeters for radiation measurements.*

9. Abstract submission and presented at Postgraduate Research Conference 2015, University of Surrey, United Kingdom, 23 - 24 April 2015. **S.F. Abdul Sani***,* S.J. Hinder, G.W. Grime, V. Palitsin, G. Amouzad Mahdiraji, H.A Abdul Rashid, S.S Ahmad Shaharuddin, N. Tamchek, M.J. Maah, J. F. Watts and D.A. Bradley. *XPS and PIXE Analysis of Doped Silica Fibre for Radiation Dosimetry.*

10. Abstract submission and presented at the 2015 International Conference on Application of Nuclear Technique (ICANT 2015), Crete, Greece, 14 - 20 June 2015. **S.F. Abdul Sani**, Sean Collin, M.J. Maah, and D.A. Bradley. *Measurement of Dose from ^{223}Ra using Doped Silica Fibre.*

11. D. A. Bradley, **Siti F. Abdul Sani**, Amani I. Alalawi, S.M. Jafari, Noramaliza M. Noor, Hairul Azhar A. R, Ghafour Amouzad Mahdiraji, Nizam Tamchek, S. Ghosh, M.C. Paul, Khalid S. Alzimami, A. Nisbet, M.J. Maah, "Development of tailor-made silica fibres for TL dosimetry", *Radiat. Phys. Chem.,* vol. 104, pp. 3-9, Nov. 2014. Paper presented at 1st International Conference on Dosimetry and its Applications (ICDA-1). Prague, Czech Republic, 23 – 28 June 2013.

12. A.T. Abdul Rahman, **Siti Fairus Abdul Sani**, and D. A. Bradley, "Doped SiO_2 telecommunication fibre as a 1-D detector for radiation therapy dosimetry". AIP Conf. Proc. 1423, pp. 347-353. Paper presented at IX Latin American Symposium on Nuclaer Physics and Applications, Quito Ecuador, 18–22 July 2011.

13. A.T. Abdul Rahman, R.P. Hugtenburg, **Siti Fairus Abdul Sani**, A.I.M. Alalawi, Fatma Issa, R. Thomas, M.A. Barry, A. Nisbet and D.A. Bradley, "An investigation of the thermoluminescence of Ge-doped SiO_2 optical fibres for application in interface radiation dosimetry". Appl Radiat Isot. 2012 Jul;70 (7):1436-41 22154388.

Appendix A

XPS and PIXE Analysis of Doped Silica Fibre for Radiation Dosimetry

S. F. Abdul Sani, G. Amouzad Mahdiraji, A. S. Siti Shafiqah, G. W. Grime, V. Palitsin, S. J. Hinder, N. Tamchek, H. A. Abdul Rashid, *Member, IEEE*, M. J. Maah, J. F. Watts, and D. A. Bradley

***Abstract*—The material characteristics of doped SiO_2 fibre are studied, the electron traps in the product medium creating a situation attractive for their application in thermoluminescence (TL) radiation dosimetry. To date, rather limited research has been conducted towards gaining an essential understanding of the magnitude of TL signal and material characteristics of doped fibres. Characterization is being sought to ensure that the mechanism of TL yield in optical fibres is well understood, allowing a favourable well controlled production situation to be established. The intended end point is to specify dosimeters, not only for clinical dosimetry but also for their application in industrial/energy–industry settings. Investigation of the surface oxidation state of the Ge-doped SiO_2 optical preform has been carried out using the X-ray photoelectron spectroscopy technique. In a further development using the fibre forming technology, particle-induced X-ray emission/Rutherford back scattering measurements have been employed to ascertain dopant concentrations of Ge-doped-cladding photonic crystal fibres (PCFs) with a view to improving TL yield. Present results concern uncollapsed and collapsed-hole-PCFs.**

***Index Terms*—Doped SiO_2 fibres, dosimetry, particle-induced X-ray emission (PIXE), photonic crystal fibre (PCF), X-ray photoelectron spectroscopy (XPS).**

Manuscript received November 5, 2014; revised January 14, 2015 and February 9, 2015; accepted February 12, 2015. Date of publication February 25, 2015; date of current version March 20, 2015. This work was supported by the University of Malaya—Ministry of Higher Education of Malaysia UM-MOHE High Impact Research Grant UM.C/625/1/HIR/33. The fibres used herein were all fabricated using the University of Malaya Fibre Drawing System, supported by the University of Malaya-Ministry of Higher Education of Malaysia UM-MOHE High Impact Research Grant A000007-50001.

S. F. Abdul Sani is with the Centre for Nuclear and Radiation Physics, Department of Physics, University of Surrey, Guildford, Surrey GU2 7XH, U.K. (e-mail: ctfairussani@gmail.com).

G. A. Mahdiraji is with the Integrated Lightwave Research Group, Department of Electrical Engineering, Faculty of Engineering, University of Malaya, 50603 Kuala Lumpur, Malaysia (e-mail: ghafouram@gmail.com).

A. S Siti Shafiqah is with the Department of Physics, University of Malaya, 50603 Kuala Lumpur, Malaysia (e-mail: shafiqahshaharuddin22@gmail.com).

G. W. Grime and V. Palitsin are with the Surrey Ion Beam Centre, Nodus Laboratory, University of Surrey, Guildford, Surrey GU2 7XH, U.K. (e-mail: g.grime@surrey.ac.uk; v.palitsin@surrey.ac.uk).

S. J. Hinder and J. F. Watts are with the Surface Analysis Laboratory, School of Engineering, University of Surrey, Guildford, Surrey GU2 7XH, U.K. (e-mail: s.hinder@surrey.ac.uk; j.watts@surrey.ac.uk).

N. Tamchek is with the Department of Physics, Faculty of Science, Universiti Putra Malaysia, 43400 Serdang, Selangor, Malaysia (e-mail: nizamtm@gmail.com).

H. A. Abdul Rashid is with the Faculty of Engineering, Multimedia University, 2010 Cyberjaya, Selangor, Malaysia (e-mail: hairul@mmu.edu.my).

M. J. Maah is with the Department of Chemistry, University of Malaya, 50603 Kuala Lumpur,, Malaysia (e-mail: mjamil@um.edu.my).

D. A. Bradley is with the Centre for Nuclear and Radiation Physics, Department of Physics, University of Surrey, Guildford, Surrey GU2 7XH, U.K., and also with the Department of Physics, University of Malaya, 50603 Kuala Lumpur, , Malaysia (e-mail: d.a.bradley@surrey.ac.uk).

Color versions of one or more of the figures in this paper are available online at http://ieeexplore.ieee.org.

Digital Object Identifier 10.1109/JLT.2015.2406394

I. Introduction

In recent years, much attention has been focused on the use of standard optical telecommunication fibres for thermoluminescence dosimetry (TLD). This is due to the presence of extrinsic doping in the fibre core, providing for electron trapping and therefore luminescence when heated following exposure to radiation. The storage capacity allows for proportionality between occupied traps and radiation dose, the dose integration capability making it in principle suitable for dosimetric applications [1]. To date, such fibres with small diameter (typically $\sim$125 μm) are suggested to approximate a Bragg-Gray cavity, leading to their identification for particular application in radiotherapy dosimetry, not least in small-field, high dose gradient situations, the latter representing state-of-the-art developments in radiotherapy provision. They can also be re-used numbers of times following thermal annealing without loss in dose-response and are water and corrosion resistant, offering the possibility of the production of thermoluminescence (TL) dosimeters interesting for use in a variety of *in vivo* and interface dosimetry situations. Going beyond the use of standard telecommunication fibres and fabricating tailor-made fibres as herein, ultimately we are seeking to obtain TL yields that extend applications to dosimetry in the diagnostic and environmental dose regimes (mGy down to fractions of a μGy respectively). As such, one is looking to refine the sensitivity of these fibres, in particular to offer radiation sensitivity approaching or exceeding that of more well-established TL dosimeters such as the LiF phosphor-based commercial product TLD-100.

Present work employs the method of modified chemical vapour deposition (MCVD) for extrinsically doped optical fibre production by prefabricating a single glass rod known as the preform. The process herein utilizes $SiCl_4$ and $GeCl_4$ vapour precursor, exposed to extreme temperature, with the fusion process occurring between 2100 and 2200 °C applied in collapsing down the medium and tamped into a solid glass rod. The preform is subsequently pulled down into fibre form. This protracted processes will eventually produce defects, considerably enhancing the TL signal of the SiO_2 optical fibre; such defect centres can also be generated in the glass by either ionization or displacement damage, typically at elevated linear-energy transfer. Thus said, under certain influencing conditions in the production of the fibres from the preform, it is expected that precursor flow, temperature and drawing speed will all play an important and dominating role in the TL response, influencing the species and population of defects and characteristics of the optical fibre. Particular examples that are determined by the oxidation environment are oxygen rich and oxygen deficient defects,

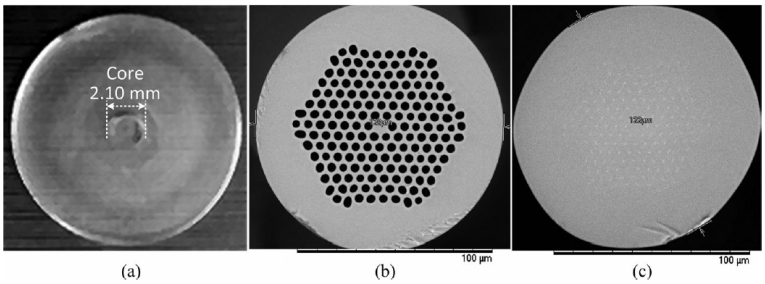

Fig. 1. (a) Polished surface Ge-doped silica preform. (b) and (c) scanning electron microscope (SEM) images from the cross section of Ge-doped-cladding uncollapsed PCF and collapsed PCF, respectively.

influencing the internal stresses within the glass [2]. The invention of microstructured optical fibres for instance photonic crystal fibres (PCFs) has further improved the TL sensitivity in radiation dosimetry [3]. Moreover, PCFs have also been used in radiation measurements in the form of optically stimulated luminescence detection mode, modelling also being undertaken [4], [5]. The dose detection sensitivity of PCFs could be due to the fusing of the outer wall surface of the stacked capillaries since such high TL response properties have been observed in single capillaries after collapsing the internal bore to form a flat fibre shape; the TL has been observed to be enhanced compared to that before collapse [6]. In addition, a more significant improvement in TL response is observed in flat fibres when extrinsic impurities are added to the collapsing/fusing area, comparison being made with undoped flat fibre. This should be taken into consideration in designing a PCF that might perhaps contain hundreds of capillaries stacked in a glass tube; collapsing all capillary holes to form a collapsed-hole-PCF would then be expected to lead to even greater TL response compared to the original PCF. However, it is not clear what silica dependent parameters change during PCF and collapsed-hole-PCF fabrication to the extent that improved luminescence response is indicated.

In this study, it is intended to investigate elemental and chemical analysis of a tailor-made Ge-doped cladding PCF and collapsed-hole-PCF, use being made of X-ray photoelectron spectroscopy (XPS) and ion beam analysis respectively, the latter accessing a combined microbeam proton-induced X-ray emission (PIXE)/Rutherford back scattering (RBS) arrangement.

II. Materials and Methods

A. Fibres Fabrication

Optical fibre is typically made from a preform of silica, comprising two essential components, the doped silica core and the outer silica cladding, such that for telecommunication purposes a difference in refractive index is produced between the core and the cladding. This refractive index profile is controlled and manipulated through the addition of dopant to the basis SiO_2 glass. The fibres, produced by a University of Malaya lead collaboration, are doped using the MCVD method. The final Ge-doped preform with 15.14 mm outer diameter and 2.10 mm core diameter contains 8.49 ± 0.07 wt% Ge [measured by electron dispersive X-ray (EDX)] in the preform core area. Samples of this preform, cut to a length of some 1.5–2 mm were then prepared, the surface being polished and cleaned in order to avoid interference during optical measurements, as shown in Fig. 1(a).

Present work focuses on the diffusion of Ge (and Si) in tailor made doped PCFs. The PCFs is fabricated at the University of Malaya using the stack-and-draw method. A Ge-doped silica tube preform made with the aid of the MCVD process [fabricated with the same doping concentration and MCVD process parameters as the preform shown in Fig. 1(a)] is used here for fabricating the PCF. The Ge-doped tube preform is drawn into capillaries, to obtain a diameter of a few millimeters (1.26 mm diameter is used in this study for seven-ring PCF). Prior to stacking, the capillaries undergo preparation processes such as cutting to a shorter length of 30–40 cm, fusing one end, and cleaning [7]. The capillaries are then stacked into a Suprasil F300 silica tube with outer and inner diameters of 25 and 19 mm, respectively. The central capillary is exchanged with a similar size solid rod to form a solid-core-PCF. After fixing the capillaries in the tube, the PCF preform is drawn into PCF cane of 1.5–2 mm diameter. A mild vacuum pressure is applied during the PCF cane fabrication to close all interstice holes between capillaries. A PCF cane is then pulled into the standard fibre size of $\sim$125 μm at 1980 °C with solid core diameter of 8.27 μm as shown in Fig. 1(b), hereafter referred to as uncollapsed PCF. A new type of PCF, herein called a collapsed PCF [see Fig. 1(c)], is also fabricated in this study with almost the same core and cladding diameter as the uncollapsed PCF. A PCF cane fabricated from the same PCF preform is used to draw the collapsed PCF at a slightly higher furnace temperature (by 10 °C) by applying a vacuum pressure from the top of the PCF cane to make sure all the capillary holes are fully collapsed.

Both optical fibres have been fabricated with similar drawing tension ranges from 20 to 25 g, the one difference being in collapsed PCF that an additional vacuum pressure was applied.

The small tolerance in optical fibre drawing is expected to have negligible effect on radiation characteristics of optical fibre. As an example, Girard *et al.*, have shown that fibre drawing tension ranges from 22 to 70 g has no effect or negligible effect on radiation induced attenuation (RIA) over an observed $\sim$500–1600 nm wavelength for a Ge-doped core optical fibre [8]. Alessi *et al.*, have shown the lack of tension variation

effect of drawing condition on the fibre radiation response by comparing the RIA of two fluorine-doped optical fibres over ~200–500 nm fabricated with 30 and 140 g tension, with the samples exposed to 400 kGy [9]. In another study, Alessi *et al.*, demonstrated the insignificance of drawing condition variation on structural and radiation sensitivity of an optical fibre fabricated with different tensions from 35 to 80 g, and evaluated with different measurements (Raman spectroscopy, electron paramagnetic resonance and RIA) [10].

B. Surface Analysis Using XPS

The Ge-doped optical silica preform used herein was cleaned using an ultrasonic bath, repeated three times, cleaned in three different solvents; methanol, ethanol and propanol. The sample analysis was performed under ultra-high vacuum conditions in a ThermoFisher Scientific (East Grinstead, U.K.) Theta Probe spectrometer. The instrument employs a monochromatic Al Kα X-ray source (hν = 1486.6 eV). The area of analysis was approximately 800 μm diameter. The pass energy was set at 50 eV for core level high-resolution spectra of all elements of interest and at 300 eV for all survey spectra. The preform sample was held in place on the instrument sample stage by a Cu/Be clip. All data were obtained and quantified using the manufacturer's Avantage v4.84 software, which incorporates the appropriate sensitivity factors and corrects for the electron energy analyser transmission function [11]. All spectra were charge referenced against the C1s peak at 285 eV to correct for charging effects during acquisition.

C. PIXE Analysis

The sample preparation is covered in detail by Abdul Sani *et al.* [12]. The University of Surrey provides the EPSRC (Engineering and Physical Sciences Research Council) national ion beam facility. The microbeam facility used herein is based on a 2 MV Tandetron accelerator, described in detail by Simon *et al.* [13]. The samples were irradiated on the microbeam line to a beam of 2.5 MeV protons with the beam normal to the sample, use being made of a spot size of 2×2 μm^2, measured using a copper grid and a proton current of between 0.3 and 0.8 nA. The characteristic X-ray photon emissions were detected using a SGX Si-Li detector (Sensortech Ltd, High Wycombe, U.K.) of 80 mm^2 active area and 140 eV energy resolutions at 5.9 keV, mounted at a scattering angle of 45° to the beam. In order to reduce the intensity of the Si Kα X-rays and to avoid spectrum degradation by high energy recoiling protons the Si-Li detector was fitted with a two-layer absorber consisting of 130 μm beryllium foil and 50 μm Kapton foil.

Scanning was carried out over the cross-sectional area of the optical fibres implanted in the resin block, producing a pixel-by-pixel map of the sample elemental composition. For each sample, elemental maps were collected for localisation and then a line of points was set up in order to obtain the required concentration profiles. This was done in preference to a continuous line scan along the profile because this allows the local sample matrix composition to be determined at each point, permitting more accurate analysis. Although this is superficially a simple system (only three atoms, Si, O, Ge), PIXE spectrum processing is complicated by the fact that in the high concentration regions of the sample, the yield of the Ge K lines is strongly affected by self-absorption and so the Ge concentration must be determined independently or an iterative process must be used. Since the O is not visible in the PIXE spectra, and it is not possible to iterate assuming atomic stoichiometry, RBS was used to provide an independent measurement of Ge. Pairs of simultaneously collected RBS and PIXE spectra were processed using the 'Q factor' method [14] implemented in OMDAQ2007 [15]. In this method the actual beam charge and the local sample matrix (both of which are required for accurate thick target PIXE analysis) are calculated from the RBS spectrum and transferred automatically to the PIXE processing software within OMDAQ2007. The method requires a determination of the ratio of solid angles of the PIXE and RBS detector and also the parameters used in the model of the variation of the PIXE detector efficiency with X-ray energy. This is done during each run as part of the setting-up process using a standard reference material (lead glass BCR 126A [16]) as described in [17]. RBS spectra were fitted using the simulation module of OMDAQ2007 which incorporates non-Rutherford cross sections. The PIXE spectra were processed using GUPIX [18] accessed via the automated OMDAQ2007 user interface. Fig. 2 shows PIXE spectrum for a Ge concentration region.

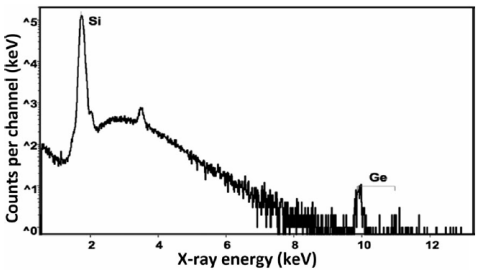

Fig. 2. PIXE spectrum for a point in a Ge concentration region of Ge-doped SiO_2 PCF uncollapsed fibre. The total run time was 2.5 min using beam current of ~150 pA of 2.5 MeV protons corresponding to a beam dose of 22.5 nC.

OMDAQ2007 provides real-time spectrum quality monitoring and so each point was analysed until the statistical precision of the Ge Kα line area was better than 5% and the total number of counts in the RBS spectrum was greater than 50 000 or for a maximum of 10 min. With the beam currents available this corresponds to an accumulated charge of up to 300 nC.

III. Results and Discussion

A. Determination of Oxidation Charge State Using XPS

In XPS, the solid material is bombarded with low energy X-rays to provoke the photoelectron emission from the outermost atomic layers of the surface, allowing identification of the elemental composition (except for H and He). The energy of the emitted photoelectrons is then analyzed by the electron spectrometer and the data presented as a graph of intensity against electron energy. The kinetic energy of the electron is the

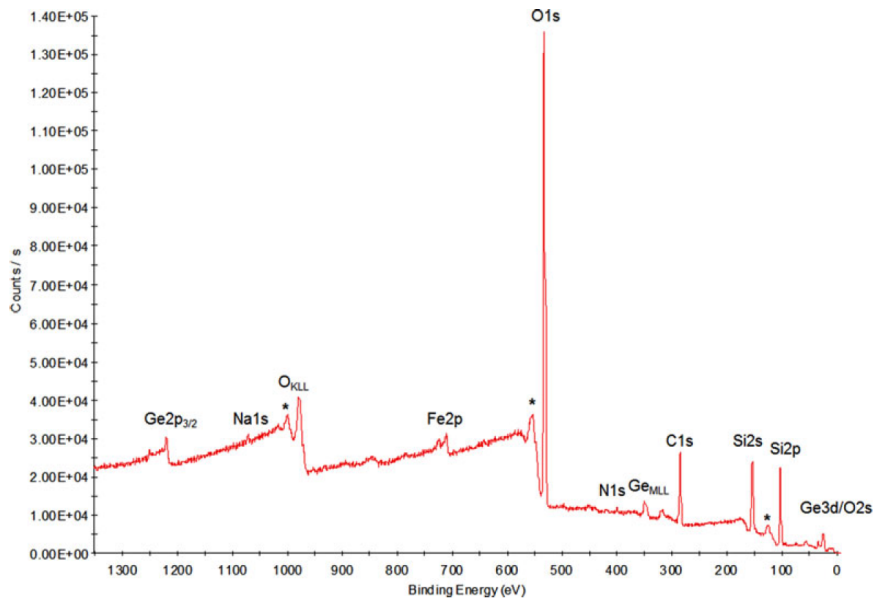

Fig. 3. A survey spectrum is shown for the Ge-doped perform, revealing the XPS transitions made accessible using Al Kα radiation (1486.60 eV), the features marked with an asterisk are electron energy loss features due to plasmon excitation.

experimental quantity measured by the spectrometer, but this is dependent on the photon energy of the X-rays employed. Fig. 3 shows the presence of elements on the sample surface with the different peaks corresponding to electrons photoejected from the different core levels of the material. The narrow scan provides the high resolution Ge2p3 core level peak shown in Fig. 4. The binding energy and atomic percentage of the detected elements are presented in Table I. It is observed in Fig. 3 that the O1s peak ($\sim$527 eV) is the most intense peak in the spectrum, followed by the C1s component peak ($\sim$282 eV), which is attributed to the hydrocarbon components. Adventitious carbon contamination detection, resulting from exposure to the atmosphere is commonly used as a charge reference for XPS spectra so as to calibrate the binding energy scale for XPS measurements with non-conducting specimens; a binding energy of 284.8 eV has been set for this purpose. The presence of Fe2p, N1s and Na1s in the preform under investigation is due in part to contamination during sample handling.

Following core-ionization by photoelectron emission, an outer shell electron can fill the created vacancy and the energy released can result in the emission of an Auger electron. The energy of the Auger transition shows dependence on chemical state, more exactly than do the binding energies of the individual electrons involved in the transitions. Therefore, the Auger electrons emitted from surface under the action of X-ray bombardment allows analysis of prominent spectral features and are used to determine the chemical shift of metal surfaces, referred to as the Auger parameter (α') without interference of surface charging. Originally defined by Wagner [19], [20], the Auger parameter was calculated using (1):

$$\alpha' = \mathrm{Ek(C1C2C3)} + \mathrm{Eb(C)} \quad (1)$$

where Ek(C1C2C3) is the kinetic energy of the Auger transition involving electrons from C1, C2 and C3 core levels and Eb(C) is the binding energy of the core level C. The kinetic energy of the $\mathrm{Ge_{LMM}}$ Auger electrons is shown in Fig. 5, indicating the kinetic energy value to be 1137 eV. The observed $\mathrm{Ge_{LMM}}$ lineshape and oxidation state shift of 2354.39 eV with respect to pure germanium indicate that the germanium is predominantly in the form of GeO_2 (+4 oxidation state) within the core [21].

The oxidation state of germanium is of significance because GeO_2 is known to play an important role in the optical fibre performance. The difference in refractive index induced by GeO_2 between the core and cladding structure allows the light signal to propagate, enabling long distance optical telecommunication. Naturally, oxygen interstitials occupy bond-centered position of the Ge-Ge bond axis forming a tetrahedral structure similar to silicon. Since the formation energy of GeO_2 is much lower (-106 kJ/mol^{-1}) compared to silicon, the oxygen diffusion rate is higher which leads to increased oxygen-related defects. Mostly, these defects are embedded in an amorphous Si and Ge matrix, being created in the preform during the high temperature fabrication processes.

In recent years, as a result of numerous Ge-doped silica studies, knowledge of oxygen-related defects in Ge has rapidly increased, their signature properties being discussed with emphasis on seeking to understand and utilise these for possible application in optical, electrical and dosimetric scenarios.

The oxygen-related defect centre been attributed to a diamagnetic Ge oxygen deficient centre (GODC), and previous researches have pointed out that its most probable microscopic structure is that of a twofold coordinated Ge (= Ge ••), where the (=) represents the bonds with two oxygen atoms, and (••)

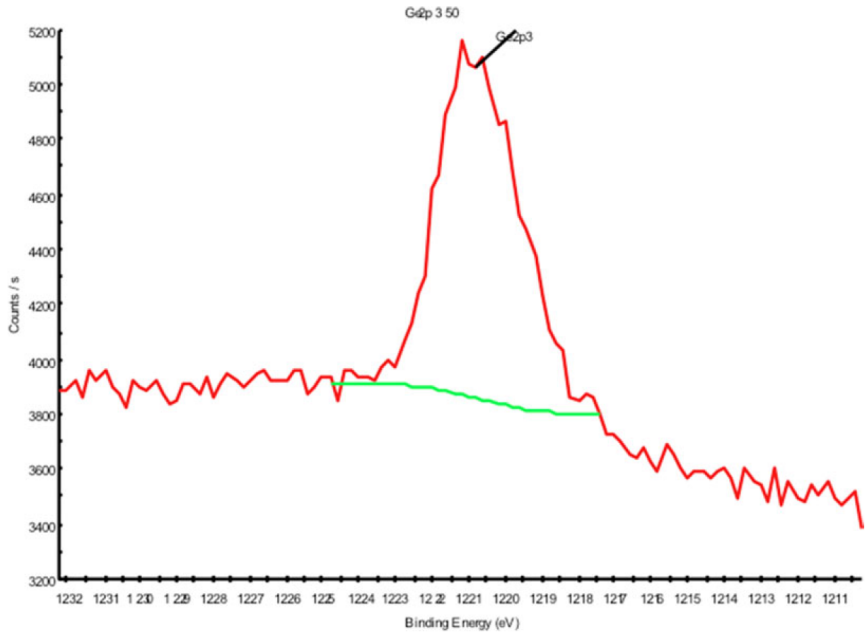

Fig. 4. A narrow high resolution scan of the Ge2p3 spectrum, revealing the peak binding energy to be located at 1217.39 eV with the atomic percentage of 0.82%.

TABLE I
SUMMARY XPS ANALYSIS FOR GE-DOPED OPTICAL SILICA PREFORM

Name	Binding Energy (eV)	Atomic Percentage
Ge2p3	1217.39	0.82
Si2p	99.80	18.70
O1s	527.20	60.30
C1s	282.20	17.35
Fe2p	705.00	1.37
N1s	396.89	0.95
Na1s	1068.81	0.51

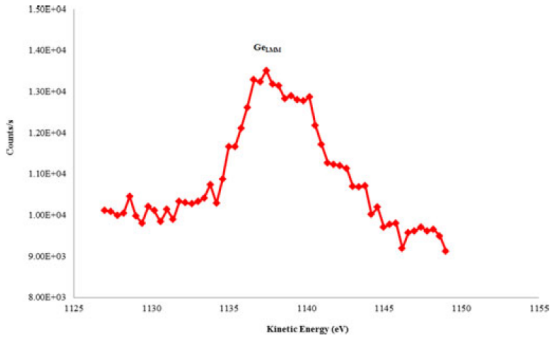

Fig. 5. Narrow scan, providing high resolution determination of the kinetic energy for Ge_{LMM} Auger electrons, showing the kinetic energy to be 1137 eV.

denotes a lone electron pair: from this structural model the defect takes the name Ge lone pair centre (GLPC) [22], [23]. Previous work has provided evidence for the presence of GLPC defects induced by ionising radiation where the absorption band peaks at 5.15 eV, showing two photoluminescence bands at 4.3 and 3.1 eV [23], [24]. The absorption band has been associated to an electronic transition from a point defect ground state (S_0) to its first excited singlet state (S_1). The α_E band is attributed to the inverse transition of absorption ($S_1 \rightarrow S_0$) while, in this energy level scheme, the β band is associated to the transition from the first excited triplet state (T_1), supplied by an intersystem-crossing (ISC) process ($S_1 \rightarrow T_1$), to the S_0 [25], [26]. The other absorption change is the generation of the Ge electron centre (GEC), where an electron is trapped at a fourfold coordinated Ge site. Fujimaki *et al.* [23] has explained in detail the generation mechanism of the GEC in Ge-doped SiO_2 glass through absorption and ESR measurements with three different photon sources, showing electrons are released from the GLPCs and the GEC are generated. Some defects providing absorption at 5.1 eV strongly contribute to the generation of the paramagnetic centres, referred to as Ge(1) and Ge(2). These two signatures of Ge(1) and Ge(2) structures have attracted debate, in one case with Ge(1) being assigned to the GEC of which all the next-nearest four neighbours are silicons while Ge(2) is assigned to the GEC which has one Ge atom at the next-nearest neighbours [27]. By comparison, in the work of Anoikin *et al.* [28], they have been respectively assigned to the GEC and the hole-centre

of the GODC, the latter donating an electron to GEC. Furthermore, thermally stimulated luminescence (TSL) measurements, availed by laser irradiation, have helped clarify that the reverse reaction can be induced thermally, whereby electrons are detrapped from the GECs and are captured by the GLPC. Morever, the ESR spectra for Ge(1) and Ge(2) are assigned to the GEC and a hole trapped at the GLPC, respectively [23].

The GODC formation is accounted for by internal stresses. In the stressed regions, regular bonds are ruptured to produce pairs of oxygen-deficient and oxygen redundant centres. Germanium atoms in SiO_2 are directly substituting for the silicon atoms in the crystalline quartz, as the Ge^{4+} ion is isoelectronic with Si^{4+}, so only the 4+ valence state is present before irradiation. This indicates that GODC is an electron donor. Studies at 77K have found that the GeO_4 tetrahedra that trap electrons in x-irradiated Ge-doped silica glass, denoted Ge(1) and Ge(2), possess a degree of quartz-like local structure [29]. All of these defects result from trapping of radiation-induced electrons on substitutional Ge^{4+} ions present in the original diamagnetic materials. These features suggest that the main generation mechanism of twofold coordinated Si defects involves the displacing of O from bonding configuration, due to knock-on or radiolysis processes. Such a generation process should depend on the structure of the material (for example on the strength of Si–O bonds).

Fig. 6(a) shows the Ge2p3 photoelectron spectrum of the sample. By fitting the measured spectrum, the binding energy of the Ge was found to be 33.32 eV with a FWHM of about 3.02 eV. Comparing this energy with elemental Ge3d of 29.1 eV [NIST], the energy is shifted to about 4.22 eV. According to Schmeisser [30], an average chemical shift per oxidation state for Ge3d core level is about 0.85 eV which brings about an oxidation state of greater than 4. Fig. 6(b) shows that the O2s photoelectron is found at 25 eV, about 1 eV [31] more than the typical value. The quantitative ratios of the photoelectron peak intensity yields a [O/Ge] of about ∼3.3 for the present material.

Under high temperature fabrication, the mobility of Ge atoms is increased thus allowing transform to GeO_x states. Therefore, during prolonged treatments at this temperature, GeO_x precipitates are easily formed. However when heat is suddenly removed, the GeO_x form 'strained GeO_2' to achieve equilibrium states. This leaves vacancies (Frenkel defects), which are responsible for the formation of GEC and GODC centres.

B. Determination of Dopant Concentration using PIXE Analysis

Typical PIXE and RBS spectrum for a collapsed PCF of 125 μm diameter, obtained with a 2.5 MeV proton beam are shown in Fig. 2. Similar PIXE and RBS spectra were obtained for the uncollapsed PCF investigated herein. Fig. 6 represents the elemental maps of Si and Ge for both uncollapsed and collapsed PCFs. PIXE and RBS analysis also detected the presence of other elements, including P, and Al, due in part to sample handling. However, the concentration of these elements has been found to be relatively small and as such can be considered to have little effect upon the TL yield of these fibres.

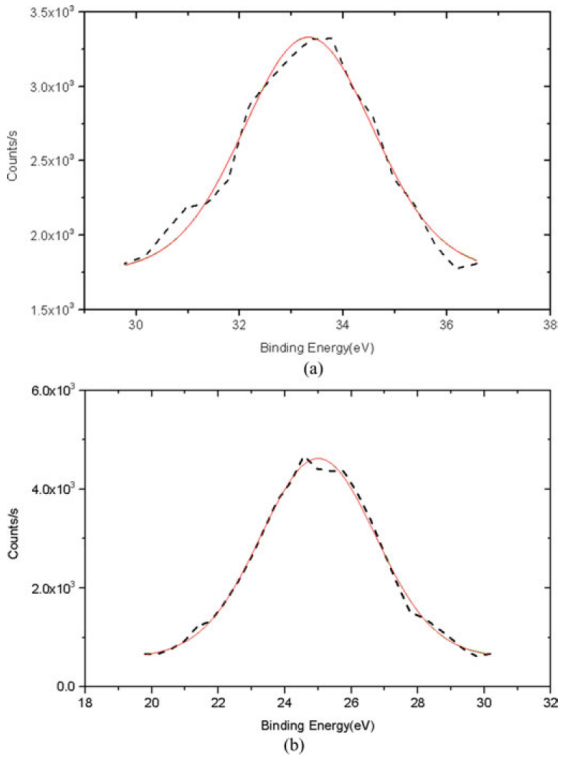

Fig. 6. (a) The X-ray photoelectron for Ge2p3, (b) O2s. The dotted line is the subtracted counts per second using the Shirley background and the solid line is the fitted curve.

A complementary analysis for the concentration of Si and Ge obtained by line scanning across the uncollapsed and collapsed PCFs are presented in Figs. 8 and 9, respectively. The lower Ge concentration measured from the fibre cross-section area in uncollapsed PCF, being in the range of 0.0238–0.1826 compared to that in collapsed PCF of 0.0376–0.2183, is in agreement with the line scans in Figs. 8 and 9. This is mainly due to large beam size, 2×2 μm^2. In each PIXE measurement, the elemental concentration in uncollapsed PCF might be a result of a mixture between Ge, Si, and/or air holes, while in collapsed PCF it might be a mixture of Ge and Si. However, there is a very large difference between the Ge concentration measured in the preform compared to that observed in uncollapsed and collapsed PCFs. Besides the small percentage diffusion of elements during the fibre drawing process, it should also be noted that the measurements in the preform were directly from a large core area of around 2.10 mm doped with Ge.

In the case of PCFs, the elemental analysis has been performed within the PCFs cross-sectional area, including the Ge-doped cladding and an 8.27 μm pure silica central core. The Ge-doped cladding is made of capillary fibres with a thin layer of Ge core existing in the inner layer of the capillaries, where

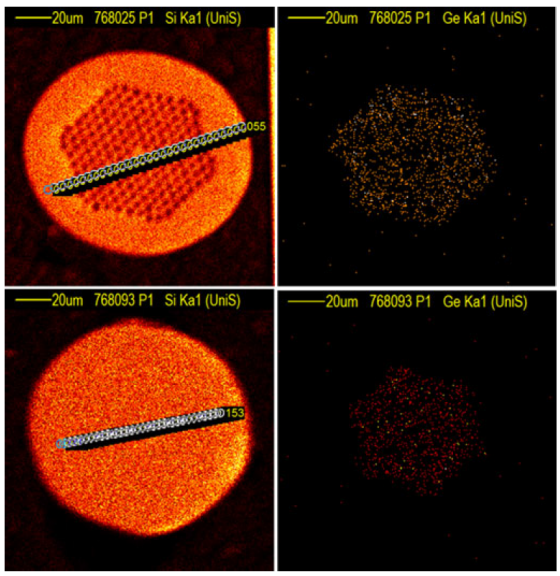

Fig. 7. Elemental maps across the transverse cross section of an uncollapsed PCF (top) and collapsed PCF (bottom), showing the relative presence of the identified elements, Si, and Ge respectively. Also identified are the locations of the point scans.

the area of the Ge layer is approximately 52 times smaller than the area of the pure silica capillary cladding (here one refers to the core and cladding area of the preform shown in Fig. 1(a), assuming these to have the same core to cladding area ratio compared to the Ge-doped preform tube used for PCF fabrication). The output of the elemental analysis is thereby an average of Ge and Si from the collapsed PCF cross sectional area, which is expected to have a Ge concentration which is some 52 times lower than that of the preform core. This is in agreement with the maximum Ge concentration observed from the collapsed PCF cross section compared to the preform, of about 39 times (8.49 wt% in preform measured by EDX divided by 0.2183 wt% in collapsed PCF measured by PIXE). The difference between the expected Ge concentration in collapsed PCF (with a Ge concentration some 52 times lower) and the measured concentrations (39 times lower) is mainly due to the use of two different elemental measurement methods, i.e., EDX and PIXE.

Here it is to be noted that the issue of spatial resolution in electron beam induced X-ray analysis (EDX) is complex, the reasoning behind the assertion of superior spatial resolution of the PIXE-based method is as follows: while the beam diameter in electron probe machines is routinely significantly smaller than that achieved in the proton microprobe, the spatial resolution is primarily determined by the shape of the excitation volume beneath the surface of the sample. For electrons, this is a 'teardrop' created by multiple scattering of the primary electrons from electrons in the sample. The effective dimensions of this are determined by the primary beam energy, the material of the sample and the mass absorption coefficient of the X-ray being observed. For electrons with energy sufficient to excite the germanium K-lines, the depth and diameter of the excitation volume may be in the micrometre range. For MeV protons, the excitation volume is a cylinder with a diameter equal to the diameter of the beam at the surface (1 μm) and a length dependent on beam energy and the material of the sample. For present samples, the penetration depth before the beam starts to broaden significantly is around 80 um, and since X-rays from this depth will be attenuated by the overlying material, the resolution is effectively equal to the beam diameter, offering superior spatial resolution.

However, it is to be emphasised that the primary reason for the choice of PIXE is the much lower detection limit. X-rays from the germanium in the lesser doped samples were not visible using the electron probe technique.

Recently, we have measured the Ge concentration of conventional optical fibre fabricated from the same preform presented in Fig. 1(a) using PIXE, showing a Ge concentration of around 10–12 wt% in the fibre core area [12]. Considering the highest Ge concentration of 12 wt%, this confirms that the Ge concentration in collapsed PCF cross section is about 55 times lower than the Ge concentration in the conventional fibre, due to the averaged concentration between Ge and Si.

In respect of the uncollapsed PCF, in addition to Si and Ge, air holes are also present. Each air hole has a diameter of around 4.3 μm and a wall thickness between two adjacent holes of some 2.0 μm. Averaging the elements Si, Ge, and air holes in the cross section area of uncollapsed PCF would result in a very much lower Ge concentration for this fibre. It should be noted that in the uncollapsed PCF, if the fibre samples under measurement are not exactly aligned to be perpendicular to the applied PIXE beam then there would be a greater probability for part of the beam area to be focused on the inner wall surface of the capillaries (where the Ge layer is available) instead of the hollow area. The results in Fig. 8 and the range of Ge concentrations suggest that the uncollapsed PCF was not very far from exact perpendicularity with the applied beam, otherwise a much lower Ge concentration might have been observed from the surface of this fibre.

The variations of Ge concentration in the line scan presented in Fig. 8 are the result of inexact knowledge of the focusing point of the PIXE beam over the uncollapsed PCF cross-section area. With a 2×2 μm^2 PIXE beam size, the possibility of having the beam located in an area involving Si, Ge, and/or air is very high. Thus, as the line scan in Fig. 8 shows, the Ge concentration to the two sides of the PCF central core is not symmetric, being mainly dependent on the position of the applied PIXE beam in the surface of the PCF, a situation similarly applicable for Si concentration variation.

The lower Ge concentration in the central core of the PCFs is due to the pure silica rod used in these PCFs. However, the small Ge concentration at the central core of PCFs shown in Figs. 8 and 9 suggest that besides a small diffusion of Ge that might be induced from the cladding part into the core, the line scan did not pass through the exact central core or diameter

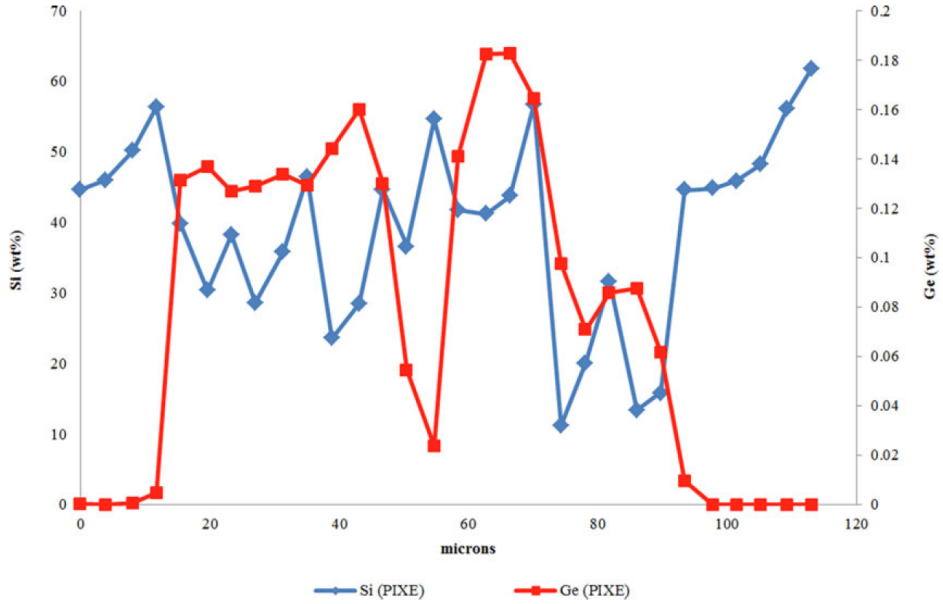

Fig. 8. The distribution of Si and Ge along a line scan for a Ge-doped uncollapsed PCF.

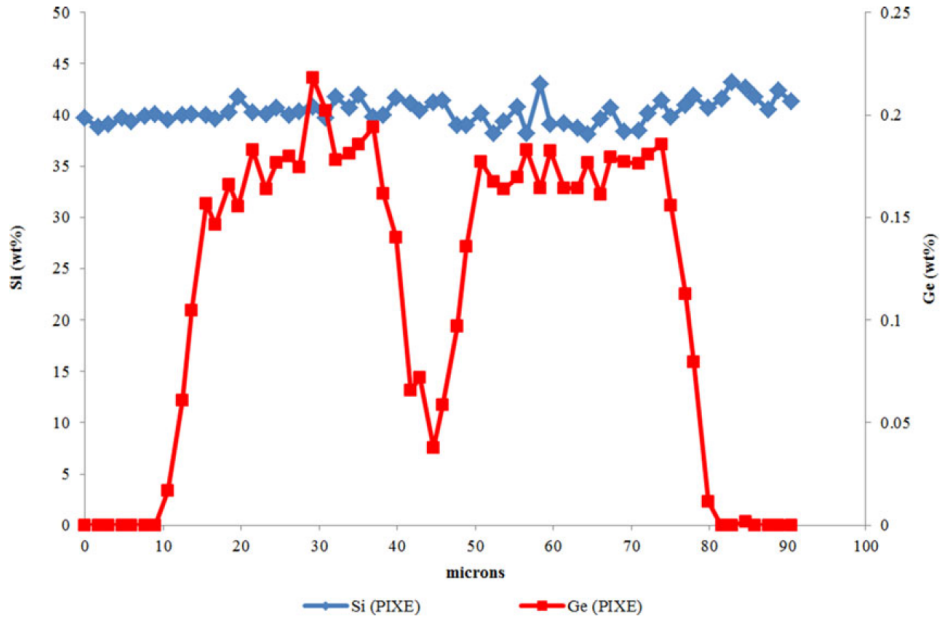

Fig. 9. The distribution of Si and Ge along a line scan for a Ge-doped collapsed PCF.

of the PCFs. Instead, it passes through a hypotenuse close to the core, resulting in an average Ge concentration overlapped between the pure silica central core and the Ge doped capillaries in the cladding. This is clearly observed from Fig. 7 (top), the line scan failing to pass exactly through the central core of the PCF.

The lower Ge concentration at the outer diameter of the PCFs (for example before 15 and after 95 μm in Fig. 8) is due to the

use of pure silica tube that is used to stack the capillaries inside this jacket.

An appreciable presence of carbon is visible (Fig. 2), which affects the quantitation. It is possible that this is the embedding medium, which has entered the lumen of the fibres. Given that the PIXE analysis assumes a 'flat homogenous slab' approximation, the presence of variable amounts of carbon in the vicinity of each point leads to scatter in the results (Fig. 8).

IV. Conclusion

In support of the design of tailor made SiO_2 fibre TLD of improved performance, obtained through control of the processes of fabrication, we seek to investigate the surface chemical charge state of the Ge-doped SiO_2 optical preform and dopant concentrations of Ge-doped PCFs using the XPS technique and PIXE/RBS measurements respectively. The binding energy of Si2p and Ge2p3 were found to be 99.80 and 1217.39 eV respectively, the atomic percentages from the XPS analysis being 18.70% and 0.82% respectively. The observed Ge_{LMM} lineshape and oxidation state shift of 2354.39 eV with respect to pure germanium indicate the dopant to be in the predominant form GeO_2 (+4 oxidation state) within the core. Present PIXE/RBS measurements have demonstrated the characteristics of uncollapsed and collapsed PCFs. The proton energy used (2.5 MeV) is the optimum for PIXE analysis in this system. The 'noise' in the silicon profile in the uncollapsed PCF is due to the fact that the analysis points were not selected to fall on either the core (Ge), the air hole or the wall (Si) and so there is a large variation. The output of the elemental analysis from the collapsed PCF cross-section area is the average of Ge and Si, diffusing away from the centre into the fibre cladding. These results are expected to help in understanding the influence of the doped silica structure, also involving characterisation of the fundamental parameters that control thermoluninescence yield of the media under investigation.

Acknowledgment

The authors would like to thank the scientific and technical staff of the Structure Analysis Laboratory and Micro Structural Studies Unit, University of Surrey and Surrey Ion Beam Centre for their help in carrying out surface and elemental analysis and proton irradiations. They would also like to acknowledge the TM R&D/MMU lab, sited at the Multimedia University, for fabricating the fibre preforms. They want to extend their thanks to David Griscom for his advice.

References

[1] A. L. Yusoff, R. P. Hugtenburg, and D. A. Bradley, "Review of development of a silica-based thermoluminescence dosimeter," *Radiat. Phys. Chem.*, vol. 74, no. 6, pp. 459–481, Dec. 2005.

[2] L. Skuja, M. Hirano, H. Hosono, and K. Kajihara, "Defects in oxide glasses," *Phys. Status Solid*, vol. 2, no. 1, pp. 15–24, Jan. 2005.

[3] M. Ghomeishi, G. A. Mahdiraji, F. R. M. Adikan, and S. Hashim, "The thermoluminescence response of undoped silica PCF for dosimetry application," in *Proc. Conf. Lasers Electro-Opt. Pacific Rim*, Jun. 2013, pp. 1–2.

[4] S. Girard, J. Baggio, and J.-L. Leray, "Radiation-induced effects in a new class of optical waveguides: the air-guiding photonic crystal fibres," *IEEE Trans. Nucl. Sci.*, vol. 52, no. 6, pp. 2683–2688, Dec. 2005.

[5] N. J. Florous, K. Saitoh, T. Murao, and M. Koshiba, "Radiation dose enhancement in photonic crystal fiber Bragg gratings: Towards photoionization monitoring of irradiation sources in harsh nuclear power reactors," in *Proc. Conf. Lasers Electro-Opt.*, 2007, vol. 1, pp. 1–2.

[6] D. A. Bradley, G. A. Mahdiraji, M. Ghomeishi, E. Dermosesian, F. R. M. Adikan, H. A. A. Rashid, and M. J. Maah, "Enhancing the radiation dose detection sensitivity of optical fibers," *Appl. Radiat. Isotopes*, (2014), http://dx.doi.org/10.1016/j.apradiso.2014.12.005i

[7] G. A. Mahdiraji, D. M. Chow, S. R. Sandoghchi, F. Amirkhan, E. Dermosesian, K. S. Yeo, Z. Kakaei, M. Ghomeishi, S. Y. Poh, S. Y. Gang, and F. R. M. Adikan, "Challenges and solutions in fabrication of silica-based photonic crystal fibers: An experimental study," *Fiber Integr. Opt.*, vol. 33, pp. 85–104, Oct. 2014.

[8] S. Girard, C. Marcandella, A. Alessi, A. Boukenter, Y. Ouerdane, N. Richard, P. Paillet, M. Gaillardin, and M. Raine, "Transient radiation responses of optical fibers: Influence of MCVD process parameters," *IEEE Trans. Nucl. Sci*, vol. 59, no. 6, pp. 2894–2901, Dec. 2012.

[9] A. Alessi, S. Girard, M. Cannas, S. Agnello, A. Boukenter, and Y. Ouerdane, "Influence of drawing conditions on the properties and radiation sensitivities of pure-silica-core optical fibers," *J. Lightw. Technol.*, vol. 30, no. 11, pp. 1726–1732, Jun. 2012.

[10] A. Alessi, S. Girard, C. Marcandella, L. Vaccaro, M. Cannas, A. Boukenter, and Y. Ouerdane, "Influence of the manufacturing process on the radiation sensitivity of fluorine-doped silica-based optical fibers," *IEEE Trans. Nucl. Sci*, vol. 59, no. 4, pp. 760–766, Aug. 2012.

[11] S. J. Hinder, C. Lowe, J. T. Maxted, C. Perruchot, and J. F. Watts, "Intercoat adhesion failure in a multilayer organic coating system: An X-ray photoelectron spectroscopy study," *Prog. Org. Coatings*, vol. 54, no. 1, pp. 20–27, Sep. 2005.

[12] S. F. Abdul Sani, G. W. Grime, V. Palitsin G. A. Mahdiraji, H. A. A. Rashid, M. J. Maah, and D. A. Bradley, "Micro-PIXE analysis of doped SiO_2 fibres intended as TL dosimeters for radiation measurements," *X-Ray Spectrometry*, vol. 44, pp. 33–40, 2015.

[13] A. Simon, C. Jeynes, R. P. Webb, R. Finnis, Z. Tabatabaian, P. J. Sellin, M. B. H. Breese, D. F. Fellows, R. van den Broek, and R. M. Gwilliam, "The new surrey ion beam analysis facility," *Nucl. Instrum. Meth. Phys. Res. B: Beam Interact. Mater. Atoms*, vols. 219/220, pp. 405–409, Jun. 2004.

[14] G. W. Grime, "The 'Q factor' method: Quantitative microPIXE analysis using RBS normalisation," *Nucl. Instrum. Meth. Phys. Res. B: Beam Interact. Mater. Atoms*, vols. 109/110, pp. 170–174, Apr. 1996.

[15] Oxford Microbeams Ltd. (2014, Nov. 19). [Online]. Available: http://www.microbeams.co.uk/download.html

[16] European Commission, Joint Research Centre, Institute for Reference Materials and Measurements (IRMM), Certified Reference Materials 2015, Retieseweg 111, B-2440 Geel, Belgium.

[17] I. Gomez-Morilla, A. Simon, R. Simon, C. T. Williams, Á. Z. Kiss, and G. W. Grime, "An evaluation of the accuracy and precision of X-ray microanalysis techniques using BCR-126A glass reference material," *Nucl. Instrum. Meth. Phys. Res. B: Beam Interact. Mater. Atoms*, vol. 249, nos. 1/2, pp. 897–902, Aug. 2006.

[18] J. L. Campbell, N. I. Boyd, N. Grassi, P. Bonnick, and J. A. Maxwell, "The Guelph PIXE software package IV," *Nucl. Instrum. Meth. B*, vol. 268, pp. 3356–3363, 2010.

[19] C. D. Wagner, *Electron Spectroscopy*, D. A. Shirley, Ed. Amsterdam, The Netherlands: North-Holland, 1972, p. 861.

[20] C. D. Wagner, "Auger lines in X-ray photoelectron spectrometry," *Anal. Chem.*, vol. 44, no. 6, pp. 967–973, 1972.

[21] C. D. Wagner, "Chemical shifts of Auger lines, and the Auger parameter," *Discuss. Faraday Soc.*, vol. 60, pp. 291–300, 1975.

[22] K. Awazu, H. Kawazoe, and M. Yamane, "Simultaneous generation of optical absorption bands 5.14 and 0.452 eV in 9 SiO_2:GeO_2 glasses heated under H_2 atmosphere," *J. Appl. Phys.*, vol. 68, pp. 2713–2718, 1990.

[23] M. Fujimaki, T. Watanabe, T. Katoh, T. Kasahara, N. Miyazaki, Y. Ohki, and H. Nishikawa, "Structures and generation mechanisms of paramagnetic centers and absorption bands responsible for Ge-doped SiO_2 optical-fiber gratings," *Phys. Rev. B*, vol. 57, pp. 3920–3926, 1998.

[24] A. Alessi, S. Agnello, F. M. Gelardi, S. Grandi, A. Magistris, and R. Boscaino, "Twofold coordinated Ge defects induced by gamma-ray irradiation in Ge-doped SiO_2," *Opt. Exp.*, vol. 16, no. 7, pp. 4895–4900, Mar. 2008.

[25] M. Leone, S. Agnello, R. Boscaino, M. Cannas, and F. M. Gelardi, "Optical absorption, luminescence, and ESR spectral properties of point defects in silica," in *Silicon-Based Materials and Devices: Properties and Devices*, H. S. Nalwa, Ed. San Diego, CA, USA: Academic, 2001.
[26] L. Skuja, "Isoelectronic series of twofold coordinated Si, Ge, and Sn atoms in glassy SiO_2: A luminescence study," *J. Non-Cryst. Solids*, vol. 149, pp. 77–95, 1992.
[27] T. E. Tsai, D. L. Griscom, and E. J. Friebele, "On the structure of Ge-associated defect centres in irradiated high purity GeO_2 and Ge-doped SiO_2 glasses," *Diffus. Defect Data*, vol. 53–54, pp. 469–476, 1987.
[28] E. V. Anoikin, A. N. Guryanov, D. D. Gusovskii, V. M. Mashinskii, S. I. Miroshnichenko, V. B. Neustruev, V. A. Tikhomirov, and Y. B. Zverev, "Photoinduced defects in silica glass doped with germanium and cerium," *Sov. Lightw. Commun.*, vol. 1, pp. 123–131, 1991.
[29] D. L. Griscom, "Trapped-electron centers in pure and doped glassy silica: A review and synthesis," *J. Non-Cryst. Solids*, vol. 357, nos. 8/9, pp. 1945–1962, Apr. 2011.
[30] D. Schmeisser, R. D. Schnell, A. Bogen, F. J. Himpsel, D. Rieger, G. Landgren, and J. F. Morar, "Surface oxidation of germanium," *Surf. Sci.*, vol. 172, pp. 455–465, Feb. 1986.
[31] T. L. Barr, M. Mohsenian, and L. M. Chen, "XPS valence band studies of the bonding chemistry of germanium oxides and relates systems," *Appl. Surf. Sci.*, vol. 51, pp. 71–87, Dec. 1991.

S. F. Abdul Sani received the B.Sc. degree physics from the University of Surrey, Surrey, U.K., in 2011, where she is currently working toward the Ph.D. degree in the field of radiation physics.

G. Amouzad Mahdiraji received the B.Eng. degree in electrical power engineering in Iran in 2002, the M.Eng. degree in communication and computer engineering from Universiti Kebangsaan Malaysia, Selangor, Malaysia, in 2006, and the Ph.D. degree from Universiti Putra Malaysia, Serdang, Malaysia, in 2009, in the field of communications and networks engineering, majoring in optical communication. From May 2009 to August 2010, he was a Lecturer in the School of Engineering, UCSI University. Afterward, he joined to the Centre of Excellence for Wireless and Photonics Networks at UPM for around 1 year as a Postdoctoral Student. From November 2011 to 2012, he worked as a Visiting Research Fellow in the optical fiber fabrication group in the Photonics Research Group (PRG), Department of Electrical Engineering, University of Malaya, Kuala Lumpur, Malaysia. Since then, he has been working in the same department as a Senior Lecturer. Apart from optical communication systems, his current research interests include design and fabrication of microstructured optical fiber for different sensing applications.

A. S. Siti Shafiqah received the B.Eng. and M.Eng. degrees in mechanical engineering from the Tokyo University of Science, Tokyo, Japan, in 2010 and 2012, respectively. She is currently working toward the Ph.D. degree in physics at the University of Malaya, Kuala Lumpur, Malaysia.

G. W. Grime received the B.A. and D.Phil. degrees in physics from the University of Oxford, Oxford, U.K., and has extensive experience in developing techniques and multidisciplinary applications for MeV ion microbeam analysis. In 1980, he was part of the team which developed the first submicrometer nuclear microbeam. Now at the University of Surrey, Surrey, U.K., his research interests include continuing development of submicrometer focusing systems and the inclusion of other analytical methods such as mass spectrometry into ion beam microanalysis.

V. Palitsin received the M.Sc. degree in physical electronics from Tashkent Technical University, Tashkent, USSR, and the Ph.D. degree in physics from the University of Warwick, Warwick, U.K. He is currently a Research Fellow in the Surrey Ion Beam Centre, University of Surrey, Surrey, U.K.

S. J. Hinder received the Ph.D. degree in Nottingham, U.K., in 2001. He is currently a Research Fellow and Operations Manager at the Structure Analysis Laboratory and Micro Structural Studies Unit, University of Surrey, Surrey, U.K.

N. Tamchek received the B.Sc. degree in optics/astrophysics from Kanazawa University, Kanazawa, Japan, in 2001, and the M.Sc. and Ph.D. degrees from the University of Malaya, Kuala Lumpur, Malaysia, in 2004 and 2010, respectively, both in the field of photonics. From 2010 to 2011, he was a Postdoctoral Student in MOSTI-UM. He is currently a Lecturer at Universiti Putra Malaysia, Serdang, Malaysia.

H. A. Abdul Rashid (M'04) received the B.Eng. degree in electronic and electrical engineering from University College London, London, U.K., in 1997. He then received the M.Eng.Sc. degree in signal processing and the Ph.D. degree in optical communication systems in 2001 and 2007, respectively, both from Multimedia University (MMU), Selangor, Malaysia. He then obtained an Executive Certificate in Strategy and Innovation from the MIT Sloan School of Management in 2010. He is currently a Professional Engineer with the Board of Engineers, Malaysia, and a member of the IEM. He is a Professor at the Faculty of Engineering, MMU. He is currently the Director of Research Management Center, MMU, where he oversees research planning, management, and monitoring in the university. He has served MMU for over 17 years in several capacities including the Dean of Research and the Director for Research Collaborations. He currently leads a team of researchers, collaborating with Telekom Research and Development Sdn. Bhd. (TM R&D) focusing on designing and fabrication of specialty optical fiber for communications and sensors. His research team has accumulatively attracted grants close to RM7.2 million from Ministry of Science, Technology and Innovation (MOSTI) and Telekom Malaysia (TM). His current project is into new optical communication transmission band and its amplification methods, funded by Telekom Malaysia Bhd (TM). The output from this project leads to improvement in transmission bandwidth, allowing greater broadband experience. The project has started to strike commercialization interest from industry like FiberHome (China) and Alnair Labs (Japan)

M. J. Maah received the B.Sc. (Hons.) degree in chemistry from the University of Malaya, Kuala Lumpur, Malaysia, in 1979. He started his academic career as a Chemistry Tutor at Pusat Asasi Sains University Malaya (PASUM) and later went to the University of Sussex, Brighton, U.K., to complete his M.Sc. degree in organometallic chemistry. This was the year he worked collaboratively with Prof. Sir H. Kroto, a Nobel Laureate in Chemistry. In 1985, he went again to Sussex University for his D.Phil. degree—continuing on the pioneer work he initiated during his M.Sc on the coordination chemistry of ligands containing P–C multiple bonds under the supervision of Prof. J. Nixon. Other than research, he is actively involved in chemical education and had been consultants to several ministries and industries in Malaysia. He has held several academic administrative positions in University Malaya (UM) including the Head of Department, Director, Dean of several establishments in UM and DVC (Research and Innovation) and the Deputy Vice Chancellor (Academic and International). He is the Chairman of the Malaysia Chemistry Olympiad Committee and heads several scientific committees involving government ministries and societies. He was recently seconded to the Ministry of Science, Technology and Innovation (MOSTI) as Undersecretary of the BIOTEK Division. He is currently a Professor of inorganic chemistry at the Department of Chemistry, University of Malaya.

J. F. Watts received the Ph.D. and D.Sc. degrees from dUniv Paris-Sud, Paris, France. He has extensive experience in the application of surface analysis to applied problems in materials science. His research fields include adhesion between inorganic and organic phases and their subsequent failure, and surface characterisation of polymeric materials. He is currently the Director of UMI and of the Centre for Materials, Surfaces and Structures, School of Engineering. He obtained honours and awards of the Alcoa Foundation Award (1992), the Robert L Patrick Fellowship of the Adhesion Society (2006) design and fabrication of microstructured optical fiber for different sensing applications. He is a Chartered Engineer (CEng), Fellow of Institute of Material (FIM), Fellow of the Institute of Physics (FInstP), Chartered Physicist (CPhys).

D. A. Bradley received the B.Sc. (physics), M.Sc. (radiation physics), and Ph.D. degrees. He is currently a Professor at Radiation and Medical Physics and was for six years the Secretary of the International Radiation Physics Society. He has been the Editor-in-Chief of the Elsevier journals *Applied Radiation and Isotopes* and *Radiation Physics and Chemistry* and a member of an Experts Steering Group of the IAEA for the project "Strengthening Medical Physics through Education and Training." Presently, he is the Editor-in-Chief of the *British Journal of Radiology*. Throughout the 1990s, he was an Adjunct Associate Professor with the Atomic Physics Theory Group at the University of Pittsburgh. He is a Fellow of the Institute of Physics (FInstP), Fellow of Institue of Physics and Engineering in Medicine (FIPEM).

Appendix B

Research article

X-RAY SPECTROMETRY

Received: 9 September 2014 Revised: 28 November 2014 Accepted: 30 November 2014 Published online in Wiley Online Library: 30 December 2014

(wileyonlinelibrary.com) DOI 10.1002/xrs.2575

Micro-PIXE analysis of doped SiO_2 fibres intended as TL dosimeters for radiation measurements

S. F. Abdul Sani,[a]* G. W. Grime,[b] V. Palitsin,[b] G. A. Mahdiraji,[c] H. A. Abdul Rashid,[d] M. J. Maah[e] and D. A. Bradley[a,f]

Sample elemental concentrations can be determined using the microbeam proton-induced X-ray emission (PIXE) technique, providing non-destructive simultaneous low-background multi-element analysis. Present interest concerns analysis of Ge-doped SiO_2 fibres intended as high spatial-resolution thermoluminescence (TL) dosimeters for radiation measurements in place of their more typical applications in telecommunications. During fibres fabrication, defined amounts of the Ge dopant are added, the dopant more usually having a determining role in the transmission properties of the fibre. Characteristic X-rays produced in PIXE analysis provide information on the relative distribution of elements within a sample, as in for instance Ge and Si concentrations, the Ge acting as point defect centres that promote TL. With the dopant tending to diffuse in and away from the fibre core, it is essential to define the sample matrix composition in order to accurately evaluate the X-ray yield. This is determined in part using simultaneous Rutherford Back Scattering analysis. In present work, PIXE/Rutherford Back Scattering measurements have been employed to ascertain dopant concentrations of fibres that have been fabricated at the University of Malaya with a view to improving TL yield. Present results concern cylindrical fibres, nominally with 4%, 6% and 8% weight peak Ge concentrations and flat fibres of nominal 6% weight Ge concentration. For the cylindrical fibres, Ge dopant concentration has been found to be in the range of 2.41–4.56%, 6.44–8.29% and 10.27–12.25% weight, respectively, while for the flat fibres, the Ge concentration range is broader, at 0.07–6.55% weight. Copyright © 2014 John Wiley & Sons, Ltd.

Introduction

Over the past decade and more, optical telecommunication fibres have been widely investigated for application as thermoluminescence dosimeters (TLD), offering relatively high TL yield as a result of extrinsic doping of the fibre core.[1,2] As a result of irradiation, electrons are excited into the point defect traps that have been created by the doping process so that in principle, the concentration and storage capacity of these traps can provide a medium suitable for dosimetric applications. To date, the main dosimetric attributes that have been associated with such small diameter optical fibres (typically ~100 μm) have included the following: the possibility of producing a dosimeter with excellent spatial resolution; a wide dynamic range of dose sensitivity, from a fraction of a grey to many tens of grey and beyond, providing for applications in radiotherapy and high dose industrial dosimetry; water and corrosion resistance; reusability; and modest cost. Ultimately, we are seeking to fabricate in-house, enhanced TL yield fibres that would extend applications to diagnostic and environmental radiation doses (milligray down to fractions of a microgray, respectively). As such, one is looking to offer radiation sensitivity approaching or exceeding that of more well-established TL dosimeters such as the LiF phosphor-based commercial product TLD-100.

The TL response of commercial doped SiO_2 optical fibres has been investigated by a number of workers, demonstrating promising TL properties with respect to ionising radiation, including for photons,[3–7] electrons,[4,8] protons,[9] alpha particles,[10] fast neutrons[11] and synchrotron radiations.[12]

Optical fibre is typically made from a preform of silica, comprising two essential components, the doped silica core and the outer silica cladding, such that for telecommunication purposes, a difference in refractive index is produced between the core and the cladding. This refractive index profile is controlled and manipulated through the addition of the dopant. As an example, a particularly popular process is to flow and deposit a gaseous mixture of $GeCl_4$ and $SiCl_4$ within an initially pure silica hollow tube. Simultaneously, the tube is collapsed down to produce what is referred to as a preform, using a high-temperature drawing and fusion process[13] producing an inner core of Ge_2O_3 in amorphous SiO_2.

* Correspondence to: Siti Fairus Abdul Sani, Centre for Nuclear and Radiation Physics, Department of Physics, University of Surrey, Guildford, Surrey, GU2 7XH, UK. E-mail: s.abdulsani@surrey.ac.uk

a Centre for Nuclear and Radiation Physics, Department of Physics, University of Surrey, Guildford, Surrey, GU2 7XH, UK

b Surrey Ion Beam Centre, Nodus Laboratory, University of Surrey, Guildford, Surrey, GU2 7XH, UK

c Integrated Lightwave Research Group, Department of Electrical Engineering, Faculty of Engineering, University of Malaya, Kuala Lumpur, 50603, Malaysia

d Faculty of Engineering, Multimedia University, 2010 Cyberjaya, Selangor, Malaysia

e Department of Chemistry, University of Malaya, Kuala Lumpur, 50603, Malaysia

f Department of Physics, University of Malaya, Kuala Lumpur, 50603, Malaysia

In brief, for present purposes, the optical properties of silica (specifically the amorphous form) are based on the trapping processes usually reported for crystalline media. It has previously been noted that the TL response of the SiO_2 optical fibre is considerably enhanced by the presence of structural defects in the material, including those produced by extrinsic doping.[2] Such defect centres can also be generated in the glass by either ionisation or displacement damage, typically at elevated linear-energy transfer.[14,15] Thus said, with regard to production of the fibres from the preform, it is expected that pulling parameters such as vacuum pressure [used for the flat fibres (FFs)], pulling speed, use of a high pulling temperature of >2000 °C and the fast cooling/quenching rate to room temperature will all play an important and dominating role in the TL response, influencing the species and population of defects and characteristics of the optical fibre.

The extrinsically doped silica fibre used herein is composed of silicon ($Z=14$) and oxygen ($Z=8$) doped with germanium ($Z=32$), fabricated via the standard Modified Chemical Vapour Deposition (MCVD) method, utilising $SiCl_4$ and $GeCl_4$ vapour precursor. The cladding layer is exclusively deposited with $SiCl_4$; conversely in the core, deposition of this occurs together with $GeCl_4$. The Ge atoms (valence 4) directly substitute the Si atoms (also valence 4) in silica (SiO_2) when Ge is added to the silica glass, therefore affecting the O bonds between Si and Ge atoms; O bonds are lost and form oxygen deficiency centres. The formation of these defects also affects the internal stresses within the glass, it being well understood that the silica fibres become more brittle and therefore less mechanically stable with increasing dopant concentration.

To date, rather limited research has been conducted towards gaining an essential understanding of the magnitude of TL signal and material characteristics of doped fibres. The work of Yusoff *et al.*,[2] as an instance, concerns TL yield and structural characteristics of sol–gel glass. Dopant diffusion in optical fibres is fundamentally important, determining both the transmission properties of the fibre and in defining the eventual TL yield of the medium. For doped silica fibres, to establish an underpinning basis for the TL yield, we wish to define the extent of diffusion of the Si and Ge in the core and inner cladding of single-mode optical fibre. In turn, this reflects the underlying influence of fibre drawing and subsequent heat treatment processes.

The overarching aim of the project is to improve SiO_2-fibre TLD performance through control of the processes of fabrication. In support of this, and to ascertain dopant concentrations of tailor-made fibres, ion beam study has been undertaken using a combined microbeam proton-induced X-ray emission (PIXE)/Rutherford Back Scattering (RBS) analysis arrangement. The key advantages of the PIXE method, other than its generally non-destructive nature, are the availability of simultaneous multi-elemental analysis, the short data collection time and the very low background, avoiding primary bremsstrahlung production, with parts per million detection limits.[16]

Material and methods

Fibres fabrication

Present research focuses on the diffusion of Ge (and Si) in tailor-made doped cylindrical silica optical fibres (CFs) and FFs. The fibres, produced by the University of Malaya lead collaboration, are investigated for three groups of Ge-doped fibres of nominal dopant concentrations 4%, 6% and 8% weight. Absolute values are determined using Surrey University ion beam centre facilities, assessing the characteristic X-rays produced in PIXE analysis. As previously outlined, the optical fibres are doped using the MCVD method, with precursor $SiCl_4$, $GeCl_4$ and oxygen (O_2) being made to flow into rotating high purity silica tube. The vapour mixture is subsequently oxidised using a high-temperature H_2/O_2 burner/furnace operating in the temperature range 1300–2100 °C and moved forwards and backwards in a number of passes depending on the target dopant concentration value. As the vapour mixture approaches the hot zone, the vapour is turned into a white soot-like powder, to be distributed along the substrate tube by the thermophoretic process, yielding a temperature-dependent particle-size deposition profile. Subsequent to soot deposition, the tube temperature is increased to 1800–2100 °C in order to sinter the soot particles, the powder being considered to be fully sintered when the material is judged by eye to be sufficiently transparent. The sintered preform is subsequently collapsed and sealed by further elevation of temperature.[17]

The FF used herein has been fabricated using a conventional 5 m high fibre drawing tower, the latter being located at the Flat Fibre

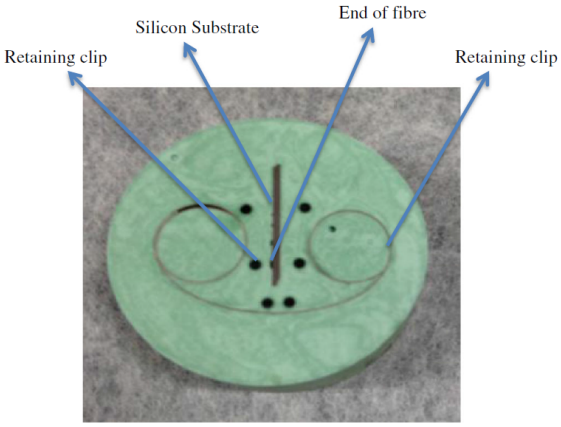

Figure 1. Optical fibres were implanted in circular resin blocks for proton-induced X-ray emission analysis. The large black dots are the only visible part of retaining clips that are embedded in the resin to prevent the fibres from floating in the initially non-solid resin. The other items seen in the figure are a circular retaining clip, also to prevent the fibres from floating. Barely visible along the left-hand edge of a centrally located linear silicon substrate are the ends of the fibres under investigation, appearing as small dots; the silicon substrate was required in order to provide a more rigid structure that would allow the face of the resin blocks to be ground into a flat surface without flexing of the fibres.

Table 1. Dimensions of nominal 6% and 8% weight Ge-doped SiO_2 fibres used in proton-induced X-ray emission analysis

Sample dimension	Fibre type	
	Cylindrical fibre (μm)	Flat fibre (μm)
1	604 ± 30	200 × 750 ± 20
2	483 ± 20	165 × 620 ± 20
3	362 ± 10	100 × 350 ± 20
4	241 ± 10	85 × 270 ± 5
5	120 ± 10	60 × 180 ± 5

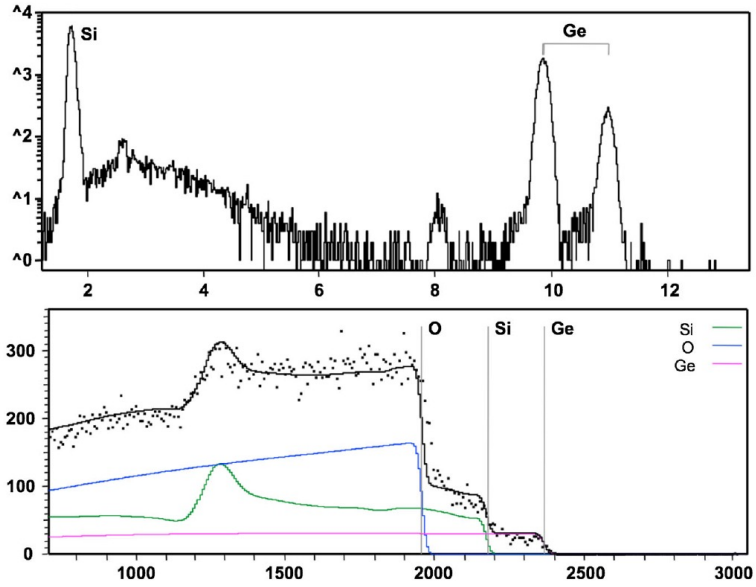

Figure 2. Proton-induced X-ray emission (top) and Rutherford Back Scattering spectra for a point in a high Ge concentration region of a doped quartz fibre (Si 42%, Ge 9.5%, O 42% w/w). In each graph, the vertical axis is counts per channel and the horizontal axis is X-ray energy or proton recoil energy, both in kiloelectron volt. In the Rutherford Back Scattering spectrum, the surface energies of O, Si and Ge are marked and the solid lines show the fit calculated by OMDAQ2007. (The coloured lines are the partial spectra for each element). The total run-time was 2.5 min using beam current of ~150 pA of 2.5 MeV protons corresponding to a beam dose of 22.5 nC.

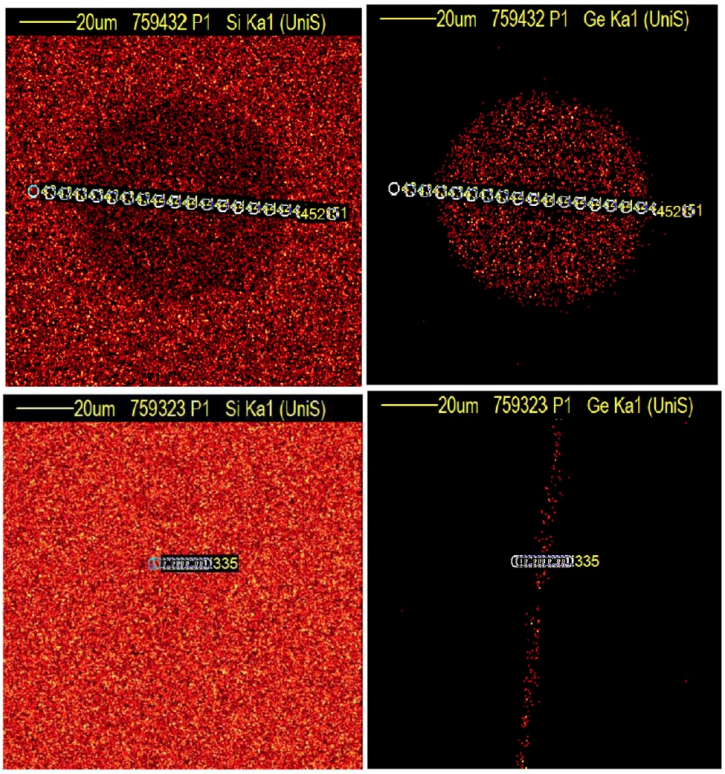

Figure 3. Typical elemental maps across the transverse cross section of a SiO_2 cylindrical fibre, 483 μm outer diameter (top) and flat fibre, 165 × 620 μm (bottom), showing the relative presence of the identified elements, Si and Ge, respectively. Also identified are the lines along which the point data were obtained.

Laboratory, Department of Electrical Engineering, University of Malaya. Unlike the more conventional case of a CF formed from a preform doped silica solid rod, the doped FF preform is a hollow silica tube with the internal faces containing the deposited dopant. In this work, to produce the FF, the preform is a commercially available uncollapsed silica tube co-doped with $SiCl_4$ and $GeCl_4$.[18] Application of a vacuum leads to quasi-complete collapse of the preform into a flattened shape, with additional TL yield resulting from the stresses produced at the inner contacting faces of the flattened fibre during the cooling process.

Sample preparation

The Ge-doped optical fibres have been cut into approximate 2.0 cm lengths using an optical fibre cleaver (Fujikura, Japan). Preparing for irradiation, the optical fibres, attached to a silicon substrate (see caption of Fig. 1), were embedded in a 25 mm diameter circular resin casting. The mould was filled with a liquid synthetic resin made of Durocit Liquid and Durocit Powder, which then harden to form what is referred to as a cold mounting resin (Struers, Denmark). Clips were used to hold the samples in the resin to prevent

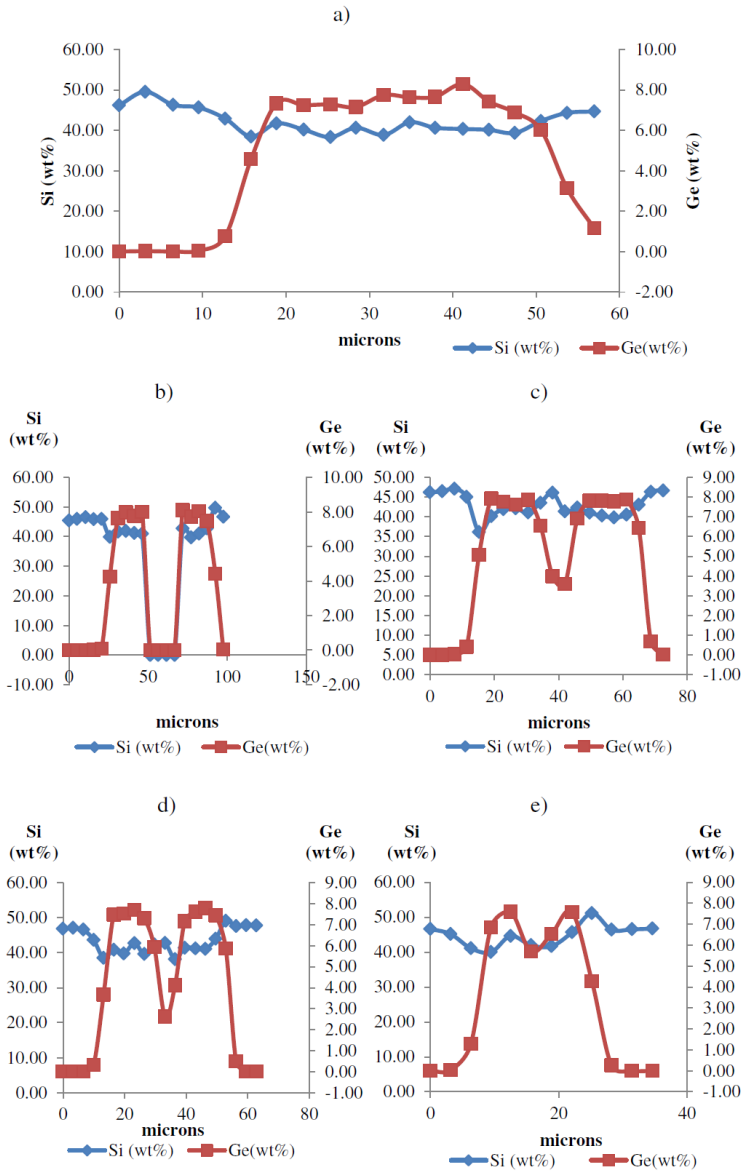

Figure 4. The distribution of Si and Ge along a line scan for nominal 6% weight Ge-doped cylindrical fibres of different dimension: (a) 604 μm, (b) 483 μm, (c) 362 μm, (d) 241 μm and (e) 120 μm. The data for the largest fibre, i.e. that represented in (a) is clearly for one-half of the core diameter, the full data showing symmetry between one-half and the other, as in (b)–(e).

them from floating in the initial resin solution. For the hardened resin, Struers Pedemax-2 and Struers Accutom-5 were used, respectively, to grind the resin blocks in order to present a flat cross section to the beam and to customise the blocks to the desired thickness (~15 mm). In order to minimise sample charging, conductive adhesive tape was fixed to the surface of each resin block, leaving a small window around the samples in the block. Three nominal 4% weight Ge-doped SiO_2 fibres of 125.0 ± 2.0 μm diameter were the first such fibres to be investigated by PIXE analysis; the dimensions of nominal 6% weight and 8% weight for both CFs and FFs are detailed in Table 1.

Microbeam setup

The University of Surrey provides the Engineering and Physical Sciences Research Council a national ion beam facility. The microbeam facility used herein is based on a 2 MV Tandetron™ accelerator, described in detail by Simon *et al.*[19] The samples were irradiated on the microbeam line to a beam of 2.5 MeV protons with the beam normal to the sample, being made of a spot size of 2 × 2 μm, and measured using a copper grid and a proton current of between 0.3–0.8 nA. The resin blocks were mounted inside the target chamber, which was designed to include a moving sample stage and can be used for simultaneous PIXE and RBS analysis. The characteristic X-ray photon emissions were detected using a SGX Si–Li detector (Sensortech Ltd, High Wycombe, UK) of 80 mm^2 active area and 140 eV energy resolution at 5.9 keV, mounted at a scattering angle of 45° to the beam. In order to reduce the intensity of the Si Kα X-rays and to avoid spectrum degradation by high energy recoiling protons, the Si–Li detector was fitted with a two-layer absorber consisting of 130 μm beryllium foil and 50 μm Kapton foil.

Scanning was carried out over the cross-sectional area of the optical fibres implanted in the resin block, producing a pixel-by-pixel map of the sample elemental composition. For each sample, elemental maps were collected for localisation, and then, a line of points was set up in order to obtain the required concentration profiles. This was performed in preference to a continuous line scan along the profile because this allows the local sample matrix composition to be determined at each point, permitting more accurate analysis. Although this is superficially a simple system (only three atoms, Si, O and Ge), PIXE spectrum processing is complicated by the fact that in the high concentration regions of the sample, the yield of the Ge K lines is strongly affected by self-absorption, and so, the Ge concentration must be determined independently or an iterative process must be used. Because the O is not visible in the PIXE spectra and it is not possible to iterate assuming atomic stoichiometry, RBS was used to provide an independent

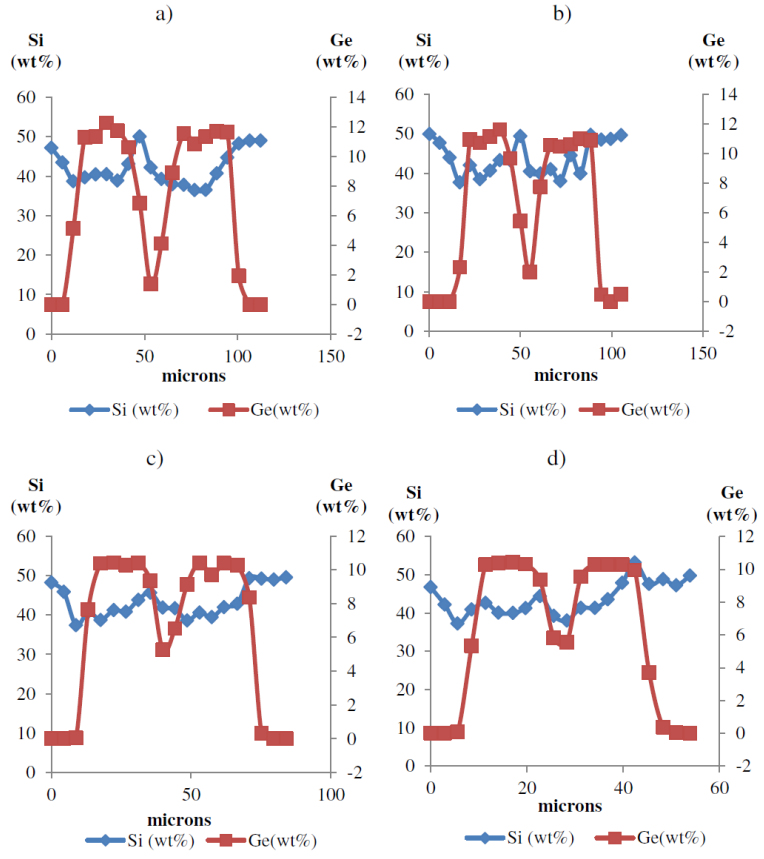

Figure 5. The distribution of Si and Ge along a line scan for nominal 8% weight Ge-doped cylindrical fibres: (a) 604 μm, (b) 483 μm, (c) 362 μm and (d) 241 μm.

measurement of Ge. Pairs of simultaneously collected RBS and PIXE spectra were processed using the 'Q factor' method[20] implemented in OMDAQ2007.[21] In this method, the actual beam charge and the local sample matrix (both of which are required for accurate thick target PIXE analysis) are calculated from the RBS spectrum and transferred automatically to the PIXE processing software within OMDAQ2007. The method requires a determination of the ratio of solid angles of the PIXE and RBS detector and also the parameters used in the model of the variation of the PIXE detector efficiency with X-ray energy. This is performed during each run as part of the setting-up process using a standard reference material (lead glass BCR 126A[22]) as described in the study of Gomez-Morilla *et al.*[23] RBS spectra were fitted using the simulation module of OMDAQ2007, which incorporates non-Rutherford cross sections. The PIXE spectra were processed using GUPIX (Guelph PIXE Group GUPIX and GUPIXWIN Department of Physics University of Guelph Guelph, Ontario, Canada N1G 2W1)[24] accessed via the automated OMDAQ2007 user interface. Figure 2 shows PIXE and RBS spectra for a high Ge concentration region.

OMDAQ2007 provides real-time spectrum quality monitoring, and so, each point was analysed until the statistical precision of the Ge Kα line area was better than 5% and the total number of counts in the RBS spectrum was greater than 50 000 or for a maximum of 10 min. With the beam currents available, this corresponds to an accumulated charge of up to 300 nC.

Results and discussion

Typical PIXE and RBS spectrum for a CF of 604 μm diameter, obtained with a 2.5 MeV proton beam, are shown in Fig. 2. Similar PIXE and RBS spectra were obtained for the other CFs and FFs investigated herein. Figure 3 represents the elemental maps of Si and Ge for both CF and FF. PIXE and RBS analysis also detected the presence of other elements, including P and Al, due in part to contamination of the fibre pulling facility. However, the concentration of these elements has been found to be relatively small (nowhere greater than ~0.5%) and as such can be considered to have little effect upon the TL yield of these fibres.

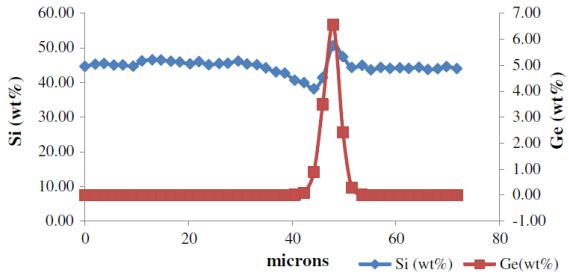

Figure 6. Typical plot of distribution of Si and Ge along a line scan for a nominal 6% weight Ge-doped flat fibre, 200 × 750 μm (flat fibre sample 1). Similar patterns were obtained for other flat fibre outer diameters.

The Ge distribution in the fibres, centrally located as designed, diffuses away from the centre into the fibre cladding, extending out to Ge concentrations measurable to well below 0.1 mol%, strongly dominated by Si in all cases. In the centre of the fibre, a pronounced dip in the Ge concentration is observed, mirroring what is seen in the refractive index profile, again attributed to Ge diffusion, in line with Ge chemistry temperature dependency.[25] Further, in many cases, there are one and sometimes two peaks in Si concentration, almost certainly because of $SiCl_4$ vapour deposition and its variations, typically with co-location discrepancies with the Ge dip of the order of 2 to 5 μm, as seen in Figs. 4–6. These illustrate some of the points discussed earlier. Also, as previously mentioned, there are challenges in terms of the increasingly brittle nature of the glass with increasing dopant concentration, the predominant effect being illustrated in Fig. 7. Here, we note that drawing of optical fibres of greater Ge concentration requires elevated drawing temperatures (by some 10–20 °C) compared with similar fibres of lower dopant concentration. This is perhaps best illustrated in efforts towards fabricating 8% weight Ge FF, incomplete closure of the inner bore to the glass fibre resulting, as shown in Fig. 7(a). Using the same drawing conditions for 6% weight Ge-doped FF (Fig. 7(b)) leads to a fully closed situation. We have therefore only used 6% weight Ge FFs in investigations herein. The dips may also be due in part to the evaporation of GeO_2, occurring because of the relatively low vapour pressure of GeO_2 compared with that of SiO_2.[16]

The results of PIXE/RBS analysis of Ge concentrations in SiO_2 fibres nominally doped to 4%, 6% and 8% weight are presented in Table 2, it being noted by Lyytikainen *et al.*[25] that dopant distribution in the fibres is affected by temperature during manufacture of fused fibre couplers and by fibre drawing. It is also apparent from Table 2 that the shape of fibre has strongly influenced the variation in Ge concentration in the fibres, specifically in the FF.

With the core region in the FFs being highly central and thinly distributed along the width of the fibre, results are clearly expected to show only a very narrow Ge-rich core thickness in the collapsed region. As such, with a scanning resolution of ~2 μm, very few scanned points are obtained in the centre of the FF, as seen in Fig. 6.

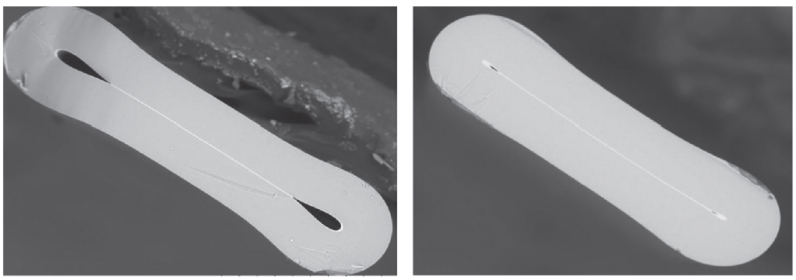

Figure 7. Flat fibre (FF) cross section images that are fabricated with the same drawing parameters (a) 8% weight Ge-doped FF, which two remaining holes and (b) 6% weight Ge-doped FF, which is fully is closed.

Table 2. Summary proton-induced X-ray emission analysis for fibres of nominal Ge concentrations 4%, 6% and 8% weight

	Ge dopant concentration (wt%)		Ge dopant concentration (wt%)		
	4%		6%		8%
Sample no.	CF	Sample dimension	FF*	CF	CF
1	0.87–1.25	1	2.43–6.55	6.01–8.29	10.61–12.25
		2	0.95–1.14	7.47–8.10	10.48–11.62
2	2.45–4.56	3	0.15–0.17	6.44–7.92	10.27–10.43
		4	0.07–0.10	7.31–7.79	10.38–10.42
3	3.10–4.26	5	0.07–0.12	6.53–7.59	—

* Note: As discussed in the text, the flat fibres results are manifestly compromised by the 2 μm spatial resolution. Further investigation of these will be required, use being made of the nanometre resolution beam line at the Surrey ion beam centre.
CF, cylindrical fibre; FF, flat fibres.

Thus, because of the limited spatial resolution, the peak Ge concentration may not have been obtained. Applying a curve fitting interpolation based on the three points that are central to the Ge distribution curve would suggest the Ge in the central core to be slightly higher than the evaluated value of 6.55 shown in Table 2. The same problem would also be expected to prevail for the Ge core thickness of the other FF samples, becoming increasingly acute with decrease in FF dimensions, the extreme of which would be that of FF sample 5 in Table 2, with a Ge core of less than 500 nm (0.5 μm).

Linearity between dose and TL response has been observed, the TL response of Ge-doped fibres of the greatest diameter producing superior response to that for smaller dimension fibres. It is clear that non-uniformities in the distribution of added dopants will have direct effect on the TL yield. Variation in TL yield obtained from each batch of Ge-doped SiO_2 fibre is almost certainly explained by point-to-point variation in doping concentration along the length of an optical fibre, as shown in Fig. 8. This is reflected in present PIXE analysis results, as seen in Fig. 9 for similar fibres (nominal 4% weight) with a much greater measured peak Ge concentration of 4.56% weight in one case compared with the other fibre with a measured peak Ge concentration of 1.25% weight

Results from these investigations can be compared against that of previous research for doped silica glass. Using the sol–gel route, a notably difficult process to control, Yusoff *et al.*[2] have reported the highest TL yield to be obtained from Ge-doped fibres at 0.25 mol%, investigating dopant concentrations from 0.01 up to 33 mol%. Hashim *et al.*[8] have found that the Ge concentration range in commercial Ge-doped fibres is 0.53–0.71 mol%. While the application of the MCVD method, as used herein, can be used to provide for different dopant concentration fibres, which may improve upon the sensitivity of existing TL systems, the TL performance can only be more fully specified by knowledge of the dopant distribution, measured in absolute terms, as herein.

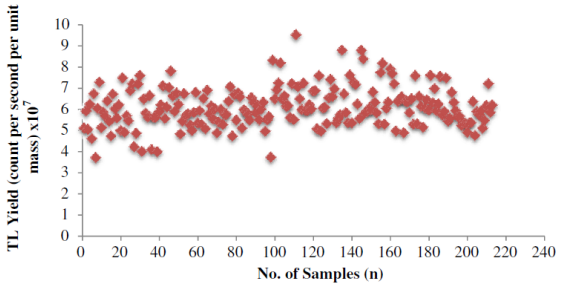

Figure 8. Response from two hundred eleven 6% weight Ge-doped cylindrical fibres of 604 μm diameter, irradiated to a fixed dose of 3 Gy using a Gulmay X-ray machine (Gulmay, UK) operated at a potential of 250 kVp. Prior to irradiation, the fibres were cut to lengths of approximately 5.0 ± 0.1 mm; variations in response arising from variation in dopant concentration along the length of a fibre are expected to be the largest influencing factor. The irradiations were conducted at the Royal Surrey County Hospital. The fibres were then readout 12 h after irradiation using a TOLEDO TLD reader (Pitman Instruments, Weybridge, UK).

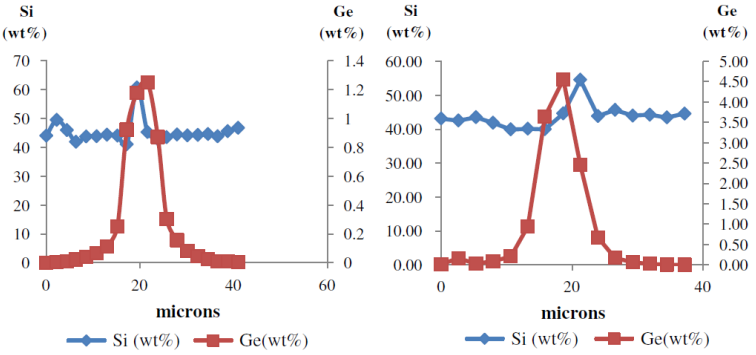

Figure 9. Line scan Si and Ge concentrations for nominal 4% weight Ge-doped cylindrical fibre of similar dimension (125 μm).

Conclusion

Present studies have been aimed at determining the absolute concentration profile of the Ge dopant in tailor-made silica fibre TL dosimeters. The PIXE/RBS method provides for such analysis, as demonstrated. This is important, with optimisation of optical fibre design relying heavily on the fabrication technique used and on accurate characterisation of the dopant profile. GeO_2, commonly used for doping the core region to alter the refractive index, produces significant TL yield in addition to enhancing light transmission along the length of the fibre. The fibre production process is typically seen to result in wide variation in dopant concentration and distribution, critical parameters in controlling the behaviour of the dosimeter. However, it does need to be commented that with regard to the FF samples, the high variation observed in doping concentration was due to the very thin Ge-rich core, being less than the dimensions scanning beam. Findings from present studies are expected to pave the way for more comprehensive investigations of TL from tailor-made doped SiO_2 fibres.

Acknowledgements

We would like to thank the scientific and technical staff of the Surrey Ion Beam Centre for their help in carrying out elemental analysis and proton irradiations. We would also like to acknowledge the TM RnD/MMU lab, sited at the Multimedia University, for fabricating the fibre preforms. The authors are grateful to the University of Malaya – Ministry of Higher Education of Malaysia UM-MOHE High Impact Research Grant UM.C/625/1/HIR/33. The fibres used herein were all fabricated using the University of Malaya Fibre Drawing System, supported by the University of Malaya – Ministry of Higher Education of Malaysia UM-MOHE High Impact Research Grant A000007-50001.

References

[1] D. A. Bradley, R. P. Hugtenburg, A. Nisbet, A. T. Abdul Rahman, F. Issa, N. Mohd Noor, A. Alalawi. Review of doped silica glass optical fibre: their TL properties and potential applications in radiation therapy dosimetry. *Appl. Radiat. Isot.* **2012**, *71*, 2–11.
[2] A. L. Yusoff, R. P. Hugtenburg, D. A. Bradley. Review of development of a silica-based thermoluminescence dosimeter. *Radiat. Phys. Chem.* **2005**, *74*(6), 459–481.
[3] Y. A. Abdulla, Y. M. Amin, D. A. Bradley, The thermoluminescence response of Ge-doped optical fibre subjected to photon irradiation, *Radiat. Phys. Chem.* **2001**, *61*, 409–410 ST – The thermoluminescence response of G.
[4] A. T. Abdul Rahman, A. Nisbet, D. A. Bradley. Dose-rate and the reciprocity law: TL response of Ge-doped SiO2 optical fibers at therapeutic radiation doses. *Nucl. Instrum. Meth. Phys. Res. Sect. A Accel. Spectrometers, Detect. Assoc. Equip.* **2011**, *652*(1), 891–895.
[5] N. M. Noor, M. Hussein, D. A. Bradley, A. Nisbet. The potential of Ge-doped optical fibre TL dosimetry for 3D verification of high energy IMRT photon beams. *Nucl. Instrum. Meth. Phys. Res. Sect. A Accel. Spectrometers, Detect. Assoc. Equip.* **2010**, *619*(1–3), 157–162.
[6] N. M. Noor, M. Hussein, D. A. Bradley, A. Nisbet. Investigation of the use of Ge-doped optical fibre for in vitro IMRT prostate dosimetry. *Nucl. Instrum. Meth. Phys. Res. Sect. A Accel. Spectrometers, Detect. Assoc. Equip.* **2011**, *652*(1), 819–823.
[7] F. Issa, N. A. A. Latip, D. A. Bradley, A. Nisbet. Ge-doped optical fibres as thermoluminescence dosimeters for kilovoltage X-ray therapy irradiations. *Nucl. Instrum. Meth. Phys. Res. Sect. A Accel. Spectrometers, Detect. Assoc. Equip.* **2011**, *652*(1), 834–837.
[8] S. Hashim, S. Al-Ahbabi, D. A. Bradley, M. Webb, C. Jeynes, A. T. Ramli, H. Wagiran. The thermoluminescence response of doped SiO2 optical fibres subjected to photon and electron irradiations. *Appl. Radiat. Isot.* **2009**, *67*(3), 423–427.
[9] S. Hashim, A. T. Ramli, D. A. Bradley, H. Wagiran, The thermoluminesce response of Ge-doped optical fibre subjected to proton irradiation in 5th National Seminar on Medical Physics. Malaysia. Medical Physics Association, Kuala Lumpur, **2006**.
[10] A. T. Ramli, D. A. Bradley, S. Hashim, H. Wagiran. The thermoluminescence response of doped SiO2 optical fibres subjected to alpha-particle irradiation. *Appl. Radiat. Isot.* **2009**, *67*(3), 428–432.
[11] S. Hashim, D. A. Bradley, M. I. Saripan, A. T. Ramli, H. Wagiran. The thermoluminescence response of doped SiO2 optical fibres subjected to fast neutrons. *Appl. Radiat. Isot.* **2010**, *68*(4–5), 700–703.
[12] A. T. Abdul Rahman, D. A. Bradley, S. J. Doran, B. Thierry, E. Bräuer-Krisch, A. Bravin. The thermoluminescence response of Ge-doped silica fibres for synchrotron microbeam radiation therapy dosimetry. *Nucl. Instrum. Meth. Phys. Res. Sect. A Accel. Spectrometers, Detect. Assoc. Equip.* **2010**, *619*(1–3), 167–170.
[13] A. C. Pugh, R. P. Stratton, D. B. Lewis. Investigation of elemental diffusion during the drawing and heat treatment of glass optical fibres. *J. Mater. Sci.* **1994**, *29*, 1036–1040.
[14] E. J. Friebele, G. H. Sigel, D. L. Griscom. Drawing-induced defect centers in a fused silica core fiber. *Appl. Phys. Lett.* **1976**, *28*(9), 516.
[15] Y. Hibino, H. Hanafusa. Consolidation atmosphere influence on drawing induced defects in pure silica optical fibres. *J. Lightwave Technol.* **1988**, *6*(2), 172–178.
[16] S. A. E. Johansson, J. L. Campbell, K. G. Malmqvist, *Particle-induced X-Ray Emission Spectrometry (PIXE)*, John Wiley & Sons, New York, **1995**.
[17] M. L. Zulkifli, S. M. Aljamimi, A. Yusoff, Y. M. Amin, S. Shafiqah, A. P. Technologies, D. Cyberjaya. Effect of $GeCl_4/SiCl_4$ flow ratio on Germanium Incorporation in MCVD process Si02 $Si0_2$. **2013**, *4*, 284–287.
[18] K. D. Dambul, G. A. Madhiraji, F. Amirkhan, M. C. Desmond, K. W. G. Gabriel, W. R. Wong, M. R. A. Hassan, S. Ismail, S. A. Ibrahimi, N. Tamc0068ek, F. R. M. Adikan, Fabrication and development of flat fibers, **2012**, 3–5.
[19] A. Simon, C. Jeynes, R. P. Webb, R. Finnis, Z. Tabatabaian, P. J. Sellin, M. B. H. Breese, D. F. Fellows, R. van den Broek, R. M. Gwilliam. The new Surrey ion beam analysis facility. *Nucl. Instrum. Meth. Phys. Res. Sect. B Beam Interact. Mater. Atoms* **2004**, *219–220*, 405–409.
[20] G. W. Grime. The 'Q factor' method: quantitative microPIXE analysis using RBS normalisation. *Nucl. Instrum. Meth. Phys. Res. Sect. B Beam Interact. Mater. At.* **1996**, *109–110*, 170–174.
[21] Oxford Microbeams Ltd. Available from http://www.microbeams.co.uk/download.html (accessed 19 November 2014)
[22] European Commission, Joint Research Centre, Institute for Reference Materials and Measurements (IRMM), Geel, Belgium.
[23] I. Gomez-Morilla, A. Simon, R. Simon, C. T. Williams, Á. Z. Kiss, G. W. Grime. An evaluation of the accuracy and precision of X-ray microanalysis techniques using BCR-126A glass reference material. *Nucl. Instrum. Meth. Phys. Res. Sect. B: Beam Interact. Mater. At.* **2006**, *249*, 897–902.
[24] J. L. Campbell, N. I. Boyd, N. Grassi, P. Bonnick, J. A. Maxwell. The Guelph PIXE software package IV. *Nucl. Instrum. Meth. B* **2010**, *268*, 3356–3363.
[25] K. Lyytikainen, S. Huntington, A. Carter, P. McNamara, S. Fleming, J. Abramczyk, I. Kaplin, G. Schötz. Dopant diffusion during optical fibre drawing. *Opt. Express* **2004**, *12*(6), 972–977.

Appendix C

Radiation Physics and Chemistry 104 (2014) 134–138

Contents lists available at ScienceDirect

Radiation Physics and Chemistry

journal homepage: www.elsevier.com/locate/radphyschem

High sensitivity flat SiO_2 fibres for medical dosimetry

Siti.F. Abdul Sani [a,*], Amani I. Alalawi [a,b], Hairul Azhar A.R [c], Ghafour Amouzad Mahdiraji [d], Nizam Tamchek [e], A. Nisbet [a,f], M.J. Maah [g], D.A. Bradley [a,h]

[a] Centre for Nuclear and Radiation Physics, Department of Physics, University of Surrey, Guildford, Surrey GU2 7XH, UK
[b] Physics Department, Faculty of Applied Sciences, Umm AL-Qura University, Makkah, P.O. Box 175, Saudi Arabia
[c] Faculty of Engineering, Multimedia University, 2010 Cyberjaya, Selangor, Malaysia
[d] Photonics Research Group, Faculty of Engineering, University of Malaya, 50603 Kuala Lumpur, Malaysia
[e] Department of Physics, Faculty of Science, Universiti Putra Malaysia, 43400 Serdang, Selangor, Malaysia
[f] Department of Medical Physics, The Royal Surrey County Hospital NHS Trust, Guildford, GU2 7XX Surrey, UK
[g] Department of Chemistry, University of Malaya, 50603 Kuala Lumpur, Malaysia
[h] Department of Physics, University of Malaya, 50603 Kuala Lumpur, Malaysia

HIGHLIGHTS

- Studies of a novel undoped flat fibre fabricated for medical dosimetry.
- Investigation of the TL response of the undoped flat fibres, TLD-100 chips and Ge-doped fibres in megavoltage potentials.
- The sensitivity of the flat fibres is found to be markedly higher than that of Ge-doped fibre, being comparable to the TLD-100.

ARTICLE INFO

Article history:
Received 19 June 2013
Accepted 30 March 2014
Available online 5 April 2014

Keywords:
Thermoluminesence
Dosimetry
Flat fibre
Ge-doped optical fibre

ABSTRACT

We describe investigation of a novel undoped flat fibre fabricated for medical radiation dosimetry. Using high energy X-ray beams generated at a potential of 6 MV, comparison has been made of the TL yield of silica flat fibres, TLD-100 chips and Ge-doped silica fibres. The flat fibres provide competitive TL yield to that of TLD-100 chips, being some 100 times that of the Ge-doped fibres. Pt-coated flat fibres have then been used to increase photoelectron production and hence local dose deposition, obtaining significant increase in dose sensitivity over that of undoped flat fibres. Using 250 kVp X-ray beams, the TL yield reveals a progressive linear increase in dose for Pt thicknesses from 20 nm up to 80 nm. The dose enhancement factor (DEF) of $(0.0150 \pm 0.0003)\,nm^{-1}$ Pt is comparable to that obtained using gold, agreeing at the 1% level with the value expected on the basis of photoelectron generation. Finally, X-ray photoelectron spectroscopy (XPS) has been employed to characterize the surface oxidation state of the fibre medium. The charge state of Si2p was found to lie on 103.86 eV of binding energy and the atomic percentage obtained from the XPS analysis is 22.41%.

1. Introduction

Dosimetry is fundamental to many applications of radiations, with numerous investigations made of a wide range of dosimeter forms, including radiation-induced attenuation in optical fibres (Huston et al., 2001), radioluminescence (RL) and optically stimulated luminescence (OSL) (Justus et al., 1997; Aznar et al., 2004; Benevides et al., 2007). Thermoluminescence dosimetry (TLD) is well-established, often considered to be the most widely used and cost-effective approach to radiation dosimetry, not least in regard to radiation therapy (Hashim et al., 2006).

While phosphor TLD media such as LiF have been widely exploited in medical dosimetry, these have several acknowledged defects, including potential hygroscopic issues and relatively poor (~mm) spatial resolution (Izewska and Rajan 2005). In recent years, a number of investigations have concerned the TL properties of doped silica (SiO_2) optical fibres, overcoming the particular limitations of existing TLD systems (Hashim et al., 2009), pointing to intercavitary and interstitial measurement applications and high sensitivity over a wide range of dose rates and absorbed doses (Yusoff et al., 2005). The TL response of commercial doped SiO_2 optical fibres has been investigated for photons (Abdulla et al., 2001;

* Corresponding author.
E-mail address: s.abdulsani@surrey.ac.uk (Siti.F. Abdul Sani).

http://dx.doi.org/10.1016/j.radphyschem.2014.03.043
0969-806X/

Abdul Rahman et al., 2010b; Issa et al., 2011; Noor et al., 2010, 2011); electrons (Hashim et al., 2009; Abdul Rahman et al., 2010b); protons (Hashim et al., 2006); alpha particles (Ramli et al., 2009); neutrons (Hashim et al., 2010) and synchrotron radiation (Abdul Rahman et al., 2010a). The TL yield is dictated by the concentrations and types of intrinsic or extrinsic defects within the medium. In practice, variations in these are reflected in the sensitivity of the dosimeter (Chen and McKeever 1992; Youssef, 2003), a situation resolved by selection through sensitivity screening should the intention be to use the dosimeter in practice. Present studies represent the X-ray response of undoped flat fibres and commercial Ge-doped SiO_2 fibres, compared against the standard photon TL material, TLD-100, all unscreened.

Noting that Pt-based cisplatin drugs have immunochemo- and radio-therapeutic effects of use in improving loco-regional and systemic tumour control (Abundes-Velasco et al. 2007; Bhide et al., 2012; Guida et al., 2008), we further explore the potential of flat fibres for investigation of the high-Z photoelectron-generated local dose enhancement. In this we use nm-thick Pt-coatings to the silica fibre dosimeters. As an aside, the untoward effect observed in clinical use of X-rays of enhanced dose local to Pt implants (Cheung and Tang, 2007) is something that our fibres would also be able to measure.

Finally, we are seeking to explore the defects-basis of the SiO_2 TL underpinning our work. In this, we investigate the elemental, chemical and electronic state of the silica using X-ray photoelectron spectroscopy (XPS). This non-destructive surface-sensitive quantitative spectroscopic technique is based on the lossless emission of photoelectrons from the sample surface, the escape depth varying from 0.1 nm to 1 nm depending on the kinetic energy of the photoelectron. As such, the surfaces under study must be studied under stringently clean conditions.

2. Materials and methods

2.1. Samples and their preparation

We compare single-mode doped SiO_2 telecommunication fibres, undoped SiO_2 flat fibres and TLD-100 chips. For the first, use was made of INOCORP (Canada) fibres comprising a 9.0 μm Ge-doped core in a SiO_2 cladding of diameter (124.7 ± 1.0) μm plus a polymer coat of diameter (250 ± 10) μm. Following polymer removal the doped fibres have been cut into approximate 0.5 cm lengths. The undoped flat fibres have been fabricated using a 5 m fibre drawing tower located in the Department of Electrical Engineering, University of Malaya (Dambul et al., 2012). The flat fibres have been fabricated using a high grade amorphous SiO_2 tube (Suprasil F300), outer and inner dimensions 25 mm and 19 mm. As the SiO_2 tube preform is pulled down into capillary form (Fig. 1(left)) of around 1–2 mm diameter, vacuum pressure is applied to collapse the capillary into the flat form (Fig. 1(middle) and Fig. 2). The dimensions of the flat fibres, obtained by digital calipers (DURATOOL), are detailed in Table 1. The TLD-100 (LiF:Mg, Ti), comprises 99.99% ^{7}Li, in the form of a disc of diameter 8.81 mm and 0.35 mm thickness. To avoid surface abrasion and

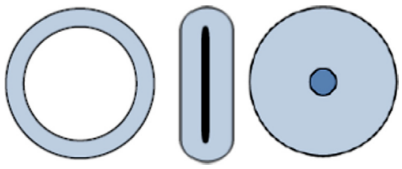

Fig. 1. From left to right are not-to-scale schematic representations of capillary fibre, flattened capillary fibre (flat fibre) and the common form of doped single mode telecommunication fibre (from Alawiah et al., 2013).

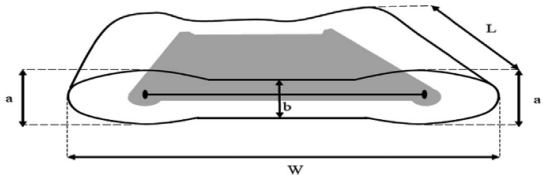

Fig. 2. Expanded schematic of pure silica flat optical fibre (from Alawiah et al., 2013).

Table 1
Mean dimensions of eleven undoped silica flat fibres (FF) (see Fig. 2).

Dimension	(*mm*)
a	1.13
b	1.00
W	3.72
L	10.00
Weight (g)	0.085

contamination, vacuum tweezers (Dymax 5, Surrey, UK) have been used to handle the TL materials. To minimize light exposure, all three types of dosimeter were kept in darkened conditions before and subsequent to irradiation, until readout.

2.2. Annealing

Before making irradiations, the samples (all unscreened) were first annealed in a furnace (Carbolite, UK). This was carried out to provide for a stable situation, for both background and TL signal, the annealing allowing elimination of previous irradiation history, standardizing the thermal history as well as sensitivity, also erasing the unstable low-temperature glow peaks. For annealing, the samples were retained in an alumina ceramic boat and covered with Al foil, annealing being performed at 400 °C for a period of 1 h. Subsequently, to minimize thermal stress, the samples were left in the oven for 18 h to finally equilibrate at room temperature.

2.3. Flat fibres coating

The undoped flat fibres were arranged to be Pt-coated on one side only (to allow read out using the uncoated side), use being made of a sputter coating unit (Emitech K575X) located at the Surrey Materials Institute. The fibres were coated with 20 nm, 40 nm, 60 nm and 80 nm of Pt. The sputter current was set to 70 mA and the 20 nm terminate value was selected. Upon each cycle completion, one of the fibres was taken out of the sputterer and the rest would be coated for another 20 nm. The procedure was repeated until all four thicknesses of coated fibres were obtained. Pressure sensitive adhesive (Blu-Tack) was used to secure the fibres on the specimen stage (glass slide).

2.4. Sample irradiation

For comparative sensitivity the samples were irradiated at the Royal Surrey County Hospital (RSCH), use being made of a Clinac™ 2100C linear accelerator (LINAC). The TL media was exposed to 6 MV X-rays to give a dose of 3 Gy. The source to sample surface distance (SSD) was set at 100 cm, with a field size of 20 cm × 20 cm. Subsequent to Pt coating the flat fibres were irradiated to tube X-rays produced at an accelerating potential of 250 kVp, again to a dose of 3 Gy. In all cases, the fibres were placed at the centre of the field, with the coated side facing towards the

X-ray tube, aligned with the applicator of the X-ray unit with a 3 cm stand off distance from the phantom to the applicator.

2.5. Readout

After irradiation, the samples were read out using a Toledo TLD reader (Vinten, Sandy, UK), with a N_2 gas atmosphere set at 0.5 bar to inhibit the effects of chemi- and triboluminescence. During readout, the following time-temperature cycle was used: a preheat temperature of 120 °C for 28 s; readout temperature of 300 °C for 25 s; a heating cycle rate of 38 °C/s. Lastly, an internal annealing temperature of 300 °C was used for 28 s to provide initial erasing of any residual signal. The arrangement provided for an optimal glow curve.

2.6. X-ray photoelectron spectroscopy (XPS)

This was carried out using an XPS Thermo Scientific Theta Probe located at the Structure Analysis Laboratory and Micro Structural Studies Unit of the University of Surrey. The sample analysis was performed in an ultra-high vacuum (UHV), the electron flux being evaluated with minimum error at each value of kinetic energy. The arrangement also minimises re-contamination of the freshly cleaved sample, noting that in XPS instruments the electron counting detectors are typically 1 m distant from the sample. With a high voltage potential applied between the filament and anode to accelerate electrons towards the target, electron bombardment of the target produces core vacancies, causing photoelectrons and emission of fluorescence X-rays. The photoelectrons enter an energy analyzer coupled to an electron detector. The facility is typically operated at an anode voltage of 15 kV and a current of 20 mA to produce sufficiently intense photoelectron peaks. Prior to use, the sample holder, sample stub (ESCALAB) and fibres were cleaned using an ultrasonic bath, repeated using three different solvents; methanol, ethanol and propanol. To ensure minimal charge collection the stub was coated with ~50 nm gold.

3. Results and discussion

Using the 6 MV photon beam, eleven of each of the TLD-100 chips, Ge-doped fibres and flat fibres were simultaneously irradiated to obtain their comparative TL yield (Fig. 3). Interest focuses on the previously unexplored sensitivity of the flat fibres. Fig. 3 shows the much greater TL response of the flat fibres compared to the Ge-doped fibres, of the order of 100 times that produced by the Ge-doped fibres, being also similar to that from TLD-100. This is due in good part to the differential mass of the two dosimeter types, the Ge-doped fibre mass being approximately 1000 times less than that of the flat fibre, and also due to the undoped nature of the flat fibres. In undoped optical fibres, the defect centres are mainly induced during the fibre pulling process (Friebele et al., 1976; Hibino and Hanafusa, 1988). Thus said, it is expected that pulling parameters such as vacuum pressure, pulling speed, high pulling temperature of above 2000 °C and fast cooling/quenching rate in room temperature play an important role in the TL response, influencing the species and population of defects and characteristics of optical fibre. The deformation of the circular shape into a flat shape produces stresses on the circumference of the neck-down region of the preform that generate additional structural defects. The shear stress applied to viscous state induces non-bridging oxygen hole centres (NBOHCs) and breakage of the strained Si–O bonds in the continuous random silica network defining the amorphous silica (Hibino and Hanafusa, 1988). The findings are supported by theoretical predictions (Roushdey, 2011).

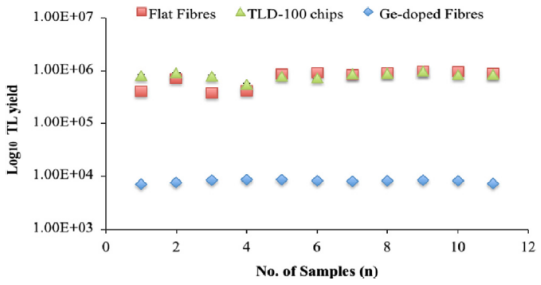

Fig. 3. Logarithmic plot of the TL yield distribution for flat fibres, TLD-100 chips and Ge-doped fibres subjected to 6 MV photon irradiation. (*Note*: the error bars are smaller than the data points).

The sensitivity of undoped flat fibres is increased through application of high atomic number coating to enhance photoelectron production. In this case, Pt ($Z=78$) was used as a coating material. The dose enhancement factor (DEF) is described as the ratio of dose deposited in the Pt-coated fibre to the dose deposited in the uncoated fibre. The results in Fig. 4 show a linear increase in dose enhancement factor (DEF) from 20 nm up to 80 nm. At 80 nm the DEF attains its highest value of 1.20 ± 0.03, leading to a summary DEF of $(0.0150 \pm 0.0003)\ nm^{-1}$. The result is comparable to the previous study of Alalawi et al. (2013) using gold, which showed a DEF of $(0.0160 \pm 0.0001)\ nm^{-1}$. The difference of 6% between the DEF of Au and Pt coatings is in line with the photoelectric effect probability difference of 5%.

In XPS, atomic concentrations (with a lower limit of approximately 0.1 at%) can be quantified. Fig. 5 shows the presence of a number of elements on the sample surface, the different peaks corresponding to electrons photoejected from the different core levels of the material. A higher resolution scan is observed in Fig. 6, showing the Si2p core level peak. In essence, the peak positions reflect binding energies, providing information about the chemical state for a material. The peak binding energy of Si2p is at 103.86 eV. The atomic concentration of the Si2p state obtained from he XPS analysis is found to be 22.41%.

4. Conclusion

In present study, the sensitivity of the undoped flat fibre has been found to be markedly higher (by a factor of 100) than that of Ge-doped fibre, being comparable to that of TLD-100. The study results are suggestive of defects generation occurring as a result of the collapsing technique in producing the flat fibres, providing a TL response from the optical fibres that can improve upon existing TL system sensitivities. Following on from this, investigation has been

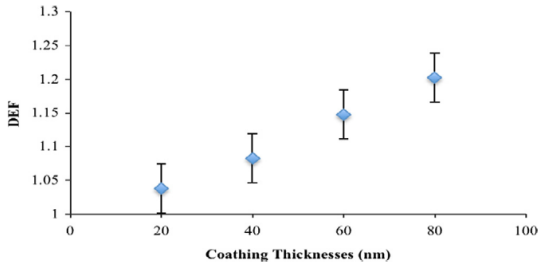

Fig. 4. Dose enhancement factor (DEF) for different thicknesses of platinum coating.

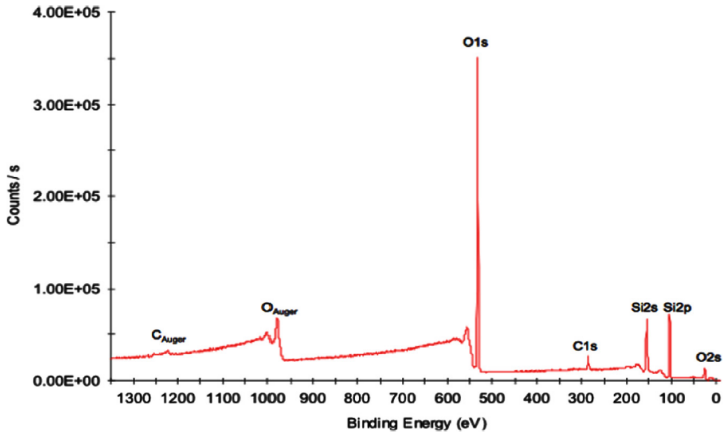

Fig. 5. XPS survey spectrum of an undoped flat fibre, analysed over the cross-section of the fibre using a 400 μm focal spot.

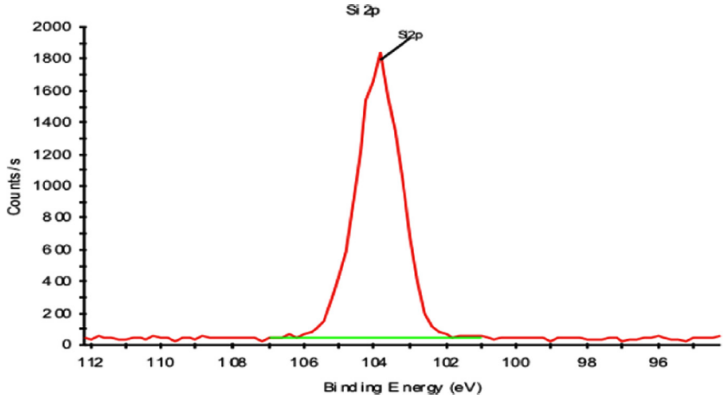

Fig. 6. High resolution scan of Si2p core level peak.

made of the effect of different thicknesses of platinum coating on the thermoluminescence response of the tailor-made undoped SiO_2 flat fibres. The results show a dose enhancement factor of $(0.0150 \pm 0.0003)\,nm^{-1}$, which is comparable to that obtained using gold-coated fibres, the latter validated by Monte Carlo simulations. Information of the identification of elements near the surface and oxidation states of transition metals has been investigated using the XPS method. The charge state of Si2p was found to be associated with a binding energy of103.86 eV, the atomic percentage of the Si2p state being 22.41%.

Acknowledgement

Receipt of a University of Malaya-Ministry of Higher Education UM-MOHE High Impact Research Grant UM.C/625/1/HIR/33.is acknowledged. The authors are grateful for help from staff at the Royal Surrey County Hospital, the Department of Physics and the Structure Analysis Lab of the University of Surrey. SFAS acknowledges receipt of a Majlis Amanah Rakyat (Malaysia) research studentship. We further acknowledge permission from SPIE for reproduction of Figs. 1 and 2 from the 2013 paper of Alawiah et al., 'Thermoluminescence characteristics of flat optical fibre in radiation dosimetry under different electron irradiation condition', Proc. of SPIE. Vol. 8775, 87750S.

References

Abdul Rahman, A.T., Bradley, D.A., Doran, S.J., Thierry, B., Bräuer-Krisch, E., Bravin, A., 2010a. The thermoluminescence response of Ge-doped silica fibres for synchrotron microbeam radiation therapy dosimetry. Nucl. Instrum. Methods Phys. Res., Sect. A 619, 167–170.

Abdul Rahman, A.T., Nisbet, A., Bradley, D.A., 2010b. Dose-rate and the reciprocity law: TL response of Ge-doped SiO_2 optical fibers at therapeutic radiation doses. Nucl. Instrum. Methods Phys. Res., Sect. A 652 (1), 891–895.

Abdulla, Y.A., Amin, Y.M., Bradley, D.A., 2001. The thermoluminescence response of Ge-doped optical fibre subjected to photon irradiation. Radiat. Phys. Chem. 61, 409–410.

Abundes-Velasco, A., Zabal-Cerdeira, C., García-Montes, J.A., De los Ríos-Ibarra, M.O., Gallegos, J.E., Peña, G.Q., 2007. Treatment of seven patients with coarctation of the aorta treated using a Mexican-made platinum/iridium stent. Arch. Med. Res. 38 (8), 853–857.

Alalawi, A.I., Hugtenburg, R.P., Abdul Rahman, A.T., Barry, M.A., Nisbet, A., Alzimami, K.S., Bradley, D.A. 2013, Measurement of Dose Enhancement Close to High Atomic Number Media using Optical Fibre Thermoluminescence Dosimeters. http://dx.doi.org/10.1016/j.radphyschem.2013.05.017.

Alawiah, A., Intan, A.M., Bauk, S., Abdul Rashid, A., Yusoff, Z., Mokhtar, M.R., Wan Abdullah, W.S., Mat Sharif, K.A., Mahdiraji, G.A., Mahamd Adikan, F.R., Tamchek, N., Noor, N.M., Bradley, D.A., 2013. Thermoluminescence characteristics of flat optical fibre in radiation dosimetry under different electron irradiation conditions. Proc. SPIE 8775, 87750S.

Aznar, M.C., Andersen, C.E., Botter-Jensen, L., Back, S.A.J., Mattsson, S., Kjaer Kristoffersen, F., Medin, J., 2004. Real-time optical-fibre luminescence dosimetry for radiotherapy: physical characteristics and applications in photon beams. Phys. Med. Biol. 49, 1655–1669.

Benevides, L.A., Huston, A.L., Justus, B.L., Falkenstein, P., Brateman, L.F., Hintenlang, D.E., 2007. Characterization of a fiber-optic-coupled radioluminescent detector for application in the mammography energy range. Med. Phys. 34, 2220–2227.

Bhide, S.A., Gulliford, S., Schick, U., Miah, A., Zaidi, S., Newbold, K., Nutting, C.M., Harrington, K.J., 2012. Dose–response analysis of acute oral mucositis and pharyngeal dysphagia in patients receiving induction chemotherapy followed by concomitant chemo-IMRT for head and neck cancer. Radiother. Oncol. 103 (1), 88–91.

Chen, R., McKeever, S.W.S., 1992. Theory of Thermoluminescence and Related Phenomena. World Scientific, New York.

Cheung, J.Y., Tang, F.H., 2007. The calculation of dose enhancement close to platinum implants for skull radiography. Health Phys. 93 (4), 267–272.

Dambul, K.D., Mahdiraji, G.A., Amirkhan, F.A., Chow, D., Gan, G., Wong, W.R., Abu Hassan, M.R., Tee, D.C., Ismail, S., Ibrahim, S.A., Tamchek, N., Mahamd Adikan, F.R., 2012. Fabrication and development of flat fiber. Proc. PGC 1 (3), 13–16.

Friebele, E.J., Sigel, G.H., Griscom, D.L., 1976. Drawing-induced defect centers in a fused silica core fiber. Appl. Phys. Lett. 28, 516–518.

Guida, C., Maione, P., Rossi, A., Bareschino, M., Schettino, C., Barzaghi, D., Elmo, M., Gridelli, C., 2008. Combined chemo-radiotherapy for locally advanced non-small cell lung cancer: current status and future development. Crit. Rev. Oncol. Hematol. 68 (3), 222–232.

Hashim, S., Ramli, A.T., Bradley, D.A., Wagiran, H., 2006. The Thermoluminesce Response of Ge-doped Optical Fibre Subjected to Proton Irradiation. In: Fifth National Seminar on Medical Physics. Malaysia. Medical Physics Association, Kuala Lumpur.

Hashim, S., Al-Ahbabi, S., Bradley, D.A., Webb, M., Jeynes, C., Ramli, A.T., Wagiran, H., 2009. Thermoluminescence response of doped SiO_2 optical fibres subjected to photon and electron irradiations. Appl. Radiat. Isot 67, 423–427.

Hashim, S., Bradley, D.A., Saripan, M.I., Ramli, A.T., Wagiran, H., 2010. The thermoluminescence response of doped SiO_2 optical fibres subjected to fast neutrons. Appl. Radiat. Isot 68, 700–703.

Hibino, Y., Hanafusa, H., 1988. Consolidation-atmosphere influence on drawing-induced defects in pure silica optical fibers. J. Lightwave Technol. 6, 172–178.

Huston, A.L., Justus, B.L., Falkenstein, P.L., Miller, R.W., Ning, H., Altemus, R., 2001. Remote optical fiber dosimetry. Nucl. Instrum. Methods Phys. Res., Sect. B 184, 55–67.

Issa, F., Latip, N.A.A., Bradley, D.A., Nisbet, A., 2011. Ge-doped optical fibres as thermoluminescence dosimeters for kilovoltage X-ray therapy irradiations. Nucl. Instrum. Methods Phys. Res., Sect. A 652 (1), 834–837.

Izewska, J., Rajan, G., 2005. Radiation dosimeters. In: Podgorsak, E.B (Ed.), Radiation Oncology Physics: A Handbook for Teachers and Students. International Atomic Energy Agency, Vienna (IAEA).

Justus, B.L., Rychnovsky, S., Miller, M.A., Pawlovich, K.J., Huston, A.L., 1997. Optically stimulated luminescence radiation dosimetry using doped silica glass. Radiat. Prot. Dosim. 74, 151–154.

Noor, N.M., Hussein, M., Bradley, D.A., Nisbet, A., 2010. The potential of Ge-doped optical fibre TL dosimetry for 3D verification of high energy IMRT photon beams. Nucl. Instrum. Methods Phys. Res., Sect. A 619, 157–162.

Noor, N.M., Bradley, D.A., Nisbet, A., 2011. An investigation of the suitability of Ge-doped optical fibres in mailed thermoluminescence dosimetry audits of radiotherapy dose delivery. Radiother. Oncol. 99 (1), S196–S197.

Ramli, A.T., Bradley, D.A., Hashim, S., Wagiran, H., 2009. Thermoluminescence response of doped SiO_2 optical fibres subjected to alpha-particle irradiation. Appl. Radiat. Isot 67, 428–432.

S. Roushdey, Defect Related Luminescence in Silicon Dioxide Network: A review., In: Crystalline Silicon—Properties and Uses, S. Basu, (Ed.), (InTech, Rijeka, 2011), pp. 135–172.

Youssef, A.A., 2003. The Thermoluminescence Response of Ge-doped and Er-doped Optical Fibres in Radiation Therapy. Ph.D. Thesis. University of Malaya.

Yusoff, A.L., Hugtenburg, R.P., Bradley, D.A., 2005. Review of development of a silica-based thermoluminescence dosimeter. Radiat. Phys. Chem. 74, 459–481.